Multiphase Flow and Hysteresis Phenomena in Oil Recovery by Water Alternating Gas (WAG) Injection

By

S. Mobeen Fatemi

BSc., MSc.

Submitted for the degree of **Doctor of Philosophy** in

Petroleum Engineering

Heriot-Watt University

Institute of Petroleum Engineering

March 2015

ABSTARCT

Water flooding and gas injection are two widely used improved oil recovery techniques that can be applied individually or combined as water alternating gas (WAG) or simultaneous gas and water (SWAG) injection. Laboratory data on WAG and SWAG injections for non-water-wet systems are very limited especially for near-miscible (very low IFT) gas-oil systems. Near-miscible gas injection represents a number of processes of great importance to reservoir engineers including high pressure hydrocarbon gas injection and CO_2 flooding.

Simulation of these processes (WAG and SWAG injections) requires three-phase relative permeability (k_r) data. Most of the existing three-phase relative permeability correlations (such as Stone-I, Stone-II or Baker) have been developed for water-wet conditions and are unable to adequately account for all the complex multi-phase and multi-physics processes involved in these oil recovery techniques. Another major problem in the prediction of the performance of Water Alternating Gas (WAG) process is the uncertainty associated with the changes in three-phase relative permeability (k_r) values of oil, gas and water in different cycles, which is known as cyclic hysteresis.

The current approach in the industry (except hysteresis model proposed by Larsen and Skauge) is to use two-phase bounding imbibition and drainage relative permeabilities along with a two-phase hysteresis model (such as Land, Carlson or Killough to generate two-phase scanning curves) and input the result into a three-phase correlation (Stone-I, Stone-II, Baker etc) to simulate hysteresis in WAG injection. The other approach in the industry to account for hysteresis in WAG injection is the WAG-hysteresis model (proposed by Larsen and Skauge) coupled with Stone-I correlation. None of these models and approaches is developed and assessed based for low oil/gas IFT and/or non-water-wet system. Nevertheless, the majority of oil reservoirs are believed to be mixed-wet and hence, prediction of the performance of WAG injection in these reservoirs is associated with significant uncertainties.

Accurate determination of relative permeability values and their hysteresis behaviour is crucial for obtaining a reliable prediction of the performance of water-alternating-gas (WAG) injection in oil reservoirs. Performing reliable laboratory experiments is the key to evaluating the performance of these oil recovery techniques under different reservoir and operational conditions. The experimental data can be also used for assessment of different relative permeability and hysteresis models, and developing new methodologies for reliable simulation of WAG and SWAG injections (if required).

The content of the thesis can be divided into two sections: a) two-phase flow and b) three-phase flow.

I present the results of comprehensive series of two-phase and three-phase (WAG injections) coreflood experiments for a gas/oil system at near-miscible (IFT= 0.04 $mN.m^{-1}$) conditions. Two different cores; a high-permeability (1000 mD) and a lower permeability (65 mD) core were used in the experiments and both water-wet and mixed-wet conditions were examined. Experimental data have been used to obtain reliable relative permeabilities and investigate their cyclic hysteresis behavior.

In the first section of the thesis (two-phase flow), effects of different parameters such as permeability, wettability (water-wet and mixed-wet), immobile water and saturation history on two-phase flow of oil and gas at near-miscible condition have been

investigated. Contrary to the open literature reports which are based on high IFT oil/gas, the results (for very-low oil/gas IFT) showed the importance of the wettability and immobile water saturation on the recovery profiles and estimated relative permeabilities. In addition contrary to the near-miscible liquid-liquid systems, it was observed significant hysteresis effect in the gas-liquid system.

I have also investigated different two-phase systems (gas-oil, gas-water and oil-water) in mixed-wet systems. This is crucial, considering the importance of the two-phase systems as a backbone to better understand three-phase flow as well as their importance as an input to two-phase hysteresis models (for simulation of WAG including hysteresis). The investigation in this study shows that currently available two-phase hysteresis models in simulators (Carlson and Killough) are not able to capture the observed cyclic hysteresis behavior in these systems. The results suggest that for mixed-wet systems, it is necessary to consider irreversible hysteresis loops for both the wetting and non-wetting phases. Such capability currently does not exist in reservoir simulators due to lack of appropriate predictive tools. Results highlight the differences between cyclic hysteresis behaviors of the relative permeabilities in these three systems.

In the second section of the thesis, I first evaluated the performance of different injection scenarios in the mixed-wet system. These processes include primary waterflooding (WF), primary gasflooding (GF), WAG injection (either starting with water injection or gas injection), and SWAG injection (with different gas/water ratios). For some of these processes (WF, GF and WAG injection started with primary WF) the effect of wettability was also investigated. The results show that in both the water-wet and mixed-wet cores, the performance of WAG injection is better than water injection and gas injection alone. The results show that in mixed-wet core, oil recovery by the WAG test which had started with water injection was higher than the WAG test started with gas injection. WAG injections had superior performance over SWAG injections. SWAG performed better compared to primary gas injection. However, surprisingly, SWAG resulted in lower oil recovery compared to primary waterflood in the mixed-wet system. Compared to the other injection strategies, a very high pressure drop across the core was observed during SWAG injection indicating injectivity problems with the application of the process in mixed-wet rocks.

Using results of the WAG injection experiments, I also investigated the cyclic hysteresis effect on three-phase relative permeabilities of each phase (gas, oil and water). The results show the importance of properly accounting for irreversible k_r hysteresis loops in the processes involving cyclic injection under three-phase flow conditions. Gas relative permeability (k_{rg}) dropped in successive cycles under both water-wet and mixed-wet conditions. k_{rg} hysteresis was larger in the water-wet system compared to the mixed-wet case. The results also reveal saturation history dependency for oil relative permeability (k_{ro}), which tends to increase in successive gas injection periods. The improvement in k_{ro} was larger in the water-wet system. In both water-wet and mixed-wet systems, the largest k_{rw} hysteresis happens for the transition from two-phase (oil/water system) to three-phase system (from 1st water injection into 1st gas injection) and the subsequent WAG cycles does not show much hysteresis for k_{rw} in the experiments. I addressed some serious shortcomings of the existing reservoir simulators for reliable simulation of oil recovery processes involving three-phase flow and flow reversal.

ACADEMIC REGISTRY
Research Thesis Submission

Name*:*	Seyyed Mobeen Fatemi		
School/PGI:	Institute of Petroleum Engineering		
Version: *(i.e. First, Resubmission, Final)*	Final	Degree Sought (Award **and** Subject area)	PhD; Petroleum Engineering

Declaration

In accordance with the appropriate regulations I hereby submit my thesis and I declare that:

1) the thesis embodies the results of my own work and has been composed by myself
2) where appropriate, I have made acknowledgement of the work of others and have made reference to work carried out in collaboration with other persons
3) the thesis is the correct version of the thesis for submission and is the same version as any electronic versions submitted*.
4) my thesis for the award referred to, deposited in the Heriot-Watt University Library, should be made available for loan or photocopying and be available via the Institutional Repository, subject to such conditions as the Librarian may require
5) I understand that as a student of the University I am required to abide by the Regulations of the University and to conform to its discipline.

* *Please note that it is the responsibility of the candidate to ensure that the correct version of the thesis is submitted.*

Signature of Candidate*:*		Date:	

Submission

Submitted By *(name in capitals):*	S. Mobeen Fatemi
Signature of Individual Submitting:	
Date Submitted:	

For Completion in the Student Service Centre (SSC)

Received in the SSC by *(name in capitals):*			
Method of Submission *(Handed in to SSC; posted through internal/external mail):*			
E-thesis Submitted (**mandatory for final theses)**			
Signature:		Date:	

DEDICATION

To my beloved parents ***Hossein*** *and* ***Fatemeh****,*

My dearly loved wife ***Andisheh***

my kind siblings ***Moein*** *and* ***Matin***

and my lovely children who we don't have them yet because of this thesis!

ACKNOWLEDGEMENTS

I would like to express the sincere gratitude and respect to The Godfather, my dear supervisor Prof. Mehran Sohrabi, who provided the opportunity and encouragement during my studies. My second supervisor Prof. Mahmoud Jamiolahmady is also gratefully acknowledged for his support and inspiration during my PhD studies. My heartily regards go to dear my Grand-supervisor (supervisor of my PhD supervisor in his PhD studies), Prof. Dabir Tehrani for his constructive and tough comments throughout the JIP project studies as well as his kindness towards me and my wife. I also owe a great deal of debt to The Maestro, Mr. Shaun Ireland for his kindness! and patience all through training The Mobster and taking care of my wonder in Shaunland (mistakenly called Laboratory sometimes). My kind friends Kamran Ahmed and Graeme Robertson are also thankfully acknowledged for their invaluable help during conducting experimental work of the JIP project.

I should also acknowledge the financial support of the Iranian Ministry of Science, Research and Technology (MSRT) over the first 3.5 years of my PhD studies at Heriot-Watt University. My special thanks go to my dear MSc. Supervisors at Sharif University of Technology, Prof. Cyrus Ghotbi and Prof. Riyaz Kharrat as well as Prof. Davood Rashtchian for supporting my MSRT Scholarship and encouraging me to continue my studies in the UK. I also like to appreciate thesis examiners Dr. Reza Fassihi and Dr. James Somerville for their constructive comments in the Viva session.

Special thanks go to my dear friends Jalal Fahimpour, Hamed Amini, Amir Farzaneh, Hamidreza Shahverdi, Omid Shahrokhi, Mehrzad Nasriani and Heron Gachuz for the enjoyable and memorable time we had in Edinburgh.

Last but not the least, I wish to greatly acknowledge my beloved parents, my beautiful wife and my kind siblings for their continuous support and believing in me.

TABLE OF CONTENTS

LIST OF TABLES

LIST OF FIGURES

NOMENCLATURE

α	residual oil saturation correction factor in WAG hysteresis model
θ	contact angle
σ	interfacial tension
ρ	density
μ	fluid viscosity
Δp	pressure drop across the core
k_r	relative permeability
mD	10^{-3} Darcy, permeability unit
r	radius of pore
BT	breakthrough
CSS	cyclic steam stimulation
FAWAG	foam assisted water alternating gas injection
FCM	first contact miscible
GF	gas flooding
GOR	gas oil ratio
HCPVI	hydrocarbon pore volume injected
IFT	interfacial tension
IGIP	initial gas in place
IOIP	initial oil in place
K	absolute permeability
MCM	multiple contact miscible

MME	minimum miscibility enrichment
MMP	minimum miscibility pressure
P_c	capillary pressure
PV	pore volume
S_{gro}, S_{gto}	residual or trapped gas saturation due to oil imbibition
S_{gtw}	trapped gas saturation after water injection
S_{oi}, S_{gi}, S_{wi}	initial saturation of oil, gas and water
S_{org}	residual oil saturation after gas injection
S_{orw}, S_{otw}	residual or trapped oil saturation after water injection
S_{wim}	immobile water saturation
S_{wrg}	residual water saturation after primary gas injection
S_{wro}	residual water saturation after primary oil injection
SG	sight-glass
SWAG	simultaneous water and gas
MW	mixed-wet
WAG	water alternating gas
WF	waterflooding
WW	water-wet

LIST OF PUBLICATIONS

Journal Papers

- **Fatemi S.M.** and Sohrabi M.; (2013): Experimental Investigation of Near-Miscible Water-alternating-gas (WAG) Injection for Water-wet and Mixed-wet Systems, *SPE Journal, Volume 18, Number 1*, pp. 114-123.

- **Fatemi S.M.;** Sohrabi M.; (2013): Recovery Mechanisms and Relative Permeability for Gas/Oil Systems at Near-Miscible Conditions: Effects of Immobile Water Saturation, Wettability, Hysteresis and Permeability, *Energy & Fuels, Volume 27, Issue 5*, pp. 2376–2389.

- **Fatemi S.M.**; Sohrabi M.; Jamiolahmady M.; Ireland S., (2012): Experimental and Theoretical Investigation of Oil/Gas Relative Permeabilities Hysteresis in the Presence of Immobile Water: under Low Oil/Gas IFT and Mixed-Wet Conditions, *Energy Fuels*, Volume *26, Issue* 7, pp 4366–4382.

SPE Conference Papers

- **Fatemi S.M.;** Sohrabi M.; (2013): Experimental and Theoretical Investigation of Two- and Three-Phase Oil and Gas Trapping under Low Oil/Gas IFT Conditions: Applicable to Water Alternating Gas (WAG) Injection, SPE-166193, presented at SPE Annual Technical Conference & Exhibition to be held 30 September – 2, New Orleans, LA, USA.

- **Fatemi S.M.;** Sohrabi M; (2013): "Cyclic Hysteresis of Three-Phase Relative Permeability Curves Applicable to WAG Injection under Low Gas/Oil IFT: Effect of Immobile Water Saturation, Injection Scenario and Permeability", SPE-164918-MS, presented at 75th EAGE Conference & Exhibition incorporating SPE EUROPEC, 10-13 June, London, United Kingdom.

- **Fatemi S.M.;** Sohrabi M; (2013): Experimental and Numerical Investigation of the Impact of Design Parameters on the Performance of WAG and SWAG Injection in Water-Wet and Mixed-Wet Systems, SPE-165286, presented at SPE Enhanced Oil Recovery Conference, 2-4 July, Kuala Lumpur, Malaysia.

- **Fatemi S.M.**; Sohrabi M.; (2012): Experimental and Theoretical Investigation of Water/Gas Relative Permeability Hysteresis: Applicable to Water Alternating Gas (WAG) Injection and Gas Storage Processes, SPE-161827, presented at Abu Dhabi International Petroleum Exhibition and Conference to be held 11-14 November 2012 in Abu Dhabi, UAE.

- Sohrabi M.; **Fatemi S.M.**; (2012): Experimental Investigation of Oil Recovery by Different Injection Scenarios under Low Oil/Gas IFT and Mixed-Wet Condition: Water-Flood, Gas Injection, WAG and SWAG Injection, SPE-161074, presented at Abu Dhabi International Petroleum Exhibition and Conference to be held 11-14 November 2012 in Abu Dhabi, UAE.

- **Fatemi S.M.**; Sohrabi, (2012): Cyclic Hysteresis of Three-Phase Relative Permeability Applicable to WAG Injection: Water-Wet and Mixed-Wet Systems under Low Gas/Oil IFT, SPE-159816, presented at SPE Annual Technical Conference and Exhibition (ATCE), 8 - 10 October, San Antonio, Texas, USA.

- **Fatemi S.M.**; Sohrabi M.; Jamiolahmady M.; Ireland S., (2012): Experimental and Theoretical Investigation of Oil/Gas Relative Permeabilities Hysteresis in the Presence of Immobile Water: under Low Oil/Gas IFT and Mixed-Wet Conditions, SPE-154530, presented at SPE EUROPEC, 4 - 7 June, Copenhagen, Denmark.

- **Fatemi S.M.**; Sohrabi M.; Jamiolahmady M.; Ireland S., (2012): Recovery Mechanisms and Relative Permeability for Oil/Gas System at Near-miscible Conditions: Effects of Immobile Water Saturation, Wettability, Hysteresis and Permeability, SPE-154277, presented at SPE Symposium on Improved Oil Recovery to be held in Tulsa, United States of America.

- **Fatemi S.M.**; Sohrabi M.; Jamiolahmady M.; Ireland S.; Robertson G., (2011): Experimental Investigation of Near-Miscible Water-alternating-gas (WAG) Injection for Water-wet and Mixed-wet Systems, SPE-145191, presented at SPE Offshore Conference, 6-8 September, Aberdeen, UK.

SCA and EAGE Presentations

- Sohrabi M.; **Fatemi S.M.**; Farzaneh S.A., Jamiolahmady M.; Ireland S.; (2012): "Performance of SWAG Injection versus Alternating and Continuous Injection of Water and Gas", SCA2012-61, presented at the International Symposium of Society of Core Analysts, 26-31 August, Aberdeen, UK.

- **Fatemi S.M.,** Sohrabi M., Jamiolahmady M., Ireland M., Robertson G., (2011): Relative Permeabilities at Near-Miscible Conditions: Effects of Connate Water Saturation, Wettability, Hysteresis and Permeability, presented at 73rd EAGE Conference & Exhibition incorporating SPE EUROPEC, Vienna, Austria.

- **Fatemi S.M.**; Sohrabi M.; Jamiolahmady M.;; Ireland S.; Robertson G., Oil Recovery by Water-alternating-gas (WAG) Injection under Low Gas-oil IFT in Water-wet and Mixed-wet, presented at EAGE-IOR 2011, Cambridge, UK.

DEVEX Presentations

- Sohrabi M., **Fatemi S.M.**, Ireland S.; (2014): Enhanced Oil Recovery by Water Alternating Gas (WAG) Injection: The Opportunity and the Challenge, presented at *European Production and Development Conference DEVEX*, Aberdeen, UK, 6-7 May.

- Sohrabi M., **Fatemi S.M.,** Shahverdi H., Jamiolahmady M., Ireland S., Robertson G., (2011): Reliable Prediction of Water-Alternating-Gas (WAG) Injection Performance, *European Production and Development Conference DEVEX*, Aberdeen, UK.

1 Introduction

1.1 Background

Water injection is the most common method of oil recovery. Usually after waterflood, significant amount of oil remains in the reservoir (S_{orw}). Part of this remaining oil can be recovered by gas injection. As the gas/oil system has lower interfacial tension (IFT) than the oil/water system, hence microscopic displacement of the oil by gas at the pore level is normally better than by water. Various types of gas have been used for injection in oil reservoirs including, CO_2 (mostly in USA), hydrocarbon gas (mostly in North Sea area), nitrogen and air. CO_2 and hydrocarbon gases are used in 90% of the gas injection projects worldwide (Kulkarni and Rao, 2005).

To achieve a miscible flood process, conventionally gas injection is operated so as to maintain the pressures above the minimum miscibility pressure (MMP), which is determined for that specific crude oil and gas combination. But many of the gas injection projects although designed to be miscible, are actually near-miscible displacement at reservoir conditions (Awan et al., 2008).

Near-miscible gas injection refers to injection of gases that do not quite develop complete miscibility with the oil, but come close (Sohrabi et al., 2008 a,b). For instance, condensing–vaporising gas drives at enrichment slightly below minimum miscibility enrichment (MME) or at pressures slightly below minimum miscibility pressure (MMP) are near-miscible processes. Near-miscible gas injections appear attractive from both economic and operational standpoints (Sohrabi, 2001).

High gas mobility, due its low viscosity, causes gas fingering and early gas breakthrough which reduces the macroscopic (areal and vertical) sweep efficiency. Reservoir heterogeneities like high permeable layers and fractures (Christensen et al., 2001) may also assist gas fingering and result in premature breakthrough of gas. Therefore, continuous gas injection may not result in economically significant additional oil recovery. Decreasing gas permeability or increasing gas viscosity result in reducing mobility ratio and thereby improves sweep efficiency. Reduced mobility of the

gas phase (compared to gas injection) can be achieved by injecting water and gas alternately (Caudle and Dyes, 1958). Water alternating gas (WAG) injection improves the sweep efficiency of gas injections via controlling the mobility ratio and stabilization of the propagating front (Christensen et al., 1998); this would affect the horizontal displacement efficiency of the injection.

The vertical sweep efficiency, on the other hand, is influenced by the relation between viscous and gravitational forces. The reservoir properties affecting the vertical sweep mostly include reservoir dip angle and variation in permeability and porosity. Normally, porosity and permeability increasing towards the bottom of the reservoir will be advantageous for the WAG injection because this combination increases the stability of the front since gas which has a large tendency to override the other two fluids (water and oil) would be able to flow better towards bottom and less on top of the reservoir.

When injection pressure in the gas cycles of a WAG process is close or above the MMP (minimum miscibility pressure) of the reservoir fluid, the process is referred to the miscible WAG (MWAG). The miscible-gas front in WAG injection has poor volumetric sweep efficiency because of the low viscosity of gas whereas the residual oil saturation behind miscible front is very low. So the main objective of water slug in miscible-WAG injection is to increase the macroscopic sweep efficiency.

If the gas slugs in WAG process cannot develop miscibility with the reservoir oil, it's called immiscible WAG (IWAG). This type of WAG process has been applied with the aim of improving frontal stability or contacting unswept zones. Applications have been in reservoirs where gravity-stable gas injection cannot be applied because of limited gas resources or reservoir properties like low dip or strong heterogeneity. In addition to sweep, the microscopic displacement efficiency may be improved. Residual oil saturations are generally lower for WAG injection than for a waterflood and sometimes even lower than a gasflood, due to the effect of three-phase and cycle dependent relative permeability. Sometimes the first gas slug dissolves to some degree into the oil. This can cause mass exchange (swelling and stripping) and a favourable change in the fluid viscosity/density relations at the displacement front. The displacement can then become near-miscible.

Christensen et al. (2001) reviewed 59 field cases of WAG injection applications. Recovery by the WAG process is mostly reported to be increased by about 5%, but recovery increases of up to 20% are reported from several fields. The WAG process was almost always applied as a tertiary recovery method. Only in newer applications in the North Sea, the WAG injection has been initiated early in the field life. WAG process has been applied to rocks from very low-permeability chalk up to high permeability sandstone. Among these 59 field cases, thirty-three projects have been applied in reservoirs where sandstone is the main rock type. Twelve fields have been characterized as mainly dolomite, five fields were mainly limestone, and six applications have been in carbonate rocks (Figure 1-1).

The injection gases used in WAG projects can be classified into three groups: CO_2, hydrocarbons, and non-hydrocarbons (CO_2 excluded). CO_2 is an expensive gas and is generally used when miscible drive should be achieved, or if special options for deliverance exist. It is worth noticing that corrosion problems are often mentioned and seem impossible to avoid when using CO_2. Among the 59 reviewed projects by Christensen et al. (2001), 28 used CO_2 as injection gas (Figure 1-2). Twenty-four of the reviewed field cases used hydrocarbon gas either injected as dry gas or enriched before injection. Only two fields have used N_2 or flue gas/exhaust gas, mainly because special supplies were available nearby. In some cases combination of CO_2 and N_2 has been applied.

Among the reviewed field projects, 47 were planned to be miscible and 10 were planned to be immiscible, whereas 2 have not been classified (Figure 1-3). Only six projects have been reported from the offshore environment, all of them using hydrocarbon as injection gas in the North Sea. Three are miscible (Snorre, Brae South, and Statfjord), and three are immiscible (Brage, Gullfaks, Ekofisk). Carbonate, limestone, and dolomite reservoirs have been mostly implemented by miscible displacements. Dolomite reservoirs mainly have been flooded with CO_2. Sandstone, carbonate, and limestone reservoirs have used both hydrocarbon and non-hydrocarbon gases as injection fluids.

The slug sizes of the gas volume are mostly in the range of 0.1 to 0.3 pore volume (PV). When hybrid-WAG injection (a large slug of gas is injected, followed by a number of small slugs of water and gas) is used, the initial slug can be up to 40% hydrocarbon pore

volume (HCPV). It is important to adjust the amount of water and gas so that the best possible displacement efficiency will be achieved. Too much water will result in poor microscopic displacement, and too much gas will result in poor vertical, and possibly horizontal, sweep.

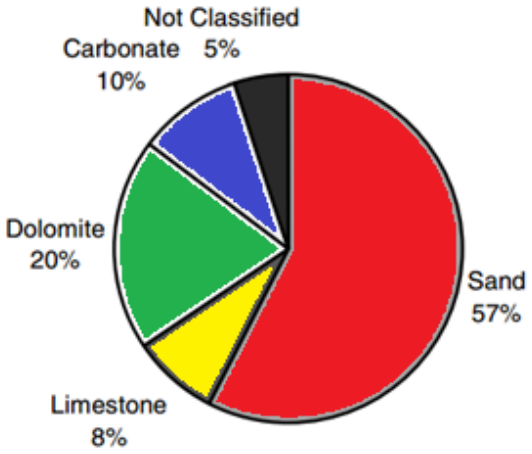

Figure 1-1: Reservoir rocks in which WAG injection has been applied in total of 59 reviewed projects (Christensen et al., 2001).

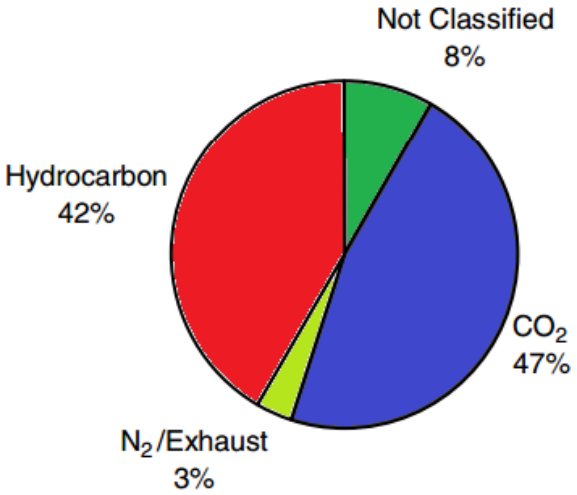

Figure 1-2: Types of gas used in WAG injection field applications (total of 59 projects) (Christensen et al., 2001)

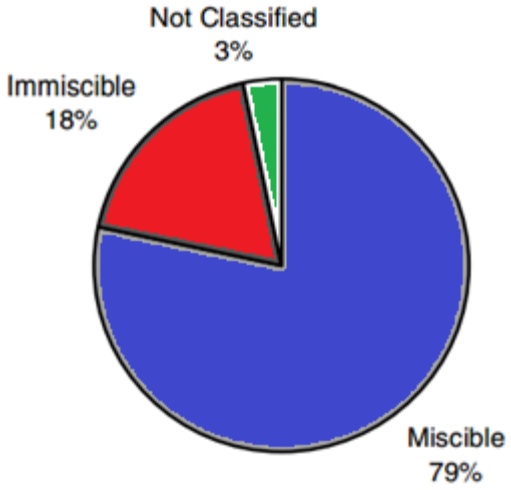

Figure 1-3: Application of miscible/immiscible WAG injections in total of 59 reviewed projects (Christensen et al., 2001).

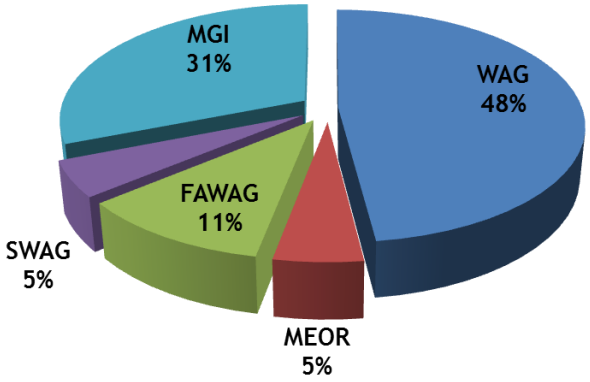

Figure 1-4: Distribution of different EOR field applications in the North Sea from total of 19 projects. (Awan et al., 2008)

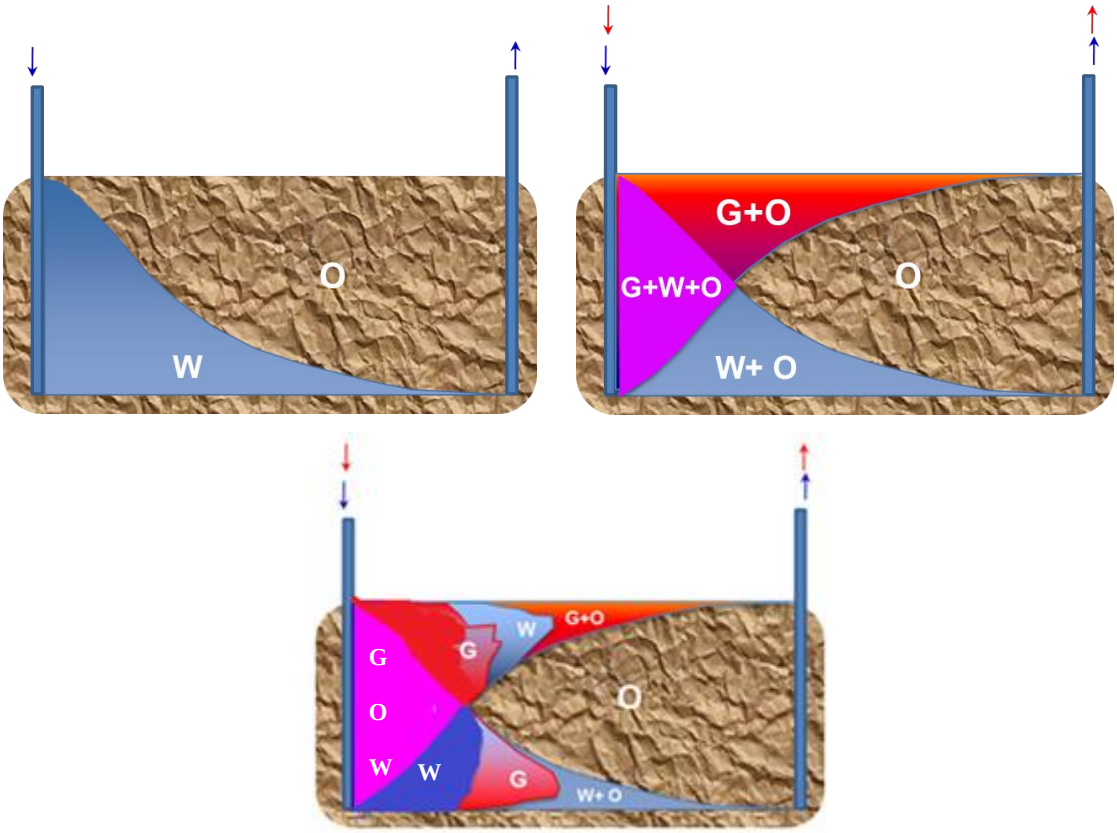

Figure 1-5: Schematic diagram of WAG injection in a real reservoir and development of different multiphase systems.

Awan et al. (2008) reviewed EOR applications in North-Sea area. Most of the EOR field applications were of the WAG injection type (Figure 1-4). Among the 19 field applications of EOR technologies, six were miscible gas injection, three were miscible WAG injection, six were immiscible WAG injection, two were FAWAG (foam assisted water alternating gas injection), one was SWAG (simultaneous water and gas injection) and one was MEOR (microbial enhanced oil recovery). All of the field reservoirs in their review produce light oil (32 to 41 °API) at depths ranging from 1740 to 3800 m subsea. The highest reservoir temperature and pressure was 165 °C and 7250 psi. In terms of rock classification, all the reviewed fields had high permeability channels. Ekofisk is a fractured reservoir with a low matrix permeability of 0.1 mD, while Gullfasks had a greatest range of permeability of 80 to 4500 mD. In both these two reservoirs immiscible WAG injection has been applied.

WAG injection is a complex form of three-phase fluid flow through porous media (Figure 1-5). Although WAG flooding has been successfully applied to many oilfields worldwide (Christensen et al. (2001) and Awan et al. (2008)), there is still an incomplete understanding of the actual mechanisms underlying oil recovery by WAG

injection especially in systems with non-uniform and non-water-wet wettability conditions (Suicmez et al., 2007). Our understanding is even more limited where the oil/gas interfacial tension (IFT) is very low (near-miscible condition) (Sohrabi et al., 2004). However most of the WAG injection projects are performed at very low oil/gas IFT range (Figure 1-3) and real reservoir rocks are rarely water-wet.

A major problem in the evaluation of WAG injection behaviour are uncertainties associated with the prediction of the wettability and spreading conditions of the system as well as the relative permeabilities values of the three phases for different injection cycles. Three-phase relative permeabilities measurement experiments (especially the steady-state method) are often time consuming and technically difficult to perform, particularly under reservoir condition. As a result, empirical models (such as Stone-I, Stone-II, Baker and etc.) are almost always used to estimate three-phase relative permeabilities from the more readily available two-phase flow data. However, most of the widely used empirical correlations are developed with an assumption that the rock is strongly water-wet (Blunt, 2000). This has contributed to a poor performance of the existing empirical equations used for determination of three-phase relative permeabilities for non-water-wet conditions (Element *et al.*, 2003).

There is a convincing body of theoretical and experimental evidence that relative permeabilities depend on many rock and fluid parameters (Avraam and Payatakes, 1999), including fluid viscosity, interfacial tension, flow rate, rock wettability, immobile water saturation, pore size distribution and of special interest to us, saturation history. Relative permeabilities are considered to be dependent on initial saturation and saturation history. This latter dependency is described in the literature as relative permeability hysteresis. The number of phases present in porous media is important when discussing hysteresis.

Several tertiary oil recovery processes have shown cycle-dependent hysteresis for relative permeability. This is especially important in EOR processes involving cyclic injection scenarios such as WAG injection and Cyclic Steam Stimulation (CSS). Multiphase flow involving saturation path reversals should be modelled with history-dependent relative permeability functions. Earlier approaches are based on two-phase flow (such as Killough (1976) and Carlson (1981) models). However, the problem of k_r hysteresis becomes significantly more complicated when moving from two-phase to

three-phase flow systems. It is now widely accepted that the cycle-dependent hysteresis in two-phase systems cannot be directly linked to three-phase flow (Skauge and Dale, 2007). Larsen and Skauge (1998) showed that when saturation oscillations occur during three-phase flow such as WAG injection, the existing two-phase hysteresis models will generally not be able to describe relative permeabilities obtained from corefloods.

It is clear that incorporating three-phase hysteresis in relative permeability curves is essential in order to obtain reliable predictions of immiscible WAG injection processes. Larsen and Skauge (1998) developed a three-phase relative permeability model to account for hysteresis effects in immiscible WAG processes which involves: (1) Hysteresis in gas relative permeability; (2) Hysteresis in water relative permeability; (3) Modification of the residual oil saturation in the Stone-I model, and (4) Coupling of residual oil saturation to trapped gas (oil relative permeability saturation history dependency). This model is currently the only available model in the commercial simulators (such as Eclipse) which has been developed specifically to reproduce the observed cyclic hysteresis behavior in three-phase flow. The model is based on their own observations during WAG injection experiments. There is insufficient published data to judge the quality of the model especially for different wettability conditions and/or oil/gas IFT conditions. Wettability is an important factor affecting gas relative permeability in three-phase flow and it determines the local distribution of the phases. A comparison with measurements from a variety of cores would be required to assess the validity of the model.

This thesis is directed as a part of the "*Characterization of Multi-phase Flow and Water Alternating Gas (WAG) Injection Studies*" JIP project, which is running at '*Centre for Enhanced Oil Recovery of Heriot-Watt University*'. The broad objective of this project is to investigate the effect of pertinent parameters on the performance of different gas based EOR processes as well as develop modified or new methodologies to predict the three-phase flow and relative permeability hysteresis under real reservoir conditions (Figure 1-6). The focus of the work performed and presented in this study is particularly about characterising three-phase flow in mixed-wet rocks and under low gas/oil IFT conditions. Using the extensive laboratory facilities, carefully designed coreflood experiments performed under two-phase and three-phase flow conditions including water injection, gas injection, WAG and SWAG injections. To be able to further investigate the effect of hysteresis on two-phase flow, cyclic injection scenarios (cyclic alternation between

imbibition and drainage) are performed in different two-phase systems (gas/oil, oil/water and gas/water). The results of the performed coreflood experiments (both two-phase and three-phase) were employed to investigate the behavior of k_r and their hysteresis effects.

Two-phase relative permeability data are required to assess different two-phase hysteresis models which are usually used in industry (coupled with a three-phase relative permeability correlation) to predict hysteresis in WAG injections. The two-phase flow studies in this work show that for all the possible systems (gas/oil, gas/water and oil/water) the performance of the existing models is poor for the conditions investigated here (mixed-wet system and/or very low oil/gas IFT).

As a part of JIP project, both two-phase hysteresis (coupled with a three-phase correlation) and three-phase hysteresis (proposed by Larsen and Skauge) approaches for simulation of WAG injection, are assessed (Shahrokhi et al., 2014). The results show that none of these approaches are able to match the observed data in the experiments.

To be able to develop modified or new methodologies for prediction of three-phase relative permeabilities hysteresis in WAG injection, experimental data are used to obtain the reliable three-phase relative permeability models. Both history matching technique (Shahverdi, 2012) and analytical solutions (presented here) are implemented to obtain three-phase relative permeabilities.

Presented experiments designed to study the hysteresis in all possible two phase system (oil/gas, oil, water and gas, water) as well as three-phase systems (WAG and SWAG injections). Based on the experiments presented in this thesis, a new methodology was then developed (called ‘WAG-HW’) for modeling of the three-phase relative permeability hysteresis in WAG injection process (Shahverdi and Sohrabi, 2013).

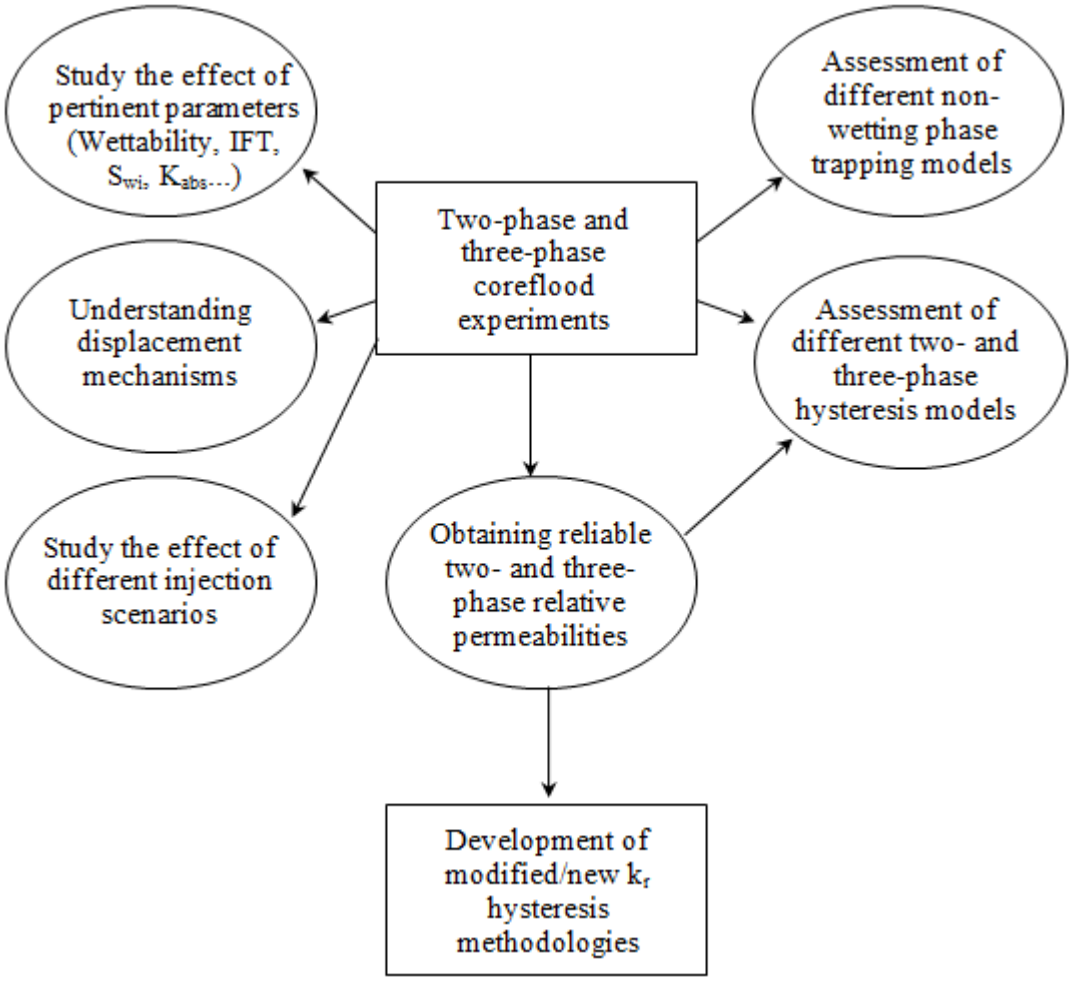

Figure 1-6: The work flow of the "Water Alternating Gas (WAG) Injection Studies JIP" at Heriot-Watt University.

1.2 Outline of the Thesis

In Chapter 2, I reviewed the pore-scale recovery mechanisms of different injection scenarios (WF, GF, WAG and SWAG injections) at different wettability conditions. These visual observations from high-pressure micromodels (Sohrabi, 2001) are quite beneficial to understand the recovery mechanisms and profiles at core-scale level (presented in this study).

Chapter 3 describes the experimental facilities and the fluids used in this work. The first part of this chapter includes a description of the coreflood rig and its important components. The fluids which have been used for this study and their physical properties are presented in the second part of this chapter.

In Chapter 4, the effect of different parameters on the fluid flow behaviour for two-phase system of gas-oil is investigated. Investigated parameters are saturation path

direction (imbibition or drainage), immobile water saturation (presence or absence), wettability (water-wet or mixed-wet) and permeability (pore size distribution). Explanations are offered for the observations based on the understanding of the pore-scale interactions and mechanisms, the distribution of fluid phases and their spreading bahaviour.

Chapter 5 deeply investigates the cyclic hysteresis effect on the estimated relative permeabilities for different two-phase systems at mixed-wet condition. The first part of the chapter studies oil/gas system under a very low oil/gas interfacial tension (IFT) of $0.04 mN.m^{-1}$. In second part of chapter 5, gas/water k_r hysteresis curves are investigated. In the last part of chapter 5, the hysteresis effect on relative permeabilities for oil/water system is investigated.

Chapter 6 investigates different injection scenarios for both water-wet and mixed-wet systems. These included water injection, gas injection, WAG injection as well as SWAG injection scenarios. SWAG-tail injection scenarios are also considered. The difference between the two WAG experiments was the order in which gas and water injections were carried out. The first WAG test started with water injection (IDIDID) whereas the second WAG experiment started with gas injection (DIDIDIDI). The difference between the two SWAG experiments was the gas/water (SWAG) ratio, which was 0.25 for the first one and 1.0 for the second SWAG test.

In Chapter 7 the cyclic hysteresis effect on three-phase relative permeabilities (during WAG injections) are investigated. The effect of pertinent parameters (wettability, immobile water saturation, injection scenario and permeability) on three-phase relative permeability hysteresis presented.

Chapter 8 presents the trapped oil and gas saturations obtained during different two-phase and three-phase (WAG injection) corefloods. The characteristic properties of rock/fluids systems (wettability, immobile water saturation, permeability, saturation history and oil/gas IFT) that influence the entrapment of gas and oil in petroleum reservoirs are investigated. A summary of the results and conclusions is presented in Chapter 9 followed by recommendations drawn from the work presented in this thesis.

Table 1-1: 65mD, Coreflood experiments at 1840 psia and 100ºF (Oil/Gas IFT = 0.04 $mN.m^{-1}$).

Exp. #	*Mobile Fluids*	*Coreflooding*	*Direction*	*Wettability*	S_{wim}
1-65-0.04-ww	Oil/Gas	Gas Injection	Drainage (D)	Water-Wet	0
S_{gi} / S_{oi} / S_{wi}				0 / 100 / 0	
S_{gf} / S_{of} / S_{wf}				69 / 31 / 0	
2-65-0.04-ww	Oil/Gas	Gas Injection	Drainage (D)	Water-Wet	0.18
S_{gi} / S_{oi} / S_{wi}				0 / 82 / 18	
S_{gf} / S_{of} / S_{wf}				60.5 / 21.5 / 18	
3-65-0.04-ww	Oil/Gas	Oil Injection	Imbibition (I)	Water-Wet	0
S_{gi} / S_{oi} / S_{wi}				100 / 0 / 0	
S_{gf} / S_{of} / S_{wf}				25.6 / 74.4 / 0	
4-65-0.04-ww	Oil/Gas	Oil Injection	Imbibition (I)	Water-Wet	0.18
S_{gi} / S_{oi} / S_{wi}				82 / 0 / 18	
S_{gf} / S_{of} / S_{wf}				30 / 52 / 18	
5-65-0.04-ww	Water/Oil	Water Injection	Imbibition (I)	Water-Wet	0.18
S_{gi} / S_{oi} / S_{wi}				0 / 82 / 18	
S_{gf} / S_{of} / S_{wf}				0 / 41.6 / 58.4	
6-65-0.04-mw	Oil/Gas	Gas Injection	Drainage (D)	Mixed-Wet	0.18
S_{gi} / S_{oi} / S_{wi}				0 / 82 / 18	
S_{gf} / S_{of} / S_{wf}				49.4 / 32.6 / 18	
7-65-0.04-mw	Oil/Gas	Oil Injection	Imbibition (I)	Mixed-Wet	0.18
S_{gi} / S_{oi} / S_{wi}				82 / 0 / 18	
S_{gf} / S_{of} / S_{wf}				38.6 / 43.4 / 18	
8-65-0.04-ww	Water/Oil	Water Injection	Imbibition (I)	Mixed-Wet	0.18
S_{gi} / S_{oi} / S_{wi}				0 / 82 / 18	
S_{gf} / S_{of} / S_{wf}				0 / 20 / 80	

	Oil/Gas	2 phase Hysteresis	DIDID	Mixed-Wet	0.18
				S_{gi} / S_{oi} / S_{wi}	
9-65-0.04-mw		*Gas Injection*	*D*	0 / 82 / 18	
10-65-0.04-mw		*Oil Injection*	*I*	64/ 18 / 18	
11-65-0.04-mw		*Gas Injection*	*D*	22 / 60 / 18	
12-65-0.04-mw		*Oil Injection*	*I*	57 / 25 / 18	
13-65-0.04-mw		*Gas Injection*	*D*	10 / 72 / 18	
				32 / 50 / 18	
	Oil/Gas	2 phase Hysteresis	IDIDI	Mixed-Wet	0.18
				S_{gi} / S_{oi} / S_{wi}	
14-65-0.04-mw		*Oil Injection*	*I*	82 / 0 / 18	
15-65-0.04-mw		*Gas Injection*	*D*	32 / 50 / 18	
16-65-0.04-mw		*Oil Injection*	*I*	65 / 17 / 18	
17-65-0.04-mw		*Gas Injection*	*D*	20 / 62 / 18	
18-65-0.04-mw		*Oil Injection*	*I*	56 / 26 / 18	
				19.5 / 62.5 / 18	
	Water/Gas	2 phase Hysteresis	DIDIDI	Mixed-Wet	0.18
				S_{gi} / S_{oi} / S_{wi}	
19-65-0.04-mw		*Gas Injection*	*D*	0 / 0 / 100	
20-65-0.04-mw		*Water Injection*	*I*	47 / 0 / 53	
21-65-0.04-mw		*Gas Injection*	*D*	23 / 0 / 77	
22-65-0.04-mw		*Water Injection*	*I*	49 / 0 / 51	
23-65-0.04-mw		*Gas Injection*	*D*	25 / 0 / 75	
24-65-0.04-mw		*Water Injection*	*I*	50 / 0 / 50	
				26.5 / 0 / 73.5	
	Water/Gas	2 phase Hysteresis	IDIDI	Mixed-Wet	0.18
				S_{gi} / S_{oi} / S_{wi}	
25-65-0.04-mw		*Water Injection*	*I*	82 / 0 / 18	
26-65-0.04-mw		*Gas Injection*	*D*	27 / 0 / 73	
27-65-0.04-mw		*Water Injection*	*I*	52 / 0 / 48	
28-65-0.04-mw		*Gas Injection*	*D*	30 / 0 / 70	
29-65-0.04-mw		*Water Injection*	*I*	50 / 0 / 50	
				30 / 0 / 70	

	Water/Oil	2 phase Hysteresis	DIDIDI	Mixed-Wet	0.18
				S_{gi} / S_{oi} / S_{wi}	
30-65-0.04-mw		*Oil Injection*	*D*	0 / 0 / 100	
31-65-0.04-mw		*Water Injection*	*I*	0 / 50 / 50	
32-65-0.04-mw		*Oil Injection*	*D*	0 / 30 / 70	
33-65-0.04-mw		*Water Injection*	*I*	0 / 52 / 48	
34-65-0.04-mw		*Oil Injection*	*D*	0 / 33 / 67	
35-65-0.04-mw		*Water Injection*	*I*	0 / 53 / 47	
				0 / 34 / 66	
	Water/Oil/Gas	WAG Injection	IDID	Water-Wet	0.16
				S_{gi} / S_{oi} / S_{wi}	
36-65-0.04-ww		*Water Injection*	*I*	0 / 84 / 16	
37-65-0.04-ww		*Gas Injection*	*D*	0 / 40 / 60	
38-65-0.04-ww		*Water Injection*	*I*	18 / 34 / 48	
39-65-0.04-ww		*Gas Injection*	*D*	7.8 / 31 / 61.2	
				23.8 / 24.6 / 51.6	
	Water/Oil/Gas	WAG Injection	IDIDID	Water-Wet	0.18
				S_{gi} / S_{oi} / S_{wi}	
40-65-0.04-ww		*Water Injection*	*I*	0 / 82 / 18	
41-65-0.04-ww		*Gas Injection*	*D*	0 / 42 / 58	
42-65-0.04-ww		*Water Injection*	*I*	24 / 29 / 47	
43-65-0.04-ww		*Gas Injection*	*D*	18 / 25 / 57	
44-65-0.04-ww		*Water Injection*	*I*	35 / 18 / 47	
45-65-0.04-ww		*Gas Injection*	*D*	27 / 15 / 58	
				46.4 / 7 / 46.9	
	Water/Oil/Gas	WAG Injection	IDIDID	Mixed-Wet	0.18
				S_{gi} / S_{oi} / S_{wi}	
46-65-0.04-mw		*Water Injection*	*I*	0 / 82 / 18	
47-65-0.04-mw		*Gas Injection*	*D*	0 / 20 / 80	
48-65-0.04-mw		*Water Injection*	*I*	24 / 16 / 60	
49-65-0.04-mw		*Gas Injection*	*D*	7 / 14 / 79	
50-65-0.04-mw		*Water Injection*	*I*	28 / 12 / 60	
51-65-0.04-mw		*Gas Injection*	*D*	11 / 10 / 79	
				39.8 / 3.7 / 56	

	Water/Oil/Gas	WAG Injection	DIDIDIDI	Mixed-Wet	0.18
				S_{gi} / S_{oi} / S_{wi}	
52-65-0.04-mw		*Gas Injection*	*D*	0 / 0.82 / 0.18	
53-65-0.04-mw		*Water Injection*	*I*	0.53 / 0.29 / 0.18	
54-65-0.04-mw		*Gas Injection*	*D*	0.05 / 0.19 / 0.76	
55-65-0.04-mw		*Water Injection*	*I*	0.31 / 0.16 / 0.53	
56-65-0.04-mw		*Gas Injection*	*D*	0.2 / 0.14 / 0.74	
57-65-0.04-mw		*Water Injection*	*I*	0.34 / 0.11 / 0.55	
58-65-0.04-mw		*Gas Injection*	*D*	0.12 / 0.1 / 0.78	
59-65-0.04-mw		*Water Injection*	*I*	0.32 / 0.07 / 0.61	
				0.39 / 0.06 / 0.55	
60-65-0.04-mw	Water/Oil/Gas	SWAG Injection	$S_o\downarrow$, $S_w\uparrow$, $S_g\uparrow$	Mixed-Wet	0.18
S_{gi} / S_{oi} / S_{wi}		(Q_g/Q_w=0.25)		0 / 82 / 18	
S_{gf} / S_{of} / S_{wf}				8.2 / 27.2 / 67.6	
61-65-0.04-mw	Water/Oil/Gas	Gas Injection*	$S_o\downarrow$, $S_w\downarrow$, $S_g\uparrow$	Mixed-Wet	--
S_{gi} / S_{oi} / S_{wi}				8.2/ 27.2 / 67.6	
S_{gf} / S_{of} / S_{wf}				30 / 26 / 44	
	Water/Oil/Gas	WAG Injection**	ID	Mixed-Wet	--
				S_{gi} / S_{oi} / S_{wi}	
62-65-0.04-mw		*Water Injection*	*I*	30 / 26 / 44	
63-65-0.04-mw		*Gas Injection*	*D*	11 / 25 / 64	
				30 / 24.1 / 45.9	
64-65-0.04-mw	Water/Oil/Gas	SWAG Injection	$S_o\downarrow$, $S_w\uparrow$, $S_g\uparrow$	Mixed-Wet	0.18
S_{gi} / S_{oi} / S_{wi}		(Q_g/Q_w=1.0)		0 / 82 / 18	
S_{gf} / S_{of} / S_{wf}				15.4 / 27.2 / 57.4	

* performed at the end of the SWAG experiment 60-65-0.04-mw
** performed after SWAG-Tail Gas injection 61-65-0.04-mw

Table 1-2: 65mD, Coreflood experiments at 1200 psia and 100ºF. (Oil/Gas IFT = 2.70 $mN.m^{-1}$)

Exp. #	***Mobile Fluids***	***Coreflooding***	***Direction***	***Wettability***	S_{wim}
	Water/Oil/Gas	WAG Injection	IDIDIDID	Mixed-Wet	0.18
				S_{gi} / S_{oi} / S_{wi}	
65-65-2.70-mw		*Water Injection*	*I*	0 / 82 / 18	
66-65-2.70-mw		*Gas Injection*	*D*	0 / 31.1 / 68.9	
67-65-2.70-mw		*Water Injection*	*I*	23.1 / 30.8 / 45.9	
68-65-2.70-mw		*Gas Injection*	*D*	11.9 / 29.2 / 58.9	
69-65-2.70-mw		*Water Injection*	*I*	25.2 / 29 / 45.8	
70-65-2.70-mw		*Gas Injection*	*D*	13.9 / 28.1 / 58	
71-65-2.70-mw		*Water Injection*	*I*	27.1 / 27.6 / 45.3	
				13.8 / 27.0 / 59.2	
	Water/Oil/Gas	WAG Injection	DIDIDIDI	Mixed-Wet	0.18
				S_{gi} / S_{oi} / S_{wi}	
72-65-2.70-mw		*Gas Injection*	*D*	0 / 82 / 18	
73-65-2.70-mw		*Water Injection*	*I*	47 / 35 / 18	
74-65-2.70-mw		*Gas Injection*	*D*	25 / 8.8 / 66.2	
75-65-2.70-mw		*Water Injection*	*I*	41.5 / 8.2 / 50.3	
76-65-2.70-mw		*Gas Injection*	*D*	31 / 6.8 / 62.2	
77-65-2.70-mw		*Water Injection*	*I*	44.6 / 6.4 / 49	
78-65-2.70-mw		*Gas Injection*	*D*	31.5 / 6 / 62.5	
79-65-2.70-mw		*Water Injection*	*I*	43.5 / 6 / 50.5	
				32.1 / 5.7 / 62.2	
80-65-0.04-mw	Oil/Gas	Gas Injection	Drainage (D)	Mixed-Wet	0.18
S_{gi} / S_{oi} / S_{wi}				0 / 82 / 18	
S_{gf} / S_{of} / S_{wf}				51.5 / 30.5/ 18	

1.3 References

Awan A.R., Teigland R., and Kleppe J., (2008): A Survey of North Sea Enhanced-Oil-Recovery Projects Initiated During the Years 1975 to 2005, SPE Reservoir Evaluation & Engineering, Volume 11, Number 3, pp. 497-512.

Avraam and Payatakes, (1999): Flow Mechanisms, Relative Permeabilities, and Coupling Effects in Steady-State Two-Phase Flow through Porous Media. The Case of Strong Wettability, Industrial and Engineering Chemistry Research, Volume 38, Issue 3, pp. 778–786.

Blunt M.J., (2000): An empirical model for three-phase relative permeability, SPE Journal, Volume 5, Issue 4, pp. 435–445.

Carlson F.M, (1981): Simulation of Relative Permeability Hysteresis to the Nonwetting Phase, presented at SPE Annual Technical Conference and Exhibition, 4-7 October, San Antonio, Texas.

Caudle, B. H. and Dyes, A. B.: 1958, Improving miscible displacement by gas–water injection, Petroleum Transactions, AIME, Volume 213, pp. 281-283.

Christensen J.R., Stenby E.H., Skauge A., (2001):"Review of WAG field Experiences", SPE-71203-PA, SPE Reservoir Evaluation & Engineering, Volume 4, Issue 2, pp. 97 - 106.

Christensen J.R., Stenby E.H., Skauge A., (2001):"Compositional and relative permeability hysteresis effects on near miscible WAG", presented at SPE/DOE Improved oil recovery symposium, 19–22 April, Tulsa, Oklahoma, USA.

Element D.J., Masters J.H.K., Sargent N.C., Jayasekera A.J. and Goodyear S.G., (2003): Assessment of Three-phase Relative Permeability Models Using Laboratory Hysteresis Data, SPE 84903, Proceedings of the SPE International Improved Oil Recovery Conference in Asia Pacific, Kuala Lumpur, Malaysia.

Killough J.E., (1976): Reservoir Simulation with History-Dependent Saturation Functions, SPE Journal, Volume 16, Number 1, pp. 37-48.

Kulkarni M.M. and Rao D.N.; (2005): Experimental investigation of miscible and immiscible Water-Alternating-Gas (WAG) process performance. Journal of Petroleum Science and Engineering, Volume 48, Issue 1-2, pp. 1-20.

Larsen J.A. and Skauge A. (1998): Methodology for Numerical Simulation with Cycle-Dependent Relative Permeabilities, SPE Journal, Volume3, Number 2, pp.163-173.

Shahrokhi O., Fatemi S.M., Sohrabi M., Ireland S., Ahmed K., (2014): Assessment of Three Phase Relative Permeability and Hysteresis Models for Simulation of Water-Alternating-Gas (WAG) Injection in Water-wet and Mixed-wet Systems, SPE-169170, SPE Improved Oil Recovery Symposium held in Tulsa, Oklahoma, USA, 12–16 April.

Shahverdi H., (2012): Characterization of Three-phase Flow and WAG Injection in Oil Reservoirs, PhD Thesis submitted to Institute of Petroleum Engineering at Heriot-Watt University, Edinburgh, Scotland, UK.

Shahverdi H. and Sohrabi M., (2013): An Improved Three-Phase Relative Permeability and Hysteresis Model for the Simulation of a Water-Alternating-Gas Injection, SPE Journal, Volume 18, Issue 5, pp. 841-850.

Skauge A. and Dale E.I., (2007): Progress in Immiscible WAG Modelling, SPE-111435-MS, presented at SPE/EAGE Reservoir Characterization and Simulation Conference, 28-31 October, Abu Dhabi, UAE.

Sohrabi M., (2001): Water Alternating Gas Injection (WAG) Studies, PhD Thesis submitted to Institute of Petroleum Engineering at Heriot-Watt University, Edinburgh, Scotland, UK.

Sohrabi M., Tehrani D.H., Danesh A., Henderson G.D., (2004): Visualization of Oil Recovery by Water-Alternating-Gas Injection Using High-Pressure Micromodels, SPE-89000, SPE Journal, Volume 9, Number 3, pp. 290-301.

Sohrabi M., Danesh A., Tehrani D.H. and Jamiolahmady M., (2008a): "Microscopic Mechanisms of Oil Recovery By Near-Miscible Gas Injection", Transport in Porous Media, Volume 72, Number 3, pp. 351-367.

Sohrabi M., Danesh A. and Jamiolahmady M., (2008b): "Visualisation of Residual Oil Recovery by Near-miscible Gas and SWAG Injection Using High-pressure Micromodels", Transport in Porous Media, Volume 74, Number 2, pp. 239-257.

Suicmez V.S., Piri M. and Blunt M.J., (2007): Pore-scale Simulation of Water Alternate Gas Injection, Transport in Porous Media, Volume 66, Number 3, pp. 259-286.

2 Pore-Scale Recovery Mechanisms

In this chapter the previous works performed on micromodel by Sohrabi (2001) and his co-workers around the visualisation of recovery mechanisms of waterflooding, gasflooding, WAG and SWAG injection will be reviewed. It should be mentioned that in their experiments, fluids (gas, oil and water) have been pre-equilibrated and as a result the compositional effects were not present.

2.1. Review of the Micromodel Studies

2.1.1 Primary Waterflooding (WF): Water-Wet System

During the primary waterflood in water-wet system, Sohrabi et al. (2004) observed that water flows on the sides of the pores, rather than forming a distinct water front. This was referred as “corner filament flow”. The water filaments were seen to thicken progressively, leaving oil filaments in the middle of the pores; as a result of the pore-network structure, the residual oil was very continuous. Figure 2-1 shows a section of the micromodel before and after primary waterflooding in water-wet system.

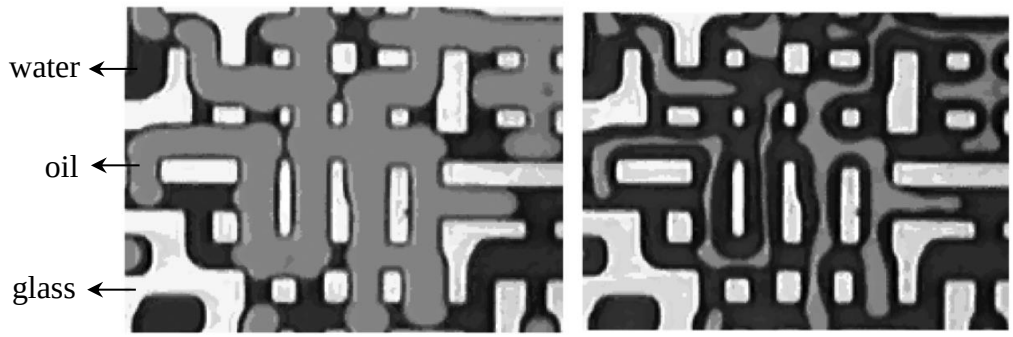

Figure 2-1: Water/oil distribution before (left) and after (right) primary waterflood (Sohrabi et al., 2004).

2.1.2 Primary Waterflooding (WF): Oil-Wet System

Figure 2-2 shows section of micromodel used in oil-wet experiments (Sohrabi et al., 2004). The curvature of the water and oil phases inside the pores confirms the oil-wet nature of the pores. During water injection, there was no spontaneous flow of water into the micromodel (unlike water-wet experiments), nor was there any layer or corner flow. This is due to the fact that porous medium was strongly oil-wet and the incoming water was a non-wetting phase. For the oil-wet system, Sohrabi et al. (2004) observed that displacement of the oil by the injected water is all piston-like. In addition, in the water-wet model, during waterflooding, no oil-filled pores were bypassed, and residual oil saturation was mainly uniform in the form of oil filaments in the middle of the pores. However, as can be noticed from Figure 2-3, in an oil-wet model, some of the oil pores are completely bypassed by the incoming water. Interestingly, Sohrabi et al. (2004) noticed that two-phase fluid distribution after waterflooding in oil-wet system is similar to that for primary drainage of water (by oil) in the water-wet case, but with the positions of the oil and water phases being reversed (Figure 2-3).

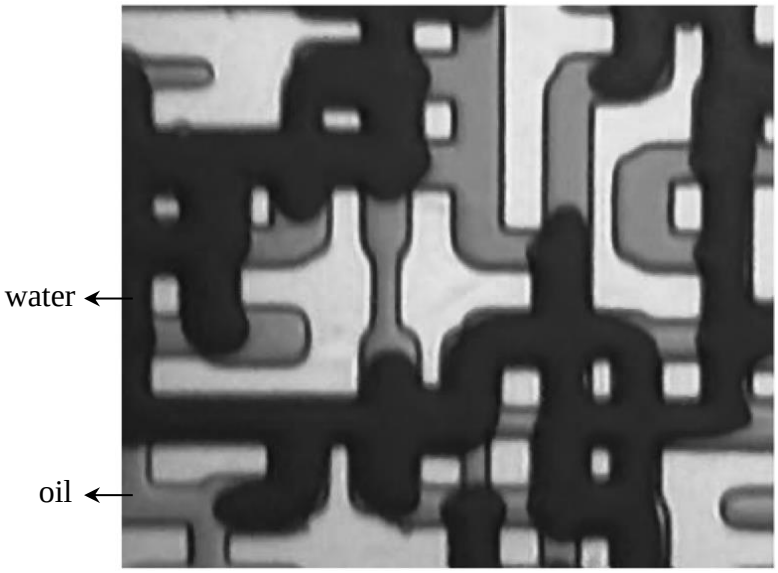

Figure 2-2: A magnified section of the oil-wet micromodel showing the oil-wet nature of the pores (Sohrabi et al., 2004).

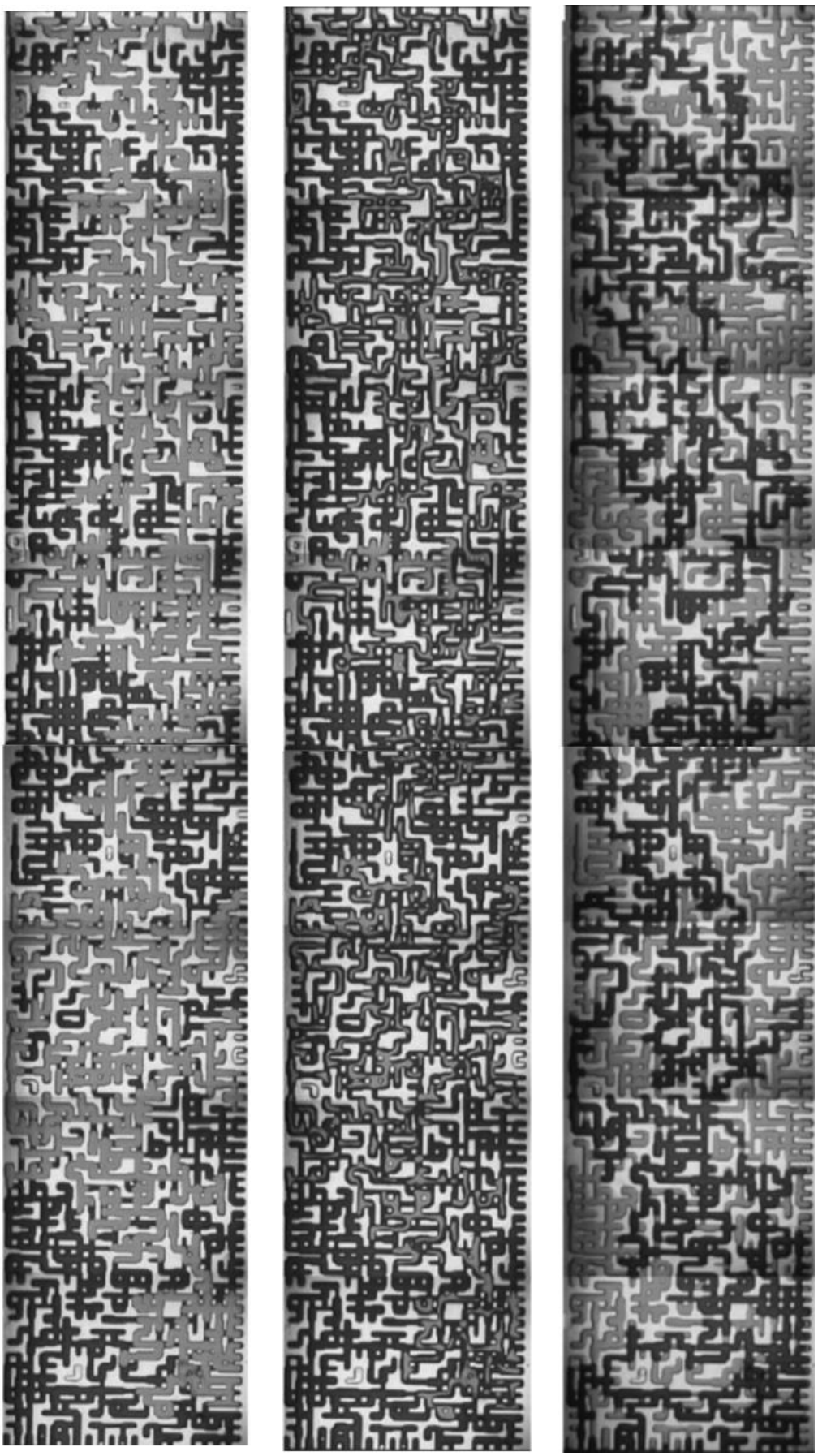

Figure 2-3: oil and water distribution in micromodel after: Primary drainage of water by oil in water-wet system (left), primary waterflooding of oil in water-wet system (middle), primary waterflooding of oil in oil-wet system (right). (Sohrabi et al., 2004)

2.1.3 Near-Miscible Gas Injection (S_{wim}=0%)

Initially, the micromodel was fully saturated with equilibrated oil (S_{oi} = 100%). Then the near-miscible gas was injected into the micromodel ($IFT_{o/g}$ = 0.08 $mN.m^{-1}$). As the gas flowed through the micromodel, a distinct piston type frontal advance (at the pore level) was observed for the incoming gas (Sohrabi et al., 2008a). The drainage of oil happened through the wetting layers in the angular corners. Figure 2-4a shows a part of the micromodel during near-miscible gas injection where the main gas front has just passed. A significant part of the original oil in place has been recovered at this stage for this low-IFT gas injection. Some of the oil has been by-passed by the main gas front. Sohrabi et al. (2008a) argued that this pore-level bypassing is always present in oil recovery by gas floods even at zero IFT (complete miscibility). Figure 2-4b shows that the recovery of the bypassed oil continued behind the main gas front and complete oil recovery has been achieved by near-miscible gas injection. This extra oil recovery, in near-miscible gas injection, had not been observed, in high-IFT (low-pressure immiscible) gas injection (Sohrabi 2001). Image analysis of micromodel experiments showed that a typical immiscible gas (gas–oil IFT around and greater than 1 $mN.m^{-1}$) injection ultimately recovered less than 60% of the original oil in place. Whereas, a typical near-miscible gas injection (gas–oil IFT of 0.08mNm^{-1}), had a much higher oil recovery and ultimately up to 95% of the original oil in place was recovered.

In near-miscible gas injection, due to a very low gas–oil IFT the capillary forces are no longer dominant; therefore the threshold capillary pressure resisting the entry of the gas into the pores occupied by bypassed oil is very small. Hence, the gas pressure can easily overcome the capillary barrier and moves the interface into the oil phase. This provides an effective driving force to transfer the bypassed oil into the main flow stream. Once the oil has been transferred into the main flow stream, its flow is further enhanced by coupling with the flow of the gas. The presence and simultaneous flow of gas and oil in the same pore has been shown (Williams and Dawe 1988) to be very effective for very low IFT (nearly miscible) systems. As a result of this mechanism, production of the by-passed oil takes place behind the main gas front. Sohrabi et al. (2008a) discuss that this mechanism of the bypassed oil recovery does not take place in immiscible gas floods nor does it occur in miscible gas floods. In immiscible (high-IFT) gas injection with spreading oil layers, although the bypassed oil maintains its connectivity with the main flow stream through the oil wetting films, however, oil recovery by this film flow mechanism is negligible especially if an effective driving force (e.g., gravity) is absent.

The rather large capillary pressure at the gas/oil interface resists the entry of the gas into the bypassed oil in the first place, it also hinders simultaneous flow of gas and the oil films in the main flow stream. In miscible gas floods, on the other hand, there would be no interface between gas and oil. The system would be basically single phase and no simultaneous flow of gas and oil could take place. Bypassed oil recovery, in miscible gas injection, can happen due to molecular diffusion and/or dispersion but not by the mechanism explained for near-miscible gas injection.

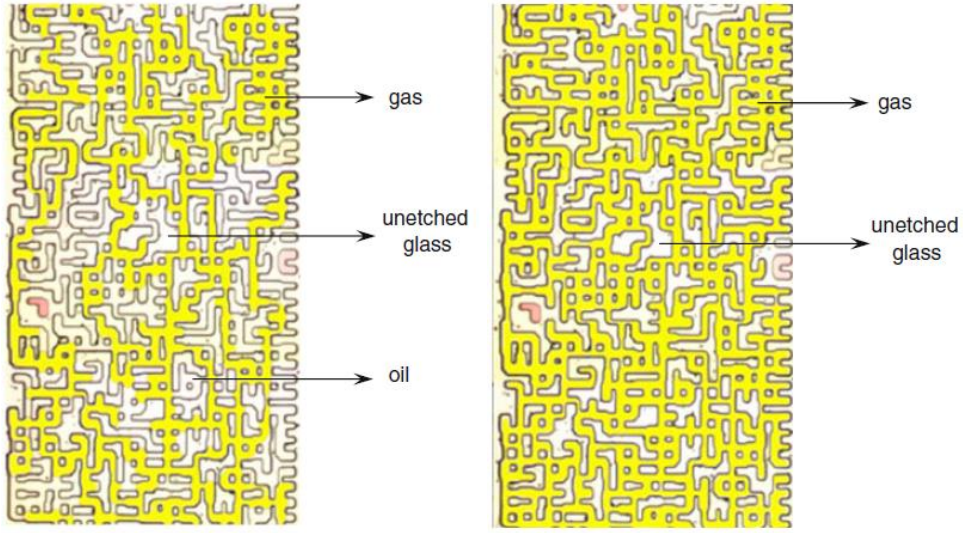

Figure 2-4: A section of the horizontal micromodel during near-miscible gas; left: bypassed oil during gas injection; right: complete recovery of this oil with extension of the gas injection beyond breakthrough (Sohrabi et al., 2008a).

2.1.4 Tertiary Gas Injection (after WF): Water-Wet System

Before start of gas injection, primary waterflooding was performed. Water flooding continued until no more oil production or changes in fluids distribution was observed. At the end of this water flood, near-miscible gas injection commenced (Sohrabi et al., 2008a). Gas was injected from the same end as water was. During gas injection, as soon as the invading gas came in contact with the residual oil, the gas front was covered with a small amount of oil (Figure 2-5). As the gas advanced further, an oil bank was formed and moved ahead of the gas front. The oil bank, moving ahead of the gas front, supplied oil to pores where residual oil was present. This resulted in thickening of those oil filaments, which came in contact with the invading gas or the oil front ahead of it. Figure 2-6 shows a part of the model during gas injection. Sohrabi et al. (2008a) divided oil phase in two types. The first type is oil in the form of some filaments surrounded with thick water layers. This is the oil that has not been contacted by the incoming gas. The second type is thick oil ganglia in contact with the gas channel. These have been formed by fluid redistribution or by local oil transfer brought about by the gas injection.

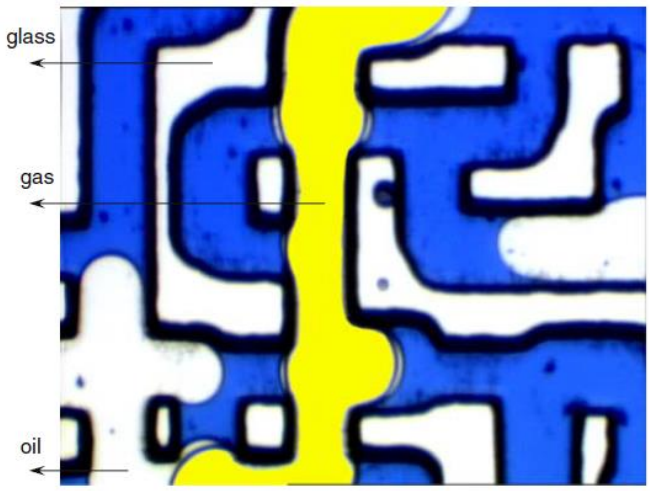

Figure 2-5: A magnified section of the micromodel demonstrating fluid distribution during near-miscible gas injection after primary waterflooding. The oil layers are visible between the gas and the water, which formed during invasion of the pores by the gas front (Sohrabi et al., 2008a).

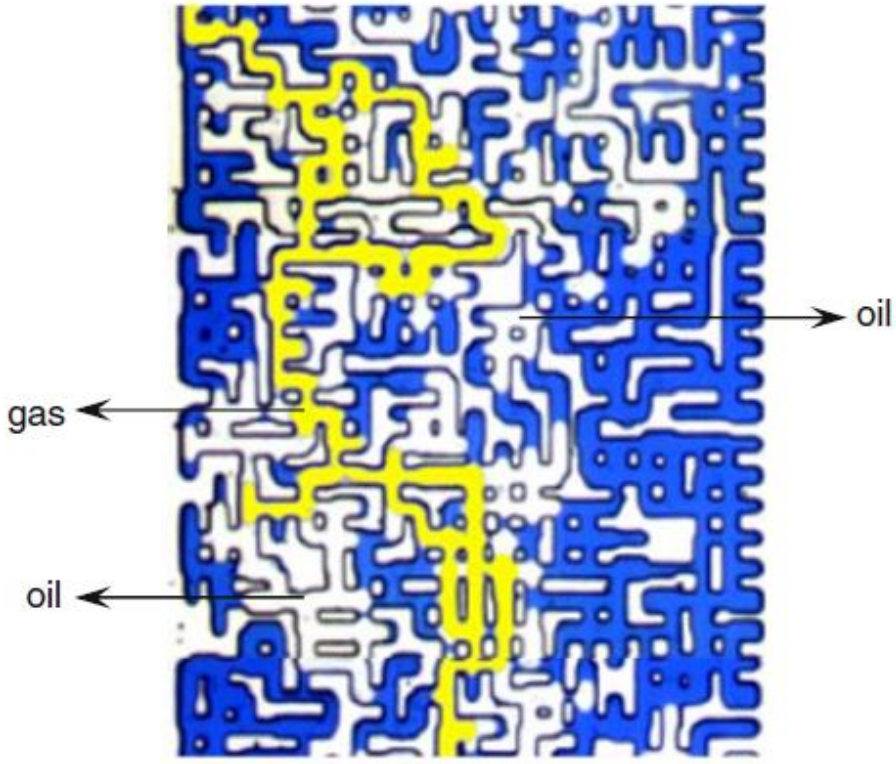

Figure 2-6: Fluid distribution within the micromodel during near-miscible gas injection. The main gas front has just left the micromodel (Sohrabi et al., 2008a).

As it can be seen, despite a very low gas–oil IFT, the gas has made only a single channel through the network of pores. Compared to secondary gas floods (Figure 2-4a), the efficiency of this tertiary gas flood has been rather poor with a significant amount of oil being bypassed by the gas front. Sohrabi et al. (2008a) provided two main reasons for this. First, in water flooded micromodel the water saturation is high, which tends to restrict the movement of the gas and shields the residual oil from being contacted by the gas. The second reason is the topology of the porous medium, which causes some of the oil that has been contacted by gas or its associated oil bank, to become trapped in dead-end (physically closed by rock surfaces) or semi dead-end (restricted by water at one or more ends) pores.

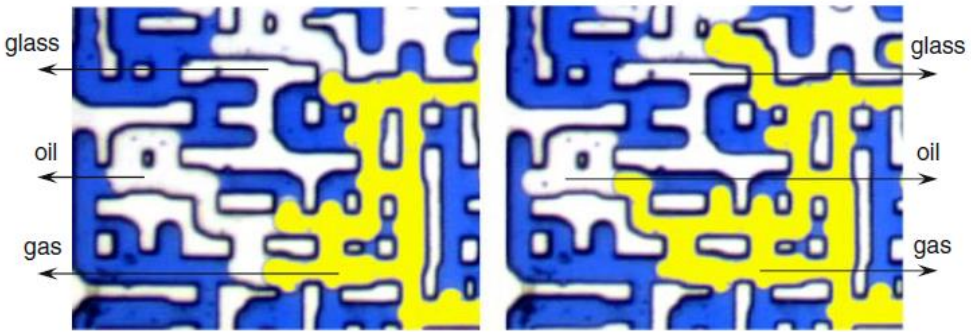

Figure 2-7: A section of the micromodel during tertiary gas injection. (a) main gas front has just passed (b) the same section after 1 h of additional gas injection, when gas channels have widened and oil ganglia have shrunk (Sohrabi et al., 2008a).

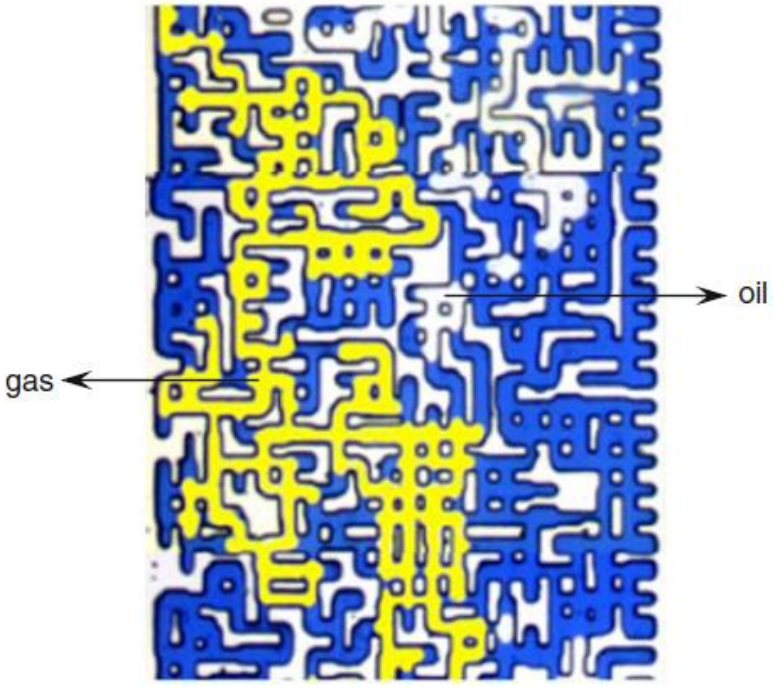

Figure 2-8: Fluid distribution within the micromodel 1 hour after gas breakthrough. The gas channel has widened by pushing some of the contacted residual oil out of the porous medium (Sohrabi et al., 2008a).

Sohrabi et al. (2008a) observed that the flowing oil (present as thick layers on the sides of the flowing gas) would repeatedly swell and shrink. This was indicative of the transport of the oil alongside the flowing gas. The flow of the bypassed oil was accompanied by the widening of the gas channel by advancement of the gas–oil menisci into the bypassed oil-filled pores (Figure 2-7). Figure 2-8 shows the distribution of the fluids within the same part of the micromodel as was shown in Figure 2-6. Comparison of Figure 2-8 and Figure 2-6 revealed that the saturation of the by-passed oil, behind the main gas front, kept reducing and eventually led to a complete recovery of all the contacted oil. Sohrabi et al., 2008a mentioned that although the efficiency of the gas injection has been affected by the presence of water, nevertheless, similarly to the primary gasflood, near-miscible gas injection has resulted in complete oil recovery of the contacted oil.

2.1.5. Water Alternating Gas (WAG) Injection: Water-Wet System

WAG injection started with a tertiary gas injection right after primary waterflooding. During the first-cycle gas injection, the invading gas first came in contact with water and formed some gas/water interfaces. The gas continued to advance by direct displacement of water (Sohrabi et al., 2004). Water layers between the moving gas and the stationary oil filament shrank by draining through the wetting layers. The water films finally ruptured, allowing the gas to directly contact the oil filament, which was in the middle of the pore surrounded by water (Figure 2-9).

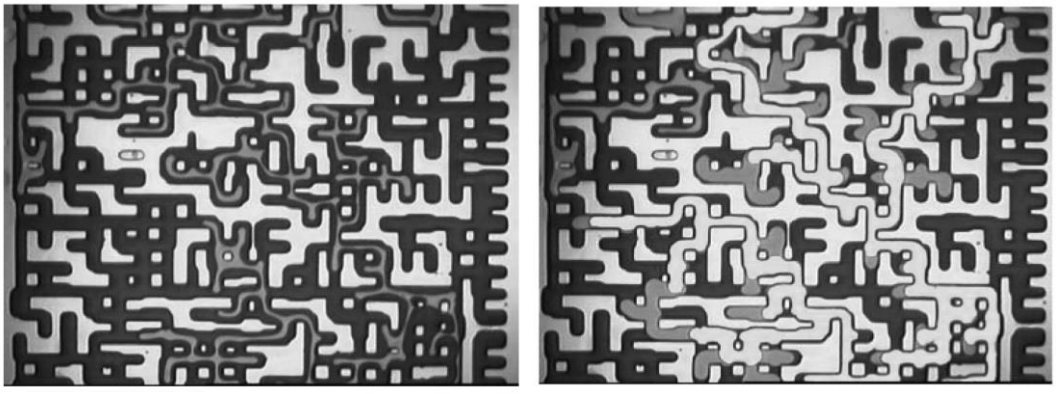

Figure 2-9: left: Water-wet micromodel after initial waterflood; right: water-wet micromodel after first gas injection (Sohrabi et al., 2004).

From this point on, the advancement of the gas front in the micromodel is either by direct displacement of water or by double displacements in which gas displaces the oil, which in turn displaces the water. As the residual oil (remained after the initial waterflood) is rather continuous (in the form of narrow oil filaments in the middle of some pores), the gas preferentially invades oil-containing pores (Sohrabi et al., 2004). At the end of the first-cycle gas injection, water injection commenced. During this water injection, water films around the thick oil blobs (which formed during the preceding gas injection) began to thicken and soon appeared as thick layers. As these water layers grew in thickness, the oil was forced into the gas channels (pores occupied by the continuous gas phase). Some of this oil would be recovered by two processes: (1) flow through the layers of oil that were connected all the way to the outlet, and (2) double displacement. Finally, when the water layers became thick enough, the continuous gas path became fragmented and disconnected, and no more oil and/or gas production was observed (water was being injected, and only water was being produced by the film flow). In addition to some oil production, this alternating injection of gas and water brought about some favourable redistribution of the fluids within the porous medium. Sohrabi et al. (2004) observed that due to this fluid redistribution, when gas was injected in subsequent WAG cycles, it did not follow the same path as the previous gas did. The result was that during the second-cycle gas injection, new pores were invaded, which effectively means improved recovery efficiency for gas injection. The redistribution of fluids was also observed during further WAG cycles, but the additional recovery of oil after the second cycle was not significant.

2.1.6 Water Alternating Gas (WAG) Injection: Oil-Wet System

In oil-wet system (as opposed to the water-wet case) oil is the wetting phase, water is the non-wetting phase, and gas is the intermediate phase. Considering that the gas/oil IFT is less than the water/oil IFT; therefore, gas, not water, is here the intermediate phase, and the system is a non-spreading system (i.e., none of the liquids spreads over the other). Sohrabi et al. (2004) discussed that due to the of lack of spreading water and/or gas layers, the only phase which is hydraulically connected all the way between the inlet and the outlet is the oil, and both water and gas have formed disconnected clusters. This is in contrast with the water-wet case, in which the water was hydraulically connected through the wetting films and the oil through the spreading films.

During the first gas-injection period, the gas was observed to preferentially enter oil-filled pore throats because of gas/oil IFT being less than that of gas/water IFT. In some pore throats, which were occupied by water, the water would completely block the progress of the gas front. In these cases, the gas pressure would rise, and eventually the blocked pore would momentarily open, letting some gas escape toward the next oil-filled pore, and the pore throat would close again by water. This mechanism will be repeated and so on. Sohrabi et al. (2004) observed that double displacements rarely happen in oil-wet system (as opposed to water-wet case). These effects make circumstances in favour of gas invading oil-filled pores, thereby resulting in higher oil recovery compared with that of water-wet model experiments.

As the main structure of the water phase was not much disturbed during the previous gas injection (because gas had invaded mainly oil-filled pores), water had to do little to re-establish a continuous path from the inlet toward the outlet of the model. Some gas snap-off was observed during this water injection stage, which was caused by oil that was displaced by the water (Sohrabi et al., 2004).

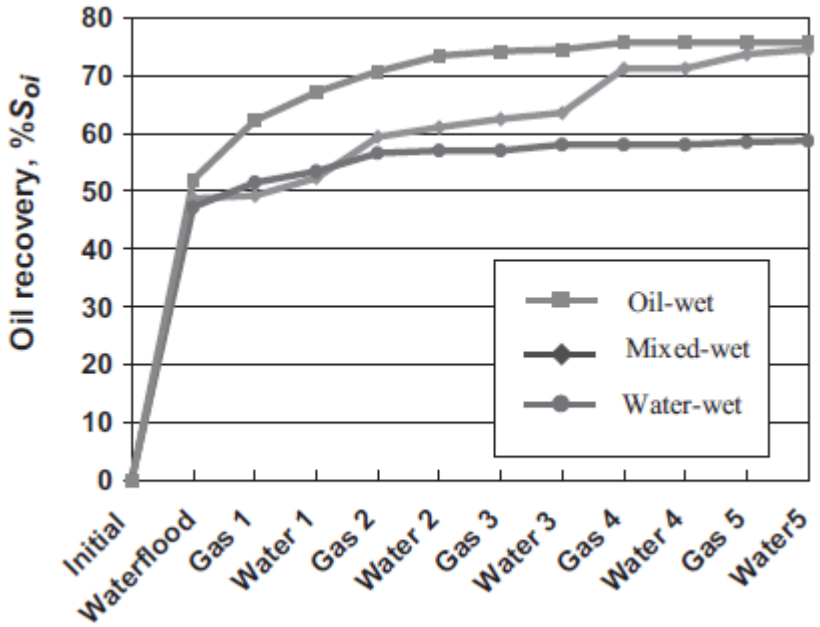

Figure 2-10: Oil recovery (as percentage of initial oil in place) for the five cycles of WAG injection in different micromodel wettabilities (Sohrabi et al., 2004).

Figure 2-10 compares oil recovery during WAG injection experiments at different wettability conditions (Sohrabi et al., 2004). For the water-wet model experiment, the initial waterflood recovered approximately 47% of the initial oil in place (IOIP). Five

cycles of WAG injection recovered an additional 11% of IOIP. The extra oil recovered after two cycles of WAG injection was only approximately 1% of initial oil in place. This shows that the majority of the benefit of WAG injection in the water-wet model has come after the first two cycles. Figure 2-10 also shows that oil recovery for the oil-wet model experiment is the highest. The initial waterflood produced 52% of the IOIP, and the subsequent WAG injection recovered an additional 23% of IOIP. Same as water-wet experiment, very little oil was recovered after the second WAG cycle. In the mixed-wet model experiment, the initial waterflood produced 50% of the IOIP, and the subsequent WAG injection recovered an additional 28% of IOIP. The flow mechanisms observed during mixed-wet model experiments were combination of the processes observed in water-wet and oil-wet model tests. An odd feature of the mixed-wet experiments (compared to water-wet and oil-wet model experiments) was that oil recovery was not limited to the first two or three cycles (Sohrabi et al., 2004).

2.1.7 Simultaneous Water and Gas (SWAG) Injection: Water-Wet System

First a primary waterflooding performed until no more oil production or changes in fluids distribution was observed. At the end of this waterflood, simultaneous injection of the near-miscible gas and water (SWAG) commenced with the 50% of the total injection rate being gas and the remaining 50% being water (Sohrabi et al., 2008b). Inside the porous pattern, no slug or bubble flow of water and gas was observed. Instead, water and gas were observed to flow separately with water creeping in the porous medium from the sides of the pores (layer flow) and gas moving in the middle of the pores (piston wise).

As the SWAG injection continued, the gas–oil and water–oil interfaces approached each other and thereby invading the oil-occupied pores. However, the advancement of gas–oil interface has been much faster than the advancement of the water–oil interface (Figure 2-11 and Figure 2-12). As SWAG injection continued more of the contacted by-passed oil was recovered and eventually all of the oil, which had been contacted by gas, was produced (Sohrabi et al., 2008b).

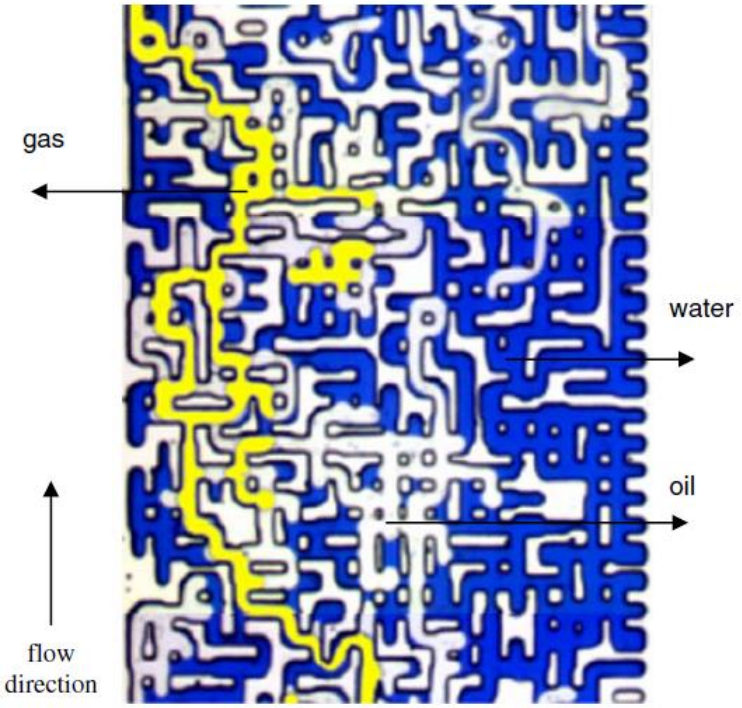

Figure 2-11: Fluid distribution within the water-wet micromodel during near-miscible SWAG injection with an injection gas fractional flow of 0.5 (Sohrabi et al., 2008b).

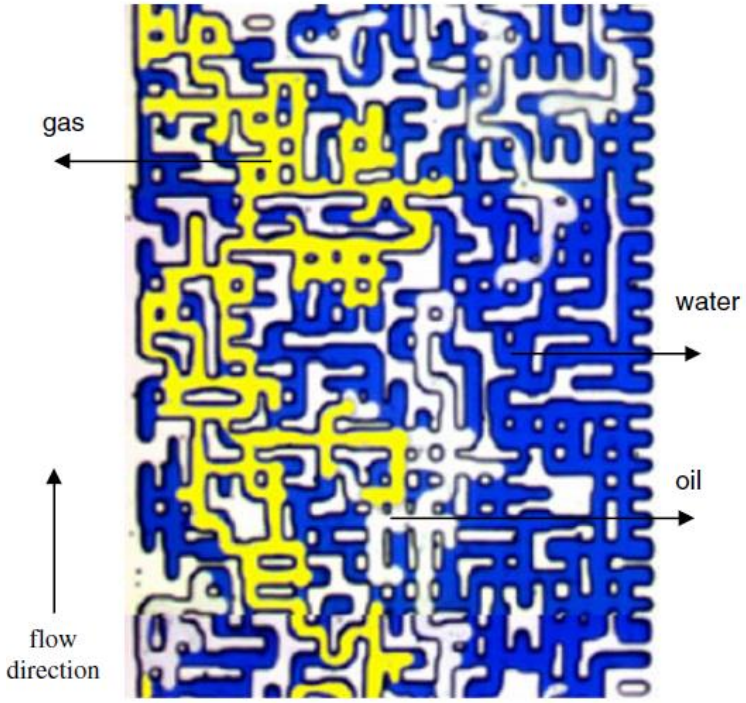

Figure 2-12: Fluid distribution within the water-wet micromodel after 1 h near-miscible SWAG injection with an injection gas fractional flow of 0.5. Almost all of the residual oil that had come in contact with the gas has been recovered (Sohrabi et al., 2008b).

2.2. References

Sohrabi M., (2001): Water Alternating Gas Injection (WAG) Studies, PhD Thesis submitted to Institute of Petroleum Engineering at Heriot-Watt University, Edinburgh, Scotland, UK.

Sohrabi M., Tehrani D.H., Danesh A., Henderson G.D., (2004): Visualization of Oil Recovery by Water-Alternating-Gas Injection Using High-Pressure Micromodels, SPE-89000, SPE Journal, Volume 9, Number 3, pp. 290-301.

Sohrabi M., Danesh A., Tehrani D.H. and Jamiolahmady M., (2008a): "Microscopic Mechanisms of Oil Recovery By Near-Miscible Gas Injection", Transport in Porous Media, Volume 72, Number 3, pp. 351-367.

Sohrabi M., Danesh A. and Jamiolahmady M., (2008b): "Visualisation of Residual Oil Recovery by Near-miscible Gas and SWAG Injection Using High-pressure Micromodels", Transport in Porous Media, Volume 74, Number 2, pp. 239-257.

Williams J.K. and Dawe R.A., (1988): Photographic Observation of Unusual flow Phenomena in Porous Media at Interfacial Tensions below 0.1 mN/m, Journal of Colloid and Interface Science, Volume 124, Number 2, pp. 691-696.

3. Rocks/Fluids, Facilities and Procedures

3.1 WAG Coreflood Rig:

Figure 3-1 show the schematic diagram of the high pressure coreflood rig used in this study. The main parts of the coreflood rig are as follow:

3.1.1 High Pressure High Temperature Oven

A temperature controlled air bath is used to house the injection fluids (storage cells), lines and sight-glass.

3.1.2 Storage Cells

Six 1000 cm^3 storage cells were set inside the oven. Two cells assigned to each phase. This way it was possible to pre-equilibrate the fluids as well as retract the fluids inside the oven (at test temperature and pressure).

3.1.3 Pressure Gauges

To evaluate and record different pressures before, during and after each coreflood, Quartzdyne gauges have been installed in the rig. These gauges made it possible to monitor pressure changes across the core, overburden pressure, as well as the pressure in each of the 6 storage cells. The accuracy of these Quartzdyne gauges is ±0.001 psi.

3.1.4 Sight-glass separator

While running the experiment, the effluent from core flows into the sight-glass separator where the water, oil and gas would be separated from each other based on their densities. Sight-glass made it possible to record the effluent production at the test temperature and pressure. Considering the large volume of the core samples used in the experiments, it was necessary to dynamically retract the fluids from sight-glass separator. The volume of this separator is around 95 cm^3. Volumes of the fluids have been recorded in each time step. A camera used to read the level of the phases interface (with the accuracy of ±0.05cm^3 for each recording point).

3.1.5 Pumps

DBR pumps were used to inject into or withdraw from the core (production from core was performed from sight-glass separator). Two DBR pumps were assigned for each fluid (gas, oil or water). Each pump was connected to the bottom of a storage cell inside the oven (e.g. gas-1, gas-2, oil-1 and etc). Gas and oil pumps (4 of the DBR pumps) have a travel distance around 1000 cm^3, while the brine pumps (the other two) have a travel distance of 500 cm^3. Assigning separate pumps for each storage cell, made it possible for us to use them for pre-equilibration purpose as well as injecting or retracting more than one phase (two or three phases) at the same time. The accuracy of the pumps was 0.1 $cm^3.hr^{-1}$. Pumps connections to the bottom of cells are labelled as P1, P2 and etc. in Figure 3-1.

3.1.6 Coreholder

To be able to perform x-ray scans of the core and to give enough space for the x-ray source and detector to travel along the core length, the x-ray compatible coreholder has been kept in a separate x-ray transparent temperature controlled frame. The connecting lines into/from this frame were covered by a thermal insulation cover to prevent temperature loss.

3.1.7 X-ray Facility

The coreflooding rig used for the experiments is equipped with an x-ray scanner, which allowed us to obtain accurate and repeatable scans of the core before, during, and after the experiments. The results of the x-ray scans are used to obtain distribution and saturation of different phases (water, oil, and gas) along the core. Core heterogeneities, distribution of irreducible water saturation, and front propagation can also be determined and monitored. X-ray results are also used to check for any experimental artefacts such as capillary end effects, which in this study was not an issue because long cores were used in the experiments.

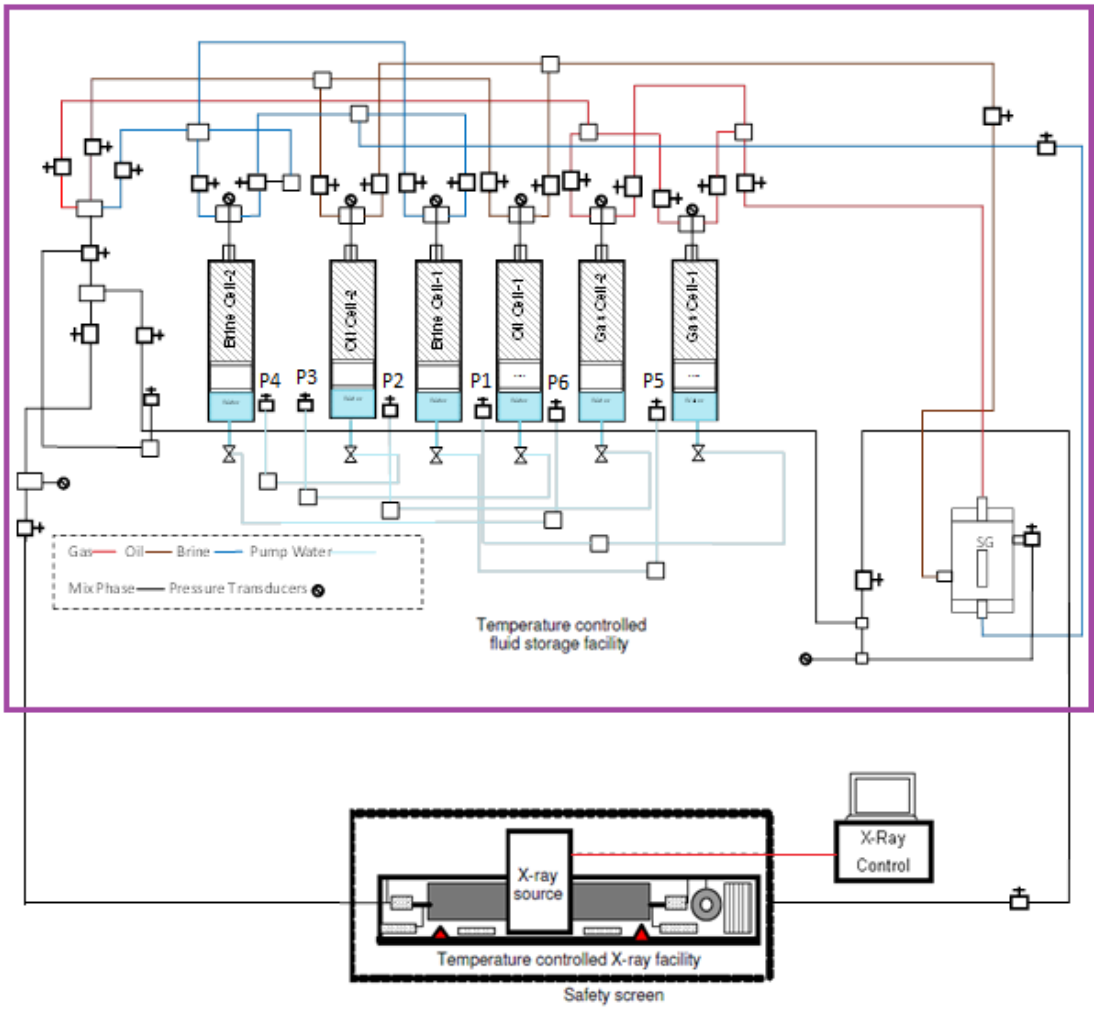

Figure 3-1: Schematic representation of coreflood facility including x-ray saturation monitoring system.

3.2 Core Samples and Fluids

3.2.1 Core Samples

Two different sandstone cores with one order of magnitude difference in absolute permeability were used in this study. Table 3-1 shows the physical properties of the cores. Before performing the coreflood experiments, a core-characterization procedure was followed to determine the suitability of the core for k_r experiments and also to determine its physical properties.

Table 3-1: Physical properties of core samples used in experiments.

Core	*Permeability (mD)*	*Length (cm)*	*Diameter (cm)*	*Porosity (frac.)*
C-1	1000	67.1	4.98	0.17
C-2	65	60.5	5.08	0.18

The core was first thoroughly cleaned by injecting large amounts of solvents (acetone and methanol) followed by nitrogen. The core was then placed in an oven to ensure that it was completely dried. The dry weight of the core was then measured as well as its dimensions. The core was also scanned to examine its homogeneity (by porosity profiling) before performing the coreflood tests. To obtain the porosity of the core along its length using x-ray, the following procedure was performed. First, the dried empty core was scanned. Then, it was made 100% saturated with brine and re-scanned. Using the scan results, the following equation, was used to determine the porosity for each volume element (the whole length of the core has been divided into 60 virtual segments to scan each part separately).

$$\Phi = (CT_{wr} - CT_{ar})/(CT_w - CT_a) \quad \text{(Eq. 3-1)}$$

The subscripts *w* and *a* represent water and air CT numbers, respectively, whereas *wr* and *ar* refer to water- and air saturated rock, respectively. For further details of the process of porosity calculation by x-ray, refer to Akin and Kovscek (2003). Figure 3-2 shows the profile of the porosity of the 65mD core sample obtained from x-ray analysis. As can be seen, apart from some normal fluctuations, the porosity value is relatively the same along the length of the core, which indicates that there are no major heterogeneities in the core. The average porosity of the core obtained from x-ray data was 18.3%, which was comparable with the average value obtained using brine and helium pore volume measurement techniques (18.2%).

Mineralogy analysis of the rock samples from these two Clashach sandstones shows they are homogenous and mostly formed from quartz with small traces of feldspar and very small evidence of pyrite. No clay was observed in the mineralogy analysis (Figure 3-4).

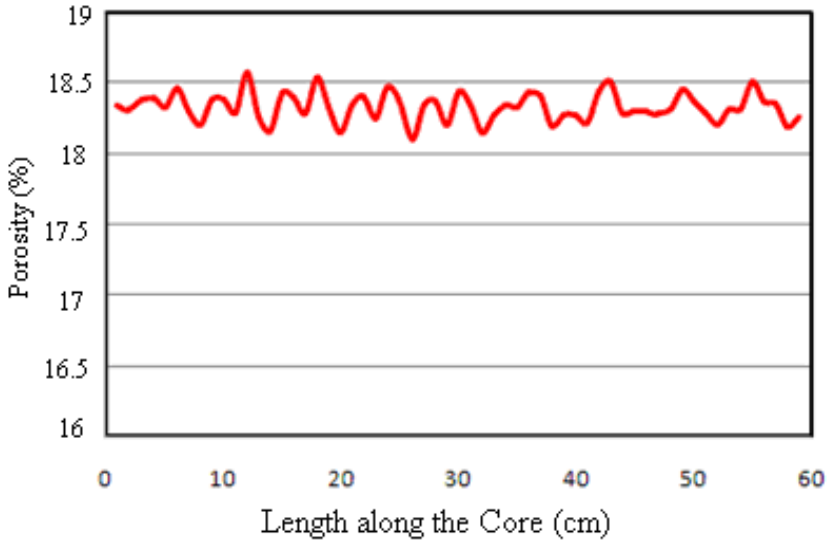

Figure 3-2: Porosity profile of 65mD core sample along the length (obtained from X-ray data analysis).

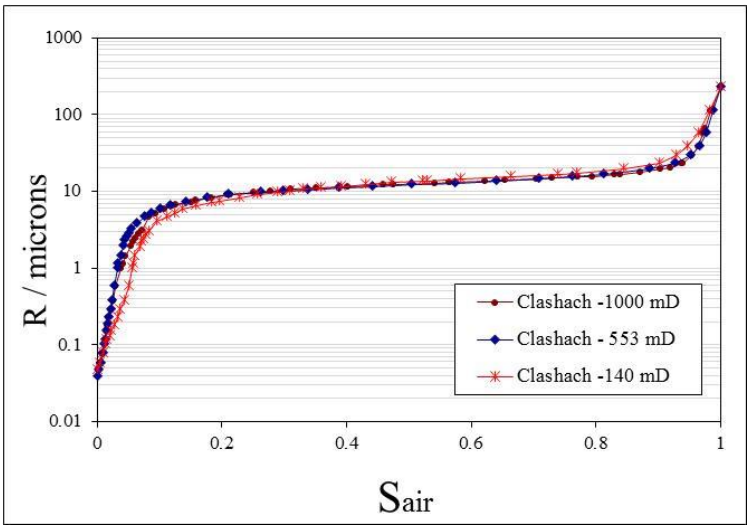

Figure 3-3: Pore size distribution of different Clashach samples, which shows very similar pore size distribution among these cores with different absolute permeability.

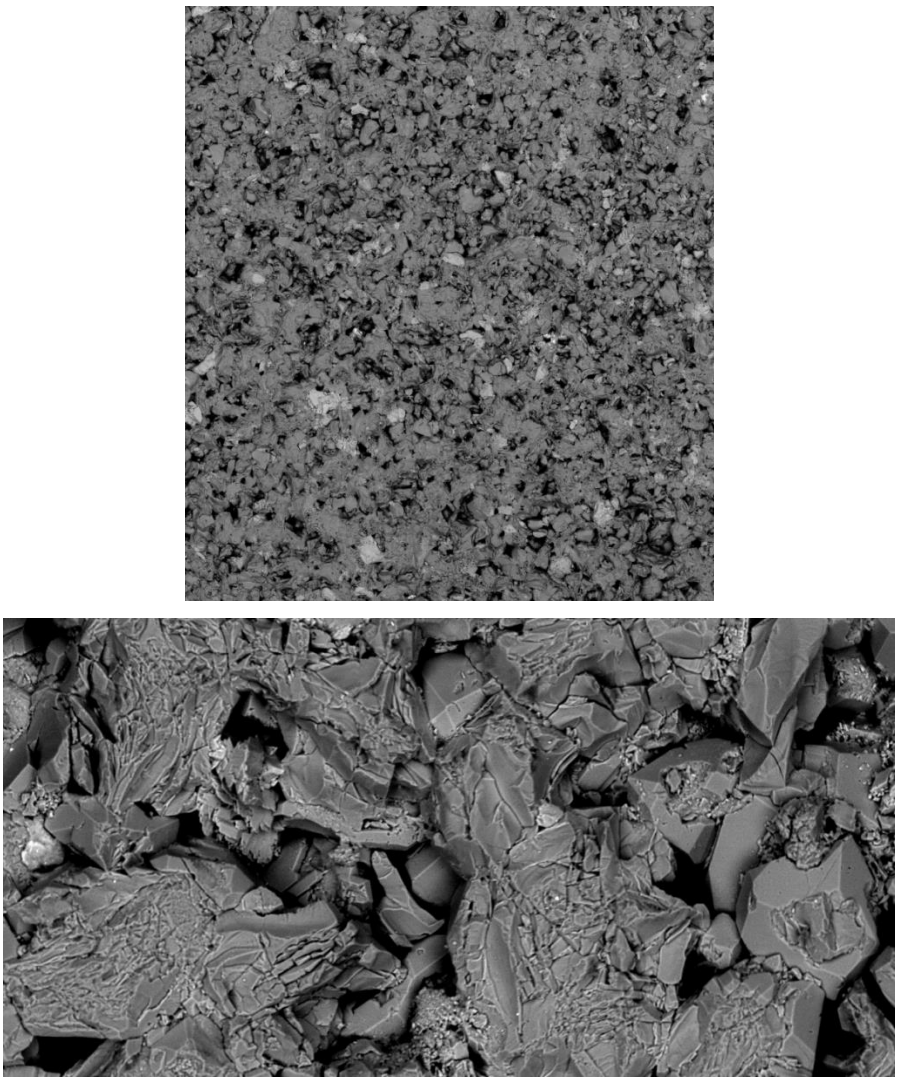

Figure 3-4: Fine images from Clashach sandstone rock samples; a) showing homogeneity of the rock in terms of grain and pore size distribution, horizontal scale = 15 mm; b) showing quartz crystals in the sample, horizontal scale is less than 1 mm.

3.2.2 Fluids (Gas, Oil and Brine)

The brine used in the experiments was a synthetic brine sample made of 16 g sodium chloride (NaCl) and 4 g calcium chloride ($CaCl_2$) in 2000 cm^3 of degassed distilled water (Table 3-2). It should be mentioned that the brine used in the tests did not represent any particular reservoir brine and was used with the main aim of reducing possibilities of adverse reactions between the core and water during waterflood experiments.

Table 3-2: Physical properties of synthetic brine

Salinity (mg/L)	Density @ 38°C (g/L)	Viscosity @ 38°C (cp)
1000	992.96	0.68

The hydrocarbon fluid system used in the experiments consisted of an equilibrium binary mixture of methane (C_1) and n-butane (n-C_4). Figure 3-5 shows the P-T phase diagram of the gas-oil mixture with the critical point of 1,870 psia (12893.1961 kPa) and 100°F (37.77°C) (red rectangle). As can be seen, the conditions of the pressure and temperature at which the experiments (purple triangle) have been conducted [1,840 psia (12686.3534 kPa) and 37.77°C] are very close to those of the critical point of the system, and hence, the gas and oil were nearly miscible (very low gas/oil IFT). The IFT between oil/gas under the test conditions was measured, which was equal to 0.04 $mN.m^{-1}$ (Table 3-3).

Table 3-3: Measured fluid properties for C1-nC4 binary mixture at 100°F and 1840 psia.

ρ_g ($kg.m^{-3}$)	ρ_L ($kg.m^{-3}$)	μ_g (mPa.s)	μ_L (mPa.s)	IFT ($mN.m^{-1}$)
211.4	317.4	0.0249	0.0405	0.04

The hydrocarbon mixture was made by mixing 73.6 mole% methane and 26.4 mole% n-butane at 2,250 psi (15 513.2038 kPa) and 100°F (37.77 °C). Then, the pressure of the mixture was reduced to the test pressure of 1840 psia (at the same temperature) and the oil and gas were separated and kept in isolated cells. In order to minimise mass transfer between fluids during the displacement experiments, the gas and oil were then mixed and pre-equilibrated with the synthesized brine at the conditions of the experiments (1840 psia and 100°F). Mixing of the fluids was repeated several times until the final volume change in successive mixings for each fluid was minimal and in the range of ±0.5 cm^3. For detailed compositional behaviour and physical properties of C_1/C_4 mixture, refer to Gozalpour et al. (2005). Figure 3-6 through Figure 3-10 show the variation of the oil/gas IFT, as well as their viscosities and densities for different pressures at test temperature (37.77°C ~= 38°C).

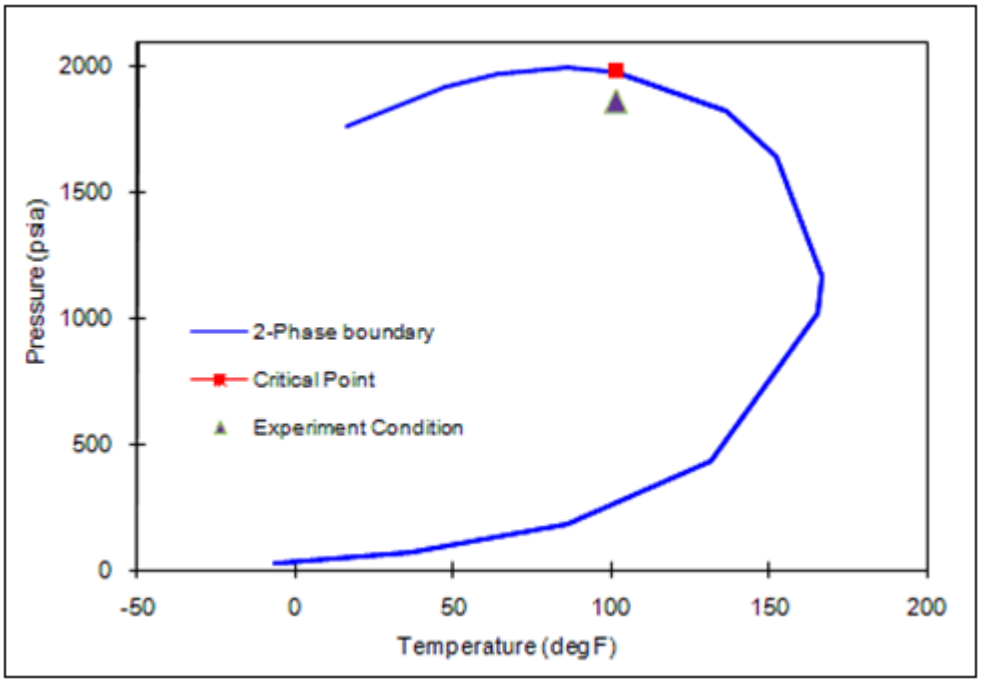

Figure 3-5: Pressure-Temperature phase diagram of C_1-nC_4 mixture used in the low IFT core flood tests.

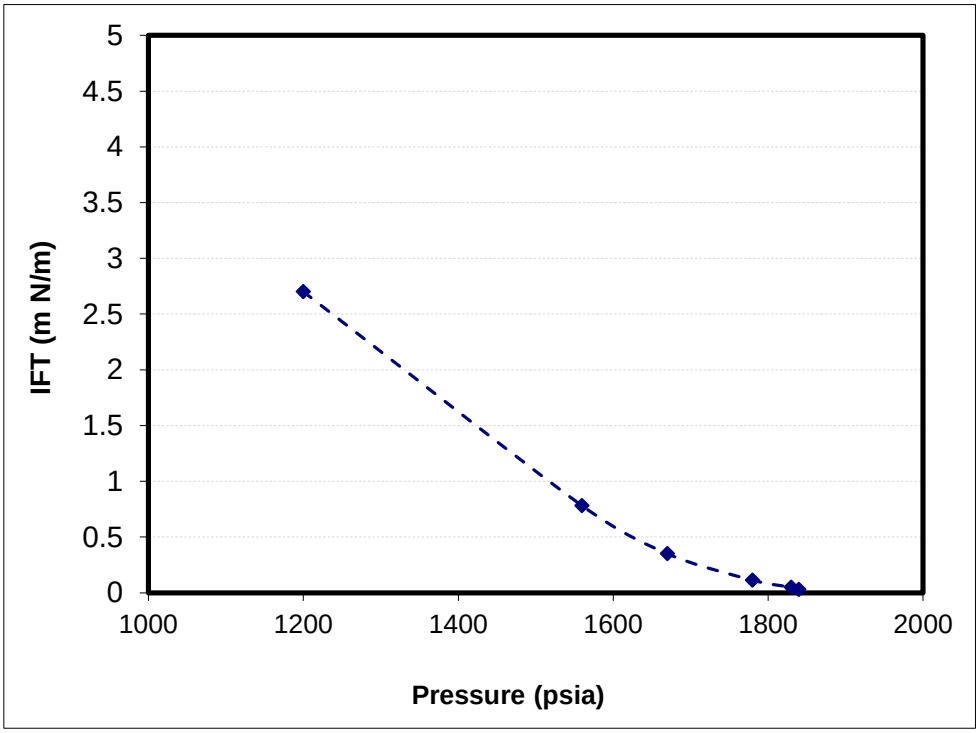

Figure 3-6: IFT between oil and gas phases used in the coreflood tests as a function of pressure at 37.77°C (~ 38°C).

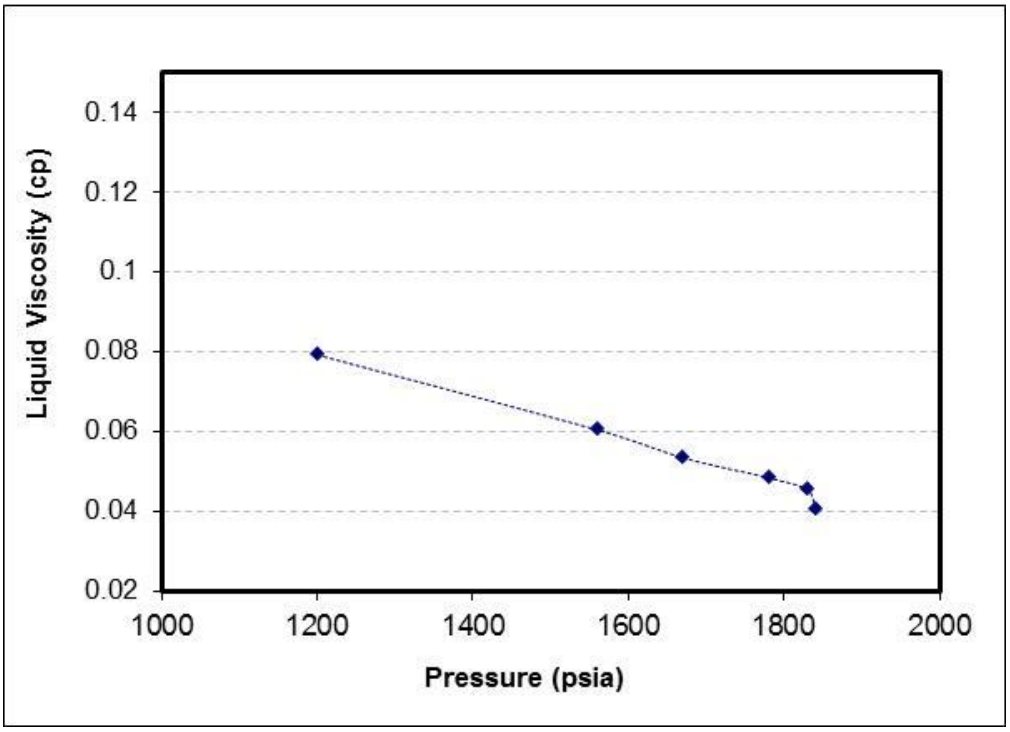

Figure 3-7: viscosity of the oil phase used in the coreflood tests as a function of pressure at 37.77°C (~ 38°C).

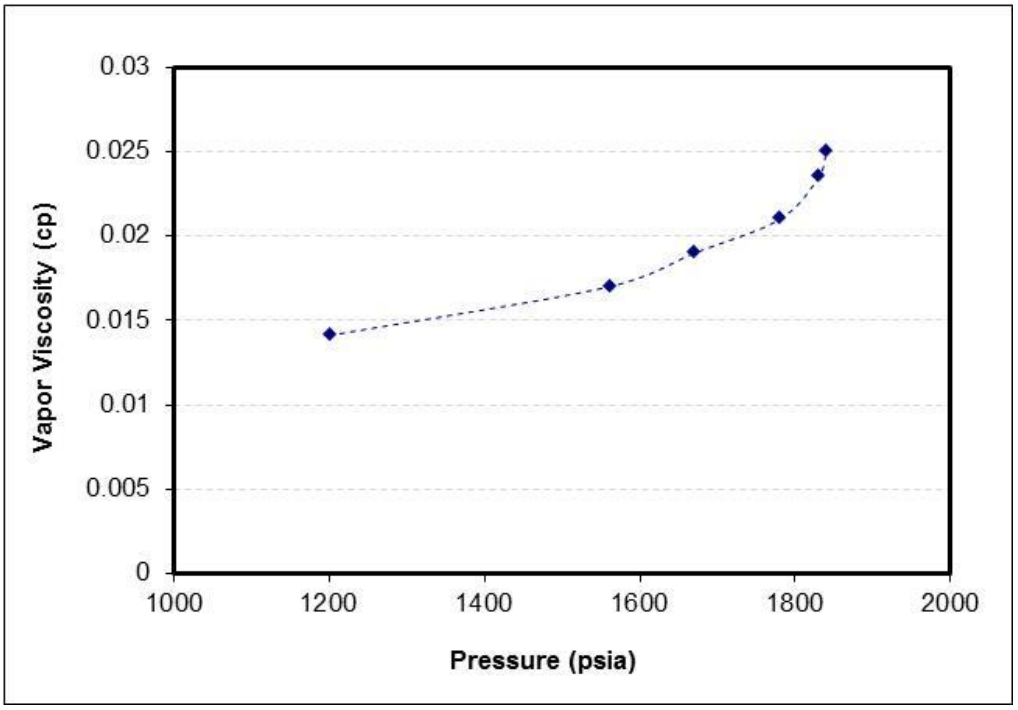

Figure 3-8: viscosity of the gas phase used in the coreflood tests as a function of pressure at 37.77°C (~ 38°C).

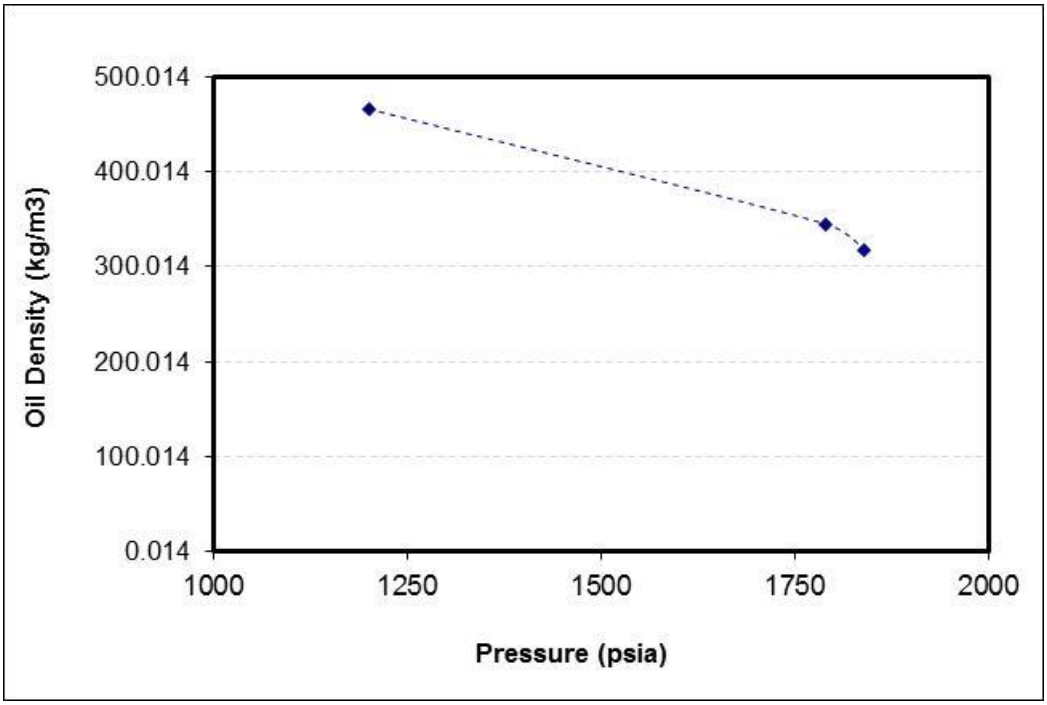

Figure 3-9: Density of the oil phase used in the coreflood tests as a function of pressure at 37.77°C (~ 38°C).

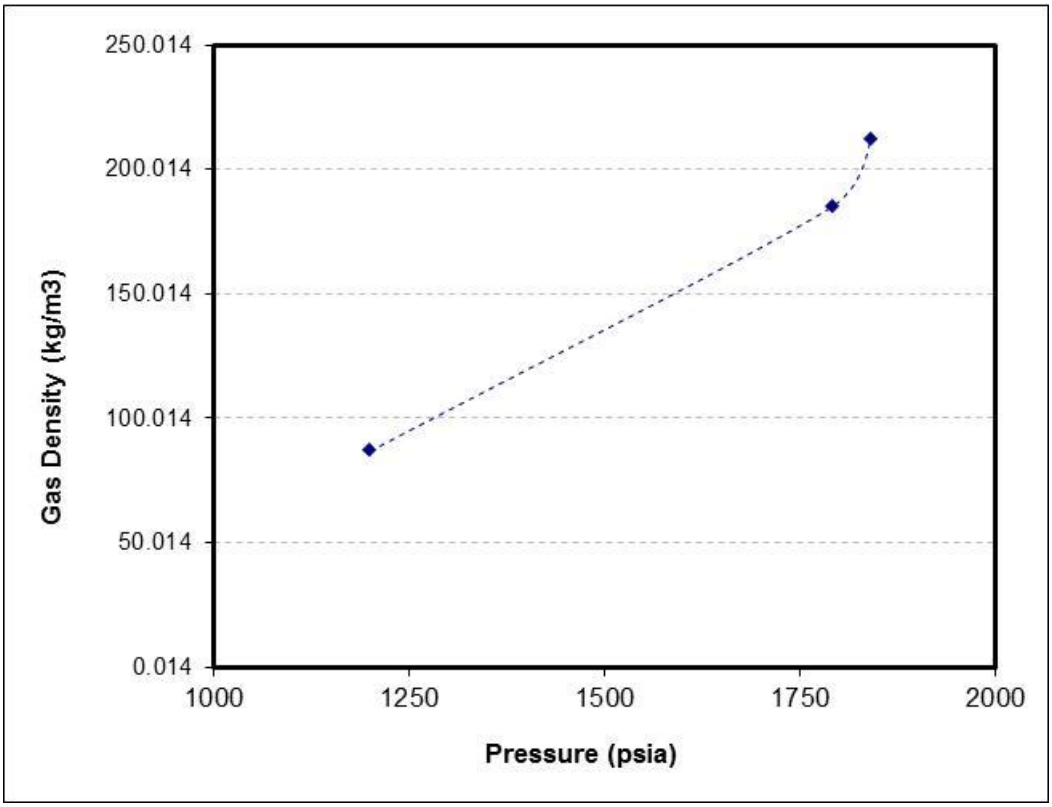

Figure 3-10: Density of the gas phase used in the coreflood tests as a function of pressure at 37.77°C (~ 38°C).

3.3 Core Preparation

3.3.1 Establishment of Immobile Water Saturation

The process of S_{wim} establishment in the laboratory is a lengthy one, because it involves a series of fluid injections and displacements. As the first step, the core was cleaned and dried, and then brine was injected into the core to make it 100% saturated with brine. Then, a mineral oil was used to push the bulk of the brine out of the core and to establish the initial (immobile) water saturation. The mineral oil was displaced using C_{10}, which in turn was removed from the core by injecting high-pressure C_1. The C_1 had been equilibrated and hydrated to ensure that there would be no further S_w reduction during these fluid displacements. Finally, the C_1 was replaced (at test temperature and high pressure) with equilibrated oil. This procedure resulted in establishing S_{wim}=18% as obtained by accurate material balance. Using the x-ray facility, the core was also scanned to investigate the uniformity of the irreducible water saturation profile in the core.

There are several different CT methods (Akin and Kovscek, 2003) for in-situ saturation determination in two-phase flow: (a) linear interpolation between pure states (b) fluid CT numbers, and (c) linear regression. In the current study, the linear interpolation technique has been used to interpret the scans. In this technique, it is assumed that the CT numbers of the core (saturated with two fluids) lie on the straight line connecting complete saturation by phase I (for instance, water) to complete saturation by phase II (for instance, oil). Thus, a single energy scan would be sufficient to measure two-phase saturations. The saturation of oil at each scan element can be obtained from the following equation:

$$S_o = (CT_{wr} - CT_{owr})/(CT_{wr} - CT_{or})\ ;\ S_w = 1 - S_o \qquad \text{(Eq. 3-2)}$$

in which *wr* refers to the CT number for the core 100% saturated with water, *owr* refers to the state of the core in which both oil and water exist at the same time (two-phase), and *or* is the CT number for the case in which the core is 100% saturated with the oil. Considering the large difference between densities of the oil and water phases in the presented experiments and the resolution of the X-ray device, there was a significant difference between CT_{wr} and CT_{or}, which resulted in accurate determination of the oil and water in place saturations. This is also true for gas and water phases and the above formula is also used for measuring gas and water saturations (see Chapter 8).

Figure 3-13 shows immobile water saturation profile along the 65mD core for both water-wet and mixed-wet samples. As can be clearly seen from this figure, for both wettability conditions the established immobile water saturation is homogenous along the core, and the local value is very close to the average value obtained from material balance (18%). Another important feature is that the value and distribution of the immobile water saturation is very close for both wettability conditions studied in this work (as will be discussed later). During the water establishment process in water-wet system, water phase resides mostly in the very small pores of the rock. Nevertheless considering the water-wetness of the rock, there is a high possibility that water remains continuous (but in very thin layers). For the mixed-wet system under study here (considering the followed procedure as will be discussed in next section), very small pores would remain water saturated (and of course water-wet), but the injection of the crude oil and aging at higher temperatures makes larger pores (or at least parts of them) hydrophobic (less or even non water-wet) and as a result oil components would attach the grains surfaces in these pores and pushing water phase out towards medium to smaller pores. This water would either thicken the water wetting layers in water-wet pores or possibly trapped inside the oil wetting layers (since there was no water production out of the core during the crude oil injection, aging (section 3.3.2) and cleaning (section 3.3.4)). Considering the homogeneity of the rock sample, the established S_{wim} for water-wet and mixed-wet systems will be closed (Figure 3-13) which is crucial for the objective of this study regarding the effect of wettability. This makes it possible for to directly compare the experimental results from the water-wet sample with those of the mixed-wet sample because they are not affected by saturation history, the initial water saturation value, or its distribution along the core.

3.3.2 Core Wettability Alteration Procedure

To be able to have a sound comparison between the results of the experiment carried out on the water-wet core with those obtained for the same core after changing its wettability to mixed-wet, it is important to have the same initial water saturation S_{wim} in both cores. Therefore, immobile water saturation was first established in the core by injecting a mineral oil, which was then displaced with a suitable crude oil. The injection of the crude oil into the core continued until no further mineral oil recovery was taking place. At this point, the rate of injection decreased to 1-2 $cm^3.hr^{-1}$ and the oven temperature was raised to 140–176 °F (60–80 °C) and the core was allowed to age for 3 weeks. During the aging period, crude oil injection continued at a very slow rate. In

order to achieve a uniform oil distribution long the length of the core, the direction of oil injection was changed halfway through the ageing period. . This process is expected to make the core mixed-wet. In general, mixed-wet systems are divided into three different wettability types (Skauge and Ottesen, 2002), known as: MWS type (with smaller pores to be oil-wet or non-water wet), MWL (with large pores to be non-water wet) and finally FW in which a fraction of the pores is water-wet and the rest is non-water wet. For FW definition different wettability conditions can occur in the pores with different pore sizes and even a type in which a pore might be partly water-wet and partly non-water wet. As would be discussed in Chapter 8, the results show that the mixed-wet system under investigation here is most likely to be fractionally wet, whereby parts of the core remain water-wet (where immobile water protects the surfaces of the rock from coming in contact with the crude oil during the aging process) and parts of the core would be made oil-wet (Salathiel, 1973). For further discussion of wettability alteration by crude oils and the mechanisms involved in this process, see Buckley et al. (1998).

Figure 3-14 and Figure 3-15 show scanning electron microscope (SEM) pictures for thin sections of water-wet and mixed-wet samples, respectively. For water-wet system, water droplets were not formed on the grains of the untreated core thin section and grain surfaces are covered by a layer of water phase, which indicates that the sand grains were strongly water-wet. For the case of mixed-wet system, rock grains in a thin section showed signs of wettability alteration from water-wet toward oil-wet because water on the grain surfaces formed droplets rather than films. It should be mentioned that for the case of the mixed-wet system, the contact angle of the water droplet on the grains is different from one point to another, which shows that different wettability conditions have been developed even in a pore.

3.3.3 USBM Wettability Index Test

Using Semi-Dynamic capillary measurement technique (Lenormand et al., 1993), USBM wettability index of the water-wet sample measured to be 0.45 with the Amott-Harvey index of 0.79 which showed water-wet nature of the rock. USBM index of the mixed-wet sample was determined by measuring the capillary pressure curves, using the centrifuge technique. Mixed-wet core plug had a USBM index of - 0.02, which shows that the core wettability was mixed-wet with an average neutral wettability.

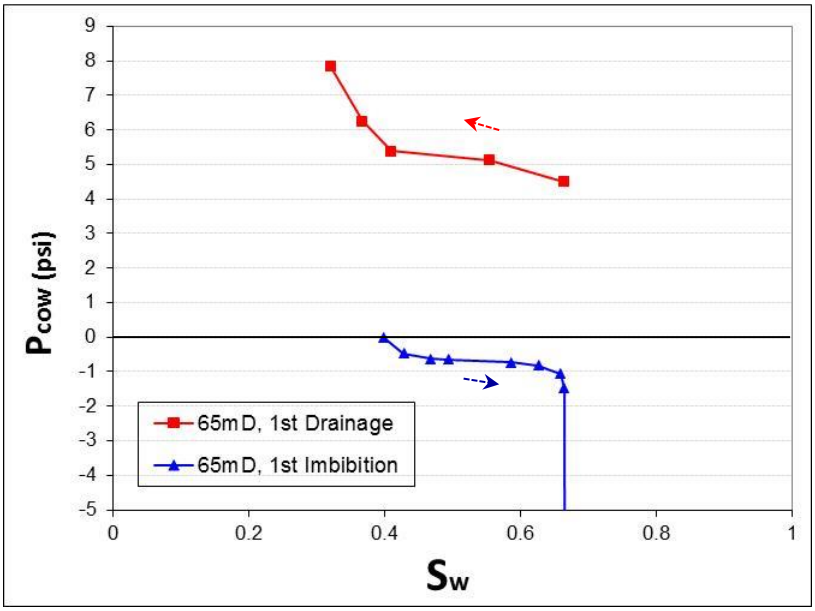

Figure 3-11: Two-phase oil/water capillary pressure of 65mD water-wet rock versus water saturation for primary drainage and 1st imbibition processes calculated by J-function from P_{cow} of 900 mD water-wet clashach core (obtained using SDM approach).

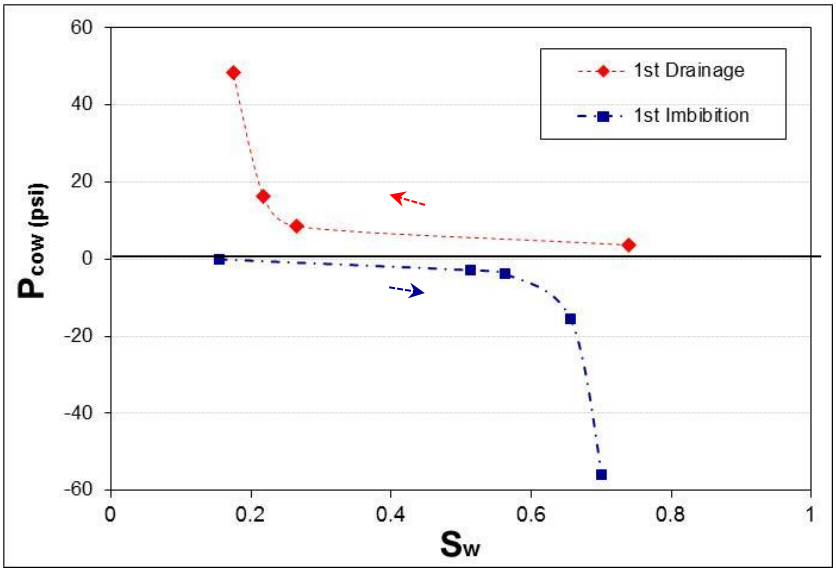

Figure 3-12: Two-phase oil/water capillary pressure of 65mD mixed-wet rock versus water saturation for primary drainage and 1st imbibition processes calculated by J-function from P_{cow} of 1000 mD mixed-wet clashach core (obtained using centrifuge approach).

3.3.4 Cleaning the Core after Wettability Alteration

After the aging period, the core went through another period of cleaning to make sure that the aging crude had been displaced from the core and would not contaminate the test fluids. This is a delicate task because the crude oil has to be displaced without aggressive cleaning of the core, which would result in total removal of the adsorbed organic material (which caused wettability alteration) and hence rendering ineffective the wettability alteration process. In this study, crude oil was displaced with decane.

Decane injection at high pressure continued until the core effluent looked clear (with no evidence of crude oil). Decane was then removed by high-pressure methane injection, which itself was displaced with equilibrated oil. The porosity profile of the core along its length and its immobile water saturation were determined the same as has already been discussed for the water-wet sample (which for the two wettability conditions were in good agreement). The core effective permeability to oil (in presence of immobile water) was also measured to make sure that the process of wettability alteration had not affected the connectivity of the pores in the rock. The calculated effective permeability for the mixed-wet core was almost same as that obtained for the water-wet core.

3.3.5 Three-phase Saturation Measurement using X-ray

Using the x-ray facility, the core was also scanned during three-phase flow studies (WAG and SWAG injections) to investigate the propagations of the fronts as well as in-situ saturation monitoring. The x-ray data are also used to check for any experimental artefacts such as capillary end effect. There are several different CT methods (Akin and Kovscek, 2003) for in-situ saturation determination in three-phase flow: (a) linear regression, (b) dual energy scan. In the current study, the linear regression technique has been used to interpret the x-ray scans.

In this method, a two-phase flood is conducted until irreducible water saturation, S_{wirr} , is achieved and a scan, CT_{oirr}, is taken at this saturation. Then, three-phase flow is initiated and the water and oil saturations are obtained using Equations 3-3 and 3-4, assuming that the saturations are linearly related to CT numbers. The remaining saturation can be obtained by material balance. This method was used by Siddiqui et al. (1996) to obtain three-phase saturations of water, benzyl alcohol and decane.

$$S_w = S_{wirr} + ((CT - CT_{oirr})/(CT_{wr} - CT_{oirr}))(1 - S_{wirr}) \quad \text{(Eq. 3-3)}$$

$$S_o = ((CT_{wr} - CT)/(CT_{wr} - CT_{oirr}))(1 - S_{wirr}) \quad \text{(Eq. 3-4)}$$

As an example Figure 3-16 shows calculated saturations along the length of the core during first two cycles of the WAG injection (started with waterflooding) performed in the 65 mD mixed-wet sample at 1840 psia.

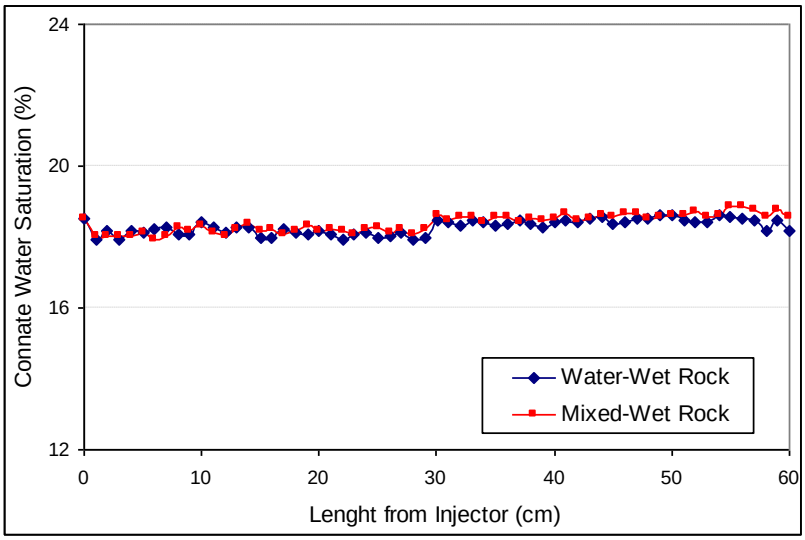

Figure 3-13: Immobile water saturation profile along the core sample (65mD) for both water-wet and mixed-wet conditions.

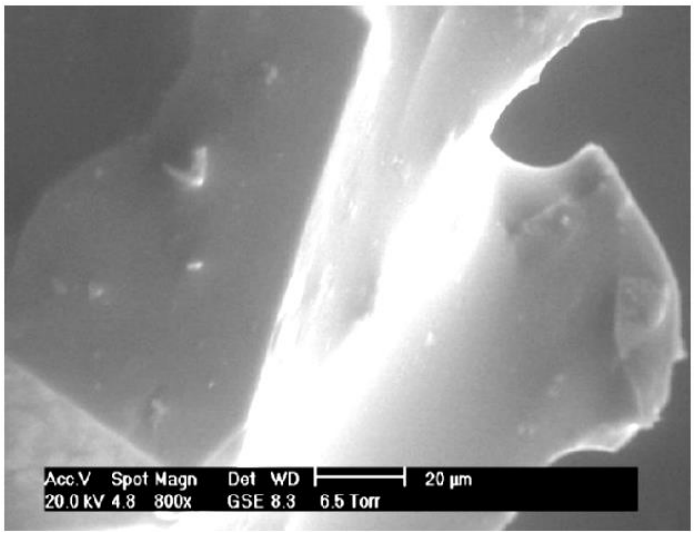

Figure 3-14: scanning electron microscope (SEM) pictures for thin sections of water-wet sample, showing water droplets spreads on the surface of the grains.

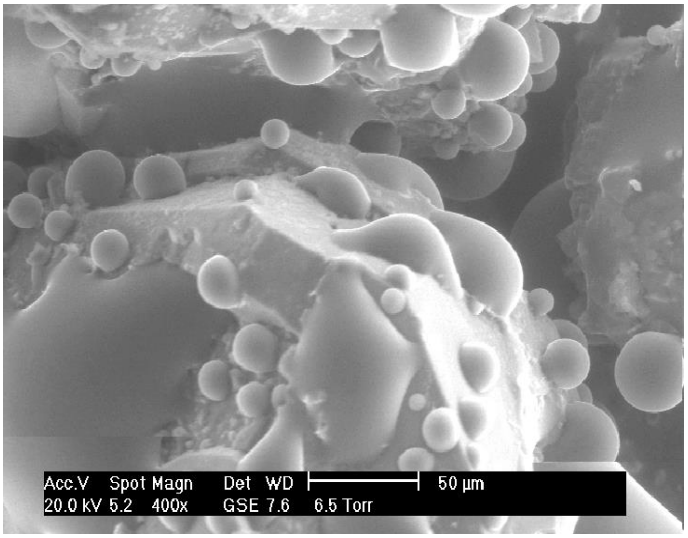

Figure 3-15: scanning electron microscope (SEM) pictures for thin sections of mixed-wet sample, showing water droplets makes various range of contact angles on the surface of grains.

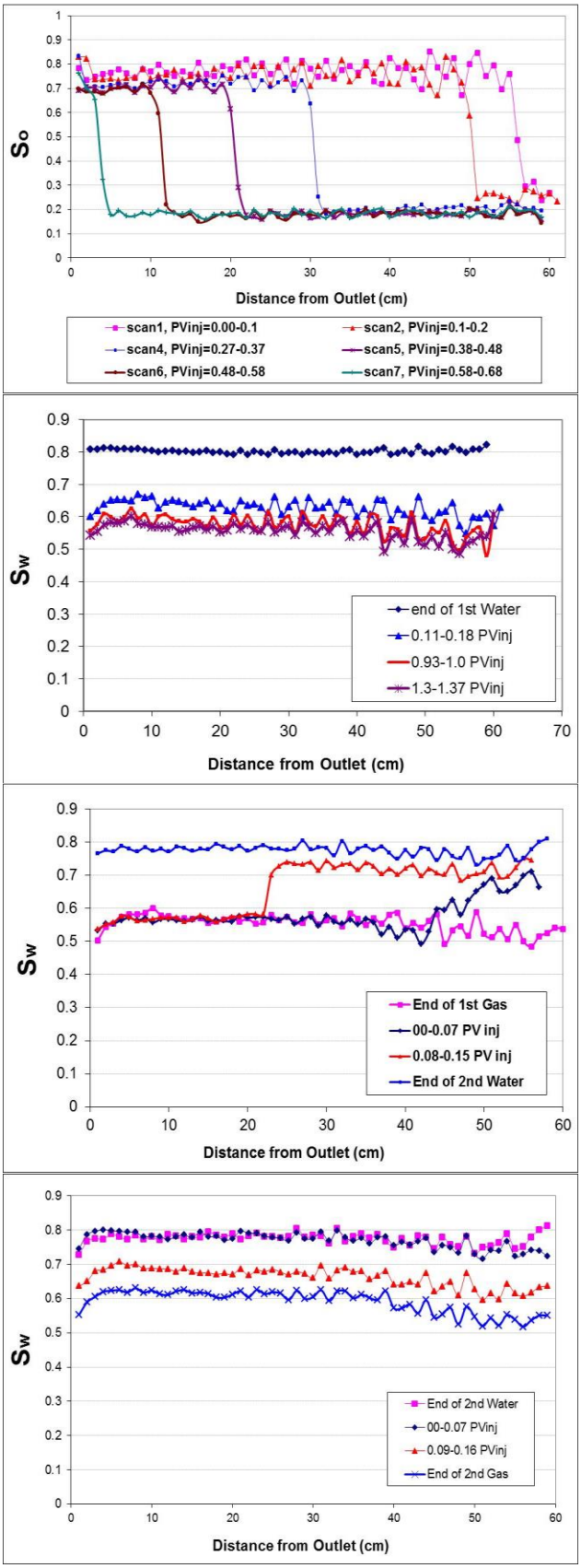

Figure 3-16: Distribution of saturations along the length of the core at different stages of the WAG injection started with primary waterflooding; from top to bottom a) local oil saturation during primary waterflooding, b) local water saturation during 1st gas injection, c) local water saturations during 2nd water injection and d) local water saturations during 2nd gas injection (65 mD, mixed-wet, 1840 psia)

3.4 References

Akin, S. and Kovscek, A.R. (2003): Computed tomography in petroleum engineering research. In Applications of Computerized X-ray Tomography in Geology and Related Domains, ed. P. Jacobs, F. Mees, R. Swennen, and M. Van Geet, No. 215, 23–38. London: Geological Society.

Buckley, J.S., Liu, Y., and Monsterleet, S. (1998): Mechanisms of Wetting Alteration by Crude Oils. SPE J. Volume 3, Issue 1, pp. 54–61.

Gozalpour, F., Danesh, A., Todd, A.C. et al. (2005): Viscosity, density, interfacial tension and compositional data for near critical mixtures of methane + butane and methane + decane systems at 310.95 K, Fluid Phase Equilibria, Volume 233, Issue 2, pp. 144–150.

Lenormand, R., A. Eisenzimmer, and C. Zarcone (1993): "A Novel Method for the Determination of Water/Oil Capillary Pressures of Mixed Wettability Samples." SCA 9322 presented during the International Symposium of the Society of Core Analysts, Houston, TX (Aug. 9-11).

Salathiel, R.A., (1973): Oil Recovery by Surface Film Drainage in Mixed-Wettability Rocks, Journal of Petroleum Technology, Volume 25, Number 10, pp. 1216-1224.

Siddiqui S., Hicks P.J. and Grader A.S. (1996): Verification of Buckley-Leverett three-phase theory using computerized tomography. Journal of Petroleum Science and Engineering, Volume 15, pp. 1-21.

Skauge A. and Ottesen B.; (2002): A summary of experimentally derived relative permeability and residual saturation on North Sea reservoir cores, SCA2002-12, proceedings of the international symposium of the society of core analysts, 22–25 September, Monterey, California, USA.

4. Effect of Different Parameters on Fluid Flow in Two-Phase Gas-Oil System

Near-miscible gas injection represents a number of processes of great importance to reservoir engineers including hydrocarbon gas injection and CO_2 flood. Very little experimental data is available in the literature on displacements involving very low-IFT (interfacial tension). This chapter presents the results of a series of two-phase and three-phase (in the presence of immobile water saturation) gas injection (drainage) and oil injection (imbibition) coreflood experiments for an gas/oil system at near-miscible (IFT= 0.04 $mN.m^{-1}$) conditions. Two different cores; a high-permeability (1000 mD) and a lower permeability (65 mD) core were used in the experiments and both water-wet and mixed-wet conditions were examined.

The results show that despite a very low gas-oil IFT, there is a significant hysteresis between the imbibition and drainage oil and gas relative permeabilities (k_r) curves in the 65mD core. Hysteresis was less for 1000mD core (compared to the 65 mD core) but it still could not be ignored. Near-miscible k_r hysteresis was significant for both water-wet and mixed-wet systems. Presence of immobile water in the water-wet cores improved oil relative permeabilities but reduced gas relative permeabilities in both imbibition and drainage directions. As a result, oil recovery for gas injection experiments improved when the rock contained immobile water. Both oil and gas relative permeabilities reduced when the rock wettability was altered to mixed-wet from water-wet and as a result, oil recovery by gas injection in the mixed-wet rock was less than that obtained under water-wet conditions. Explanations are offered for these observations based on the understanding of the pore-scale interactions and mechanisms, the distribution of fluid phases and their spreading bahaviour.

The results help to better understand the impact of some of the important parameters pertinent to k_r and its hysteresis especially in very low IFT gas-oil systems and mixed-wet rocks. Understanding these effects and behavior is important for improved prediction of the performance of different gas injection scenarios including water-alternating gas (WAG) injection in oil reservoirs.

4.1. Introduction

Proper core preparation for special core analysis (SCAL) can be difficult and time consuming. Among different core preparation procedures, establishing immobile water saturation and restoring wettability of reservoir rocks are especially difficult. As a result, usually SCAL analyses are performed on cleaned core samples which are water-wet and/or without establishing immobile water saturation. However, it is generally accepted that many oil reservoirs are mixed-wet (Jerauld and Rathmell, 1997; Salathiel, 1973; Delshad *et al.* 2003). According to Salathiel and Delshad *et al.* in a mixed-wet system, the oil-wet pores correspond to the largest pores in the rock, and the small pores are water-wet. To investigate the effect of wettability imbibition and drainage displacement tests are performed under water-wet as well as mixed-wet conditions.

Another important parameter is IFT (interfacial tension) and its effects on relative permeability. It is known that at conditions away from the critical point of the system where IFT is high (base IFT), multiphase relative permeability functions may be considered constant, i.e., independent of flow rate and IFT. These constant functions are commonly referred to as immiscible relative permeability functions. At the other extreme (IFT=0), relative permeability curves reduce to linear functions of the fluid saturation. These straight lines are referred to as miscible relative permeability functions. In this work, the focus is "near-miscible" relative permeabilities which would lie in the region between these two limits. The aim of the present chapter is to highlight the impact of some of the pertinent parameters of reservoirs which should not be ignored during SCAL analysis and reservoirs simulations. These are; immobile water saturation, saturation history, pore size distribution (permeability) and wettability. In this section, first near-miscible displacement is defined and then the highlights of the literature on the effect of IFT on the shape of relative permeability curves and their hysteresis behaviour are reviewed. Also effects of immobile water saturation and wettability on the performance of gas injection are reviewed.

4.1.1 Near-Miscible Gas Injection

Under near-miscible conditions, injected gas does not develop complete miscibility with the oil but come close. Examples of gas injections at these conditions are condensing/vaporizing gas-drives, gasfloods at enrichments slightly below minimum miscibility enrichment (MME) or at pressures slightly below minimum miscibility pressure (MMP), (Shyeh-Yung and Stadler, 1995). Near-critical conditions also occur in

volatile oil or gas condensate systems near their bubble or dew point pressures. Many laboratory and some field implementations have indicated that near-miscible and miscible gas injection performs in a comparable manner. However the general performance can be influenced by a number of physical properties. Thomas et al. (1994) stated that for samples which exhibit predominantly very small pore throats and have a very small standard deviation, IFT optimization (approaching miscibility condition) will be more important. He concluded that low IFT is a necessary condition for efficient recovery from most reservoirs, but in many cases zero IFT is unnecessary unless the pore size distribution is extremely tight and the rock is oil-wet. Shyeh-Yung and Stadler (1995); Wylie and Mohanty (1997) demonstrated that oil recovery efficiency does not decrease substantially with lower enrichment as long as the solvent (hydrocarbon gas) is at multiple contact miscible (MCM) condition.

Near-miscible gas drives appear more attractive compared to miscible ones, from both economic and operational standpoints (Burger et al. 1994; Thomas et al. 1994; Pande 1992). A leaner injectant (lower LPG or NGL enrichment in dry gas) is less expensive than a richer injectant. A lower-pressure process also reduces costs because the injectant density is lower and costs of compression are reduced at near-miscibility (Sohrabi et al., 2008a).

For a reliable reservoir performance prediction using numerical simulations, accurate relative permeabilities are needed. Considering the differences in flow mechanisms for near-miscible systems compared to high IFT systems as proposed by Sohrabi et al. (2008a, 2008b), it is important to investigate the effects of key parameters such as wettability, hysteresis and immobile water saturation on gas-oil relative permeabilities under near-miscible conditions and understand the possible differences with immiscible and miscible systems.

4.1.2 IFT Effects on Recovery Mechanisms

Hartman and Cullick (1994) noted that a typical high IFT (10-30 $mN.m^{-1}$) gas displacement behaves differently compared to a low IFT (< 2 $mN.m^{-1}$) near-critical fluid system displacement. They showed that at low IFT, slugs of both phases can flow in the same poreways, with the wetting phase being continuous and the non-wetting phase being discontinuous. The presence and simultaneous flow of gas and oil in the same pore has been shown (Williams and Dawe 1988; Jamiolahmady 2000) to be a very

effective recovery mechanism for very low IFT (nearly miscible) systems. As a result of this mechanism, oil recovery from the by-passed oil can take place behind the main gas front which results in almost complete recovery of the oil which has been contacted by the near-miscible gas (Sohrabi et al., 2008a; 2008b). Williams and Dawe (1988) and Gray and Dawe (1991) used etched glass micromodel to visualize the involved displacement mechanisms at very low IFT. They showed at IFT below 0.1 $mN.m^{-1}$, the non-wetting phase flowed as discrete ganglias. As the IFT decreased, the ganglia distorted into long thin filaments that continually split and coalesced, particularly at pores throats. Also, the wetting phase was not necessarily continuous throughout the model, and could also flow as long thin strings, even at very low saturations. They also observed emulsion flow at low saturation of either of phases.

Sohrabi et al. (2008a, 2008b) observations in high-pressure micromodel experiments demonstrated that the recovery mechanisms which occur in near-miscible gas injection processes are different compared to those in immiscible or in completely miscible processes. They observed that the mechanism of the bypassed oil recovery (which is linked to the coupled flow of the oil and gas in the same pores) does not take place in immiscible gas floods nor does it occur in miscible gas floods. In immiscible (high-IFT) gas injection with spreading oil layers, although the by-passed oil maintains its connectivity with the main flow stream through the oil films, however, oil recovery by this film flow mechanism is negligible especially if an effective driving force (e.g., gravity) is absent. In immiscible systems, large capillary pressure at the gas/oil interface resists the entry of the gas into the bypassed oil in the first place. Even if the gas could enter the small pores, high IFT would slow down simultaneous flow of gas and the oil films in the main flow stream. In miscible gas floods, on the other hand, there would be no interface between gas and oil. The system would be basically single phase and no simultaneous flow of gas and oil would take place. Sohrabi et al. (2008a) state that although by-passed oil recovery, in miscible gas injection, can take place due to molecular diffusion and dispersion, those mechanisms are quite different from the efficient transport mechanisms that lead to oil recovery in near-miscible gas injection.

4.1.3 IFT Effects on Relative Permeability

Conventionally, multiphase flow in porous media is described by means of the concept of relative permeability functions. Relative permeability accounts for the decrease in effective permeability to a flowing fluid phase due to the presence of the other phase(s). Although Darcy's law (Hubbert, 1956) which is based on the assumption of strong

wetting and stable interfaces might not accurately reflect the physics of multi-phase flow at low IFT, an apparent relative permeability can estimate the macro-scale effects of the flow in porous media (Hartman and Cullick, 1989).

Bardon and Longeron (1980) investigated the effect of interfacial tension (IFT) between oil and gas phases on two-phase relative permeabilities. In their experiments they measured gas and oil (methane/n-heptane; methane/n-decane) drainage relative permeabilities for a very wide variation of IFT from 12.6 $mN.m^{-1}$ down to 0.001 $mN.m^{-1}$. Their results showed that as the IFT between oil and gas has been decreased, the oil recovery factor improved, and for very low IFT of 0.02 $mN.m^{-1}$, approximately all of the initial oil in place (IOIP) has been recovered after 2 PV (pore volume) of the gas injection. They divided their experiments into two parts: (a) IFT > 0.04-0.07$mN.m^{-1}$ and b) IFT < 0.04-0.07 $mN.m^{-1}$. For the first group, they found a single curve of relative permeability for gas (non-wetting phase) and a family of relative permeability curves for liquid. They found that wetting phase relative permeability (liquid) was higher when the IFT decreased. For the second group, they observed that the level of relative permeability curves for both oil and gas was considerably higher when the interfacial tension approaches zero. In the immediate vicinity of the critical point (0.001 $mN.m^{-1}$) the relative permeability curves are considered to be straight lines. It should be mentioned that Bardon and Longeron experiments were all performed vertical downward, when gas was displacing oil with an initial oil saturation of 100% (no immobile water saturation).

Delclaud et al. (1987) experiments on gas–oil relative permeabilities showed that interfacial tension in the range of 30-0.6 $mN.m^{-1}$ has little effect on the relative permeabilities for both wetting (oil) and non-wetting (gas) phases. Asar and Handy (1988) conducted steady-state relative permeability studies for IFTs from 0.82 $mN.m^{-1}$ to 0.01 $mN.m^{-1}$. They found that as IFT increased, oil relative permeability (wetting phase) decreased more rapidly than the gas (non-wetting phase) relative permeability. Chen *et al.* (1999) performed experiments on gas-condensate system undergoing pressure depletion. They also observed a greater change in the wetting phase (oil) relative permeability. Bardon and Longeron (1980), Asar and Handy (1988) and Chen *et al.* (1999) observations suggest that the wetting phase relative permeability curves are most sensitive to IFT changes.

Harbert (1983) performed corefloods using an alcohol, brine and oil fluid system. They found a significant effect of IFT on non-wetting phase relative permeability and a less noticeable effect on wetting phase relative permeability. Henderson *et al.* (1997, 1998) investigated the effect of IFT for gas-condensate system in the range of 9.7 $mN.m^{-1}$ - 0.019 $mN.m^{-1}$. They concluded that as IFT decreases the oil relative permeability curve remains essentially unaffected, whilst the relative permeability to gas increases significantly.

Schechter and Haynes (1992) investigated the effect of IFT for relative permeability of the binary mixture of methanol and hexane. They concluded that non-wetting phase relative permeability (hexane rich phase), increases only slightly as the IFT is reduced. The curvature of the wetting phase relative permeability decreased as the IFT was decreasing and straightens at conditions very close to critical point.

Blom et al. (2000); investigated the relative permeabilities of a binary, near critical fluid system in a glass bead-pack as a function of rate and IFT. As a fluid system, they selected the binary liquid mixture of methanol/n-hexane as a model for a near-critical gas/condensate or gas/volatile oil system. In both cases (effect of IFT and injection rate) the greatest effect was seen on the relative permeabilities of the non-wetting phase. Blom et al. (2000) observed that at very low IFT, the non-wetting phase relative permeability approaches a unit-slope line for which the non-wetting phase relative permeability is simply equal to its saturation. The wetting phase relative permeability was not affected until the interfacial tension is decreased below 0.06 $mN.m^{-1}$.

Al-Wahaibi et al. (2006) experimental results show that as the interfacial tension decreases, the non-wetting phase relative permeability increased more rapidly than the wetting phase relative permeability and hysteresis became less important. The drainage and imbibition relative permeability curves showed a clear change in shape with interfacial tension. They concluded that the relative permeability to the gas phase increases gradually as the interfacial tension decreases from 24.2 $mN.m^{-1}$ to 0.03 $mN.m^{-1}$. At very low interfacial tension, the gas phase relative permeability approaches a straight line. This is true for both drainage and imbibition relative permeability curves. However, oil relative permeabilities for both drainage and imbibition, show smaller changes with IFT. It should be mentioned that both Al-Wahaibi et al. (2006) and Blom et al (2002) used liquid-liquid system as a near-miscible system instead of hydrocarbon

liquid–vapour fluid system. The idea of replacement is according to the assumption of universal behavior of near-critical thermodynamic quantities, for either of gas/liquid equilibria and in liquid/liquid equilibria in the vicinity of critical point. Consequently, they assumed that a near-miscible binary liquid system can be used to model a near-miscible gas/liquid system. The main advantage of using a binary liquid system is that experiments can be performed at less extreme conditions than in the case of a gas/condensate system.

From the above literature one can conclude that the knowledge of how one fluid displaces another, and of how both fluids flow together, is needed for physically realistic multiphase numerical simulation. Differences in the wetting preference may account for the difference in flow behavior between different studies. The general result is that flow characteristics for systems with ultralow IFT's (< 0.01-0.04 $mN.m^{-1}$), are dramatically different from those of normal oil or gas reservoirs where the IFT's are high (~20 $mN.m^{-1}$). The IFT reduction affects relative permeability of both phases, but not usually equally. The general observation is the increased relative permeabilities and reduced curvature and less dependence of relative permeability on saturation history (less hysteresis effect) as the system approaches to the miscibility.

4.1.4 Effect of Immobile Water Saturation

In oil reservoirs, there is always some interstitial water present, which plays an important role in displacement process and recovery efficiency. In conventional gas/oil systems, in the absence of water, oil would always be the wetting phase and gas would be the non-wetting phase. However, if water is present, depending on rock wettability, oil could be wetting (oil-wet system), non-wetting (water-wet system) or partially wetting (mixed-wet system) phase and also it may or may not form spreading layers. It is well-known that every one of these conditions can have an important impact on fluid flow and displacement mechanisms.

Close to the critical point, any third, non-critical phase will be completely covered by a layer of one of the critical phases. This phenomenon is known as critical-point wetting (Cahn 1977). Consequently, for water-wet system, in near-miscible gas floods (with zero water saturation) the oil perfectly wets the solid surface (wetting layer). In presence of immobile water, oil would form a spreading layer on water wetting layers.

Saedi and Handy (1974) stated that in the presence of connate water, the effects of reduced gas-oil IFT may be even more pronounced. Their study showed that relative permeability ratio of gas to oil shifted to appreciably lower saturations in the presence of immobile water. This indicates more liquid flow at lower liquid saturations (i.e., higher oil relative permeability when immobile water is present). Owens et al. (1956), Knopp (1965) and Delclaud et al. (1987) investigated the effect of immobile water during gas injection (drainage) and stated that water saturation has no effect on gas-oil relative permeabilities. Narahara et al. (1993) concluded that gas-oil drainage relative permeabilities would not be affected in both water-wet and mixed-wet conditions by the presence of connate water as long as the following conditions are satisfied: (a) connate water is immobile, (b) relative permeabilities are expressed in terms of total liquid saturation, and (c) effective permeability of oil at connate water saturation (instead of absolute permeability for 100% oil saturated) is used as the reference to calculate relative permeabilities.

Kalaydjian et al. (1995) measured oil and gas relative permeabilities for water-wet sandstone under conditions of non-spreading and spreading and in the presence of connate water. They concluded that the presence of water affects the pore-scale distribution of the hydrocarbon phases, which in turn affects their connectivity and tortuosity. These properties affect the relative permeability of each hydrocarbon phases. They observed that oil recovery and relative permeability for gas injections (drainages), are higher for spreading than for non-spreading conditions.

Wylie and Mohanty (1997) investigated the effects of water saturation on mass transfer from bypassed regions during first contact miscible (FCM), multiple contact miscible (MCM) and immiscible gas injection. They observed that in the presence of water, the MCM gas will tend to have better recovery because many bypassed small pores would contain water as opposed to oil. At both 12 and 21% S_{wi}, complete recovery was observed with MCM gas at 1.8 HCPVI (hydrocarbon pore volume injected), suggesting the possibility that all the smaller pores are filled with water and very few larger, oil-containing pores were bypassed.

Skauge et al. (1994) summarised the effect of connate water on gas-oil displacement. The main effect has been a decrease in oil recovery with decreasing connate water saturation. Further review of the literature (Skauge and Ottesen, 2002) indicates that in

the presence of connate water there is generally an increase in oil recovery with water saturation up to a saturation range where water becomes mobile. Skauge and Ottesen (2002) concluded that S_{org} is reduced with increasing rock permeability, but the variation is only an average reduction in S_{org} from 0.15 to 0.1 for a permeability range of 1 mD to 10000 mD. They concluded that a correlation including porosity, permeability and initial oil saturation, analogous to Jerauld (1997) could not explain the observed variation in S_{org}. The higher recovery for the positive spreading system (compare to negative spreading) results from two factors (Agbalaka et al., 2008): (1) flow through the thin but continues oil films which is important for mobilizing and reconnecting the waterflood residual oil saturation (Oren et al., 1992); (2) the oil films avoided contact with the high curvature regions of the medium and maintained overall conductivity (Vizika and Lombard, 1994).

4.1.5 Effect of Wettability

The relative distribution of fluids within a porous medium is determined by the wettability of the rock, and the interfacial tensions or energies between the three phases. For water-wet systems, the hierarchy of fluid interfacial tensions ensures that water is in direct contact with the rock, and any condensed hydrocarbon liquid forms a film on the water surface, separating the gas from the water. The wettability is very important for the continuity of the phases as wetting films on the solid. These films are in hydraulic continuity over a number of pores even at very low wetting phase saturations. This phase can flow along the solid surface of the pore walls, while the non-wetting phase(s) must flow within the wetting phase. However many oil reservoirs are not strongly water-wet.

Thomas et al. (1995) concluded that for water-wet systems, miscibility (development of a zero interfacial tension), does not need to occur in order to have the optimal gas injection scheme. This is due to the fact that if a system is strongly water-wet and the water adheres more closely to the smaller pore throats, then you do not need or want to enter those pores to recover bulk of the initial oil in place. For oil-wet system where the substantial amount of the oil is associated with the smallest pore throats, one will need to approach zero IFT in order to make all of the pore throats accessible to the injected gas.

The effect of continuity of the oil film on the residual oil saturation has already been reported (Chatzis et al. 1998; Kalaydjian 1992; Oren and Pinczewski. 1994). Under water-wet condition, the residual oil saturation was found to be lowest under spreading conditions. However, for an oil-wet porous medium, the effect of spreading on the residual oil saturation was found to be less important, since it is believed that in such a case, oil phase continuity is insured along the pore walls.

Kalaydjian *et al.* (1995) experiments showed that under water-wet conditions and positive spreading, the residual oil saturation is very low (practically to zero), due to the flow of oil by film on the water wetting layers covering the pore surface. This is in contrary to what has been observed under oil-wet conditions where strong capillary retention leads to high S_{or} (> 5%). They attributed this observation to the fact that for spreading conditions the oil phase forms stable thin films on the water in presence of gas. This maintains the hydraulic continuity of the oil phase down to very low oil saturations. The absence of stable oil films on the water in the case of non-spreading leads to early disconnection of the oil in isolated blobs and the final trapping of much higher quantities of oil. Contrary to water-wet systems, Kalaydjian *et al.* (1995) experiments for oil-wet porous media showed that the spreading condition does not play an important role on the recovery kinetics or on the final oil saturation. This was attributed to the fact that in an oil-wet porous medium the continuity of the films depends on wettability rather than on the spreading coefficient. As a result, Kalaydjian *et al.* (1995) stated that for the same positive spreading coefficient, the oil recovery kinetics are different and that gravity drainage is much less efficient in the oil-wet sand-pack than in the water-wet one. This implies that different displacement mechanisms are involved. In fact, at low oil saturations in water-wet porous medium the oil forms films on the water covering the solid (spreading oil films), while in oil-wet porous media oil films are formed directly on the solid (wetting oil films). These two types of films have different characteristics (thickness, interactions with the solid) and thus different hydraulic conductivity. Kalaydjian *et al.* (1995) concluded that oil permeability in oil-wet case should be lower than in the water-wet case.

Dehghan *et al.* (2009) results of solvent injection (n-Hexane), showed that the displacement efficiency of the solvents is generally higher in strongly water-wet. In their experiments, some amounts of initial bypassed oil for water-wet system were found in pores' center while for oil-wet systems some oil was remained on the glass

surfaces. Generally it was found that for oil-wet media, in the absence of connate water, the displacement mechanism is more finger-dominated and therefore less recovery would be obtained for the oil.

Contrary to these observations, Wylie and Mohanty (1999) observed that oil recovery is higher in oil-wet media than in water-wet media due to the presence of water-shielding in water-wet media. But it should be mentioned that the S_w for water-wet and oil-wet condition were different in their experiments and recovery mechanisms were based on mass transfer between by-passed oil and gas flow (un-equilibrated fluids).

4.2 Coreflood Experiments

4.2.1 Gas Injection (Drainage) Test: 65mD, Water-wet, S_{wi}=0

One of the displacement types that occur in the reservoir during the WAG process is the displacement of oil by the injected gas slug. To determine gas-oil relative permeability curves applicable to this type of displacement, an unsteady-state gas injection test has been carried out in the 65mD core. To be able to investigate the impact of immobile water on gas-oil k_r and displacement mechanisms, this experiment was carried out with no initial water saturation, S_{wi}. Later a similar test was carried out with S_{wi} and the impact of S_{wi} was examined by comparing the results of these tests. This experiment started with the core fully saturated with the equilibrated oil at 1840 psia and 100 ºF. The equilibrated gas was then injected through the core at a constant rate of 100 $cm^3.hr^{-1}$ and at the same time the core effluent was collected in a glass separator (sight glass) at the test pressure (using a retract pump pulling back at the same rate as the injection rate). Displacement of the oil by the gas was carried out at the average core pressure of 1840 psia corresponding to a low gas/oil IFT of 0.04 $mN.m^{-1}$. During the experiment, fluids production (oil and gas), injected volumes and also the pressure at the core inlet and outlet were accurately monitored and measured.

Figure 4-1 shows the oil recovery and pressure drop across the core versus the pore volume (PV) of injected gas during this near-miscible gas injection experiment. As can be seen from this figure, for the first 0.34 PV of gas injection (before the gas breakthrough) only oil was being produced from the core outlet and the oil production volume was equal to the volume of the injected gas. After around 0.34 PV of gas injection, the gas front reached the core outlet (gas breakthrough) and thereafter both the

gas and oil were produced. Although the oil recovery rate decreased after the gas BT (breakthrough), the production of oil continued at a significant rate until the end of the experiment. The injection of gas in this test continued for almost 3.5 PV when the test was stopped. High recovery rates after BT and very low Δp across the core, are evidences which have been previously reported in the case of near-miscible gas injection (Bardon and Longeron (1980), Hartman and Cullick (1994)).

Table 4-1: Coreflood experiments presented in Chapter-4.

Exp. #	Core	Coreflooding	Direction	Wettability	S_{wim}
1	65 mD	Gas Injection	Drainage	Water-Wet	-
2	65 mD	Oil Injection	Imbibition	Water-Wet	-
3	65 mD	Gas Injection	Drainage	Water-Wet	✓
4	65 mD	Oil Injection	Imbibition	Water-Wet	✓
5	65 mD	Gas Injection	Drainage	Mixed-Wet	✓
6	65 mD	Oil Injection	Imbibition	Mixed-Wet	✓
7	1000 mD	Gas Injection	Drainage	Water-Wet	✓
8	1000 mD	Gas Injection	Drainage	Mixed-Wet	✓
9	1000 mD	Oil Injection	Imbibition	Mixed-Wet	✓

For the water-wet system, gas would act as the non-wetting phase with respect to the oil phase. As the gas injection process starts, the gas would displace oil from the larger pores first, since larger pores have smaller entrance capillary pressure to overcome and enter in. The conductivity of these pores is also higher compare to the smaller pores, and as a result the gas would bypass those smaller pores and breakthrough from the outlet. At the time of BT, the gas would be in the body of the larger pores, while oil phase is still continuous throughout the core as the wetting layers in large pores and untouched in smaller pores. The oil saturation in larger pores would be equal to (or around) the residual oil saturation to gas injection, while the oil saturation inside the smaller pores can be as high as 100%. As the process of gas injection continues, considering the very low IFT between oil-gas phases (low capillary entrance), the gas clusters that initially entered into small pores will be connected and flow in smaller pores, displacing the oil phase out, and making some wetting oil layers. Depending on the injection rate and pore size distribution of the core, BT (breakthrough) time and amount of recovery afterwards would be different from case to case. The stability of the wetting oil layers, the capillary entrance pressure for smaller pores and the effectiveness of the gas phase drag forces on the wetting layers would determine whether the gas would produce oil from the oil wetting layers or would prefer to enter new smaller pores or both.

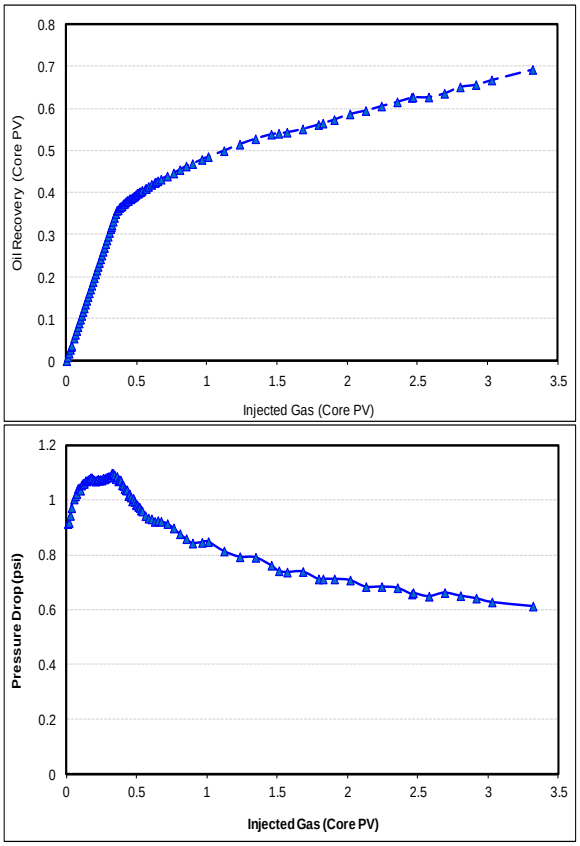

Figure 4-1: PV oil recovery (top) and pressure drop (bottom) vs. PV injected gas (gas injection, water-wet, S_{wi}=0).

4.2.2 Oil Injection (Imbibition) Test: 65mD, Water-wet, S_{wi}= 0

The results of the previous experiment in which gas injection was carried out to displace the oil from the core can be used to obtain bounding drainage k_r curves for gas/oil system. For numerical simulation of WAG process and in order to consider hysteresis effect, it is equally important to obtain imbibition gas/oil k_r curves as well as drainage (Spiteri *et al.*, 2006; Hustad and Browning, 2010). During WAG injection in an oil reservoir, an oil bank can be formed, which leads to displacement of gas (from the earlier gas injection stages) and hence imbibition gas-oil k_r curves would be needed for simulating such displacement.

To determine bounding imbibition gas/oil k_r curves for the investigated near-miscible system, another unsteady-state displacement experiment was carried out. This test began by fully saturating the core with the gas (100%) and was carried out at the same pressure and temperature as the previous test (1840 psia and 100 ºF) with no initial water saturation. The oil was then injected through the core at a rate of 100 $cm^3.hr^{-1}$. To examine repeatability of the experiments, this test was repeated. Figure 4-2 shows the measured gas recovery and pressure drop across the core during these unsteady-state oil

injection experiments. Comparison of the results of the repeated tests demonstrates excellent repeatability of the experiments. Figure 4-2 shows that, as expected, prior to oil breakthrough (which occurs around 0.6 PV oil injected) only gas is recovered from the core. However, when the oil front reaches the production end of the core (breakthrough) at 0.6 PV of oil injection, gas production decreases significantly and thereafter the core effluent is mostly oil. Production of gas after BT (albeit at a very low rates) shows that the oil is unable to completely trap the gas phase.

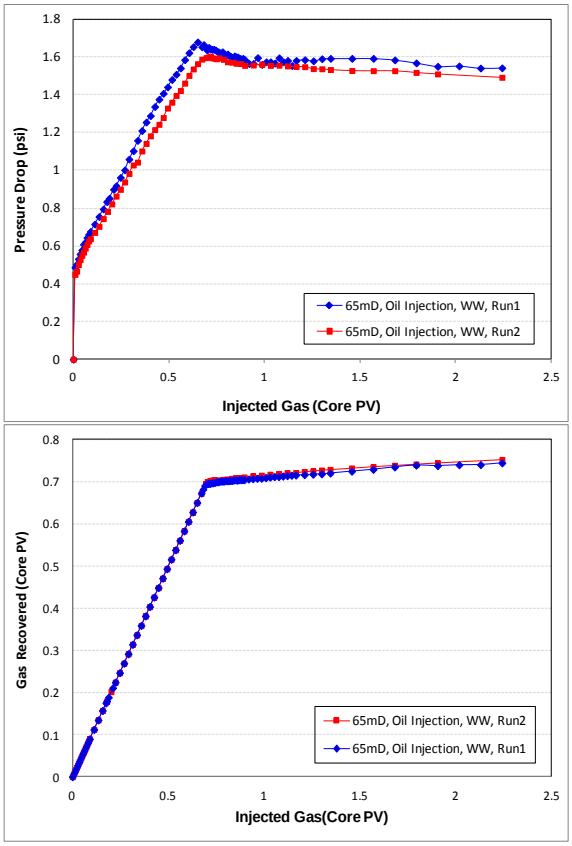

Figure 4-2: gas recovery (PV) as a function of PV of injected oil for two runs of the oil injection tests.

In a water-wet rock, oil would act as the wetting phase with respect to the gas phase. As the oil injection process starts, the oil would displace gas from the smaller pores first, since smaller pores have larger capillary imbibition force for oil. The conductivity of these pores is smaller compare to the larger pores. As the oil saturation in these pores increases, wetting phase layers will be thicker and at high enough saturations, these layers would bridge and trap the gas in between. As the oil injection continues the oil would enter larger pores. The entrapment of the gas inside a pore body is much more difficult in larger pores as oil would have established continues path towards the outlet before getting thick enough to bridge in larger pores. As the IFT between oil/gas is very low, complete trapping would not occur and a small amount of gas flow and recovery

takes place after the BT due to the possible coupled flow of the oil and gas in some medium to larger pores.

4.2.3 Gas Injection (Drainage) Test: 65mD, Water-wet, S_{wi}=18%

To examine the effect of immobile water saturation (S_{wi}) on the gas-oil relative permeability curves applicable to the displacement of oil by gas (drainage), another unsteady-state gas injection test was carried out. The test conditions were kept similar to the previous gas injection test with the only difference being the presence of immobile water saturation (S_{wi}) in the core. This experiment began with the core containing 82% oil and 18% water as an immobile phase at 1840 psia (gas-oil IFT of 0.04 $mN.m^{-1}$). Then, gas injection through the core commenced. Although the oil recovery rate decreased after the gas BT, it remained significant until the end of the experiment (due to near-miscibility condition).

4.2.4 Oil Injection (Imbibition) Test: 65mD, Water-wet, S_{wi}=18%

In this experiment again the impact of initial immobile water saturation on near-miscible gas-oil relative permeability curves has been investigated albeit for the imbibition direction. In this test the core initially contained 18% brine and 82% gas at 1840 psia (gas-oil IFT of 0.04 $mN.m^{-1}$). After the oil breakthrough (BT) which happened around 0.5 PV of oil injection, there was a sudden change of slope in the gas recovery curve and the production of gas after BT was negligible.

4.2.5 Gas Injection (Drainage) Test: 65mD, Mixed-wet, S_{wi}=18%

Having altered the wettability of the core, another gas injection was carried out with the same S_{wi}. The results of this mixed-wet experiment were then compared with their water-wet counterparts to examine the effect of wettability. To be able to compare the results of the mixed-wet cores with water-wet one, the test conditions were kept similar to the previous gas injection test in the water-wet rock with the same initial water saturation. The experiment began with the core containing 82% oil and 18% water (immobile water saturation) at 1840 psia. Then, gas injection through the core commenced and the production of fluids and also the pressure at the inlet and outlet of the core were accurately monitored and measured. The rate of oil production from the core slowed down after the breakthrough of the gas around 0.35 PV and thereafter both the gas and oil were produced. Although the oil recovery rate decreased after the gas

BT, it remained significant until the end of the experiment, which is a feature of near-miscible gas injection process.

4.2.6 Oil Injection (Imbibition) Test: 65mD, Mixed-wet, S_{wi}=18%

The objective of this experiment was also to investigate the impact of wettability on near-miscible gas-oil displacement and relative permeability curves, albeit in the imbibition direction. The test conditions were kept similar to the previous oil injection test in the water-wet rock with initial water saturation. In this test, the core was initially saturated with 18% brine and 82% gas at 1840 psia (gas-oil IFT of 0.04 $mN.m^{-1}$). The oil breakthrough took place around 0.4 PV of oil injection, where, there was a sudden change of slope of the gas recovery curve.

4.2.7 Gas Injection (Drainage) Test: 1000mD, Water-wet, S_{wi}=8%

The same procedure that was used for establishing the initial water saturation in the 65mD core was followed for the 1000 mD core too. The value of the established immobile water saturation is less for this core compare to the 65mD core due to the higher permeability of this core (and possibly larger fraction of the pores with medium to large sizes). To be able to compare the results of the water-wet 65mD core with the results of the 1000mD core, the test conditions were kept similar (1840 psia and 100 ºF, corresponding to a gas/oil IFT value of 0.04 $mN.m^{-1}$). The experiment began by a gas injection in the 1000 mD core containing 92% oil and 8% water (immobile water saturation). The rate of oil recovery from the core slowed down after the breakthrough of the gas around 0.46 PV and thereafter both the gas and oil were produced. Although the oil recovery rate decreased after the gas BT, it remained significant until the end of the experiment (which is the feature of near-miscible gas injection). For further discussion and details of the experiments on 1000mD refer to Sohrabi *et al*. (2007).

4.2.8 Gas Injection (Drainage) Test: 1000mD, Mixed-wet, S_{wi}=8%

The gas injection was carried out in the 1000 mD mixed-wet core (after changing its wettability) in order to compare its results with the similar gas injection test that had been carried out in the 65 mD mixed-wet core. A similar wettability alteration procedure as the one used for the 65mD core sample was also used for the 1000 mD core. The test conditions were kept the same for both cores (1840 psia and 100 ºF) but in the 1000 mD core the experiment began with the core initially containing 92% oil and 8% water (immobile water saturation).

4.2.9 Oil Injection (Imbibition) Test: 1000mD, Mixed-wet, S_{wi}=8%

The objective of this experiment was also to investigate the impact of permeability on near-miscible gas-oil displacement for the imbibition direction. Comparison of the results of this test with its counterpart in the 65 mD core reveals the effects of permeability of the rock. The test conditions were kept similar to the previous oil injection test in the 65mD mixed-wet rock with initial water saturation. In this test, the core was initially saturated with 8% brine and 92% gas at 1840 psia. The oil breakthrough happened around 0.65 PV of oil injection, where, there was a sudden change of slope of the gas recovery curve at which point the rate of gas production dropped to almost zero.

4.3 Results and Discussion

This section discusses k_r determination for these coreflood experiments. Using these experimentally derived k_r curves, the effect of saturation history, immobile water saturation, wettability and rock permeability (pore size distribution) will be discussed. The differences between gas/oil near-miscible systems with liquid/liquid near-miscible systems are discussed as well. A commercial simulator (SENDRA) was used in this exercise to history match the core flood results (the production and differential pressure data) and obtain the best k_r estimates. This software is a two-phase 1D black-oil simulation model used for analysing SCAL (special core analysis) experiments. Through history matching function, one can match the experimental data (pressure drop and production data) by adjusting the relative permeability curves. This is done by choosing one of the relative permeability correlations available in the simulator. The software is then automatically changing the empirical parameters in that function trying to match the experimental data (Style et al. (2004); Lomeland et al. (2005)).

As an example to show the quality of the history matching in this study, Figure 4-3 shows a set of experimental and simulated data for the pressure drop across the core, gas production and oil recovery for one of the performed gas injections (65mD, water-wet, S_{wi}=0). Figure 4-3 shows the good match achieved between the simulation and experiment data which is important for reliable estimation of the relative permeabilities curves.

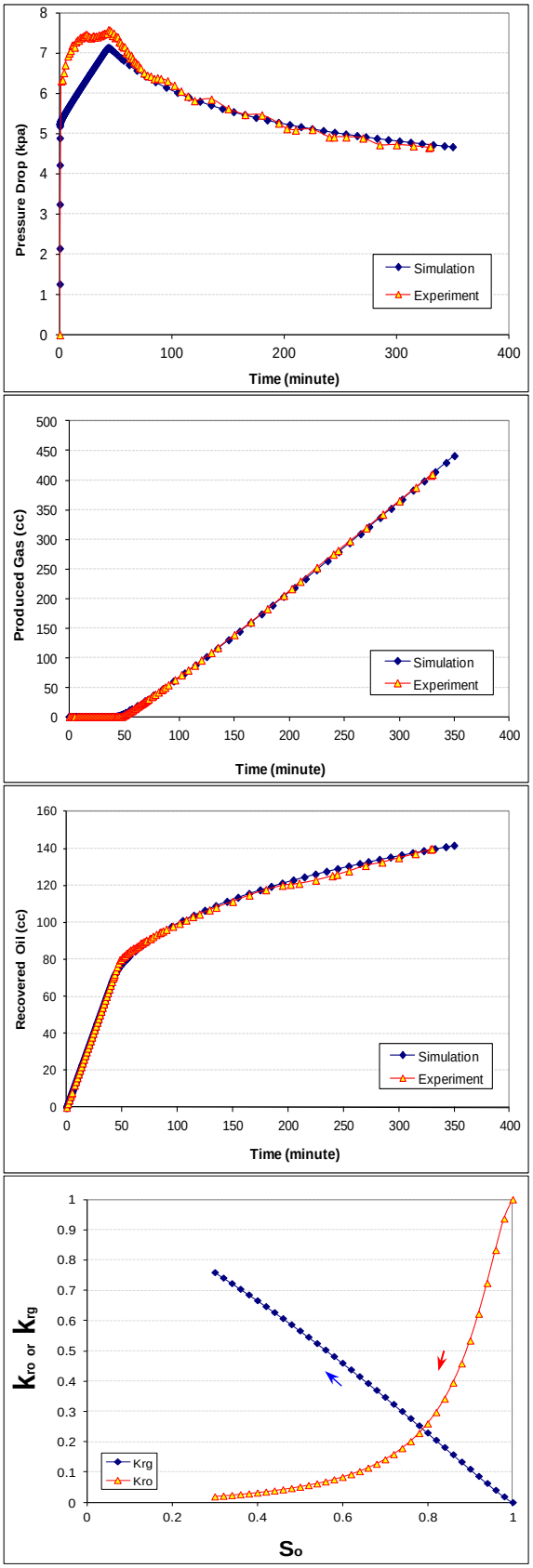

Figure 4-3: History matching of the experimental data (pressure drop, gas recovery and oil production) and estimated relative permeabilities for Gas Injection (65mD, Water-Wet, S_{wi}=0).

4.3.1 Comparison of Gas and Oil Injection Tests: 65mD, Water-wet, $S_{wi} = 0$

Figure 4-4 compares the oil recovery and pressure drop in the near-miscible gas injection (drainage) test with the gas recovery and pressure drop for the near-miscible oil injection (imbibition) test both carried out in the 65mD core using the same fluids and performed at the same pressure and temperature. As can be seen, when oil displaces gas (imbibition), at the BT, the amount of gas recovery is higher than the amount of oil recovery when gas displaces oil (drainage). This means that the oil breakthrough in the oil injection test happened after the gas breakthrough in the gas injection test. However, extrapolation of the gas and oil recovery curves in Figure 4-4 reveals that if the gas injection continues for an extended period of time (in this particular case more than 3.5 PV) then the amount of oil recovery will catch up with the gas recovery in the oil injection test and would be higher afterwards. Figure 4-4 and Figure 4-5 shows that although the IFT between oil/gas phases is as low as 0.04 $mN.m^{-1}$, there is still a significant difference between recovery mechanisms which results in different recovery profile and pressure drop behaviour and therefore totally different k_r values for imbibition and drainage displacement (see the following sections). The significant additional oil recovery after the gas breakthrough in near-miscible gas injection is attributed to the flow and recovery of the oil through highly conductive oil layers that exists in near-miscible systems. In near-miscible oil injection experiments, however, since the gas is a non-wetting phase, no gas layers can form and hence the gas left behind after the BT of the oil would be mainly isolated and fragmented.

In the vicinity of miscibility these two recovery curves and pressure drop behaviour would approach together, in the case of two liquid phases (Al-Wahaibi et al., 2006; Blom et al., 2002) which means whether wetting phase displace the non-wetting phase or vice versa, recovery curves and pressure drop behaviour would be very close. This is due to the fact that in the case of liquid/liquid system the amount of trapped non-wetting phase in imbibition would be very small and close to the residual wetting phase in drainage displacement. Considering this, Figure 4-4 highlights the difference between oil/gas system and liquid/liquid (Al-Wahaibi et al., 2006; Blom et al., 2002) system at near-miscible condition. As a result, the application of near-miscible liquid/liquid system instead of gas/liquid system to investigate near-miscible gas injections, gas/condensate or gas/volatile-oil systems is not justified and would results in erroneous conclusions and results. Liquid/liquid system has been usually applied in literature due to the simplicity of the experiments in liquid/liquid systems compared to gas/liquid (oil)

systems which would require working under high pressures. The author believes that for the same low IFT value (near-miscible condition), the behaviour of a liquid/liquid system and the associated displacement mechanisms are different with those of a gas/liquid system. This significant difference in the behaviour of the two systems is responsible for the observed significant k_r hysteresis (Figure 4-6) for the near-miscible gas-oil system in this study compared to Al-Wahaibi et al., 2006 and Blom et al., 2002 experiments which were performed on liquid/liquid near-miscible system. The same behaviour (significant trapping of the non-wet phase during imbibition) was also observed for the near-miscible gas-oil displacements experiments in mixed-wet (65 mD) core when the core contained immobile water. The experimental results performed in the higher permeability core (1000mD) have also confirmed these observations.

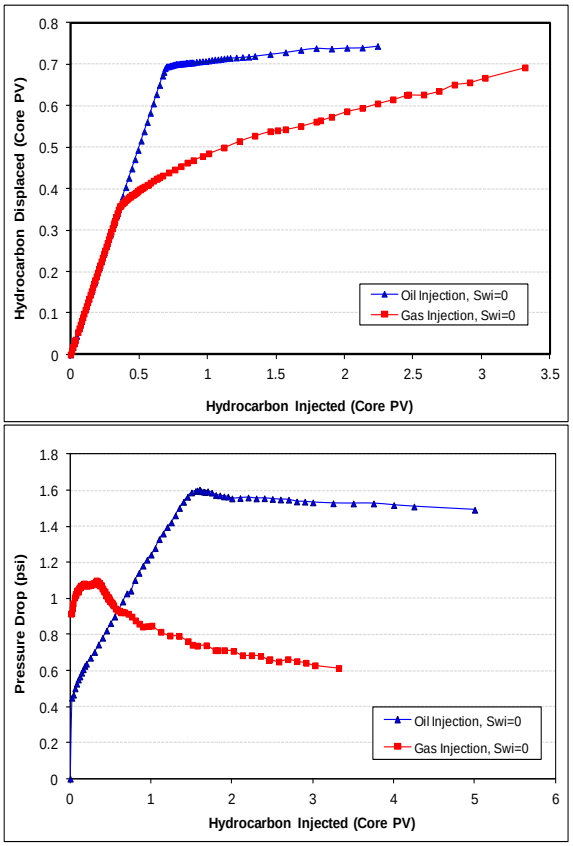

Figure 4-4: Comparison of displaced phase recovery (top) and pressure drop (bottom) during two low IFT un-steady state displacements (imbibition and drainage), (65mD, water-wet, S_{wi}=0)

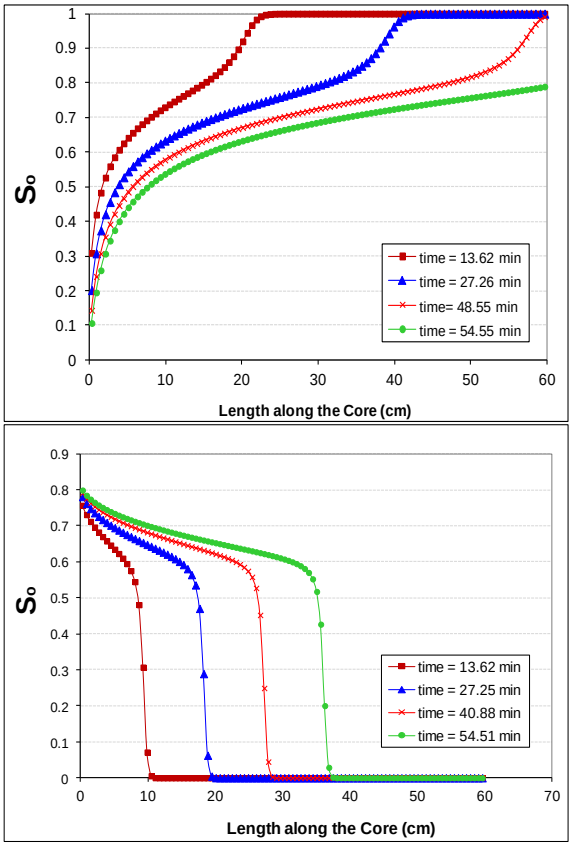

Figure 4-5: Simulated oil saturation profile along the core (after history matching) different stage of the displacement. Top: gas injection; Bottom: oil injection (65mD, water-wet, S_{wi} = 0).

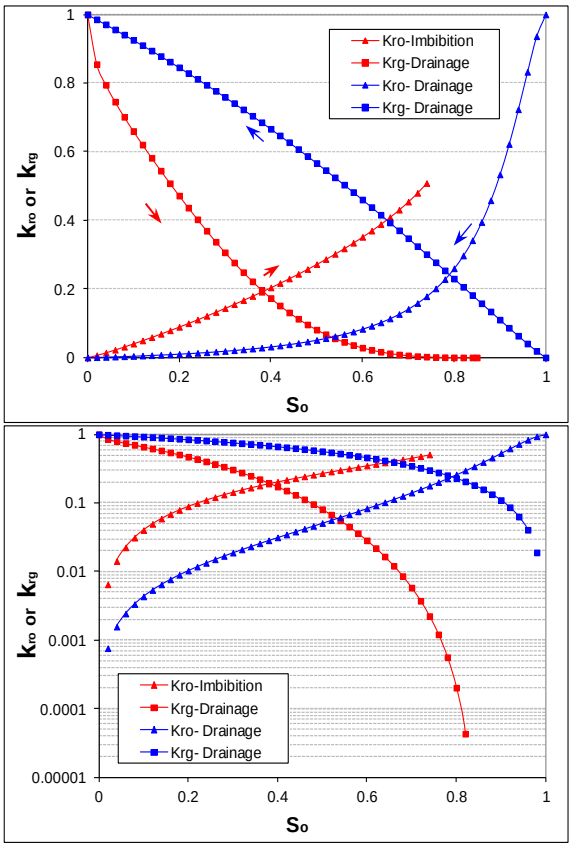

Figure 4-6: Hysteresis effect on bounding relative permeability drainage and imbibition curves (65mD, water-wet, S_{wi}=0).

4.3.2 Effect of S_{wi} on Gas Injection (Drainage): 65mD, Water-wet

Figure 4-7 shows the effect of immobile water saturation (S_{wi}) on the performance of gas injection (in water-wet system). The vertical axis in this Figure shows the oil recovery as a fraction of the initial oil in place (IOIP) and the horizontal axis is also corrected as the injected volume of the gas in terms of IOIP pore volume (which assumes the immobile water saturation as a part of the rock). As can be noted, the presence of S_{wi} has had a positive effect on the gas injection performance as it has delayed the breakthrough (BT) of the gas and has increased the amount of oil recovered during gas injection. A common approach in the simulation of multiphase flow in porous media is that the saturation values are corrected for S_{wi}, i.e. they are reported based on the hydrocarbon pore volume assuming that S_{wi} acts as a part of the rock. The results in Figure 4-7 clearly show that this assumption is invalid for the near-miscible system, since there is a clear difference in the production profiles in these two plots which have been prepared based on the hydrocarbon pore volume.

This observation can be explained in terms of the distribution of different phases at the pore level for these two cases. In the absence of immobile water (Figure 4-8a), the oil would be the wetting phase adhering on the surface of the grains (wetting layer) while the gas, as the non-wetting phase, would flow in the body of the pore. In contrast to this, in the presence of immobile water (Figure 4-8b), water would act as the wetting phase adhering on the grains surfaces (wetting layers), and oil would spread on these wetting layers as the intermediate-wet phase and form spreading layers. Lubricating the flow of oil by water wetting layers, spreading oil layers (in the presence of immobile water saturation) would be more conductive than oil wetting layers (in the absence of immobile water saturation). As a result, the performance of gas injection would be improved in the former case where water wetting layers exist.

This observation is in disagreement with previous reports by Owens et al. (1956), Knopp (1965), Delclaud et al. (1987) and Narahara et al. (1993) in which immobile water saturation had no effect on gas/oil displacement and relative permeabilities. This discrepancy can be explained by the very low oil/gas IFT in the presented experiments. Capillary pressure is a function of IFT, σ, as well as contact angle, θ, and pore radius, r, through the following equation:

$$P_{cog} = \frac{2\sigma_{og}.\cos\theta}{r} \qquad \text{(Eq. 4-1)}$$

For high oil/gas IFT systems (such as those data presented by Owens et al. (1956), Knopp (1965), Delclaud et al. (1987) and Narahara et al. (1993)), capillary forces (between oil and gas) would be high enough to prevent the gas entering into small pores. As a result, in high oil/gas IFT system, in both cases of with and without immobile water saturation, gas would not be able to enter those very small pores anyway and as a result the amount of oil recovered by gas and k_r would be unaffected by the presence or absence of immobile water saturation. In a system with very low IFT, however, oil/gas capillary pressures would be low, and the gas phase would be able to enter small pores (in the absence or presence of immobile water). Taking into account the difference between the pore level distributions of the fluids in the absence or presence of S_{wim}, the amount of oil recovery and k_r values would be affected. As a result, higher oil recovery was observed due to the oil spreading layers in the presence of immobile water saturation. The extent of the oil recovery improvement in the presence of immobile water saturation would be a function of the pore size distribution, wettability and oil/gas IFT.

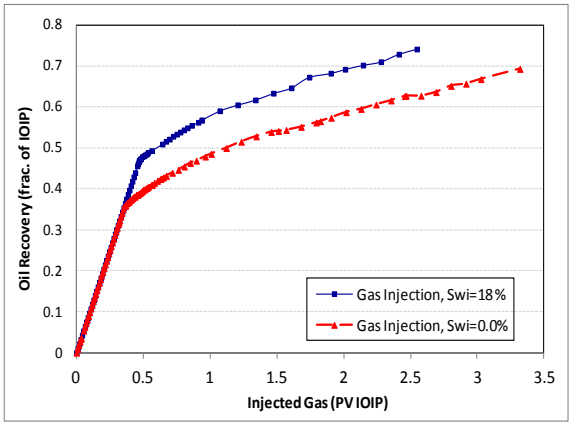

Figure 4-7: Effect of S_{wi} on oil recovery (fraction of initial oil in place) as a function of injected gas (fraction of IOIP pore volume); 65mD, Water-Wet, Drainage.

Figure 4-8: Schematics of pore level distribution of different phases (oil, water and gas) in small pores of the rock. Left: in the absence of immobile water saturation; right: in the presence of immobile water saturation (brown: grains; dark: oil; blue: water; red: gas); 65mD, Water-Wet, Drainage.

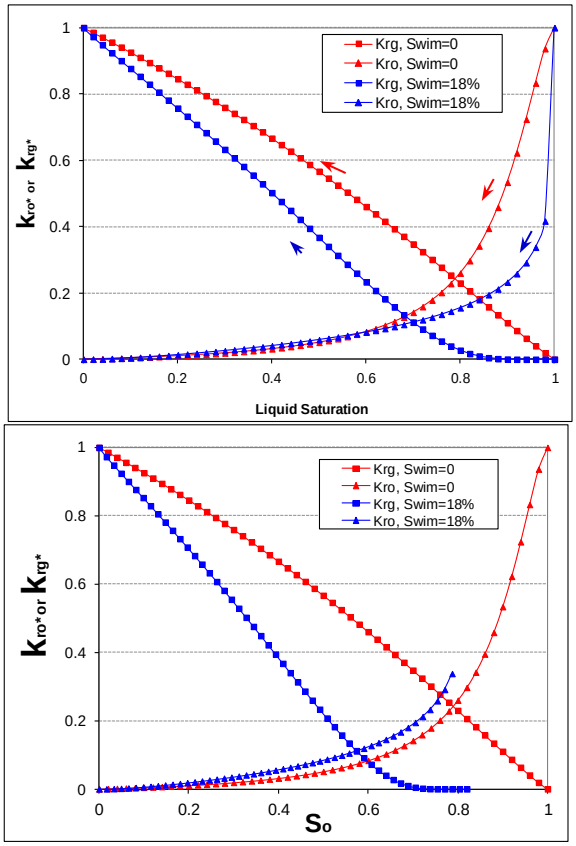

Figure 4-9: Effect of S_{wi} on oil and gas relative permeability, Top: vs. total liquid saturation; Bottom: vs. oil saturation (65mD, water-wet system, drainage).

Figure 4-9 shows the effect of immobile water on oil and gas relative permeability values for drainage displacement. Although in Figure 4-9a the conditions proposed by Narahara et al. (1993) are satisfied (a: connate water is immobile, b: relative permeabilities are expressed in terms of total liquid saturation, and c: effective permeability of oil at connate water saturation (K_{eff} = 55 mD) used as a reference to calculate relative permeabilities for the case in which S_{wi} = 18%), relative permeability are different with and without immobile water saturation. In Figure 4-9a (k_r expressed in terms of liquid saturation), oil and gas relative permeability values are less in the presence of immobile water, since for the same liquid saturation, part of the pore space is now filled with the water phase which is immobile and as a result the relative conductance of the core has been reduced. In Figure 4-9b, where oil and gas relative permeabilities are expressed in terms of the oil saturation (k_{ro} are calculate based on K_{abs} = 65 mD), k_{ro} shows improvement for the case when immobile water is present, while k_{rg} values have reduced in this case. This can be explained by the fact that for the same oil saturation value, the conductance of the oil layers are more in spreading condition (in the presence of immobile water saturation) compared to the case of wetting condition (absence of S_{wi}).

4.3.3 Effect of S_{wi} on Oil Injection (Imbibition): 65mD, Water-wet

Figure 4-10 depicts the effect of S_{wi} on the performance (gas production) of oil injection (in water-wet system). The vertical axis in this Figure shows the recovered gas as a fraction of the initial gas in place (IGIP) and horizontal axis is also corrected to represent the injected volume of the oil in terms of IGIP pore volume. As can be noted, the presence of S_{wi} has had a negative effect on the oil injection performance. The results in Figure 4-10 clearly show that the hypothesis of assuming immobile water as a part of rock is invalid for the investigated near-miscible system. This observation can be explained in terms of the pore-scale distribution of fluid phases for these two experiments. As is shown in Figure 4-11, for the entrapment of the gas phase in the body of the pore (due to bridging of the oil layers at the throats and the snap-off process) lower oil saturation (less oil) would be required when the part of the pore is occupied by water (immobile water saturation). In addition, as discussed in the previous section, the conductivity of the oil layers is higher in the presence of immobile water saturation. As a result, the oil breakthrough would happen earlier compared to the case in which immobile water is absent.

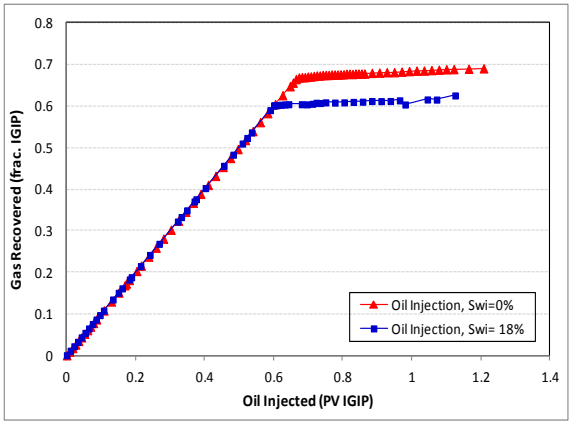

Figure 4-10: Gas production (fraction of initial gas in place) as a function of injected oil (fraction of IGIP pore volume); 65mD, Water-Wet, Imbibition.

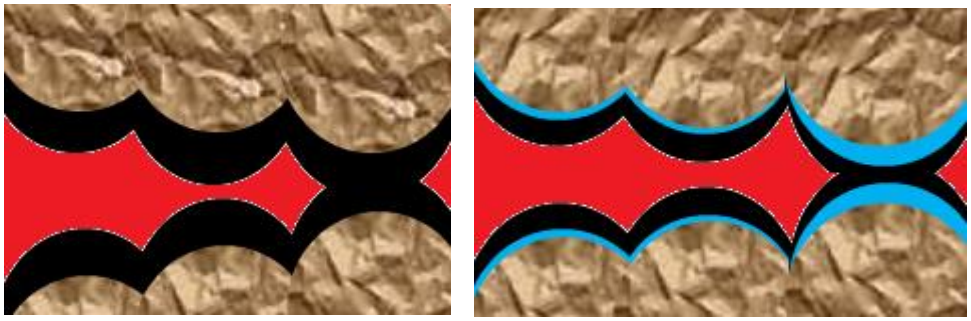

Figure 4-11: Schematics of the pore level distribution of different phases in small pores of core sample. Left: in the absence of immobile water saturation; right: in the presence of immobile water saturation (brown: grains; dark: oil; blue: water; red: gas); 65mD, Water-Wet, Imbibition.

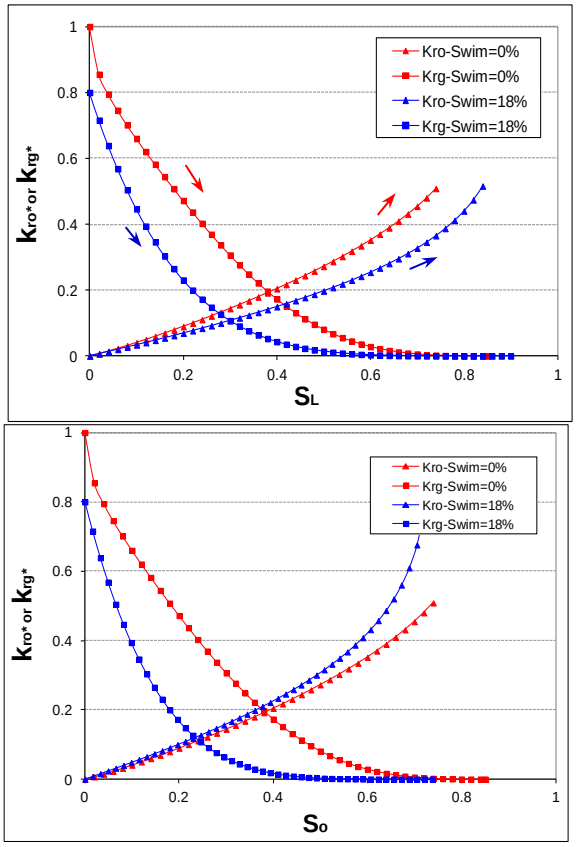

Figure 4-12: Effect of S_{wim} on oil and gas relative permeability, Top: vs. total liquid saturation; Bottom: vs. oil saturation (65mD, water-wet system, Imbibition).

Figure 4-12 shows the effect of immobile water saturation on the oil and gas relative permeability values for imbibition displacement. Although in Figure 4-12a the conditions proposed by Narahara et al. (1993) are satisfied, the relative permeability are still different as a result of the absence or presence of immobile water. Similar to what has been already explained for the case of drainage, in Figure 4-12a, where k_r expressed in terms of liquid saturation, oil and gas relative permeability are less in the presence of immobile water, since for the same liquid saturation, part of the pore space is now filled with the water phase which is immobile and as a result the flow capacity of the pore space has been reduced. In Figure 4-12b, where oil and gas relative permeability are expressed in terms of oil saturation, k_{ro} shows improvement in the presence of immobile water, while the k_{rg} values have reduced in this case. The data shown in Figure 4-9 and Figure 4-12, also show that the effect of immobile water saturation is more pronounced for non-wetting phase (gas) compared to the wetting phase (oil).

Figure 4-13 shows the oil and gas relative permeability curves for imbibition and drainage for the tests with immobile water saturation. Comparing this Figure with Figure 4-6, it can be concluded that hysteresis effect is less when immobile water is

present in the rock. In the pores in which water exist, oil would act as an intermediate-wet phase (compare to its wetting behavior in the absence of immobile water), and as a result, the hysteresis effect would be less.

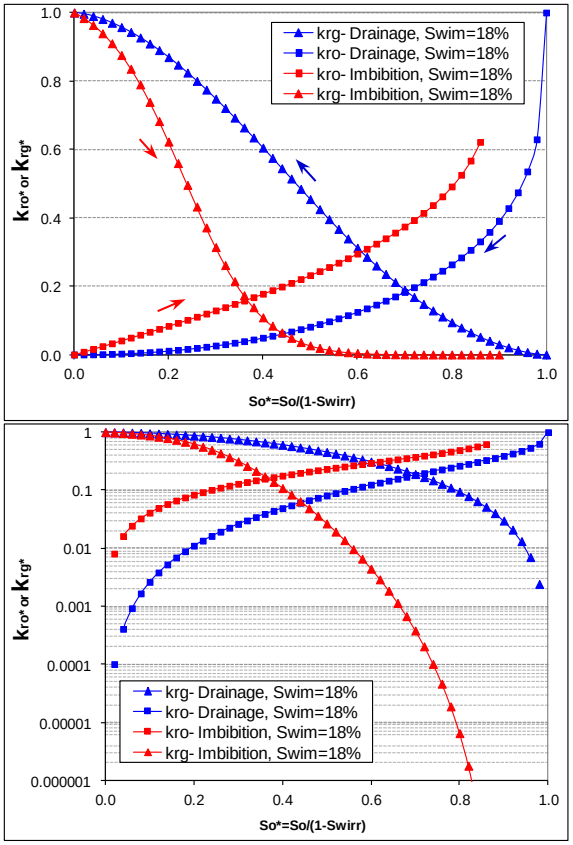

Figure 4-13: Hysteresis effect on bounding relative permeability drainage and imbibition curves (65mD, water-wet, S_{wi}=18%).

4.3.4 Effect of Wettability on Gas Injection Process

To investigate the possible effects of the rock wettability on the performance of gas injection (at near-miscible condition), the experimental results of oil recovery by gas injection in the water-wet and the mixed-wet cores (for the same S_{wi}) have been compared. Figure 4-14 shows that the gas breakthrough in the water-wet rock takes place just slightly later than that in the mixed-wet core. Earlier BT of the gas in the mixed-wet system can be due to the less accessible PV of oil by gas in this system (since in large and medium pores, oil phase is changing between oil wetting layers on the grains (less accessible to gas) to the oil spreading layers (in some pores that still water is there as a wetting phase). Figure 4-14 also shows that the oil production rate and the ultimate recovery factor achievable in the mixed-wet core are lower compared to the water-wet sample. Both these observations indicate that the performance of gas injection has been adversely affected in less water-wet system. In the mixed-wet core, the pores can be divided in two categories, partly water-wet and partly intermediate to

oil-wet. The performance of the very large pores would be more or less the same for both systems, since in the water-wet sample the water layers (if any in these pores) are very small and discontinuous and oil would be the dominant phase anyway. The difference would be more pronounced for smaller pores in which immobile water presents. For water-wet systems, oil would be connected through the spreading layers (Figure 4-15a). For the mixed-wet system, parts of these pores (which have been in contact with crude oil during wettability alteration process) are neutral to oil-wet (Figure 4-15b). In these pores, oil layers would change their action from spreading layers to the wetting layers and vice versa. As discussed earlier, the conductivity of wetting layers are less than spreading layers and as a result oil recovery in the mixed-wet system would be less compared to the water-wet case.

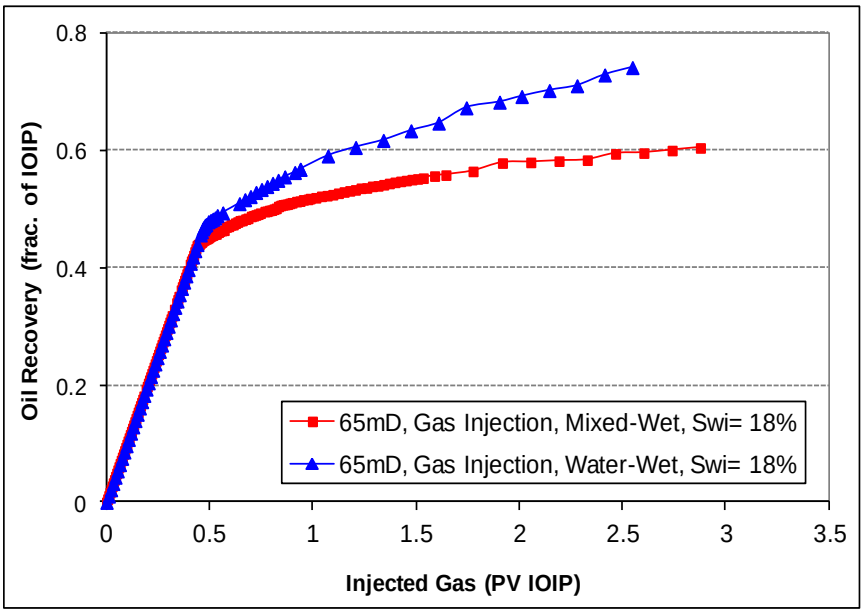

Figure 4-14: Effect of wettability on the performance of gas injection (64mD, S_{wi}=18%)

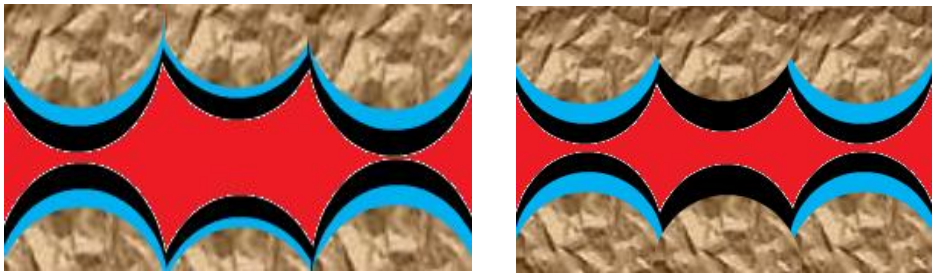

Figure 4-15: Pore level distribution of different phases in small pores of core sample. Left: water-wet system; right: mixed-wet system (brown: grains; dark: oil; blue: water; red: gas); 65mD, Drainage, S_{wi}=18%.

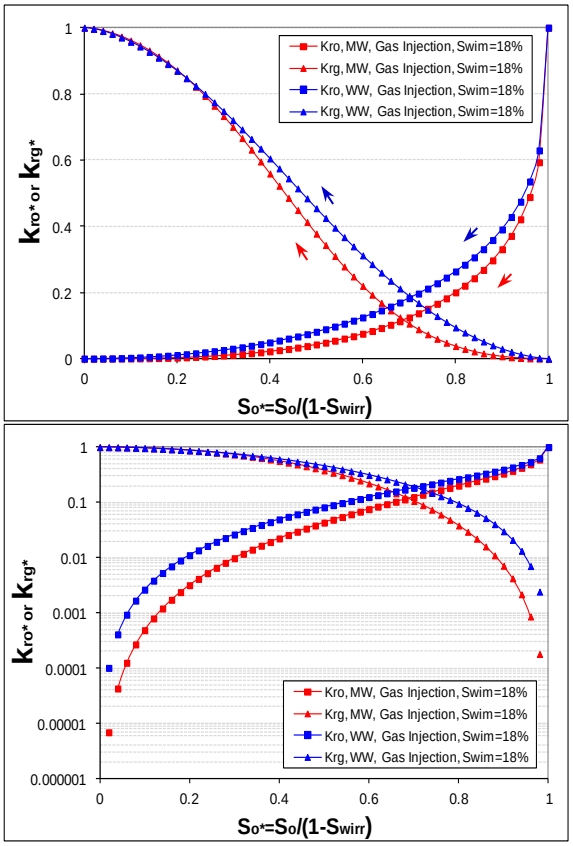

Figure 4-16: Effect of wettability on oil and gas relative permeability curves, (65mD, Drainage, S_{wi}=18%).

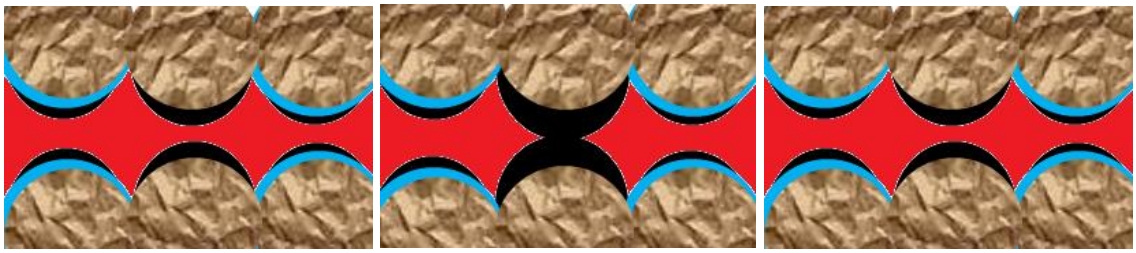

Figure 4-17: pore level distribution of different phases in small pores of mixed-wet core sample. From left to right shows the temporary formation of oil bridges which would collapse again as the gas injection and oil production continues. (brown: grains; dark: oil; blue: water; red: gas); 65mD, mixed-wet, Drainage.

Figure 4-16 shows the effect of wettability on the oil and gas relative permeability curves for the experiments with immobile water saturation. As can be seen from this figure, oil relative permeability has decreased for the mixed-wet core compared to the water-wet system. This can be explained using the same discussion which has already been provided for oil recovery. The same Figure shows that the gas relative permeability has also decreased for the mixed-wet system compared to the water-wet sample. Figure 4-17 shows the pore level distribution of different phases in the small pores of the mixed-wet system. As mentioned, the conductivity of the wetting oil layers would be less than the spreading oil layers. The oil saturation increases at these points

(non-water wet pores) and there is a chance of the layers bridging if the oil saturation is high enough (or pore throats are small enough). These bridges are not stable since local oil saturation at this pore would decrease by feeding the adjacent spreading oil layers, and as a result would collapse again (due to very low IFT and capillary pressure between oil and gas phases). Although the gas would not be trapped inside the pore body as a result of this evidence, its relative permeability would decrease. For further discussions regarding to the formation and collapse of these liquid bridges and their possible effects on relative permeability refer to Williams and Dawe (1988) and Dawe and Grattoni (2007).

4.3.5 Effect of Wettability on Oil Injection

A similar comparison to what was carried out above for the gas injection (drainage) experiments has been carried out in this section to investigate the effect of wettability alteration on the performance of oil injection (imbibition). Figure 4-18 compares the recovery of the gas by oil injection in the 65 mD core for the water-wet and mixed-wet systems. The oil breakthrough in the water-wet rock is slightly delayed compared to that in the mixed-wet rock. The same graph also shows that the ultimate recovered gas achieved for the mixed-wet core is lower compared to the case of water-wet core. This can also be explained on the basis that in the mixed-wet core, presence of partly wetting oil layers and partly spreading layers reduces the conductivity of the oil layers compared to the water-wet system in which oil phase is connected all the way through the highly conductive spreading layers. Lower conductivity of the layers in mixed-wet systems results in the accumulation of the oil in locations where the oil phase is present as wetting layers. As the oil injection continues and the oil saturation inside the core increases, there is a high chance for these layers to bridge at the pore throats and snap-off the gas phase inside the pore body (Figure 4-19). For the case of water-wet rock, due to the high conductivity of the oil spreading layers, larger oil saturation (compared to the mixed-wet system) would be required to thicken these layers and bridging at the pore throats (Figure 4-20). As a result, the process of gas snap-off would be delayed for water-wet systems compared to mixed-wet ones and higher gas recovery would be achieved. Figure 4-21 shows the effect of wettability on oil and gas relative permeability in the presence of immobile water. As can be seen from this figure, both the oil and gas relative permeability have decreased for the mixed-wet compared to the water-wet system, which is in agreement with the discussions already presented.

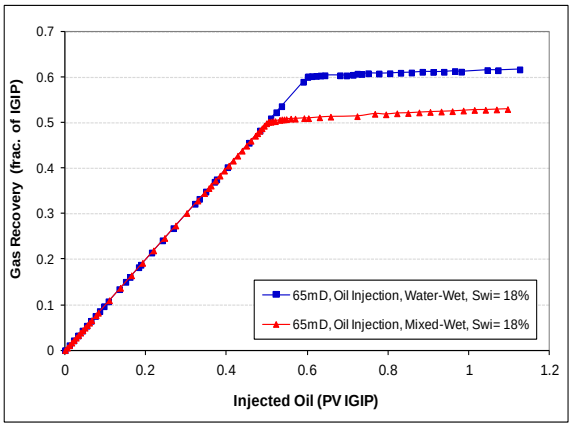

Figure 4-18: Effect of wettability on the performance of oil injection test (64mD, Imbibition, S_{wi}=18%)

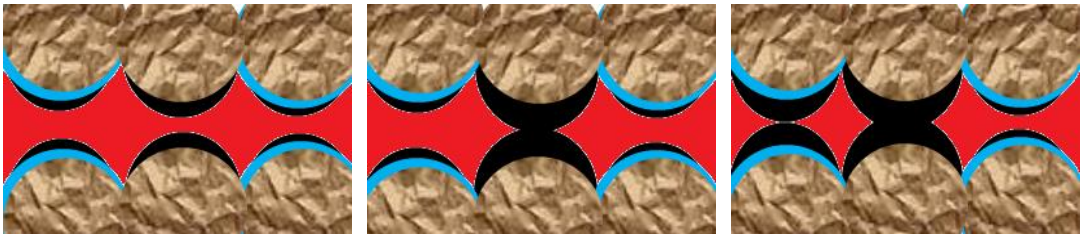

Figure 4-19: pore level distribution of different phases in small pores of mixed-wet core sample. From left to right shows the oil saturation increment and formation of stabilized oil bridges which would snap-off the gas phase inside the pore body. (brown: grains; dark: oil; blue: water; red: gas); 65mD, mixed-wet, imbibition.

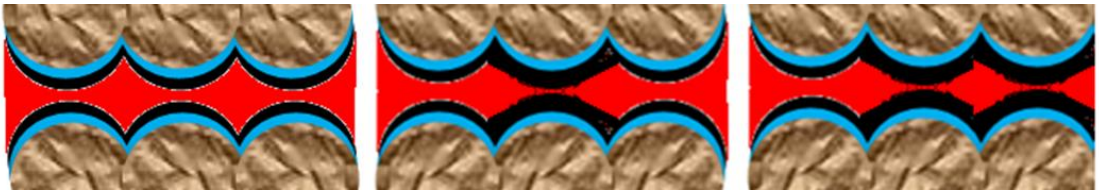

Figure 4-20: pore level distribution of different phases in small pores of water-wet core sample. From left to right shows the oil saturation increment. As the spreading layers are very conductive, formation of stabilized oil bridges (and as a result gas snap-off) would be delayed to larger saturations compared to mixed-wet system. (brown: grains; dark: oil; blue: water; red: gas); 65mD, water-wet, imbibition.

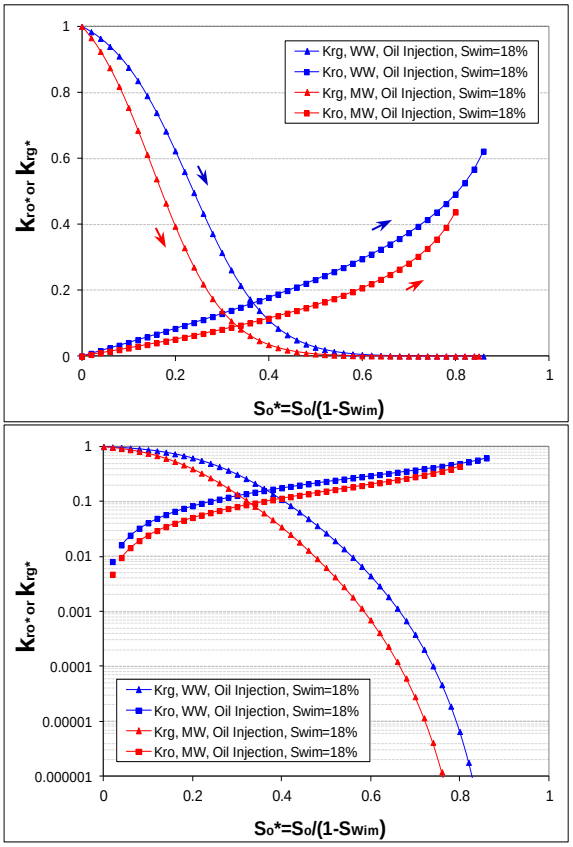

Figure 4-21: Effect of wettability on oil and gas relative permeability curves (65mD, Imbibition, S_{wi} = 18%).

4.3.6 Effect of Rock Permeability

Figure 4-22 shows the effect of wettability on the performance of gas injection for the 1000mD core. Comparing Figure 4-22 with Figure 4-14 (the 65mD core) shows that the effect of wettability is not significant in 1000mD. This is attributed to the higher permeability and larger pore sizes in the 1000mD core which decreases the effect of capillary forces. Figure 4-23 shows the hysteresis effect on oil and gas relative permeability bounding curves for the 1000mD mixed-wet rock. Comparing this Figure with Figure 4-13, which shows the corresponding k_r for the 65mD, mixed-wet core, one can conclude that although hysteresis effect is less for the high permeability (1000 mD) core, it cannot be ignored.

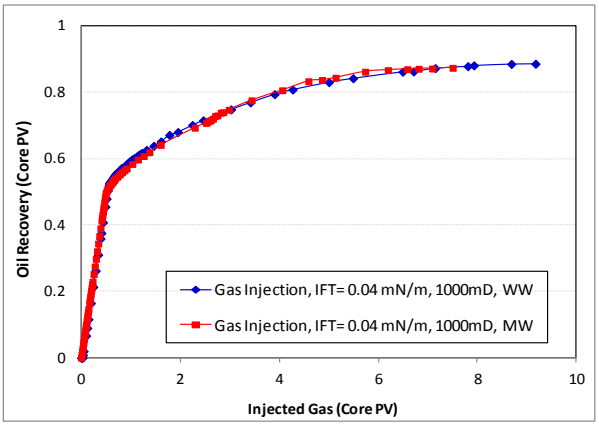

Figure 4-22: Effect of wettability on the performance of gas injection (1000mD, Drainage, S_{wi}=8%)

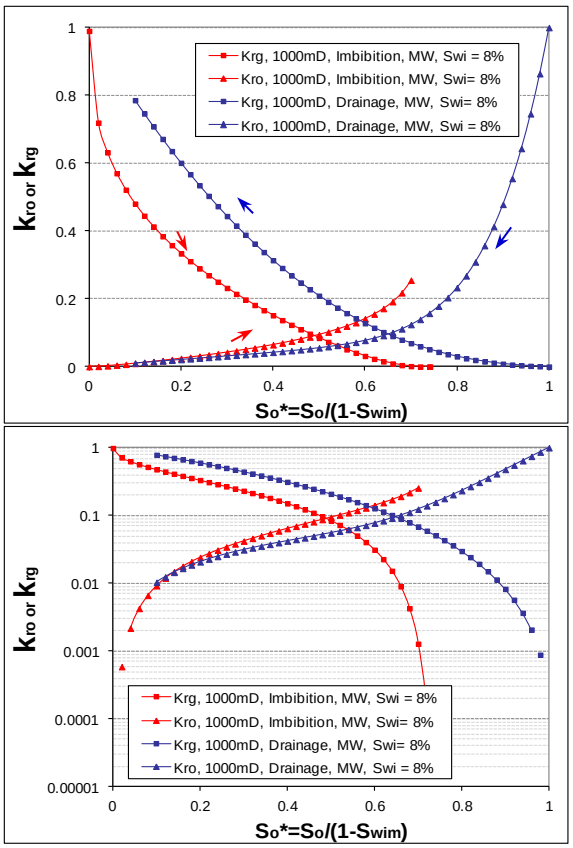

Figure 4-23: Hysteresis effect on bounding relative permeability curves in mixed-wet system for the 1000mD rock (drainage: blue; imbibition: red).

4.4 Conclusions

1. Current assumptions in the literature suggest that as a fluid system approaches miscibility, relative permeabilities of both phases, as a function of wetting-phase saturation, show linear behaviour and become diagonal lines. The results of this study show that only for non-wetting phase (gas), in drainage direction, this assumption is valid. However, for the two rocks tested in this work, the wetting phase relative permeability (oil), in both imbibition and drainage directions, and also the non-wetting-phase (gas) k_r in imbibitions direction, show significant deviation from this assumption even at the very low IFT of 0.04 $mN.m^{-1}$.

2. Based on the current assumptions in the literature, in the vicinity of miscibility, non-wetting phase relative permeabilities hysteresis diminishes and normally no hysteresis is assumed for the wetting-phase. The results presented here show that even at near-miscible conditions (IFT=0.04$mN.m^{-1}$), there is a significant hysteresis for both the non-wetting-phase (gas) and the wetting-phase (oil), in both the high permeability (1000mD) and the low permeability (65mD) rocks.

3. Low IFT liquid/liquid systems should not be used as an analogue for low IFT gas/liquid (oil) systems. The behaviour of these two systems and the involved displacement mechanisms are different and that explains why in this study significant k_r hysteresis was observed at low gas/oil IFT but other researchers using a low IFT liquid/liquid system as an analogue for low IFT gas/oil systems have not reported k_r hysteresis.

4. In agreement with literature data, hysteresis was much higher for non-wetting phase (gas) compared to the wetting-phase (oil).

5. Hysteresis for both the wetting- and non-wetting phases were less in the highly permeable core (1000mD) compared to the 65mD core sample.

6. Current assumptions in the literature also suggest that as long as connate water is immobile it does not influence the relative permeability of the phases. The presented investigation in this study shows that the effect of connate water on wetting-phase relative permeability (oil) is not significant if the k_r data is presented based on the oil (wetting phase) saturation. However, the effect of

connate water saturation on the non-wetting phase (gas) was significant and should not be ignored. This effect was more profound in gas injection (drainage) compared to oil injection (imbibitions). This shows the importance of performing SCAL (k_r) tests with representative connate water saturation (for near-miscible conditions). More study regarding the effect of connate water saturation is recommended.

7. In water-wet systems, the effect of hysteresis on relative permeability was slightly less when connate water was present compared to the cases where there was no connate water present in the rock.

8. Relative permeability of both the wetting and non-wetting phases (oil and gas) in the mixed-wet systems reduced compared to the water-wet systems. The reduction was observed for both imbibition and drainage directions. This shows the importance of performing SCAL tests under representative wettability of the reservoir rock (for near-miscible conditions and in the presence of immobile water saturation).

4.5 References

Agbalaka C.; Dandekar A.Y., Patil S.L., Khataniar S., and J.R. Hemsath, (2008): The Effect of Wettability on Oil Recovery: A Review, SPE-114496, presented at SPE Asia Pacific Oil and Gas Conference and Exhibition, 20-22 October, Perth, Australia.

Akin S. and Kovscek R., (2003): Computed Tomography in Petroleum Engineering Research (in Applications of X-ray Computed Tomography in the Geosciences), Geological Society Special Publications, 215, pp. 23-38.

Al-Wahaibi Y.M., Grattoni C.A., Muggeridge A.H., (2006): Drainage and imbibition relative permeabilities at near miscible conditions, Journal of Petroleum Science and Engineering, volume 53, issue 3-4, pp. 239–253.

Asar H. and Handy L.L., (1988): Influence of Interfacial Tension on Gas/Oil Relative Permeability in a Gas-Condensate System, SPE Reservoir Engineering, Volume 3, Number 1, pp. 257-264.

Bardon C., Longeron D.G., (1980): Influence of Very Low Interfacial Tensions on Relative Permeability, SPE Journal, Volume 20, Number 5, pp. 391-401.

Blom S.M.P., Hagoort J., Soetekouw D.P.N., (2000): Relative Permeability at Near-Critical Conditions, SPE Journal, Volume 5, Number 2, pp. 172-181.

Burger, J.E., Bhogeswara, R., Mohanty, K.K. (1994): Effect of Phase Behavior on Bypassing in Enriched Gasfloods, SPE Reservoir Engineering, Volume 9, Number 2, pp. 112-118.

Cahn, J.W; (1977): Critical Point Wetting, Journal of Chemical Physics, Volume 66, Number 8, pp. 3667-3672.

Chatzis, I., Kantzas, A., Dullien, F.A.L., (1998): On the Investigation of Gravity-Assisted Inert Gas Injection Using Micromodels, Long Berea Sandstone Cores, and Computer-Assisted Tomography, SPE 18284, SPE Annual Technical Conference and Exhibition, 2-5 October, Houston, Texas.

Dawe R.A. and Grattoni C.A. (2006), Fluid Flow Behaviour of Gas-Condensate and Near-Miscible Fluids at the Pore Scale, Journal of Petroleum Science and Engineering, Volume 55, Issues 3-4, pp. 228-236.

Dehghan A.A., Kharrat R., Ghazanfari M.H., Farzaneh S.A., (2009): Studying the Effects of Pore Geometry, Wettability and Co-Solvent Types on the Efficiency of Solvent Flooding to Heavy Oil in Five-Spot Models, SPE-123315, Asia Pacific Oil and Gas Conference & Exhibition, 4-6 August, Jakarta, Indonesia.

Delclaud J., Rochon J., and Nectoux A., (1987): "Investigation of Gas/Oil Relative Permeabilities: High Permeability Oil Reservoir Application", SPE 16966, presented at SPE Annual Technical Conference and Exhibition, Dallas.

Delshad M., Lenhard R.J., Oostrom M., and Pope G.A., (2003): A Mixed-Wet Hysteretic Relative Permeability and Capillary Pressure Model for Reservoir Simulations, SPE Reservoir Evaluation & Engineering, Volume 6, Number 5, pp. 328-334.

Gray J.D. and Dawe R.A., (1991): Modeling Low Interfacial Tension Hydrocarbon Phenomena in Porous Media, SPE Reservoir Engineering, Volume 6, Number 3, pp. 353-359.

Harbert, L.W., (1983): Low Interfacial Tension Relative Permeability, SPE-12171, presented at SPE Annual Technical Conference and Exhibition, 5-8 October, San Francisco, California.

Hartman K.J., and Cullick A.S., (1994): Oil Recovery by Gas Displacement at Low Interfacial Tension, Volume 10, pp. 197-210.

Henderson G.D., Danesh A., Tehrani D.H., Peden J.M., (1997): The Effect of Velocity and Interfacial Tension on Relative Permeability of Gas Condensate Fluids in the Wellbore Region, Journal of Petroleum Science and Engineering, Volume 17, Issues 3–4, pp. 265–273.

Henderson, G.D., Danesh, A., Tehrani, D. H., Al-Shaidi, S., Peden, J.M., (1998): Measurement and Correlation of Gas Condensate Relative Permeability by the Steady-State Method, SPE-30770 , SPE Reservoir Evaluation & Engineering, Volume 1, Number 2, pp. 134-140.

Hubbert M.K., (1956): Darcy's Law and the Field Equations of the Flow of Underground Fluids, SPE-749-G, Petroleum Transactions, AIME, Volume 207, pp. 222-239.

Hustad O.S. and Browning D.J., (2010): A Fully Coupled Three-Phase Model for Capillary Pressure and Relative Permeability for Implicit Compositional Reservoir Simulation, SPE-125429, SPE Journal, Volume 15, Number 4, pp. 1003-1019.

Jamiolahmady, M., Danesh, A., Tehrani, D.H., Duncane, D.B., (2000): A Mechanistic Model of Gas-Condensate Flow in Pores, Transport in Porous Media, Volume 41, pp. 17–46.

Jerauld G.R., (1997): Prudhoe Bay Gas/Oil Relative Permeability, SPE-35718, SPE Reservoir Engineering, Volume 12, Number 1, pp. 66-73.

Jerauld G.R. and Rathmell J.J., (1997): Wettability and Relative Permeability of Prudhoe Bay: A Case Study in Mixed-Wet Reservoirs, SPE Reservoir Engineering, Volume 12, Number 1, pp. 58-65.

Kalaydjian, F.J.M. (1992): Performance and Analysis of Three-Phase Capillary Pressure Curves for Drainage and Imbibition in Porous Media, SPE 24878, SPE Annual Technical Conference and Exhibition, 4-7 October, Washington, USA.

Kalaydjian F, Vizika O, Moulu J. and Munkerud P.K., (1995): The Role of Wettability and Spreading in Gas Injection Processes under Secondary Conditions, from De Hann H.J. (ed.): New developments in Improved Oil Recovery, Geophysical Society Special Publication, No. 84, pp. 63-71.

Knopp C.R., (1956): "Gas-Oil Relative Permeability Ratio Correlation from Laboratory Data", JPT, Volume 17, Number 9, pp. 1111-1122.

Lomeland F., Ebeltoft E., Thomas W.H., (2005): A New Versatile Relative Permeability Correlation, SCA2005-32, presented at the International Symposium of the Society of Core Analysts, 21-25 August, Toronto, Canada.

Narahara G.M., Pozzi A.L., Blackshear T.H., (1993): "Effect of Connate Water on Gas/Oil Relative Permeabilities for Water-wet and Mixed-Wet Berea Rock", SPE Advanced Technology Series, Volume 1, Number 2, pp. 114-122.

Oren P.E.; Billiotte J.; Pinczewski W.V., (1992): Mobilization of Waterflood Residual Oil by Gas Injection for Water-Wet Conditions, SPE Formation Evaluation, Volume 7, Number 1, pp. 70-78.

Oren P.E., and Pinczewski W.V., (1994): The Effect of Wettability and Spreading Coefficients on the Recovery of Waterflood Residual Oil by Miscible Gasflooding, SPE 24881, SPE Formation Evaluation, Volume 9, Number 2, pp. 149-156.

Owens W.W., Parrish D.R., and Lamoreaux W.E., (1956): "An Evaluation of Gas Drive Method for Determining Relative Permeability Relationship", Petroleum Transactions, AIME, Volume 207, pp. 275-280.

Pande, J.B., Orr, F.M. Jr., (1990): "Analytical Computation of Breakthrough Recovery for CO2 Floods in Layered Reservoirs", SPE 20177 SPE/ODE symposium on enhanced oil recovery, Tulsa, Oklahoma.

Saeidi, A. and Handy, L.L., (1974): Flow and Phase Behavior of Gas Condensate and Volatile Oils in Porous Media, SPE 4891, presented at SPE California Regional Meeting, 4-5 April 1974, San Francisco, California.

Salathiel, R.A., (1973): Oil Recovery by Surface Film Drainage in Mixed-Wettability Rocks, Journal of Petroleum Technology, Volume 25, Number 10, pp. 1216-1224.

Schechter D.S. and Haynes J. M., (1992): Relative Permeabilities of a Near Critical Binary Fluid, Transport in Porous Media, Volume 9, Number 3, pp. 241-260.

Shyeh-Yung JJ. and Stadler M.P., (1995): "Effect of Injection Composition and Pressure Displacement of Oil by Enriched Hydrocarbon Gases", SPE Reservoir Engineering, Volume 10, Number 2, pp. 109-115.

Skauge, A., Eleri, O.O., Graue, A., and Monstad, P.A., (1994): "Influence of Connate Water on Oil Recovery by Gravity Drainage," SPE/DOE 27817, presented at the SPE/DOE 9th Symposium on Enhanced Oil Recovery, Tulsa, 17-20 April.

Skauge A. and Ottesen B., (2002): A Summary of Experimentally Derived Relative Permeability and Residual Saturation on North Sea Reservoir Cores, SCA2002-12, presented at the International Symposium of the Society of Core Analysts, Monterey, California, September 23-35.

Sohrabi M., Danesh A., Tehrani D.H. and Jamiolahmady M., (2008a): "Microscopic Mechanisms of Oil Recovery By Near-Miscible Gas Injection", Transport in Porous Media, Volume 72, Number 3, pp. 351-367.

Sohrabi M., Danesh A. and Jamiolahmady M., (2008b): "Visualisation of Residual Oil Recovery by Near-miscible Gas and SWAG Injection Using High-pressure Micromodels", Transport in Porous Media, Volume 74, Number 2, pp. 239-257.

Sohrabi M., Tehrani D.H. and Al-Abri M.; (2007): Performance of Near-Miscible Gas and SWAG Injection in a Mixed-Wet Core, SCA 2007-26, presented at International Symposium of the Society of Core Analysts held in Calgary, Canada, 10-12 September.

A. Sylte, E. Ebeltoft and E.B. Petersen, (2004): Simultaneous Determination of Relative Permeability and Capillary Pressure Using Data from Several Experiments, SCA2004-17, presented at the International Symposium of the Society of Core Analysts, 5-9 October, Abu Dhabi, UAE.

Spiteri E.J., and Juanes R., (2006): Impact of relative permeability hysteresis on the numerical simulation of WAG injection, Journal of Petroleum Science and Engineering, Volume 50, Issue 2, pp. 115-139.

Thomas, F.B, Holowach, N., Zhou, X., Bennion, D.B., Bennion, D.W., (1994): Miscible or near-miscible gas injection, which is better?, SPE 27811, SPE/DOE Symposium on Improved Oil Recovery, 17-20 April, Tulsa, Oklahoma.

Thomas F. B., Erian A., Zhou X., Bennion D.B., Bennion D.W., Okazawa T., (1995): Does Miscibility Matter In Gas Injection?, Petroleum Society of Canada Annual Technical Meeting, Jun 7 - 9, Calgary, Alberta.

Vizika O. and Lombard, J.M., (1996): Wettability and Spreading: Two Key Parameters in Oil Recovery With Three-Phase Gravity Drainage, SPE Reservoir Engineering, Volume 11, Number 1, pp. 54-60.

Williams J.K. and Dawe R.A., (1988): Photographic Observation of Unusual flow Phenomena in Porous Media at Interfacial Tensions below 0.1 mN/m, Journal of Colloid and Interface Science, Volume 124, Number 2, pp. 691-696.

Wylie P. and Mohanty K.K., 1997, Effect of water saturation on oil recovery by near-miscible gas injection, SPE Reservoir Engineering, Volume 12, Number 4, pp. 264-268.

5. Hysteresis Effect in Different Two-Phase Systems (Gas-Oil, Gas-Water and Oil-Water) at Mixed-Wet Condition

Accurate determination of relative permeability values and their hysteresis behavior is crucial for obtaining a reliable prediction of the performance of water-alternating-gas (WAG) injection in oil reservoirs. The current approach in the industry (except hysteresis model proposed by Larsen and Skauge) is to use two-phase bounding imbibition and drainage relative permeabilities along with a two-phase hysteresis model (Land, Carlson or Killough) and input the result to a three-phase correlation such as Stone-I, Stone-II or Baker to simulate hysteresis in WAG injection. Recent three-phase models which incorporate the effect of hysteresis (ODD3P proposed by Hustad) are based on two-phase relative permeabilities under cyclic hysteresis. Application of ODD3P model requires relative permeabilities for all possible two-phase systems (gas/oil, oil/water and gas/water systems) under such saturation histories. This chapter reports comprehensive series of two-phase relative permeability curves obtained from coreflood experiments carried out in a mixed-wet core for water/gas, water/oil and oil/gas systems. The experimental results show that current assumption in the literature (such as in Land, Carlson and Killough models) which assumes that the relative permeability for scanning drainage curves would follow the values of the former imbibition period is not valid. The results suggest that for mixed-wet systems, it is necessary to consider irreversible hysteresis loops for both the wetting and non-wetting phases. Such capability currently does not exist in reservoir simulators due to lack of appropriate predictive tools.

The first part of the chapter studies oil/gas system under a very low oil/gas interfacial tension (IFT) of 0.04 $mN.m^{-1}$. The first set of the corefloods began by oil injection (imbibition) in the core saturated with gas and immobile water (S_{wi}). This was followed by a period of gas injection (drainage) and this sequential injection of oil and gas continued and in total, three imbibition and two drainage periods were carried out (IDIDI). In the second series of experiments, the core was initially saturated with oil and

immobile water and the experiment started with a gas injection followed by cycles of drainage and imbibitions (DIDID). The measured pressure drop and production data were history matched through simulation analysis to obtain k_{rg} and k_{ro} values for each of the imbibition and drainage cycles. The results show that both the oil and the gas relative permeability curves show cycle-dependent hysteresis despite the very low gas/oil IFT. Therefore, the current assumption in existing hysteresis models (such as Land, Carlson and Killough) that the drainage scanning k_r curves follow the preceding imbibition curve is not supported by the coreflood experiments performed in this study. When compared to the experimentally measured data, Carlson model predictions for k_{rg} in imbibition direction are poor. Killough model predictions underestimate k_{rg} and overestimate k_{ro} especially near trapped gas saturation regions. Beattie *et al.* hysteresis model is able to capture the k_{rg} and k_{ro} behavior that is observed in the performed experiments qualitatively, but it is still unable to predict the observed hysteresis quantitatively.

The second part of this chapter, reports two series of gas/water k_r hysteresis curves obtained from corefloods under mixed-wet conditions. The first set began by water injection (imbibition: I) in the core saturated with hydrocarbon gas and immobile water. Then, the injection of gas (Drainage: D) and water continued sequentially and in total, three imbibitions and two drainages were carried out (IDIDI). In the second series, the core was initially 100% saturated with water and the experiment started with drainage (gas injection) followed by successive imbibitions (water) and drainages (DIDIDI) periods. The measured pressure drop and production data were history matched to obtain k_{rg} and k_{rw} values for each imbibition and drainage. The results show cycle-dependent hysteresis for both k_{rg} and k_{rw} curves. Therefore, the current assumption in existing hysteresis models that the drainage scanning curves follow the preceding imbibition curve is not supported by experimental results of the present study. Historic behaviour of both k_{rg} and k_{rw} is qualitatively different for these two series of experiments. This shows that unlike water-wet systems, relative permeability historic behaviour in mixed-wet system can be a function of injection scenario (saturation history). In the IDIDI series, both k_{rg} and k_{rw} decreased as the alternation between imbibition and drainage injection continued. In the DIDID series, no significant hysteresis was observed for k_{rw}, but k_{rg} in drainage cycles were higher than the corresponding values in preceding imbibition cycles. In addition to WAG injection, the results presented for gas/water system and the conclusions drawn also have applications

in underground hydrocarbon gas storage which usually involves cyclic pressurization (drainage) and depressurization (imbibition) on annual basis.

The last part of this chapter, reports a series of oil/water relative permeabilities hysteresis curves obtained from corefloods under mixed-wet conditions. The core was initially saturated with water and the experiment started with oil injection (Drainage, D) followed by successive water injections (Imbibition, I) and drainages periods (DIDIDI). Contrary to the behaviour of water-wet systems, for this mixed-wet system, k_{rw} shows hysteresis during alternation between imbibition and drainage, and for each hysteresis loop the imbibition k_{rw} values are less than those of the previous drainage period. As the alternation between imbibition and drainage periods continues, the effect of hysteresis on k_{rw} becomes less and hysteresis loops become smaller. k_{ro} shows significant hysteresis for the 1st imbibition period compare to the 1st drainage period. It was found that as the alternating injection between imbibition and drainage continues, k_{ro} curves approach to the k_{ro} obtained during the primary waterflooding and k_{rw} curves approach to the primary drainage k_{rw} curve. The observed oil/water k_r hysteresis behaviour is also compared with those of water/gas system (for the same wettability condition). The results show significant differences in the k_r behaviour in these two systems and demonstrates that the current approach in the industry where for three-phase flow simulation oil-water k_r curves are often used instead of gas-water k_r values (which are not normally measured) is not valid and can lead to significant errors in prediction of reservoir simulators.

5.1 Introduction

In two-phase systems, the entire wetting phase remains continuous through the smaller pores. As the wetting phase saturation increases, it invades the next larger pores and traps some of the non-wetting phase in the pores which are invaded. Since some of the pores of the size occupied by the wetting phase contain trapped non-wetting phase, for a particular saturation, some of the wetting fluid must occupy pores of a larger size than it would occupy if there was no trapped non-wetting phase saturation. As a result wetting phase relative permeability for imbibition increases compared to the drainage case. For the same reason (entrapment of non-wetting phase) non-wetting phase imbibition relative permeability would be less than the case of drainage process. The greater the amount of entrapment, the greater is the reduction of the non-wetting phase relative

permeability for imbibition process. This means that relative permeability is a function of saturation history as well as saturation values. In other terms, the relative permeability to a fluid at a given saturation depends on whether that saturation is obtained by approaching it from a higher or lower value. This behaviour in relative permeability is known as the hysteresis effect.

The effect of saturation history on the values of relative permeabilities was first mentioned by Geffen *et al.* (1951) and Osoba *et al.* (1951). Both these works have been performed on the core samples with the native wettability of the reservoir (probably non-strongly water-wet). Geffen *et al.* investigated the effect of saturation history for relative permeability bounding curves in gas/water and oil/water systems. They concluded that for these two systems, relative permeabilities of both phases are not a single valued function of saturation. They discussed that saturation history affects the statistical distribution of the phases in the pore spaces which leads to the difference of the fluids conductivity between imbibition and drainage. It was observed that in the case of water/oil system, hysteresis effect was much larger for non-wetting phase (oil) compared to the wetting phase (water). The same was true for water/gas (air) system, in which hysteresis effect was larger for gas compared to water.

Osoba et al. (1951) experiments for bounding relative permeability curves in oil/gas (kerosene/helium) system showed the same results that the relative permeability for both phases are subject to hysteresis; Their measured relative permeability values showed hysteresis for both oil (wetting) and gas (non-wetting) phases. Oil relative permeability for imbibition was higher than drainage, while for gas, drainage relative permeability was larger than imbibition ones. Hysteresis effect was larger for non-wetting phase (gas) compared to the wetting phase (oil).

According to the literature, it is believed that for two-phase systems, hysteresis is more severe in the relative permeability to the non-wetting phase than the wetting phase. Land (1971) concluded from the results of imbibition relative permeability measurements that both directions of saturation change give equivalent results and assumed that imbibition relative permeabilities are reversible. Land (1968) stated that the hysteresis in the wetting phase relative permeability is very small, and thus difficult to distinguish from normal experimental error. For this reason Land (1971) assumed in

his hysteresis model, that for two-phase systems, characterizing the hysteretic behavior of the non-wetting phase relative permeability would be sufficient.

Figure 5-1 shows the schematic representation of Land's (1971) hysteresis model. The model does not take into account any hysteresis for the wetting phase. With regards to the non-wetting phase, hysteresis has been assumed only in imbibition direction and no hysteresis is assumed in drainage direction. This means that each drainage scanning curve would follow the preceding imbibition relative permeabilities (until turning point where it would follow the previous drainage curve). It should be mentioned that the original work of Land was performed for water/gas system under water-wet condition.

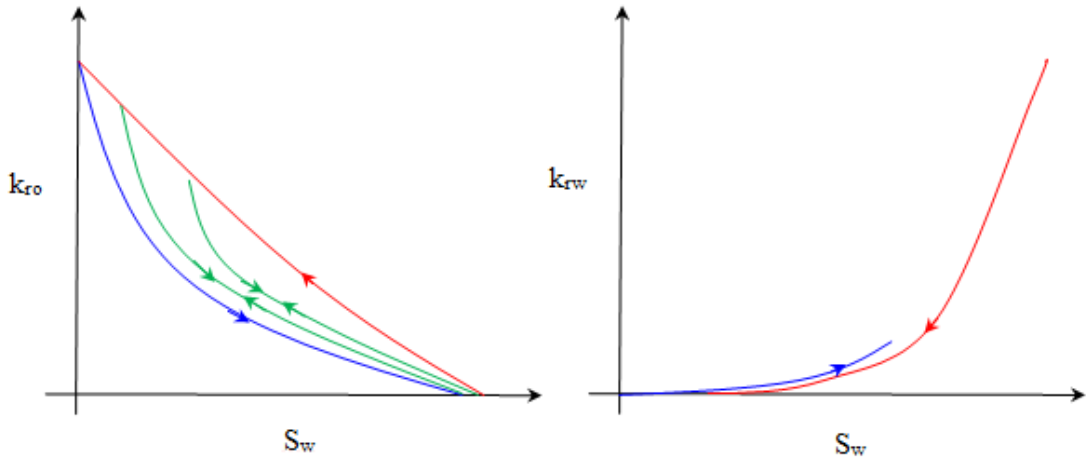

Figure 5-1: Schematic representation of Land and Carlson two-phase hysteresis models.

Killough (1976) proposed that each scanning curve can be determined by the point on the bounding curve where the reversal of the saturation direction occurred (turning point). According to his assumptions, experimental data are required only for the bounding imbibition and drainage curves, and the model provides an interpolation to the intermediate values (scanning curves). He proposed some regression parameters in his model to allow a closer match with the experimental scanning values in the case that such a data exist. What makes Killough model qualitatively different with Land model is the inclusion of hysteresis in the wetting-phase relative permeability in the case of imbibition cycles (Figure 5-2).

Although experimental observations by Evrenos and Comer (1969) and Colonna et al. (1972) supported the idea of non-reversibility of imbibition relative permeability, Killough concluded that within the accuracy of most reservoir simulations and with the

availability of the experimental data at that time, the assumption of reversible wetting phase relative permeability is not too restrictive. According to his model, once an imbibition process has begun, imbibition relative permeabilities will be traced even in the following drainage process, until the historical maximum non-wetting saturation has been reached. For non-wetting phase saturation greater than this maximum, non-wetting relative permeability follows the drainage function for the previous cycle (same as Land model). In Killough model, trapped non-wetting saturations are calculated using the expression derived by Land (1971).

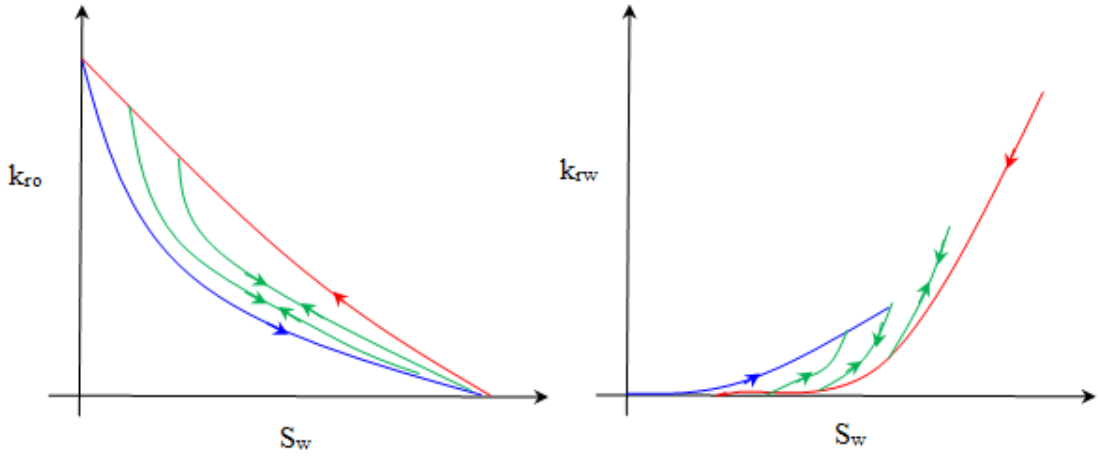

Figure 5-2: Schematic representation of Killough two-phase hysteresis model.

Carlson (1981) model does not assume any hysteresis for the wetting phase at all. With regards to the non-wetting phase relative permeability, Carlson model just assumes hysteresis for the change of injection path from drainage to imbibition, and subsequent drainage scanning curve would follow former imbibition values (same as Land and Killough models). Another assumption in Carlson model is that the curvature of non-wetting phase relative permeability, for imbibition scanning curve, would be the same (parallel) to the imbibition bounding curve. Carlson model has its own trapped non-wetting saturation formulation. As is shown in Figure 5-1, the hysteresis behaviour for relative permeability in Carlson model is qualitatively the same as Land model, the advantage of the Carlson model over Land model is its simplicity.

Much of the hysteresis data in the literature has been obtained with saturations starting at endpoint values (i.e., irreducible water saturation or residual oil saturations for water/oil system). Exceptions include the results reported by Colonna *et al.* (1972), in which the direction of saturation change was reversed at a number of intermediate saturations (cyclic hysteresis). Data such as these are more applicable to modeling

reservoir processes in which saturation of phases increase or decrease to an intermediate value, then change in the opposite direction. Examples include EOR methods such as water-alternating-gas (WAG) or Cyclic Steam Stimulation (CSS) injection.

Braun and Holland (1995), measured oil/water relative permeability cyclic hysteresis for a water-wet outcrop rock sample and a mixed-wet reservoir core. They concluded that for the oil phase, imbibition and drainage relative permeability bounding curves differ significantly. The difference was much less pronounced for the water phase relative permeability. They have also measured scanning curves as transitions between imbibition and drainage bounding curves. Similar relative permeability hysteresis behavior for oil phase was observed for both wettability conditions. The only difference was that hysteresis for the mixed-wet sample was more pronounced than for the water-wet one. Regarding reversibility of the scanning curves, they found that oil relative permeability changed reversibly (with almost no hysteresis) in the saturation range represented by the scanning curves. It should be mentioned that the range of saturation change for the k_{ro} measurement in their experiment was limited to just 10%, which usually is not expected to show much hysteresis anyway. Water relative permeability was found to be reversible over the entire ranges.

Beattie *et al.* (1991) were first to develop a relative permeability hysteresis model for cyclic injection scenarios. In their model, relative permeability scanning curves always lie on or between imbibition and drainage bounding curves. Their original work was developed for cyclic steam stimulation (CSS) process, and was proposed for water/oil systems. The approach was to define bounding imbibition and drainage relative permeabilities curves with common end points. When a saturation reversal occurs, the model calculates a scanning curve and defines how the relative permeability will move toward the appropriate bounding curve (Figure 5-3). The scanning curve exponent in their formulation determines how rapidly permeability approaches the bounding curve after a flow reversal. These values are usually very difficult to determine and have been used as history matching parameters in their original work. Beattie *et al.* expressed that the best type of exponents are those that allow relative permeability curves to move rapidly towards the drainage bounding curves but slowly towards the imbibition bounding curve. The obtained relative permeabilities therefore tend to be closer to the drainage bounding curve than the imbibition bounding curve in much of the saturation

range. As is shown in Figure 5-3, using Beattie *et al.* model, hysteresis can be applied to both wetting and non-wetting phases.

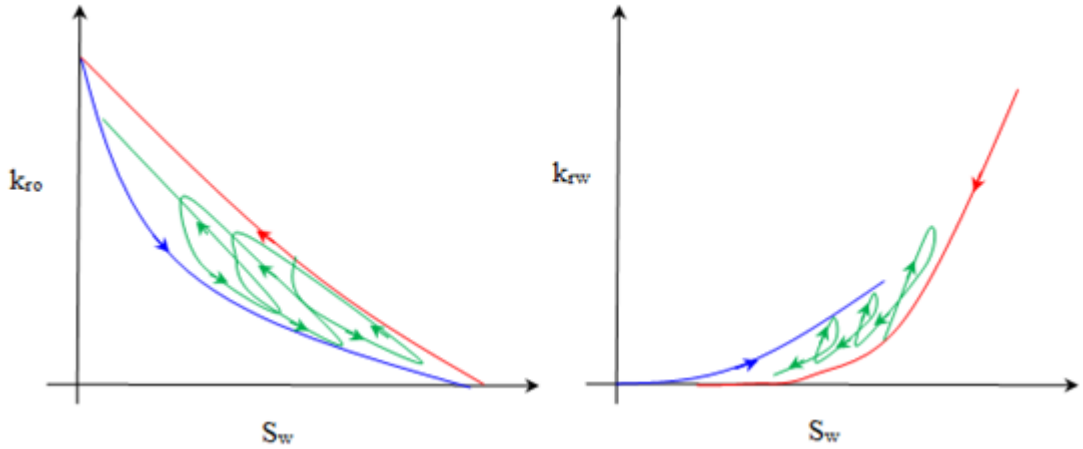

Figure 5-3: Schematic representation of Beattie et al. hysteresis model.

In addition to saturation and saturation history, reservoir rock wettability also plays an important role in relative permeability and their hysteretic behaviour (Morrow, 1990; Rao *et al.* 1992). The majority of the existing relative permeability hysteresis functions have been developed for strongly water-wet porous media (Land, Killough, Carlson, Beattie *et al.*). However, it is generally accepted that many oil reservoirs are mixed-wet (Jerauld and Rathmell, 1997; Salathiel, 1973; Delshad *et al.* 2003). According to the Salathiel and Delshad *et al.* in a mixed-wet system, the oil-wet pores correspond to the largest pores in the rock, and the smallest pores are water-wet. There are only a few relative permeability models developed for mixed-wet porous media (Delshad *et al.*, 2003; Kjosavik *et al.*, 2002).

Kjosavik *et al.* (2002) presented a two-phase relative permeability correlation for mixed-wet rocks, which was inferred from their earlier capillary pressure correlation (Skjaeveland *et al.*, 2000). The functional form is symmetric with respect to fluid-dependent properties since in a mixed-wet environment, neither fluid has priority to be the wetting phase. As a result, according to their formulation, both water and oil relative permeabilities show similar hysteretic behavior in a mixed-wet system. The advantage of their formulation is that all scanning curves are modeled by the same constants as the bounding curves. Their formulation allows that oil drainage bounding curve lies below or above the bounding oil imbibition curve, to appreciate different observations reported in the literature. The advantage of the Beattie *et al.* model compared to the Kjosavik *et al.* is its simplicity in formulation and the fact that in Beattie *et al.* model scanning curves should not necessarily form closed loops. Figure 5-4 shows a schematic behavior

of relative permeability curves according to Kjosavik *et al.* model. Both Kjosavik *et al.* and Delshad *et al.* presented two-phase hysteretic models for oil/water systems.

Literature of measured data on gas/oil systems is limited to the data reported by Jerauld (1997), in which there is no study on hysteresis effects. The measured data presented in this chapter is the first work of its own kind which tackles the relative permeability cyclic hysteresis behavior in different two-phase systems under mixed-wet conditions. In addition, the oil/gas system used in this study was at near-miscible conditions (very low interfacial tension of 0.04mN.m^{-1}), which adds to the novelty of the present work.

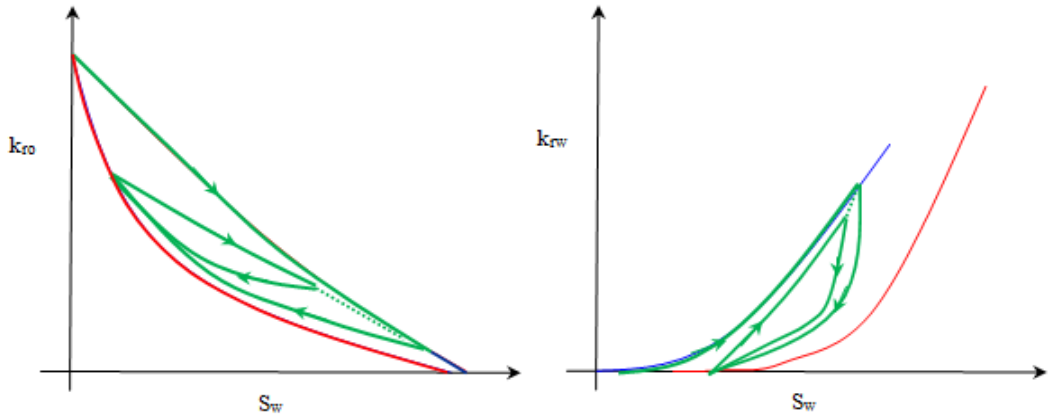

Figure 5-4: Schematic representation of Kjosavik et al. hysteresis models (the case in which k_{ro} for bounding drainage is below bounding imbibition curve).

5.2 Oil/Gas System:

The current assumptions in the literature suggest that as the miscibility is approached the hysteresis between relative permeabilities for the non-wetting phase diminishes, and usually no hysteresis is assumed for the wetting-phase (Bardon and Longernon, 1980). However, the studies presented in previous Chapter, showed that even at near-miscible conditions (IFT=0.04 mN.m^{-1}), there is a significant saturation history dependency for both the non-wetting phase (gas) and the wetting-phase (oil). This was the motivation for the present work to further investigate the effect of cyclic hysteresis for oil/gas systems under mixed-wet condition. These two-phase relative permeability data (in the presence of immobile water as the third phase) are also of interest for reliable simulation of the processes involving cyclic changes between imbibition and drainage displacement including Water-Alternating-Gas (WAG) injection. The experimentally derived relative permeability curves are used to investigate the performance of the common hysteresis models (Killough and Carlson) available in commercial simulators such as ECLIPSE and CMG. These models are widely used for inclusion of hysteresis

effects in the simulation of the WAG injection process (Spiteri *et al.*, 2006). The hysteresis model proposed by Beattie *et al.* has been also investigated (although it is not available in any commercial simulator), since it's the only hysteresis model which has been designed to capture the cyclic hysteresis behaviour. The experimental data have also been used to investigate non-wetting trapping models such as Land, Carlson.

5.2.1 Coreflood Experiments

DIDID Displacements Experiment:

This series of tests started with a gas injection into the core saturated with oil and 18.2% immobile water saturation. This gas injection period (Drainage, D) was followed by an oil injection period (Imbibition, I). The periods of gas and oil injections were repeated and in total three gas injections and two oil injections periods were carried out one after another. Therefore, this series of fluid displacements is here referred to as DIDID (Drainage-Imbibition-Drainage-Imbibition-Drainage).

1st Gas Injection (DIDID):

After establishing the immobile water saturation of 18.2% (S_{wim}=18.2 %PV), the first gas injection period began with the rate of 50 $cm^3.hr^{-1}$ and after 0.68 PV injections, rate of injection ramped to 100 $cm^3.hr^{-1}$. The increment in injection rate performed to extend the saturation interval in the experiment and as a result, to estimate more reliable relative permeability values. It should be mentioned that separate studies showed that recovery profile and estimated relative permeabilities are not rate dependent in this interval. Injection continued for an extended period until around 10 PV of gas had been injected. The residual oil saturation at this point was approximately 17%. It should be mentioned that no water production was observed during the gas injection period which confirms that the water in the core was immobile.

1st Oil Injection (DIDID):

After the first gas injection period as explained above, the first oil injection period started through the core at the rate of 50 $cm^3.hr^{-1}$ (S_{wim}=18.2%, S_{org}=17.8%, S_{gi}=64%). The injection of oil at this rate continued for more than 2 PV at which time the rate of gas production from the core dropped to practically zero and the trapped gas saturation was around 22%.

2nd Gas Injection (DIDID):

The sequential injection of gas and oil continued with another period of gas injection. At the start of this stage the saturations of fluids in the core were: S_{wim}=18.2%, S_{oi}=59.8%, S_{gr}=22%. Gas injection started with the rate of 50 $cm^3.hr^{-1}$ and after 0.40 PV injections, rate of injection ramped to 100 $cm^3.hr^{-1}$. What was different in this 2nd gas injection period (compared to the 1st gas injection cycle) was that there was no distinct gas breakthrough point since the pressure drop across the core started to decrease from the very beginning of the gas injection. Gas production from the core starts just slightly after the start of the gas injection. At this stage of the experiment, after 6 PV of gas injection, residual oil saturation (S_{org}) in the core was 25%.

2nd Oil Injection (DIDID):

The experiment continued by another oil injection period at the rate of 50 $cm^3.hr^{-1}$ (S_{wim}=18.2%, S_{or}=25%, S_{gi}=56.8%). As was the case in the previous oil injection period (1st oil injection), the gas recovery continued (albeit at a very slow rate) even after the oil BT. After around 2 PV of oil injection, the trapped gas saturation (S_{gt}) in the core was around 10%.

3rd Gas Injection (DIDID):

The last stage of this series of oil and gas displacements was the 3rd cycle of gas injection which starred with S_{wim}=18.2%, S_{oi}=72.8, and S_{gr}=10%. The same as the previous gas injection cycle, coreflood started with the rate of 50 $cm^3.hr^{-1}$ and after 0.40 PV injections, rate of injection ramped to 100 $cm^3.hr^{-1}$. Again, compared to the results of the 1st gas injection cycle, there was no distinct gas breakthrough and the gas production began shortly after the start of the gas injection (this behaviour was the same as what was observed in the 2nd gas injection cycle). After around 2 PV of gas injection through the core, and at the end of this gas injection, residual oil saturation (S_{org}) in the core was approximately 50%.

IDIDI Displacements Experiment:

In the previous set of experiment (the DIDID tests), fluid displacements began with the core initially saturated with oil (and immobile water, S_{wi}). In this series of displacements, a similar procedure was followed but the experiment began with the core saturated with gas rather than oil (and immobile water). Similarly to the previous displacements series (DIDID) the objective of this series of oil and gas displacements was to investigate and determine the effect of cyclic hysteresis for gas/oil systems under near-miscible (low-IFT) and mixed-wet conditions. Also, by comparing the results with

those of the previous set of displacements (DIDID), the effect of saturation history can be assessed further. This means that one can compare the scanning curves relative permeability for drainage and imbibition processes for these two experiments in which the initial saturations are the same (yet the history of reaching to that specified saturation would be different). The result of this comparison would show whether or not in two-phase oil/gas systems, saturation history affects scanning relative permeabilities the same way that it does bounding relative permeabilities. This second series of experiments started with an oil injection into the gas-saturated core (the core also contained 18.2% immobile water saturation). This was followed by two cycles of successive injection of gas and oil. Based on the order of oil and gas injection, this experiment is referred to as IDIDI (Imbibition-Drainage-Imbibition-Drainage-Imbibition).

1st Oil Injection (IDIDI):

The experiment began by saturating the core (containing immobile water, S_{wim}=18.2%) with the gas at 1840 psia. Then, the oil was injected through the core at the rate of 50 $cm^3.hr^{-1}$. The oil injection continued until the rate of gas production was practically zero. Similarly to the oil injection periods in the case of DIDID series, gas recovery continues (albeit at a very slow rates) even after the oil BT. At the end of this 1st oil injection period (after around 1.6 PV of oil injection), trapped gas saturation (S_{gt}) in the core was around 32%.

1st Gas Injection (IDIDI):

At the end of the preceding oil injection period, the experiment continued with a period of gas injection with the core containing S_{wim}=18.2%, S_{oi}= 49.4, and S_{gr}=32.6%. Gas injection started with the rate of 50 $cm^3.hr^{-1}$ and after 0.40 PV injections, rate of injection ramped to 100 $cm^3.hr^{-1}$. Similarly to the 2nd and the 3rd gas injection in the case of DIDID experiment, the pressure drop decreases from the beginning of the gas injection cycle and gas production started just slightly after the start of the test. After 5.2 PV of gas injection, residual oil saturation inside the core was approximately 17%.

2nd Oil Injection (IDIDI):

The experiment continued with another oil injection period at the rate of 50 $cm^3.hr^{-1}$ (S_{wim}=18.2%, S_{or}=17.5%, S_{gi}=64.3%). The oil injection continued until the rate of gas production was practically zero. Again the same as the previously mentioned oil injections, gas recovery continues (although at a very smaller rates) after the oil

breakthrough. After around 1.8 PV of oil injected, trapped gas saturation (S_{gt}) was equal to 20%.

2nd Gas Injection (IDIDI):

This series of oil and gas displacements continued with another oil injection period starting at S_{wim}=18.2%, S_{oi}=61.4%, and S_{gr}=20.4%. Gas injection started with the rate of 50 $cm^3.hr^{-1}$ and after 0.20 PV injections, rate of injection ramped to 100 $cm^3.hr^{-1}$. The same as the 1st gas injection cycle in this series and the 2nd and the 3rd gas injection cycles in the DIDID series, there was no distinct breakthrough and the gas was produced from the outlet of the core just shortly after the gas injection started. After around 5.6 PV of gas injection, the residual oil saturation was 25% PV.

3rd Oil Injection (IDIDI):

This series of fluid displacement tests finished with another period of oil injection at the rate of 50 $cm^3.hr^{-1}$. After 1.1 PV of oil injection, the 3rd oil injection cycle was stopped at which time the trapped gas saturation (S_{gt}) was approximately 20%.

5.2.2 Results and Discussion

In this section k_r determination for these experiments are discussed. A black-oil coreflood simulator (SENDRA) was used in this exercise to history match the core flood results in order to obtain k_r curves. Using these k_r curves, the effect of hysteresis will be discussed. As an example and to show the quality of the history matching, Figure 5-5 shows experimental and simulated data for the pressure drop across the core, gas recovery and oil production for the 1st gas injection period in the IDIDI series. The jump in pressure drop data is due to an increase made in injection rate during the experiment to extend the saturation change interval. Although the tail end of Dp and recovery did not match perfectly but in general Figure 5-5 shows a good match between simulation and experiment which is important for reliable estimation of the relative permeabilities curves by this method. It should be mentioned that there were simulations with better matches for Dp and oil production at the end tail, however this simulation was chosen as the best match. The reason is that this coreflood (1st gas injection in DIDIDI injection sequence) is a part of cyclic injection scenario, and the obtained set of relative permeabilities in this simulation was in the best agreement with the relative permeabilities for the rest of the corefloods both quantitatively and qualitatively (shape of the relative permeabilities). Nevertheless the tail end mismatch is very small (3 cm^3 = 1.3 % PV).

Bounding Relative Permeabilities

k_r values of the 1st drainage period in the DIDID series and the 1st imbibition period of the IDIDI series are in fact representative of bounding drainage and imbibition curves respectively. Figure 5-6 shows bounding curves for the imbibition and drainage relative permeabilities for this oil-gas system (in presence of S_{wi}). As discussed in Chapter 4, current assumptions in the literature suggest that as system approaches miscibility, the hysteresis between relative permeabilities for the non-wetting phase diminishes, and usually no hysteresis is assumed for the wetting-phase. The presented results in this study clearly show that even at near-miscible conditions of the performed experiments (IFT= $0.04 mN.m^{-1}$), there are significant hysteresis effects for both the non-wetting-phase (gas) and the wetting-phase (oil). In agreement with literature data, the observed hysteresis is much larger for non-wetting phase (gas) compared to wetting-phase (oil). Imbibition relative permeability for oil is larger than drainage values, and the gas relative permeabilities for imbibition are less than the drainage cycle (which is also consistent with experimental results in literature).

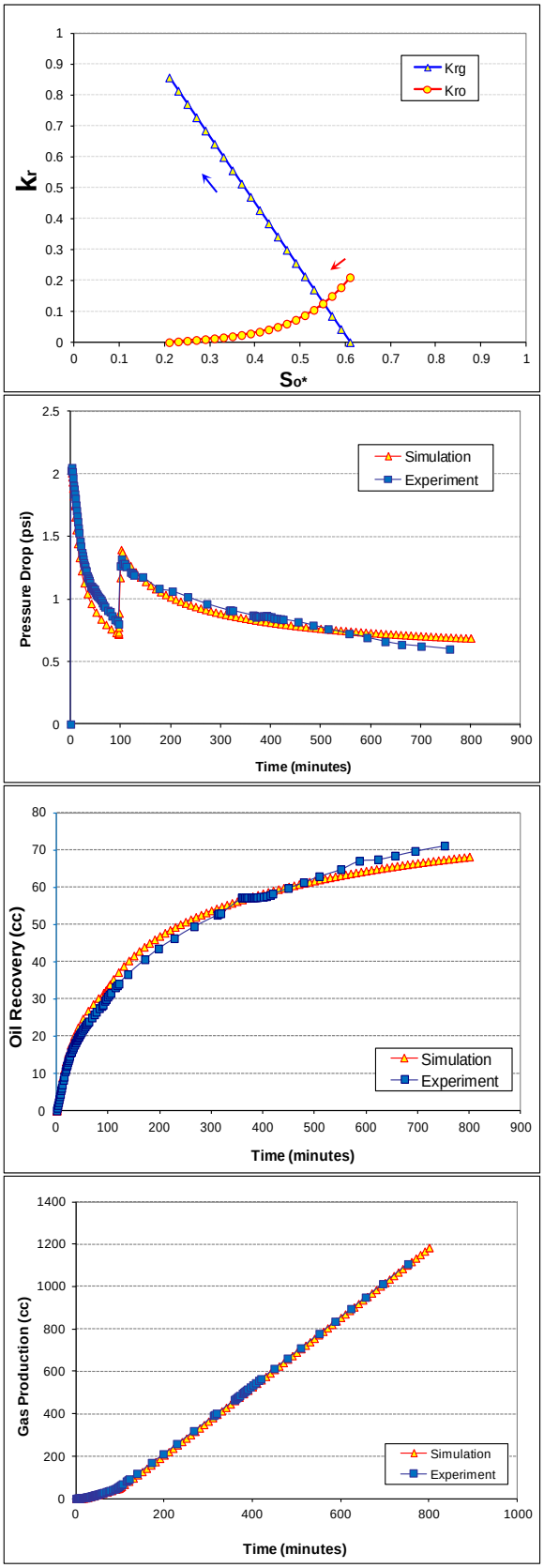

Figure 5-5: Estimated relative permeabilities and history matched data (pressure drop, gas recovery and oil production) for the 1st Gas Injection in the IDIDI experiment (65mD, mixed-wet).

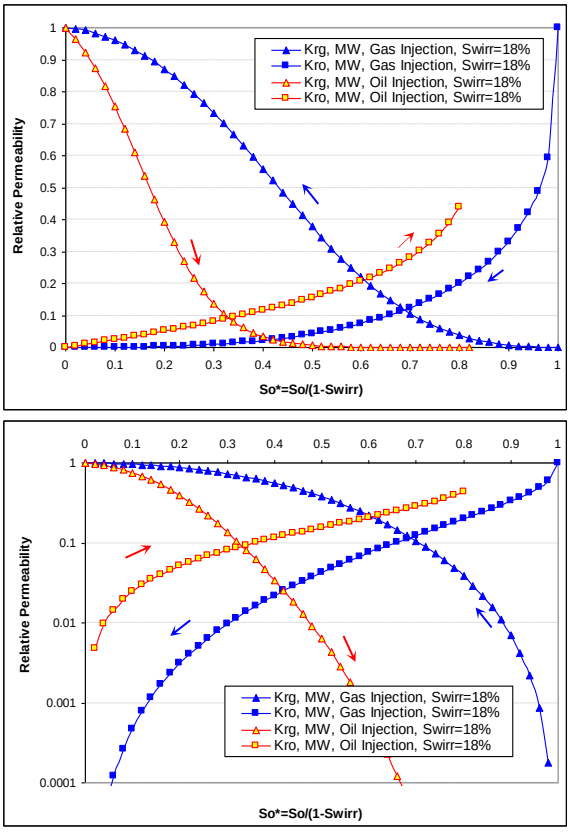

Figure 5-6: Oil and gas bounding relative permeabilities (65 mD, mixed-wet).

Experimental Scanning Relative Permeability Curves:

DIDID Experiment

Figure 5-7 shows the evolution of cyclic hysteresis effect on oil phase relative permeability in the DIDID experiment. For the sake of completeness, the imbibition bounding curve (1st oil injection of IDIDI) has also been shown by the dashed lines. The process starts with bounding drainage curve (1st gas injection) in which normalized oil saturation has decreased from 1 to 0.2. At this point, the drainage process has stopped and imbibition (oil injection) started.

Changing the direction of flow, oil relative permeability follows a new curve (red line) which lies between the previous drainage curve (bounding drainage) and the bounding imbibition curve. Scanning oil relative permeability for this imbibition is parallel to the bounding imbibition curve. Separate simulations show that the relative permeability data from the former drainage period would not match this imbibition displacement. Imbibition process stopped at normalized oil saturation of around 0.73 and another drainage displacement started in which normalized oil saturation decreased to about 0.3 (light blue curve). An important conclusion here is that the current assumption in common models such as Carlson and Killough that relative permeabilities for a drainage

displacement after an imbibition would follow those of the preceding imbibition cycle is not valid based on these experimental results; and relative permeabilities of 2nd drainage lies below the previous imbibition displacement. Scanning drainage relative permeability starts from the previous imbibition curve and sharply approaches the bounding drainage curve, and then follows the same (or quite close) values as the bounding drainage curve. As a result, it can be stated that relative permeabilities move rapidly toward the drainage bounding curves but slowly toward the imbibition scanning curve. The obtained relative permeabilities therefore tend to be closer to the drainage bounding curve than the imbibition bounding curve throughout the saturation range. This is in agreement with the assumptions made by Beattie *et al.* in their cyclic hysteresis model. Relative permeabilities of the subsequent imbibition period (2nd oil injection; red triangles) follow those of the previous drainage for a large saturation interval, which shows that cyclic hysteresis effect is less at this stage of the experiment.

An important observation here is that at normalized oil saturation of around 0.73 which is the turning point (change of displacement direction from 1st imbibition to 2nd drainage) for this hysteresis loop (2nd drainage and 2nd imbibition), the oil relative permeability is not equal to the values of the former drainage curve (at the same saturation). This means contrary to the Kjosavik *et al.* model, successive imbibition and drainage cycles do not necessarily make a closed loop. In fact, in cyclic hysteresis behaviour, as the alternation between imbibition and drainage displacements continues, the effect of hysteresis for the wetting phase relative permeability would be less. As a result, in the later stages of the injection, the wetting phase relative permeability for the successive imbibition and drainage cycles deviate from closed loop behaviour. It should be mentioned again that in Beattie *et al.* model, relative permeabilities should not necessarily make a closed loop. Figure 5-7 shows that for the last stage of this experiment (3rd gas injection; light green curve) there is no hysteresis compared to the 2nd imbibition displacement.

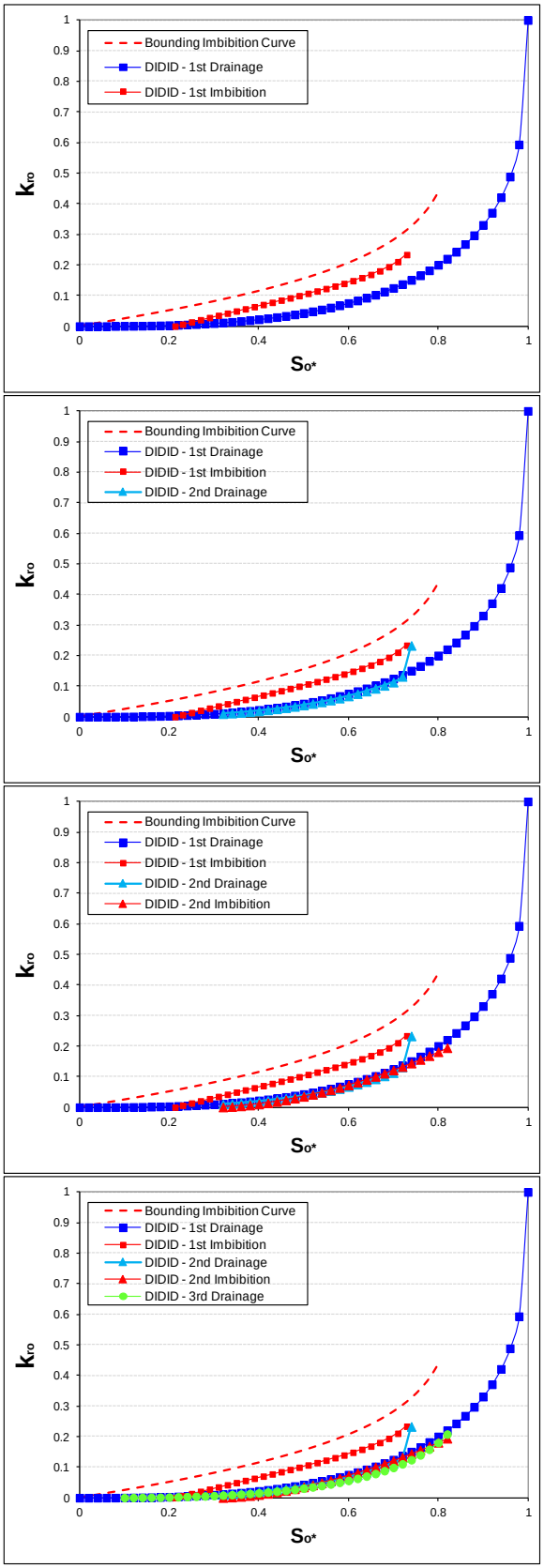

Figure 5-7: Oil phase relative permeability hysteresis for gas/oil DIDID experiment (65 mD, mixed-wet).

Figure 5-8 shows the cyclic hysteresis effect on the gas phase relative permeability in the DIDID experiment. For the sake of completeness, the same as the oil phase, the imbibition bounding curve (1^{st} oil injection of IDIDI) has been also shown by dashed curve in this Figure. The displacements start with the bounding drainage curve (1^{st} gas injection; blue) in which normalized oil saturation has decreased from 1 to 0.25. At this point the drainage process stopped and the imbibition (oil injection) started. It should be mentioned that drainage data for normalized oil saturations lower than 0.25 are just extrapolation and do not represent history matched saturation interval. Changing the direction of injection to imbibition, gas relative permeability follows a new curve (red line) which lies between the former drainage curve (bounding drainage) and the bounding imbibition. Scanning gas relative permeability for this imbibition is parallel to the bounding imbibition curves with more or less the same curvature. This observation is in agreement with all of the hysteresis models in the literature (including those of Land, Carlson, Killough and Kjosavik *et al.*). The Imbibition process stopped at normalized oil saturation of around 0.73 and another drainage displacement started in which normalized oil saturation decreased to about 0.3 (light blue curve).

An important conclusion here (as in the case of oil relative permeability), is that the current assumption in models such as Land, Carlson and Killough, that the relative permeabilities for drainage displacement after imbibition would follow those of the preceding imbibition, is not the case based on these experimental results; and that the relative permeabilities of 2^{nd} drainage lie above the former imbibition displacement. This is a behaviour which is included in recently developed hysteresis models (Beattie *et al.* and Kjosavik *et al.*). The same as the oil phase relative permeability, the gas phase drainage scanning relative permeability starts from the previous imbibition curve and sharply approaches the bounding drainage curve, and follows the same (or at least quite close) values as the bounding drainage curve. Therefore, in addition to the oil phase, it can be stated that gas drainage relative permeabilities also move rapidly toward the drainage bounding curves but imbibition scanning relative permeability moves slowly toward the imbibition bounding curve. As is obvious by comparing Figure 5-7 and Figure 5-8, the hysteresis effect is more pronounced for gas phase relative permeability than oil phase. Gas relative permeabilities of the successive imbibition (2^{nd} oil injection; red triangles) would follow a new path, which is parallel to the bounding imbibition and 1^{st} scanning imbibition curves. As the initial gas saturation for this imbibition period is less than S_{gi} for the 1^{st} imbibition displacement, trapped gas saturation would be also

less. An important result here is that contrary to the oil phase relative permeabilities, k_{rg} values make a closed loop cycles for successive imbibition and drainage cycles (as is predicted by Kjosavik *et al.* model and can be predicted by Beattie *et al.*). Figure 5-8 shows that for the last stage of this experiment (3rd gas injection; light green). Again, the gas relative permeability does not follow the values of the former imbibition displacement. The same as the previous drainage scanning curve, the 3rd drainage relative permeability starts from the previous imbibition curve and sharply approaches to the bounding drainage curve, and then follows the same (or quite close) values as the bounding drainage curve.

IDIDI Experiment

Figure 5-9 shows oil relative permeability curves obtained from the series of IDIDI displacements. The Figure also shows the drainage bounding curve (1st gas injection in DIDID series). The general hysteresis behaviour of the oil phase is the same as what has been already discussed for the DIDID experiments. Here the displacements started with a bounding imbibition curve (1st oil injection; red) in which the normalized oil saturation increased from 0 to 0.6. At this point, the imbibition process was stopped and drainage (gas injection; blue) started. It should be mentioned that imbibition data shown for the normalized oil saturations larger than 0.6 are just extrapolation and do not represent history matched saturation interval. These data have been included for comparison with those of the following imbibition displacements. Similarly to the DIDID experiment, here also the relative permeability values of the drainage scanning curve do not follow the values of the previous imbibition displacement. The 1st drainage continued until the oil normalized saturation decreased to 0.2. At this point, another imbibition displacement started, and its relative permeability followed a new path (red curve) which lies above the previous drainage displacement. An interesting observation here is that relative permeability at the turning point (S_o^*=0.6) in which the flow direction changed from 1st imbibition to 1st drainage, is the same as the previous drainage relative permeability (at the same saturation). This means that the oil relative permeability hysteresis loop is closed at this stage of the experiment. As the oil injection continues and the oil saturation increases above S_o^*= 0.6, the 2nd imbibition relative permeability follows the trend of the 1st imbibition displacement (bounding curve). At the end of the 2nd imbibition, another drainage displacement started (dark blue). Similarly to the case of the DIDID experiments, here also the scanning drainage relative permeability curves sharply approached the bounding drainage curve and they remain

very close to it for a large range of saturation. Again, the scanning drainage curves do not follow those of the previous imbibition displacement (contrary to Killough model). Once the normalized oil saturation reached to 0.32, the drainage process was stopped and another imbibition displacement started (3rd imbibition; red rectangles). The main conclusion here is that contrary to the 1st hysteresis loop (1st drainage and 2nd imbibition), the 2nd hysteresis loop (2nd drainage and 3rd imbibition) is not a closed loop. This behaviour is similar to what has been already discussed for the DIDID experiments and is in contrast with the assumptions made in Kjosavik *et al.* hysteresis model. The only hysteresis model which is able to capture the open hysteresis loops is the one proposed by Beattie *et al*.

Figure 5-10 shows gas relative permeability derived from the IDIDI experiments. For the sake of completeness, the drainage bounding curve (1st gas injection of DIDID) is also shown. The general hysteresis behaviour of the gas phase is the same as what has been already discussed for the DIDID experiments. The process starts with the bounding imbibition curve (1st oil injection; red) in which the normalized oil saturation increases from 0 to 0.6. During this displacement, the gas relative permeability drops from 1 to near zero. At this point, the imbibition process was stopped and a drainage displacement (gas injection; blue) started. Similarly to the DIDID experiments, here also the relative permeability of the drainage scanning curve does not follow the values of the previous imbibition displacement. The 1st drainage displacement continued until the normalized oil saturation decreased to 0.2. At this point, another imbibition displacement started. The relative permeability of this imbibition displacement follows a new path (red curve) which lies below the previous drainage displacement and is almost parallel to the bounding imbibition curve. At the end of 2nd imbibitions, another drainage displacement began (dark blue). The same as in the case of DIDID experiments, here the scanning drainage relative permeability curves sharply approach the bounding drainage curve and remain very close to it for a large range of saturation. Again, the scanning drainage curves do not follow those of the previous imbibition displacement (in contrast with Land, Carlson and Killough models). Once the normalized oil saturation reached 0.32, the drainage process was stopped and another imbibition displacement started (3rd imbibition; red rectangles). The main conclusion here is that contrary to the oil phase, the gas relative permeabilities make closed hysteresis loops. The same behaviour was observed for gas in the DIDID experiments,

which is in agreement with Kjosavik *et al.* and Beattie *et al.* models for non-wetting phase hysteresis.

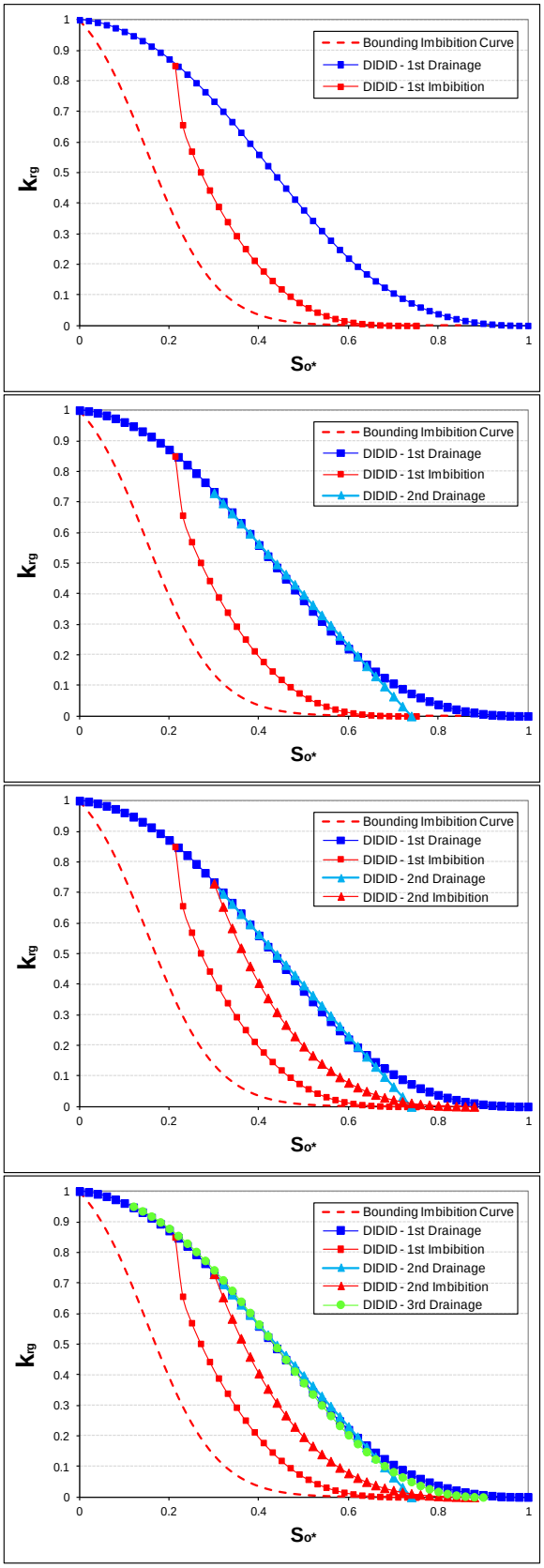

Figure 5-8: Gas phase relative permeability hysteresis for gas/oil DIDID experiment (65 mD, mixed-wet).

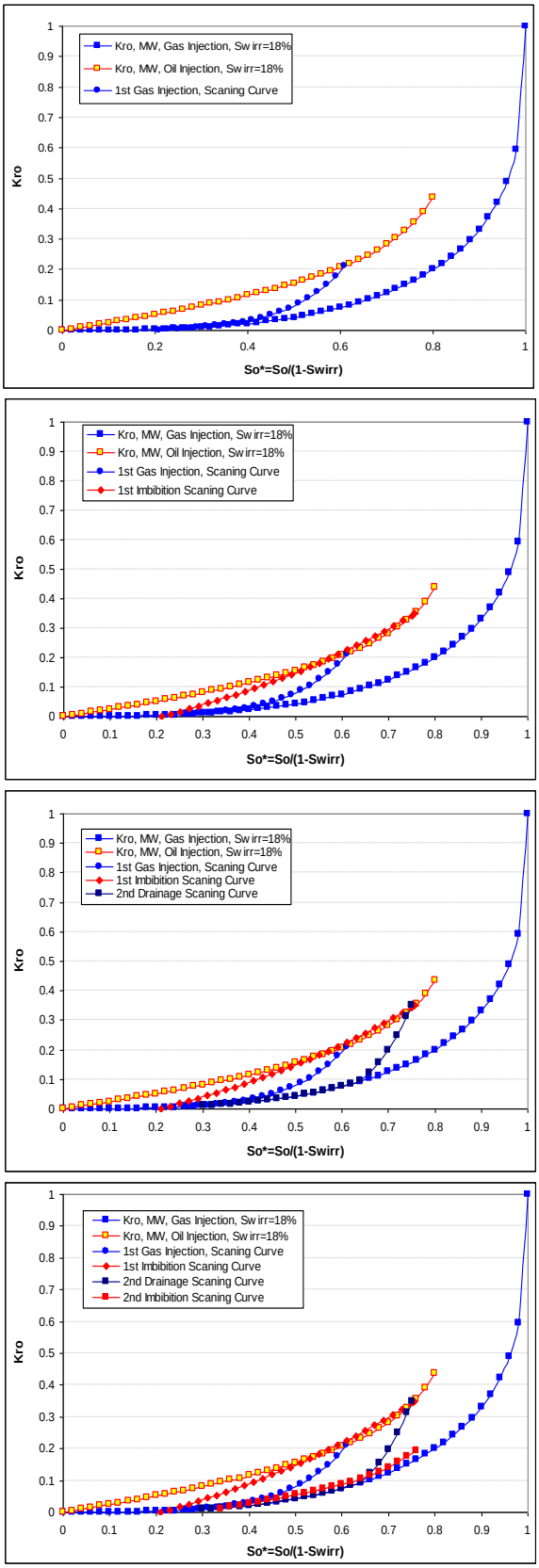

Figure 5-9: Oil phase relative permeability hysteresis for gas/oil IDIDI experiment (65 mD, mixed-wet).

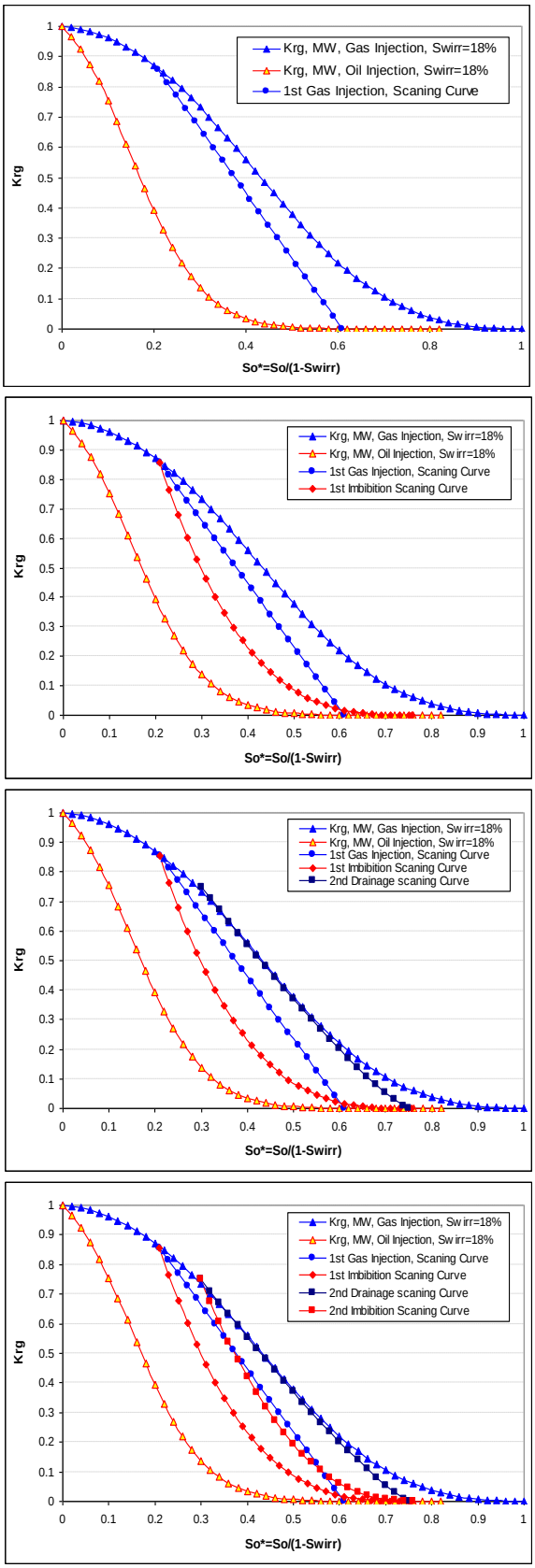

Figure 5-10: Gas phase relative permeability hysteresis for gas/oil IDIDI experiment (65 mD, mixed-wet).

Scanning Relative Permeability Curves: Assessment of Hysteresis Models

In this section predictions of some of the existing hysteresis models such as Carlson and Killough are evaluated against the experimentally derived data reported in the previous section (Figure 5-11 through Figure 5-18). As discussed earlier, both wetting (oil) and non-wetting (gas) phases show hysteresis during the flow reversal from imbibition to drainage and vice versa (drainage to imbibition). From theoretical point of view, Carlson model does not assume any hysteresis for the wetting phase (oil in this case) at all. For wetting phase relative permeability, Killough model just assumes hysteresis for change of saturation path from drainage to imbibition, and it assumes that the subsequent drainage period would not show any hysteresis and would simply follow the values of the preceding imbibition. For non-wetting phase relative permeability, Carlson model only assumes hysteresis for the change of flow path from drainage to imbibition, and the subsequent drainage scanning curve would follow former imbibition values. Another assumption in Carlson model is that it assumes that the trend of non-wetting phase relative permeability for imbibition scanning curves is the same (parallel) to the imbibition bounding curve (which is not quite supported by experimental observations in this study). Carlson model has its own trapped non-wetting phase saturation formulation that the author assessments (Chapter 8) show that it works quite well for the oil-gas system investigated in this study. Killough model hysteresis assumptions regarding the non-wetting phase hysteresis is the same as Carlson model, and the only difference is that the trapped non-wetting phase saturations (gas) would be predicted using Land's model along with a different formulation for the curvature of the scanning curve.

The assessments in Chapter 8 show that Land's model predictions overestimate experimentally measured trapped gas values. The value of trapped non-wetting phase saturation has a very significant effect on the accuracy of predicted relative permeabilities and as a result on oil recovery predictions. For example, although Killough model predictions seems to be very good in the 1st oil injection period of the oil-gas DIDID experiments (Figure 5-11), but (gas) recovery predictions are poor (underestimates) due to overestimation of the trapped gas value. Since neither Carlson nor Killough are able to adequately capture the observed k_r hysteresis behaviour, Beattie *et al.* hysteresis model was also evaluated (although this model is not included in commercial simulators). This model has been developed for oil-water systems and assumes hysteresis for both wetting and non-wetting phases in both imbibition and

drainage directions, which is qualitatively the same behaviour that it was observed for the oil-gas system here. The scanning curve exponents in their formulations (see Appendix at the end of this Chapter) determine how rapidly the relative permeabilities approach the bounding curves. These values are difficult to determine since they should be obtained through curve fitting of the experimental scanning relative permeability curves. Therefore, to be able to use Beattie *et al.* model one should have at least one scanning curve to be able to predict the rest of scanning curves. The performed assessment in this study for different imbibition and drainage cycles shows that although the general predictions of Beattie et al. model is better than Carlson and Killough, it loses its accuracy at the later stages of the experiment as the alternation between imbibition and drainage cycles continues. This means that the scanning curve exponents in their formulations, is not a constant value, and changes from cycle to the other.

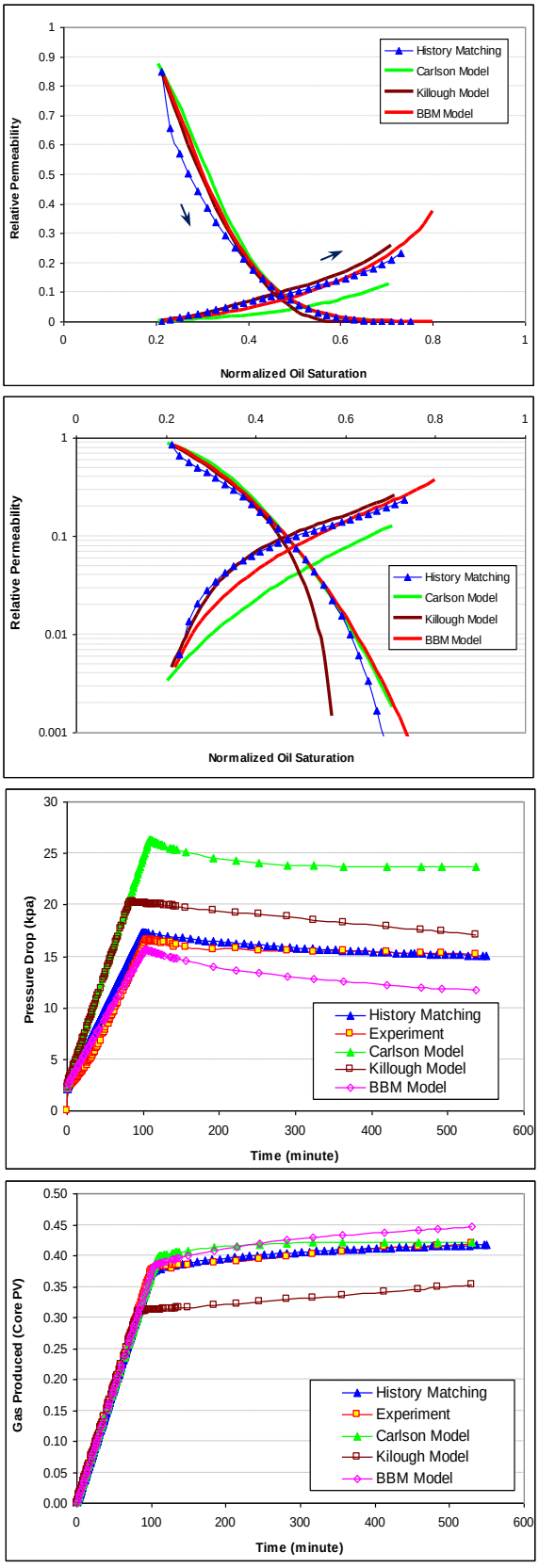

Figure 5-11: Experimental and predicted oil and gas relative permeability, pressure drop across the core and gas recovery for 1st oil injection of gas/oil DIDID experiment (65mD, mixed-wet).

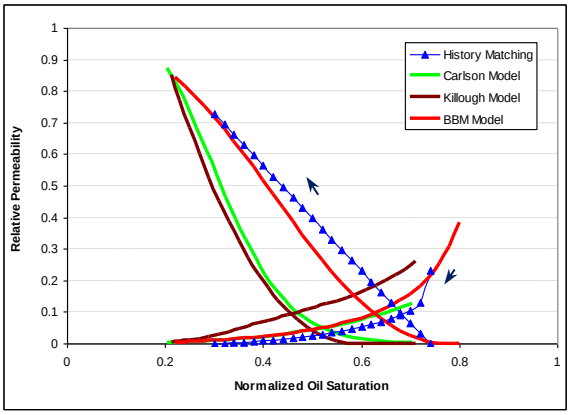

Figure 5-12: Experimental vs. predicted oil and gas relative permeabilities for 2nd gas injection of gas/oil DIDID experiment (65 mD, mixed-wet).

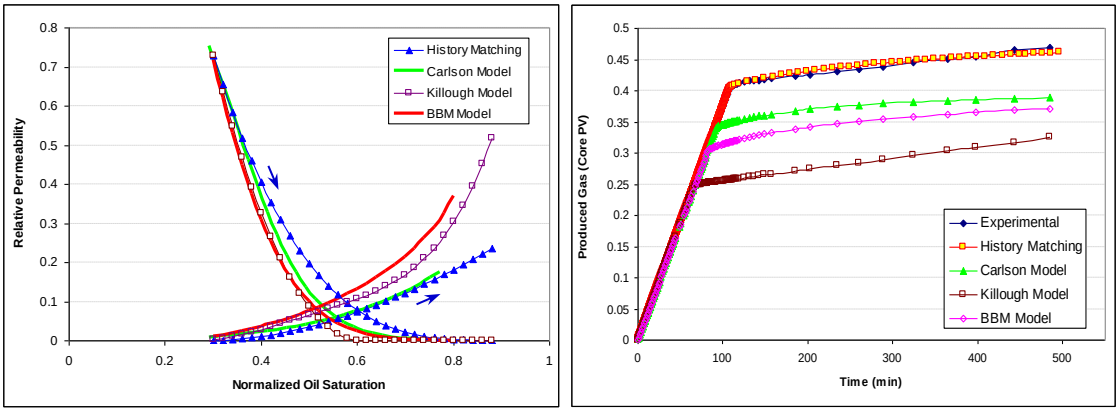

Figure 5-13: Experimental vs. predicted oil/gas relative permeability and gas recovery for 2nd oil injection of gas/oil DIDID test (65 mD, mixed-wet).

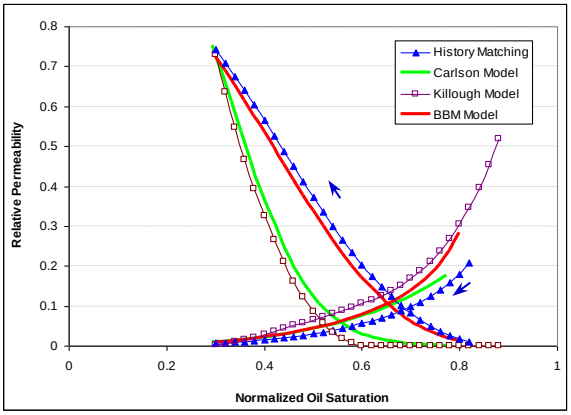

Figure 5-14: Experimental and predicted oil and gas relative permeabilities for 3rd gas injection of DIDID (65 mD, mixed-wet).

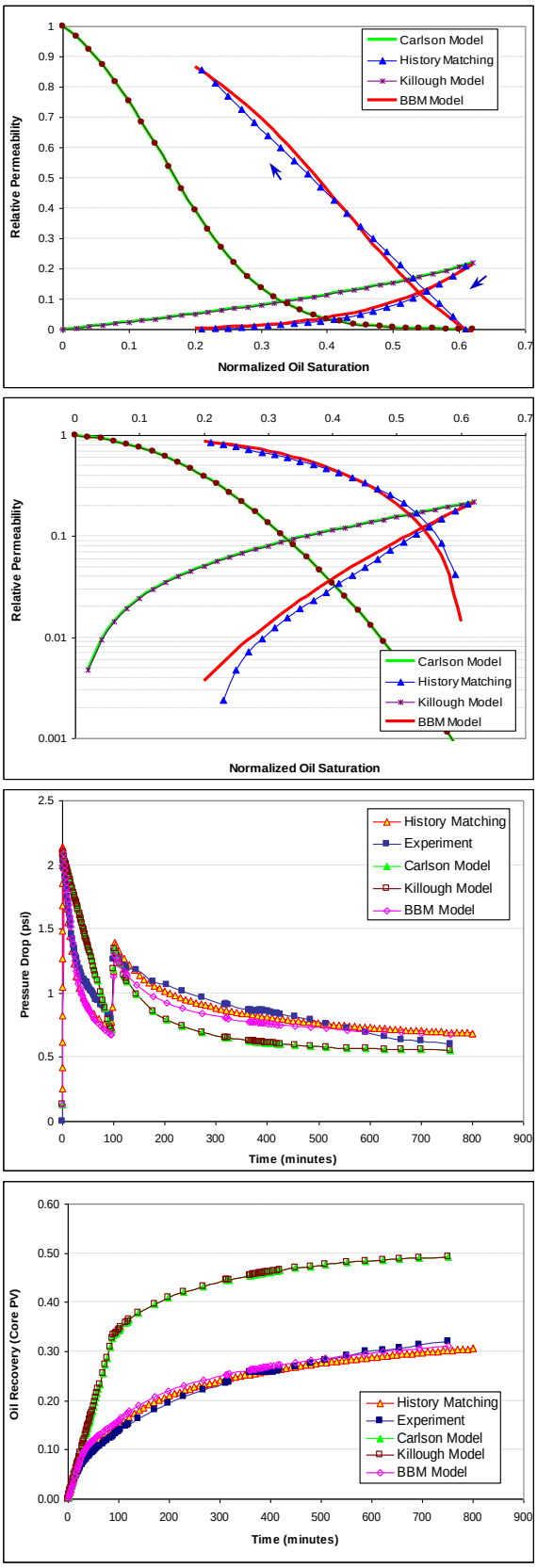

Figure 5-15: Experimental and predicted oil and gas relative permeabilities, predicted pressure drop and oil recovery for 1st gas injection of gas/oil DIDID experiment (65 mD, mixed-wet).

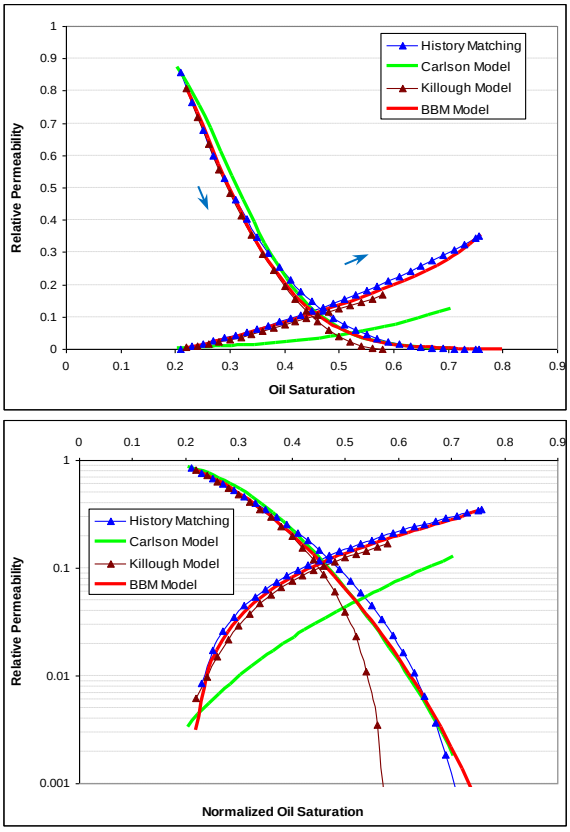

Figure 5-16: Experimental vs. predicted oil and gas relative permeabilities for 2nd oil injection of gas /oil IDIDI experiment (65 mD, mixed-wet).

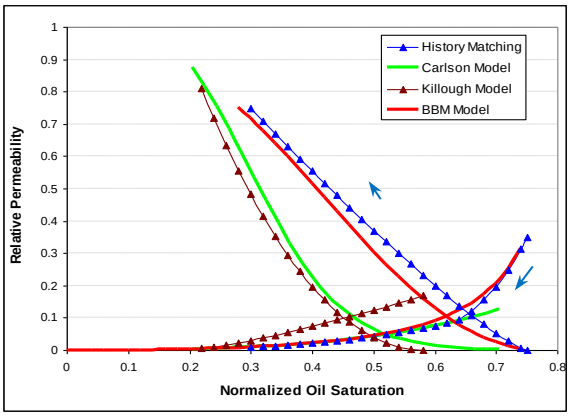

Figure 5-17: Experimental vs. predicted oil and gas relative permeabilities 2nd gas injection of gas/oil IDIDI experiment (65 mD, mixed-wet).

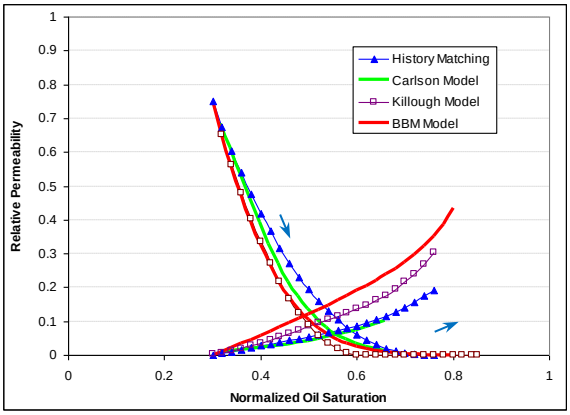

Figure 5-18: Experimental and predicted oil and gas relative permeabilities for 3rd oil injection of gas/oil IDIDI experiment (65 mD, mixed-wet).

5.2.3 Conclusions (Gas/Oil System)

This section presented two comprehensive series of gas/oil relative permeability curves obtained from history matching coreflood experiments carried out in a mixed-wet core using a gas-oil system with a very low IFT (nearly miscible). The core also contained immobile water (S_{wi}) and each set of the coreflood experiments consisted of a number of cycles of gas injections (drainage) and oil injections (imbibition). The results of the relative permeability curves were used to investigate the effects of hysteresis on gas/oil systems under the conditions of these experiments (near-miscible and mixed-wet condition).

The following conclusions can be drawn from the results of the experiments and the simulation work carried in this section:

- Despite a very low IFT (0.04 $mN.m^{-1}$) between the oil and gas, the k_r curves show significant hysteresis.
- Hysteresis is much less for wetting phase (oil) compared to the non-wetting phase (gas). This is consistent with the observations available in the literature.
- Although Carlson model predictions for the magnitude of trapped gas saturations are fair (Chapter 8), its predictions for non-wetting phase relative permeability (in imbibitions direction) were poor. This is attributed to the oversimplifying assumption in the model that the curvature of scanning imbibition curves is exactly the same as that of the bounding imbibition curve.
- Killough model predictions underestimate gas relative permeability as the oil saturation increases (especially near trapped gas saturation). This could be

because the Killough hysteresis model uses Land's model to estimate trapped gas saturation and Land's model overestimates trapped gas saturation based on the measured experimental results in this study (Chapter 8).

- Killough model overestimates the wetting phase relative permeability in imbibition, especially near the residual (trapped) gas saturation. This is again attributed to the overestimation of trapped gas saturation by Land's, which Killough model uses to predict trapped gas saturation.
- From the experimental data, it was observed that the oil and gas k_r curves show hysteresis in drainage direction compared to the preceding imbibition cycle. Neither Carlson nor Killough model predicts such behavior (neither for wetting phase nor for non-wetting phase).
- The results show that under conditions of performed experiments in study (very low gas/oil IFT and mixed-wet system), the relative permeabilities for both oil and gas phases form irreversible hysteresis loops.
- As the alternation of imbibition and drainage cycles continues, the cyclic hysteresis effects become less and at later stage the hysteresis for oil relative permeabilities diminish.
- Beattie *et al.* hysteresis model does consider hysteresis for wetting and non-wetting phases, and for both imbibition and drainage cycles. Presented assessment in this study shows that although qualitatively this model is able to capture the oil/gas relative permeability hysteresis behavior that was observed in in this study, but it is still unable to accurately predict the observed hysteresis quantitatively (which results in poor fluid recovery predictions), especially for the later cycles of imbibition and drainage.
- Based on the results, it is crucial that more flexible hysteresis models such as that of Beattie *et al.* be considered and included in commercial simulators.

5.3 Gas/Water System

The observations in the previous section were the motivation for the present work to further investigate the effect of cyclic hysteresis for gas/water systems under mixed-wet condition.

5.3.1 Coreflood Experiments

Gas-Water Hysteresis: DIDIDI

These tests started with a gas injection (drainage, D) into the core saturated with 100% water, and was then followed by a water injection period (imbibition, I). The periods of gas and water injection were repeated and in total three injection cycles, DIDIDI, were carried out.

1st Gas Injection (DIDIDI):

To perform the first gas injection, the core was first fully (100%) saturated with water. Then, the equilibrated gas was injected through the core at 1840 psia and 100 ºF. The gas injection was carried out at a rate of 50 $cm^3.h^{-1}$. The injection of gas continued after the gas breakthrough (BT) which took place after about 0.3 PV injections. After injecting 1 PV (pore volume) of gas, the gas injection rate was increased to 100 $cm^3.h^{-1}$. The increase in the injection rate was done to increase the saturation range in which the gas/water k_r could be obtained from the results of the test. It should be mentioned that based on the preliminary experiments, injection rates between 25 to 100 $cm^3.h^{-1}$ are in the range that would not affect the relative permeability data for this rock and fluid system (i.e., there was no velocity dependency here). The gas injection period continued for around 7 PV, at which time the rate of brine production was practically zero, and the residual water saturation was approximately 54%.

1st Water Injection (DIDIDI):

After the first gas injection period (with residual water saturation, S_{wrg} = 54%, and S_{gi} = 46%), the first water injection was carried out at a rate of 50 $cm^3.h^{-1}$. The injection of water at this rate continued for more than 1 PV at which time the rate of gas production from the core dropped to practically zero. When brine injection started, initially only gas was produced (due to the high initial saturation of the gas) and then the water broke through around 0.25 PV, after which no gas was produced. This is contrary to the observations for gas/oil system (presented in the previous section), in which gas recovery continued after the oil BT (although at very small rates). Bearing in mind that the core is mixed-wet and the fact that no gas was produced after water break through, it is reasonable to conclude that the snap-off process in gas-water system is stronger than

that in the gas-oil system (possibly due to the very low gas/oil IFT). After around 1.0 PV of water injection, the trapped gas saturation was around 23%.

2nd Gas Injection (DIDIDI):

The sequential injection of gas and water continued with another period of gas injection which again started at 50 $cm^3.h^{-1}$ (S_{wi}=77%, S_{gtw}=23%). The gas injection rate was increased to 100 $cm^3.h^{-1}$, shortly after the gas BT occurred (0.17 PV of gas injected). Compared to the case of 1st gas injection period, here the gas BT happened even earlier. The gas injection continued for around 7 PV.

2nd Water Injection (DIDIDI):

The experiment continued with a 2nd water injection period, which was carried out at a rate of 50 $cm^3.h^{-1}$ (S_{wrg}=50%, S_{gi}=50%). The injection of water continued at this rate after the water breakthrough, when the rate of gas production was practically zero. As was the case in the previous water injection period (1st water injection), there was no gas recovery after the water BT. Water injection extended for about 1 PV.

3rd Gas Injection (DIDIDI):

The last gas injection period of this series of water and gas displacements started at 50 $cm^3.h^{-1}$ (S_{wi}=75%, and S_{gtw}=25%). Gas injection at this rate continued until after the gas breakthrough and then the injection rate increased to 100 $cm^3.h^{-1}$. The gas BT happened even earlier than those in previous gas injection periods (after 0.13 PV of injection). In this drainage period, 5 PV of gas was injected through the core.

3rd Water Injection (DIDIDI):

This series of displacements finished by the 3rd water injection (imbibition) period, which was carried out at a rate of 50 $cm^3.h^{-1}$ (S_{wrg}=50%, S_{gi}=50%). As was the case in the previous water injections (1st and 2nd water injection), there was no gas recovery after the brine BT. After around 1 PV of water injection, the trapped gas saturation (S_{gt}) in the core was around 26.5%.

Gas-Water Hysteresis: IDIDI

Another series of gas/water displacements were carried out to further investigate and identify the hysteresis effects for gas/water system under the conditions of mixed-wettability. The immobile water saturation was first established, and then unlike the Gas/Water hysteresis experiments (DIDIDI) reported in the previous section, this series of tests was started with a brine injection into the core saturated with 82% gas and 18% S_{wim} (Imbibition: I). This brine injection period was followed by a gas injection period

(Drainage: D). The periods of water and gas injections were repeated and in total three water injections and two gas injections were carried out one after another. As a result, this series of fluid displacements has been named IDIDI (Imbibition-Drainage-Imbibition-Drainage-Imbibition).

1st Water Injection (IDIDI):

As explained above, this series of corefloods started with water injection period through the core at a rate of 50 $cm^3.h^{-1}$ (with S_{wim}=18%, S_{gi}=82%). The injection of water at this rate continued to 1.2 PV at which time the rate of gas production from the core dropped to practically zero. When brine injection started, initially only gas was produced from the core and the water breakthrough (BT) happened around 0.55 PV injections. There was no more gas production after the water breakthrough. This observation is in line with what was reported for water injection periods of gas/water DIDIDI tests. After around 0.55 PV of water injection, the trapped gas saturation was around 27% and remained constant till the end of the coreflood (after 1.17 PV injections). It is important to mention that there was a level of oil in Sight-Glass (SG) before starting the test, and during the experiment the oil level was also recorded for different times. It was noticed that the oil level remained quite the same (Figure 5-19) although the pressure drop across the core was high for imbibition stages. This is quite important since it shows that during the test, no gas was converted to the oil inside the core. The same procedure was applied for other imbibition stages as well to make sure that equilibrium conditions are met during the experiment.

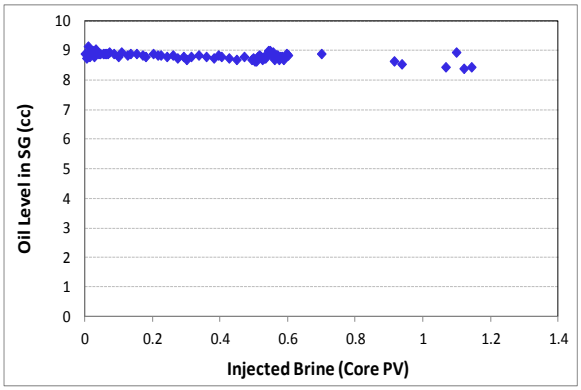

Figure 5-19: Volume of the oil in SG during the test (IDIDI: 1st Water Injection; 65mD, Mixed-wet).

1st Gas Injection (IDIDI):

To perform the first gas injection period, the equilibrated gas was injected through the core at the rate of 50 $cm^3.h^{-1}$. The injection of gas continued with this rate and an early gas breakthrough (BT) took place after 0.12 PV of gas injection. After the BT of the gas, the gas injection continued till 1.1 PV injection when rate of injection was increased to 100 $cm^3.h^{-1}$. Brine production (although at low rates) continues even after the gas breakthrough. The gas injection period continued to around 1.9 PV injections, when the saturation path was changed to the next Imbibition (water injection) period.

2nd Water Injection (IDIDI):

After the first gas injection period as described above, the second water injection period started at a rate of 50 $cm^3.h^{-1}$ (S_{wrg}=48%, S_{gi}=52%). The injection of water at this rate continued and water broke through at 0.22 PV injections. A total of 0.9 PV of water was injected and since there was no more gas production after BT, water injection stopped. After around 0.22 PV of water injection, the trapped gas saturation was around 30% (which remained constant until the end of coreflood).

2nd Gas Injection (IDIDI):

The sequential injection of gas and water continued with another period of gas injection which again started with the rate of 50 $cm^3.h^{-1}$ (S_{wi}=70%, S_{gtw}=30%). Gas breakthrough took place after 0.1 PV injections. Compared to the case of 1st gas injection period, in this period, gas BT happened even earlier (BT time for the 1st gas injection period was around 0.22 PV). The gas injection continued until 3.15 PV of gas had been injected.

3rd Water Injection (IDIDI):

This series of coreflood displacements finished by the 3rd water injection, which was carried out at a rate of 50 $cm^3.h^{-1}$ (S_{wrg}=50%, S_{gi}=50%). Water breakthrough happened after 0.21 PV of brine injected. The injection of water at this rate continued for 1 PV when the rate of gas production reduced to practically zero. As was the case in the previous water injections (1st and 2nd water injections), there was no gas recovery after the water BT, and the remaining gas was trapped inside the core (trapped gas saturation, S_{gtw}, in the core was around 25%).

5.3.2 Results and Discussion

This section discusses the determination of k_r curves for these gas/water experiments. Using these k_r curves, the effect of hysteresis will be discussed. A black-oil coreflood simulator (SENDRA) was used in this exercise to history match the core flood results in order to obtain k_r curves. As an example and in order to show the quality of the history matching in this study, Figure 5-20 shows the comparison of the experimental and simulated results of the pressure drop across the core, brine recovery and gas production for the 1st gas injection period in the DIDIDI series. The jump in pressure drop data is due to an increase made in injection rate during the experiment to extend the saturation change interval. Figure 5-20 shows a good match between simulation and experiment which is important for reliable estimation of the relative permeability curves by this method. It should be mentioned that the amount of capillary pressure (P_c) for 1st imbibition obtained using application of J-function from measured data of another Clashach sandstone (1000mD). In the saturation range of the experiment, P_c values did not affect the simulation results. As a result, to reduce the uncertainty (by decreasing the number of parameters that should be optimized during history matching), the effect of capillary pressure hysteresis in the subsequent simulations and estimations are ignored. The performance of some of the widely used hysteresis models (Carlson, Killough) available in commercial simulators will be also presented in the following sections.

Bounding Relative Permeabilities

k_r values of the 1st drainage period (gas injection in the DIDIDI series) and the 1st imbibition period (water injection in the IDIDI series) are in fact representative of bounding drainage and imbibition curves respectively. Figure 5-21 shows bounding curves for the imbibition and drainage relative permeabilities for this water-gas system. In agreement with literature data, the observed hysteresis is much larger for non-wetting phase (gas) compared to wetting-phase (water). Imbibition relative permeability for water is larger than drainage values, and the gas relative permeabilities for imbibition are less than those of drainage period (which is also consistent with experimental results in literature). Water phase k_r shows more hysteresis effect for lower water saturation values and for high enough S_w (above 0.78) the trend of k_{rw} shows that there is not much difference between imbibition and drainage values. This means that for this range of saturation, k_{rw} is just a function of its own saturation, and is not saturation history dependant. Contrary to this, the non-wetting phase (gas) k_r, shows stronger hysteresis

dependency towards high S_w values (low S_g), and trend of k_r curves shows that imbibition and drainage values are approaching each other for small S_w values.

Experimental Scanning Relative Permeability Curves:

DIDID Experiment

Figure 5-22 shows the cyclic hysteresis effect on water phase relative permeability in the DIDID experiment. The process starts with bounding drainage curve (1^{st} gas injection) in which water saturation has decreased from 1 to 0.54. At this point, the drainage process has stopped and imbibition (water injection) started. Changing the direction of flow, water relative permeability follows a new curve (blue curve) which lies slightly above the previous drainage cycle. As the alternation between imbibition and drainage cycles continues all water relative permeability curves are practically equal to each other and the bounding drainage relative permeability. So in the case of DIDIDI process, it is reasonable to conclude that water phase relative permeability does not show much cyclic hysteresis.

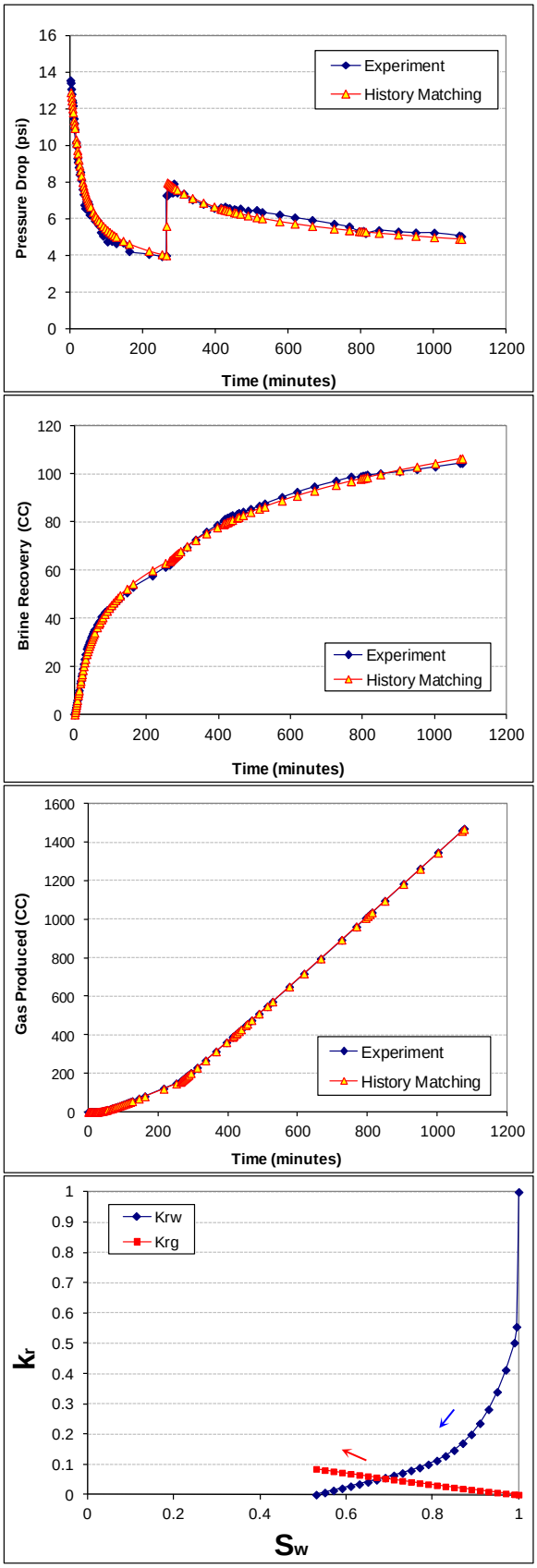

Figure 5-20: History matched data (pressure drop, water recovery and gas production) and estimated relative permeabilities for the 1st Gas Injection in the DIDID experiment (65 mD, mixed-wet, water-gas system).

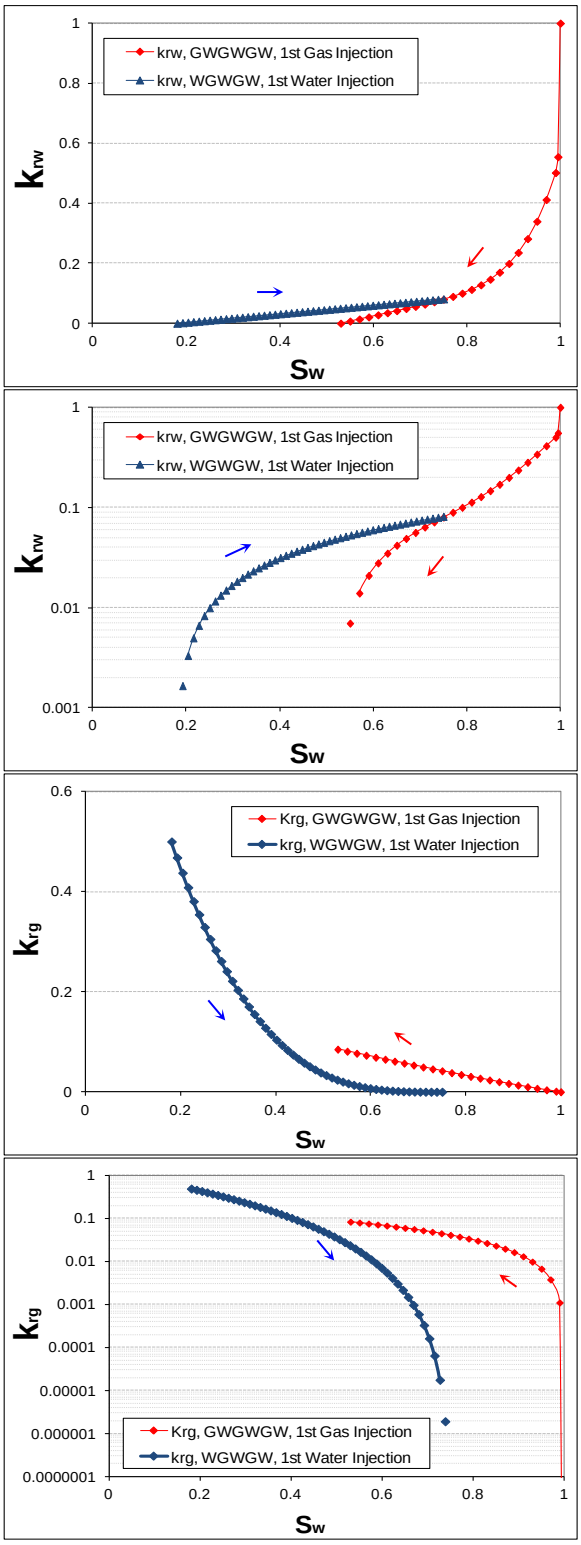

Figure 5-21: Water and gas bounding relative permeabilities (65 mD, mixed-wet, water-gas system).

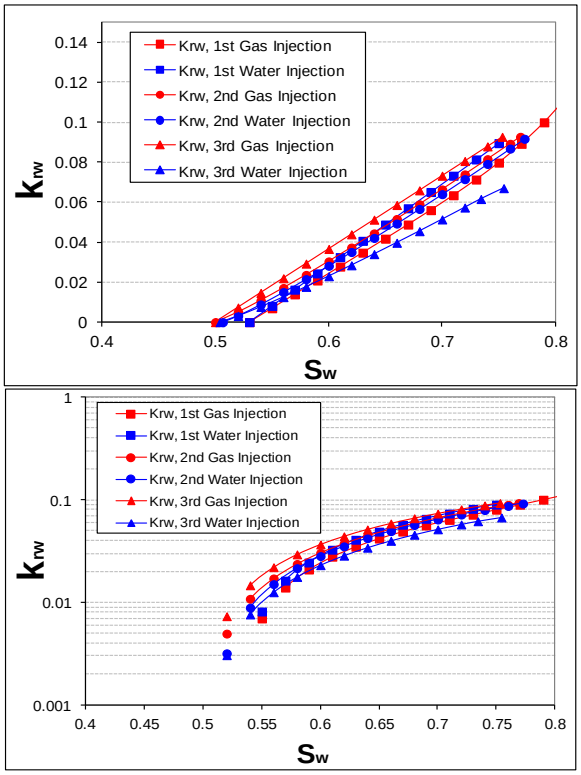

Figure 5-22: Water phase relative permeability hysteresis (65 mD, mixed-wet, water-gas system, DIDID experiment).

Figure 5-23 shows the cyclic hysteresis effect on the gas phase relative permeability in the DIDIDI experiment. The displacements start with the bounding drainage curve (1st gas injection; red triangles) in which water saturation has decreased from 1 to 0.54. During this process the gas relative permeability increased from 0 to around 0.08. It should be mentioned that 0.08 is also the value obtained from Darcy equation at the end point of the experiment (semi steady-state condition). At this low relative permeability value, the gas phase is strongly mobile due to its much less viscosity compared to water (μ_g/μ_w=0.03). At this point, the drainage process stopped and the imbibition (water injection) started. Changing the direction of injection to imbibition, gas relative permeability follows a new curve (blue curve) which lies between the former drainage curve (bounding drainage) and the bounding imbibition (1st water injection of IDIDI experiments). Scanning gas relative permeability for this imbibition is not parallel to the bounding imbibition curve. This observation is in contrast with Carlson hysteresis model.

The Imbibition process stopped at water saturation of around 0.77 and another drainage displacement started in which water saturation decreased to about 0.5 (red circles). An important conclusion here is that the current assumption in common models such as Land, Carlson and Killough, that the relative permeability for a drainage displacement

after an imbibition one would follow those of the preceding imbibition period is not the case based on these experimental results. The relative permeabilities of the 2nd drainage lie above the former imbibition displacement. This is a behaviour which is included in recently developed hysteresis models (Beattie *et al.* and Kjosavik *et al.*). The gas phase imbibition scanning relative permeability starts from the previous drainage curve and sharply approaches the bounding imbibition curve, and follows the same (or at least close to) values as bounding imbibition curve. But drainage scanning relative permeability moves slowly toward the drainage bounding curve. This behaviour is the reverse of that already observed for gas relative permeability curves in gas/oil systems. As can be seen from comparing Figure 5-22 and Figure 5-23, the cyclic hysteresis effect is more pronounced for gas phase relative permeability than water phase. Another important feature is that the hysteresis loop made by k_{rg} in the 1st imbibition and the 2nd drainage cycles, is not closed. This is in contrast to most of the existing hysteresis models including Carlson, Killough, Land and Kjosavik *et al.* models. The only exception would be Beattie *et al.* model, in which the hysteresis loops are not necessarily closed.

Gas relative permeabilities of the successive imbibition period (2nd water injection; blue circles) follow a path, which is the same as 1st water injection period. Nevertheless it is not parallel to the bounding imbibition curve. Yet, the values are very close to those of the 1st scanning imbibition curves. Figure 5-23 shows that as the alternations between imbibition and drainage cycles continue the gas relative permeability drops at different drainage stages. This means that k_{rg} for the 1st drainage cycle is higher than the 2nd drainage period, and the lowest values are those of the 3rd gas injection period. The same figure also shows that for different imbibition cycles, k_{rg} values are practically equal to each other. As the cyclic injection continues, the cyclic hysteresis effect becomes smaller for the later stages of the experiment compared to the earlier ones. This means that the reduction of k_{rg} values for the 3rd gas injection cycle (compared to the 2nd gas injection) is much less than reduction factor for the 2nd gas injection cycle (compared to the 1st gas injection). In addition to this, the hysteresis loops by 3rd drainage and 3rd imbibition, is smaller than that formed by the 1st drainage and the 1st imbibition. This shows that as expected, cyclic hysteresis is more important for earlier stages of the experiment. Possibly the most important hysteresis happened for the transition from the 1st drainage to the 1st imbibition.

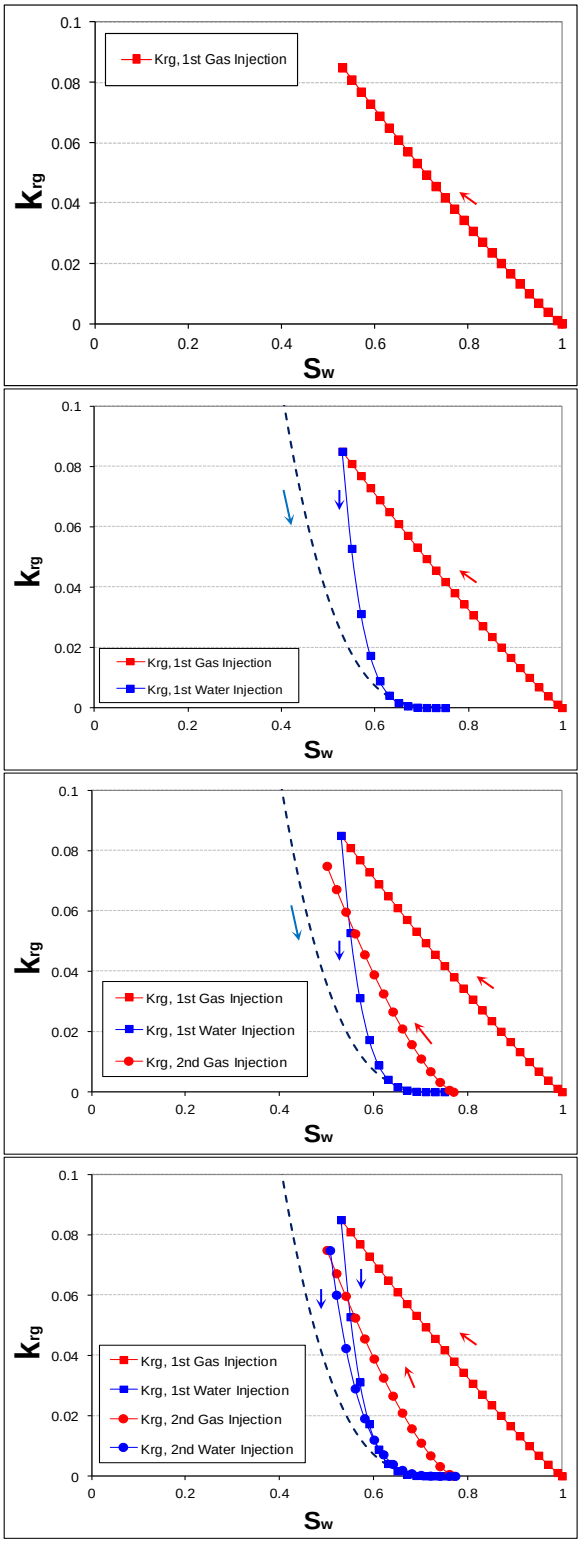

Figure 5-23: Evolution of gas phase relative permeability hysteresis (65 mD, mixed-wet, water-gas system, DIDIDI experiment).

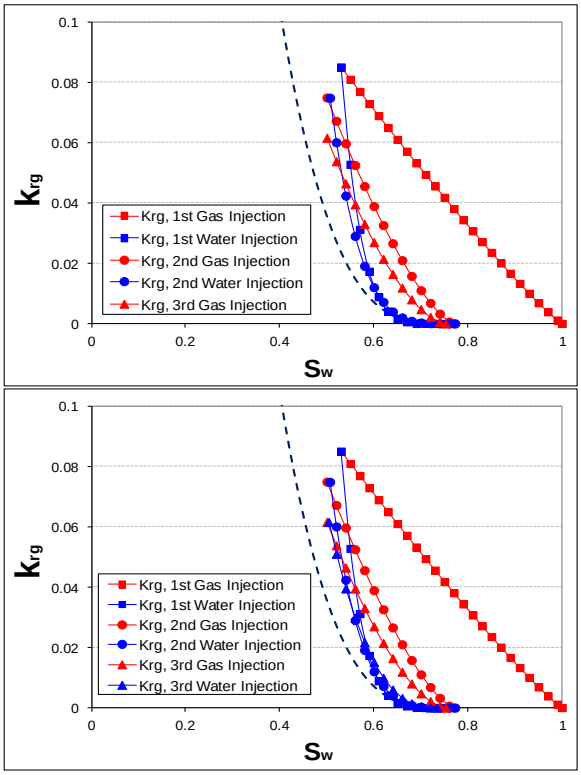

Figure 5-23: continued

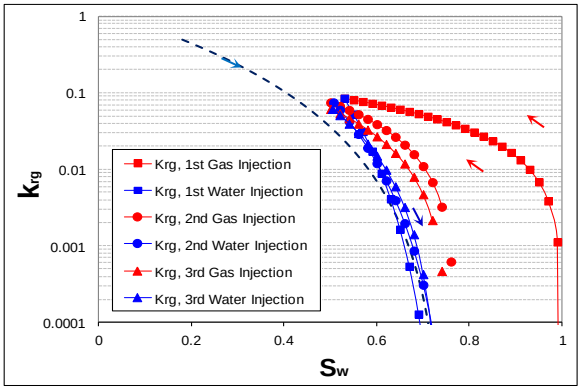

Figure 5-24: Semi-log plot of gas phase relative permeability for different stages of DIDIDI experiment (65 mD, mixed-wet, water-gas system).

IDIDI Experiment

Figure 5-25 shows water relative permeability curves obtained from the IDIDI displacements. The general hysteresis behaviour of the water phase for this series of the experiments is somehow different with what has been already discussed for the DIDIDI experiments (in which there was not much hysteresis). Here the displacements started with a bounding imbibition curve (1st water injection; blue curve) in which the water saturation increased from 0.18 (immobile water saturation) to 0.73. At this point, the imbibition process was stopped and drainage (gas injection; red) started. The water relative permeability values of the drainage scanning curve do not follow the values of

the previous imbibition displacement, rather the results shows k_{rw} reduction for the 1st drainage period compared to the previous imbibition. The 1st drainage continued until the water saturation decreased to 0.48. At this point, another imbibition displacement started, and its relative permeability followed a new path (light blue curve) which lies below the previous drainage displacement. It should be mentioned that end point relative permeability of water (at S_{gtw}) for each imbibition period are calculated directly from Darcy equation at the semi-steady state condition (when there was no more gas production and the only mobile phase was water).

An interesting observation here is that water relative permeability hysteresis loop (formed by 1st drainage and 2nd imbibition) is not closed at this stage of the experiment. This means that relative permeability of 2nd imbibition period at the turning point (S_w = 0.73) in which the flow direction changed from 1st imbibition to 1st drainage, is not the same as the previous imbibition relative permeability (at the same saturation). At the end of the 2nd imbibition, another drainage displacement started (pink curve). The results show that 2nd drainage scanning curve follow those of the previous imbibition displacement (2nd imbibition). In fact, after the 2nd imbibition period, the cyclic hysteresis effect is not that much important in the later stages of the experiment. The k_{rw} of the 2nd imbibition and all subsequent ones are very close to the bounding drainage relative permeability values. As a result, as the alternation of the injection between imbibition and drainage continues the cyclic hysteresis effect becomes less important as the k_{rw} are approaching those of the bounding drainage k_{rw}. The most important hysteresis effects are between 1st Imbibition and 1st drainage, and also between 1st drainage and 2nd imbibition.

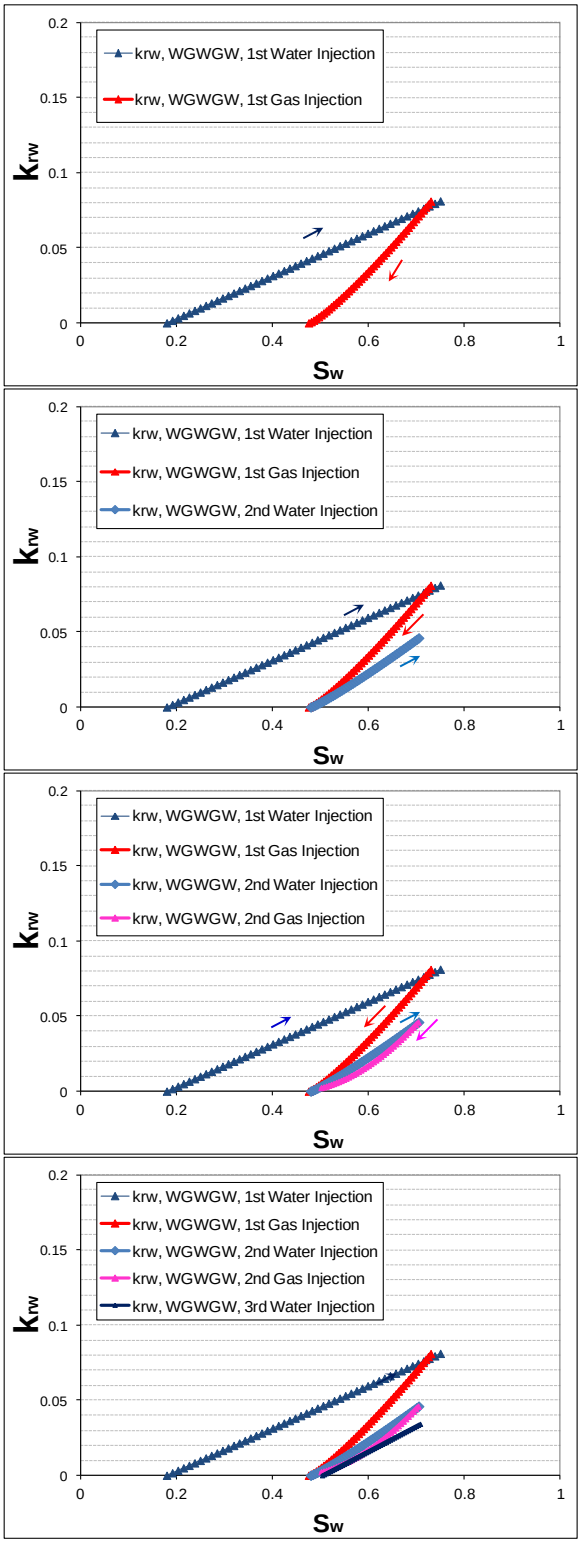

Figure 5-25: Evolution of water phase relative permeability hysteresis (65 mD, mixed-wet, water-gas system, IDIDI experiment).

Figure 5-26 and Figure 5-27 show gas relative permeability derived from the IDIDI experiments. The general hysteresis behaviour of the gas phase shows irreversible hysteresis loops as the cyclic injection continues. The process starts with the bounding imbibition curve (1st water injection; dark blue) in which the water saturation increases from 0.18 to 0.73. During this displacement, the gas saturation drops from 0.82 to 0.27 and gas relative permeability approaches zero. At this point, the imbibition process was stopped and a drainage displacement (gas injection; red) started. The relative permeability of the drainage scanning curve does not follow the values of the previous imbibition displacement. The 1st drainage displacement continued until the water saturation decreased to 0.48. It should be mentioned that k_{rg} values of the 1st drainage period are below those of the bounding imbibition curve. This (lower values of the scanning drainage curve compared to the bounding imbibition curve) is not included in most of hysteresis models (such as Carlson, Killough, Land and Beattie et al.); the only exception is the Kjosavik *et al.* model. This is contrary to Figure 5-24 where in the case of DIDIDI experiment, all k_{rg} imbibition and drainage scanning curves lie between imbibition and drainage bounding curves. At water saturation of 0.48, another imbibition displacement started. The relative permeability of this imbibition displacement follows a new path (light blue curve) which lies slightly below the previous drainage displacement. At the end of 2nd imbibition, another drainage displacement began (pink curve). Again, the scanning drainage curves do not follow those of the previous imbibition displacement (although the difference is very small). This can be explained by the fact that for the 2nd drainage cycle, trapped gas saturation (initially in place at the start of the cycle) is slightly higher than the 1st drainage cycle. This entrapment process is not reversible during the following drainage cycle and restricts the flow. In addition the gas relative permeability hysteresis loops are not closed. As the alternation between imbibition and drainage continues, the cyclic hysteresis effect becomes less important. The same as the water phase, most important hysteresis effect for the gas phase is also between 1st Imbibition and 1st drainage, and of less importance is between 1st drainage and 2nd imbibition. After the 2nd imbibition, the cyclic hysteresis effect on k_{rg} is almost vanished for the later stages of the experiment (Figure 5-28).

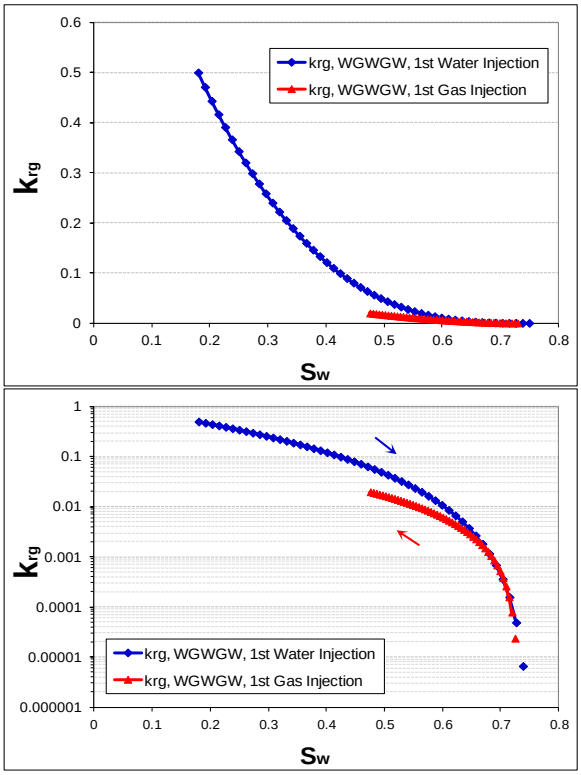

Figure 5-26: Gas phase relative permeability hysteresis between 1st imbibition and 1st drainage (65 mD, mixed-wet, water-gas system, IDIDI experiment); k_{rg} for the 1st drainage are below those of the bounding imbibition curve.

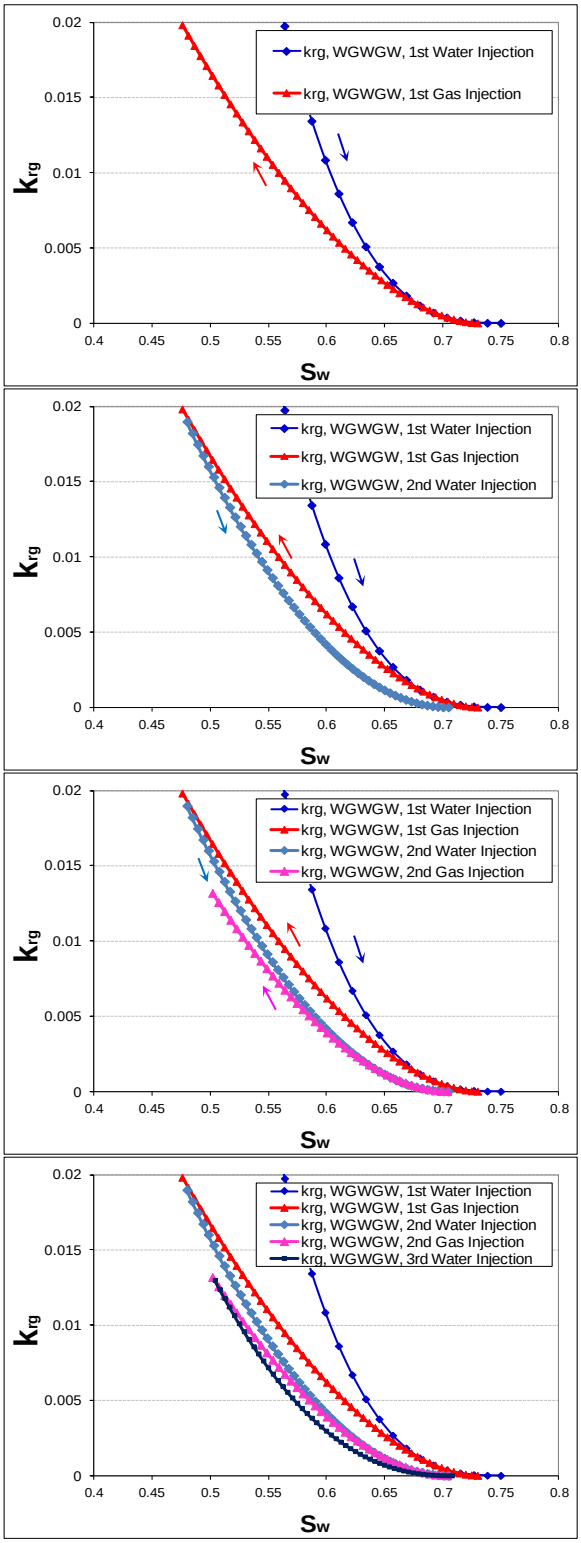

Figure 5-27: Evolution of gas phase relative permeability hysteresis (65 mD, mixed-wet, water-gas system, IDIDI experiment).

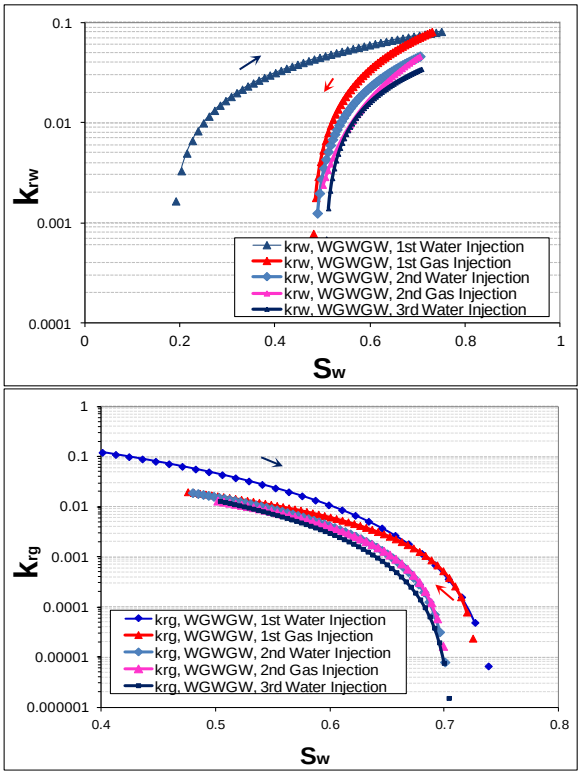

Figure 5-28: Water and gas phase relative permeability for different stages of IDIDI experiment (semi-log plot).

Comparing Figure 5-23 (k_{rg} for DIDIDI test) and Figure 5-27 (k_{rg} for IDIDI) shows that for the case of DIDIDI test there is no significant hysteresis between imbibition k_{rg} values (more or less k_r values of the 1st, 2nd and 3rd water injections are on top of each other), while for IDIDI scenario, k_{rg} shows hysteresis between different imbibition cycles (k_{rg} for the later stages of imbibition are smaller). Another feature is that for the DIDIDI test, k_{rg} for each drainage stage is higher than the former imbibition stage, while for the IDIDI, as the alternation between imbibition and drainage continues, k_{rg} for each stage is smaller than the previous stage and bigger than the successive injection periods. This means that k_{rg} values for gas/water in the mixed-wet system are saturation history dependent. This was not the case for the non-wetting phase (gas) k_r in the investigated gas/oil system. No work in the literature suggests saturation history dependency for k_{rg} in two-phase systems.

Assessment of Hysteresis Models: (Carlson and Killough)

DIDIDI Experiment

This section discusses the evaluation of the predictions of some of widely used hysteresis models (Carlson and Killough model) for water-gas two-phase systems under mixed-wet conditions (see Figure 5-29 through Figure 5-31). As discussed earlier, in the DIDIDI displacements, wetting phase (water) does not show considerable hysteresis during alternation between imbibition (water injection) and drainage (gas injection) cycles. Contrary to this, the non-wetting phase (gas) k_r showed significant hysteresis in both imbibition and drainage cycles. For wetting phase (water) relative permeabilities, using both Carlson and Killough models would be fine since there is no significant hysteresis in the experimental results.

For non-wetting phase, theoretically both models consider hysteresis for alternation from drainage to imbibition. Carlson model predicts zero trapped gas saturation for the 1^{st} imbibition cycle (Chapter 8). This means that in the case of Carlson model, gas relative permeabilities for the 1^{st} imbibition will be the same as those of 1^{st} drainage. As a result Carlson model would not be able to capture any hysteresis for the 1^{st} imbibition and all subsequent cycles. Killough model on the other hand, uses Land formulation for prediction of trapped gas saturation. Land formulation underestimates the trapped gas saturation for the 1^{st} imbibition cycle (Chapter 8), yet the prediction is much better than Carlson model. As a result of trapped gas underestimation, k_{rg} predictions by Killough model are higher than those of experimental data (Figure 5-29). Killough model does not assume any hysteresis for the change of injection from imbibition to drainage; as a result it would not predict any hysteresis for successive drainage periods.

As the alternation between imbibition and drainage periods continues, Killough model does not predict further hysteresis. There will be no hysteresis even for the successive imbibition periods since the historical turning point (S_{grw} in the 1^{st} drainage cycle) is not reached in the successive drainage stages. Figure 5-31 highlights the poor predictions of Carlson and Killough hysteresis models for the DIDIDI experiment, in terms of gas saturation changes. For both models the deviation from the experimental data becomes larger for the later cycles of the experiments. In addition to the poor prediction of saturation path, predicted injectivities for the imbibition periods of the experiment are significantly overestimated by both models. This is especially true for Carlson model

(Killough model predicted the injectivities twice the experimental observation, while Carlson model predictions are as high as 10 times of those of experimental results).

IDIDI Experiment

As discussed earlier, in the IDIDI experiment, both the wetting (water) and non-wetting (gas) phases showed some hysteresis for change of injection between imbibition and drainage. The non-wetting phase (gas) hysteresis is much less compared to what is observed in the DIDIDI experiments. However, the wetting phase (water) relative permeability hysteresis was more pronounced than in this case compared to the DIDIDI experiment. For wetting phase relative permeabilities neither Carlson nor Killough model predict any hysteresis and, for different periods of the imbibition and drainage, the relative permeability values for both phases would be the same as those of the 1st imbibition. Therefore, the prediction of these two models will be the same as each other. Figure 5-32 highlights the differences between the predicted and experimental k_r values for the 1st drainage. As can be seen, Carlson model overestimates both the wetting and non-wetting k_r values during the whole IDIDI experiment (since other experimental relative permeability values are less compared to the 1st drainage).

Figure 5-33 shows the comparison of gas saturation changes in the IDIDI experiment and the prediction of Carlson Model. As can be seen, the hysteresis model is overestimating the saturation changes during the experiment. Similarly to the DIDIDI case, the deviation from the experimental data becomes larger for the later cycles of the experiments. Predicted injectivities for the imbibition periods of the experiment are significantly overestimated by hysteresis models (around twice the experimental observations and become worse for later cycles of injection). Comparing the two injection scenarios (DIDIDI and IDIDI) shows that generally, injectivity is better (higher) in the case of DIDIDI experiments compared to the IDIDI experiments.

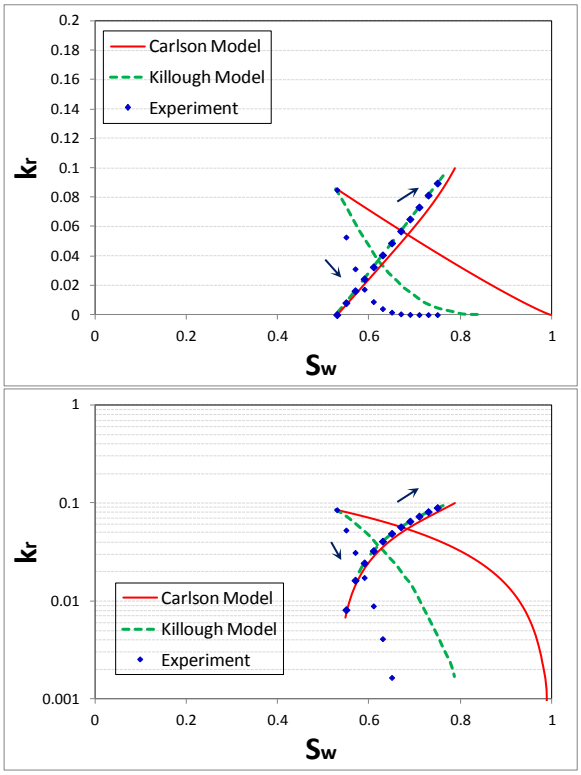

Figure 5-29: Experimental and predicted gas/water relative permeabilities (65 mD, mixed-wet, water-gas system, DIDIDI, 1st water injection).

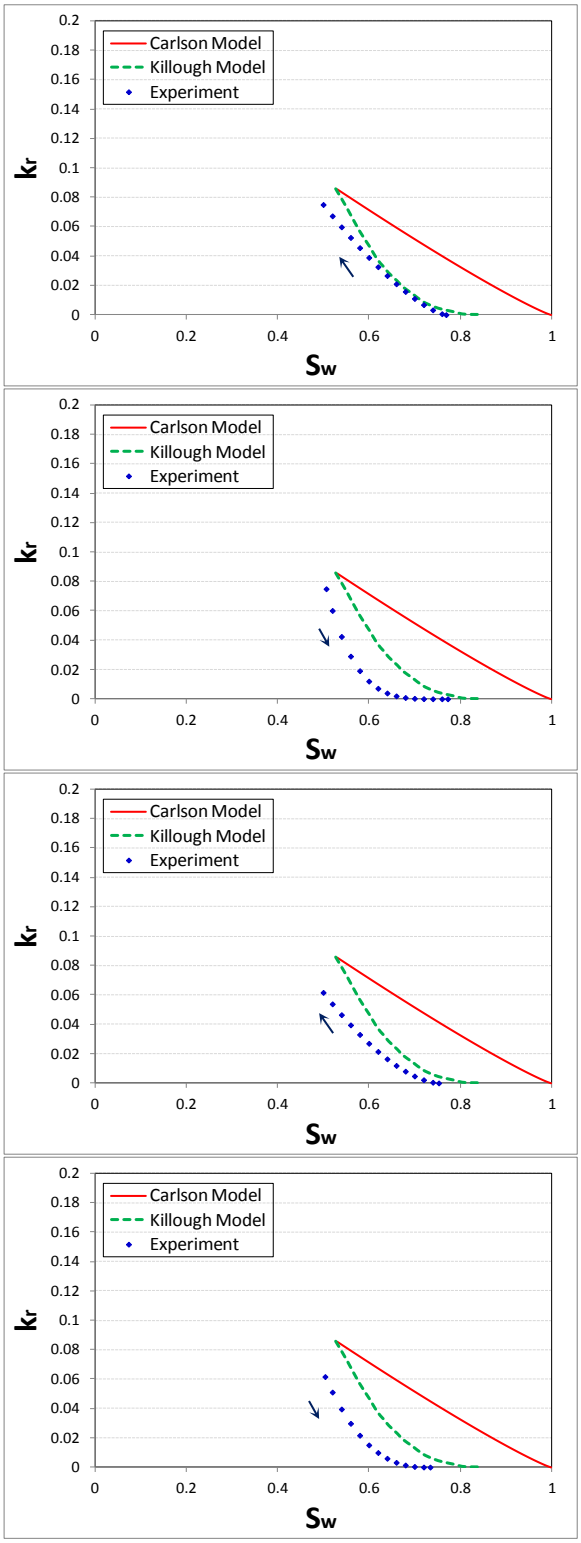

Figure 5-30: Experimental and predicted gas relative permeabilities for different stages of DIDIDI (from top to bottom: 2nd gas injection, 2nd water injection, 3rd gas injection and 3rd water injection).

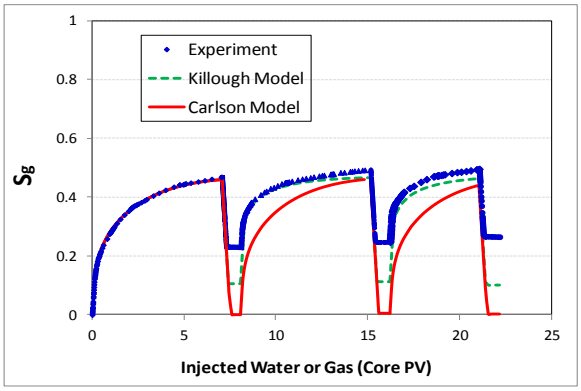

Figure 5-31: Experimental and predicted gas saturations (65 mD, mixed-wet, water-gas system, DIDIDI).

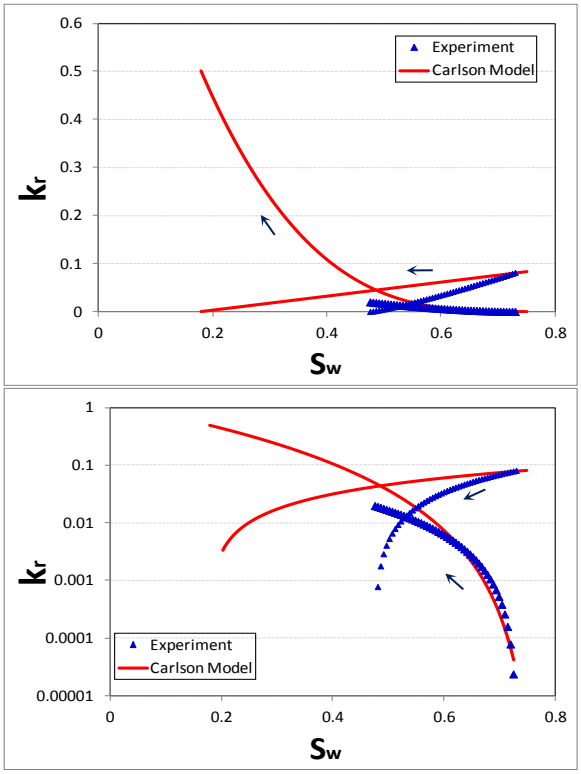

Figure 5-32: Experimental and predicted gas and water relative permeabilities (65 mD, mixed-wet, water-gas system, IDIDI, 1st gas injection).

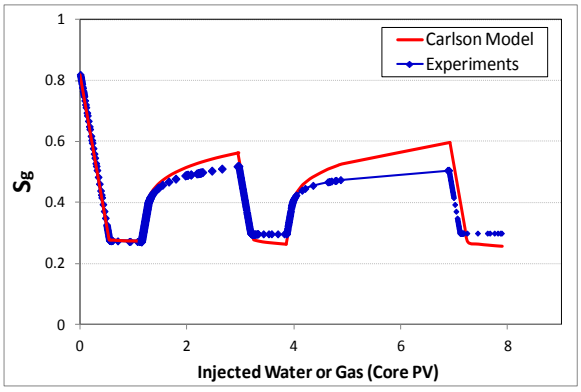

Figure 5-33: Experimental and predicted gas saturations during IDIDI experiment (65 mD, mixed-wet, water-gas system).

5.3.3 Conclusions (Gas-Water System)

General Observations

- It is observed that for the non-wetting phase (gas), relative permeability of the scanning drainage periods would not follow those of the former imbibitions. This is against the assumptions in Carlson, Land and Killough hysteresis models and shows the importance of including non-reversible hysteresis loops models such as Beattie *et al*. and Kjosavik *et al.* in commercial simulators.

- Contrary to the prediction of existing k_r hysteresis models, it was observed that although the same saturation as the former imbibition turning point is achieved in drainage periods, end-point relative permeability of gas would be less than the previous drainage period. This means that at the end of the 2^{nd} gas injection (which is at the same saturation as that of the end of the 1^{st} gas injection), k_{rg} for the 2^{nd} gas injection is less than that of the 1^{st} gas injection. Current two-phase hysteresis models assume they are the same. For both wetting (water) and non-wetting (gas) phases, the cyclic hysteresis effect is less important for the later cycles.

Gas-Water System: (IDIDI)

- Water (wetting phase) relative permeability shows hysteresis in alternating imbibition and drainage periods. Presented results show that k_{rw} values drop in successive change of injection from imbibition to drainage and vice versa. The hysteresis in k_{rw} becomes less as the number of alteration increases (later cycles).

- As the alternation between imbibition and drainage cycles continues, gas relative permeability for drainage and imbibition periods keeps decreasing. In the three-cycle water and gas injections, k_{rg} was higher for the 1^{st} water injection and was lowest for the 3^{rd} water injection cycle. Generally k_{rg} cyclic hysteresis for this series of experiments was not significant. All of the scanning k_{rg} curves fall below bounding imbibition k_{rg} curve.

Gas-Water System: (DIDIDI)

- Generally, water (wetting phase) relative permeability does not show much hysteresis during alternation between imbibition and drainage cycles (especially for higher water saturations). Compared to the k_{rw}, cyclic hysteresis is more pronounced for k_{rg}. The k_{rg} scanning curves lie between bounding drainage and bounding imbibition curves. As the cyclic injection continues, the k_{rg} from each drainage period is larger than its subsequent

imbibition k_{rg} and gas relative permeabilities approach to those of bounding imbibition curve.

5.4 Oil-Water System

5.4.1 Coreflood Experiments

Oil-Water Hysteresis: DIDIDI

The objective of this series of displacements was to investigate and identify the effect of hysteresis in the case of oil/water system under mixed-wettability conditions. The generated experimental data have been also used to investigate different non-wetting trapping models such as Lands, Carlson and Jerauld (Chapter 8). Using experimentally derived relative permeabilities the performance of hysteresis models such as Lands, Killough and Carlson have been also investigated. The experiment started with an oil injection into the core completely saturated with brine. This was followed by cycles of successive injection of this experiment has been named Drainage-Imbibition-Drainage-Drainage-Imbibition-Drainage (DIDIDI).

1st Oil Injection (DIDIDI):

The experiment began by saturating the core 100% with the brine at 1840 psia. Then, the equilibrated oil was injected through the core at the rate of 50 $cm^3.hr^{-1}$. After 1.5 PV of oil injected, rate of injection ramped to 100 $cm^3.hr^{-1}$. Oil breakthrough happened after 0.2 PV injections. Brine recovery continues (albeit at a very slower rates) even after the oil BT. At the end of this 1st oil injection period (after around 3PV of oil injection), residual water saturation (S_{wro}) in the core was around 49%.

1st Water Injection (DIDIDI):

At the end of the preceding oil injection period (1st oil), the experiment continued with a period of brine injection performed at the rate of 50 $cm^3.hr^{-1}$ (S_{wro}=49%, S_{oi}=51%). Water breakthrough happened after 0.2 PV injections. There was no oil recovery after BT (high snap-off mechanism in the case of water injection). After around 1.2 PV of brine injected, trapped oil saturation inside the core was approximately 30%.

2nd Oil Injection (DIDIDI):

The experiment continued with another period of oil injection (S_{wi}=70%, S_{otw}=30%). The oil injection continued until the rate of brine production was practically zero. Oil breakthrough happened after 0.1 PV injections and the same as the previously mentioned oil injection brine recovery continues (although at a very smaller rates) after

the oil breakthrough. After around 1.6 PV of oil injected, residual water saturation (S_{wro}) was equal to 48%.

2nd Water Injection (DIDIDI):

This series of displacements continued with another period of water injection (S_{wro}=48%, S_{oi}=52%). Test started with the oil injection rate of 50 $cm^3.hr^{-1}$, and after 0.7 PV of oil injected, rate of injection ramped to 100 $cm^3.hr^{-1}$. Water breakthrough happened after 0.19 PV injections and there is no oil production after BT. After around 1 PV of brine injection trapped oil saturation was equal to 33%.

3rd Oil Injection (DIDIDI):

This series of fluid displacements continued with a period of oil injection (S_{wi}=67%, S_{orw}=33%), started at the rate of 50 $cm^3.hr^{-1}$. Injection rate ramped to 100 $cm^3.hr^{-1}$ after 0.35 PV of oil injected and test continued after the oil breakthrough. Oil breakthrough happened after 0.09 PV injection. Brine production although at very low rates continued even after breakthrough. After around 1.5 PV of oil injected, residual water saturation (S_{wro}) was approximately 47%.

3rd Water Injection (DIDIDI):

This series of displacements finished with another water injection period which performed at the rate of 50 $cm^3.hr^{-1}$ (S_{wro}=47%, S_{oi}=53%). Water breakthrough happened after 0.19 PV injections and oil recovery stopped afterwards. After around 0.6 PV of brine injected trapped oil saturation was equal to 34%.

5.4.2 Discussion and Results

Experimental Scanning Relative Permeability Curves:

As explained earlier, the objective of this series of fluid displacement tests was to understand the effect of hysteresis for oil/water system in mixed-wettability condition. As an example Figure 5-34 shows the history matching results along with the estimated relative permeabilities for the 1st oil injection period.

Figure 5-35 and Figure 5-36 show the cyclic hysteresis effect on water phase relative permeability in this series of experiments. The process starts with bounding drainage curve (1st oil injection) in which water saturation has decreased from 1. At this point, the drainage process has stopped and imbibition (water injection) started. Changing the direction of flow, water relative permeability follows a new curve (blue curve) which lies below the k_{rw} for the former drainage period, which is contrary to the k_{rw} hysteresis

reported in the literature for oil/water system in water-wet condition. Nevertheless, this observation is line with pore-network simulations performed by Dixit *et al.* (1998) for the case in which contact angles is between 60°-90°. For the 2nd oil injection period, k_{rw} lies above those of the 1st imbibition, yet below those of 1st drainage (bounding curve), which is again in line with Dixit et al. (1998) pore-network modeling. As the alternation between imbibition and drainage periods continues, each drainage k_{rw} curve lies above those of its former imbibition period. The k_{rw} for different drainage periods are practically equal to each other and very close to the bounding drainage relative permeability. Regarding to the k_{rw} in imbibition periods, the differences are not so much for higher oil saturation (low water saturations) but as oil saturation approaches lower values (end of imbibition period), water relative permeability for 3rd imbibition is higher than 2nd imbibition period, which in turn is larger than 1st imbibition period. This is due to the residual oil saturation which increases as the alternative injection continues.

Figure 5-37 and Figure 5-38 show the cyclic hysteresis effect on the oil phase relative permeability in this series of experiment. The displacements start with the bounding drainage curve (1st oil injection). During this process the oil relative permeability increased from 0 to around 0.1. At this low relative permeability value, the gas phase is strongly mobile due to its much less viscosity compared to water (μ_o/μ_w=0.06). At this point, the drainage process stopped and the imbibition (water injection) started. Changing the direction of injection to imbibition, oil relative permeability follows a new curve (blue curve) which lies below the former drainage curve (bounding drainage). The Imbibition process stopped at water saturation of around 0.70 and another drainage displacement started in which water saturation decreased. The k_{ro} curve for the 2nd oil injection period is very close to those of the former imbibition period. As the cyclic injection continues, the oil relative permeability does not show so much hysteresis after 1st imbibition. An important conclusion here is that the current assumption in common hysteresis models (which are mostly developed based on oil/water system) such as Land, Carlson and Killough, that the relative permeability for a drainage displacement after an imbibition one would follow those of the preceding imbibition period is the case for the oil-water system.

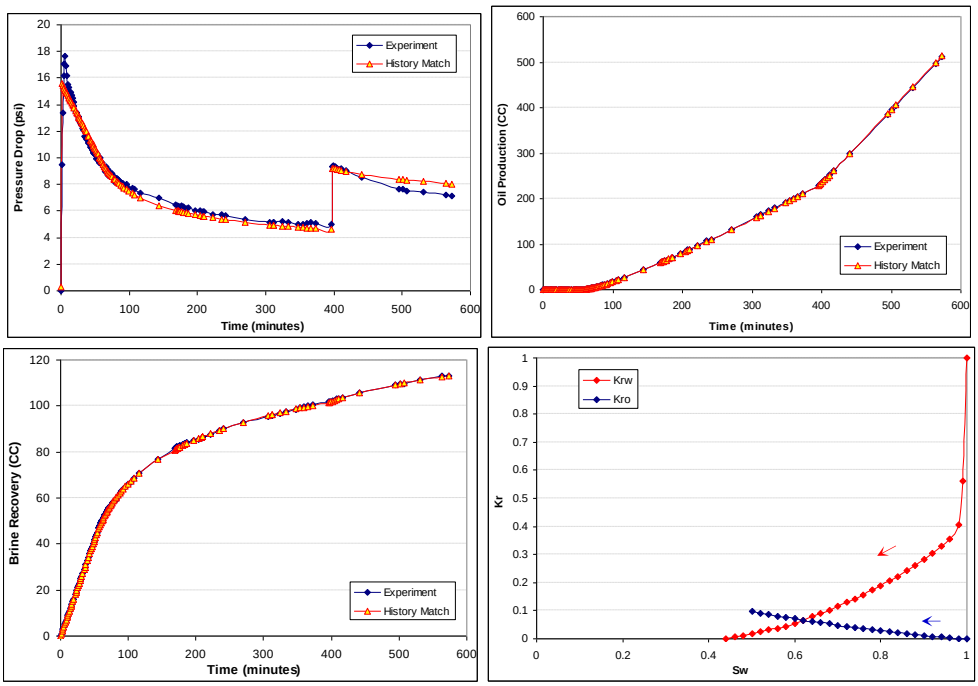

Figure 5-34: Example of history matched results for oil/water system; from left to right and top to bottom, pressure drop across the core, produced oil, brine production and oil and brine relative permeabilities (65mD, mixed-wet, water-oil system, DIDIDI: 1st oil injection).

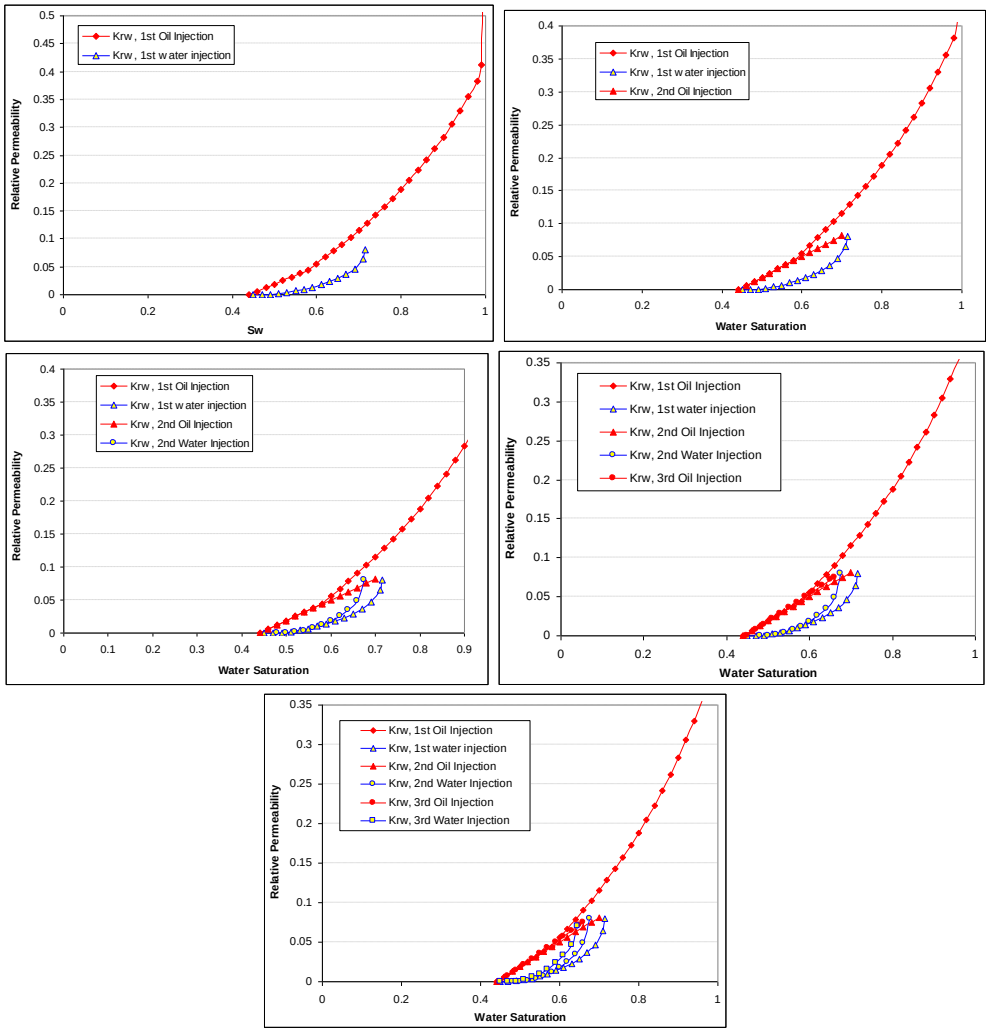

Figure 5-35: Hysteresis effect on water relative permeabilities (oil/water DIDIDI, 65 mD, mixed-wet).

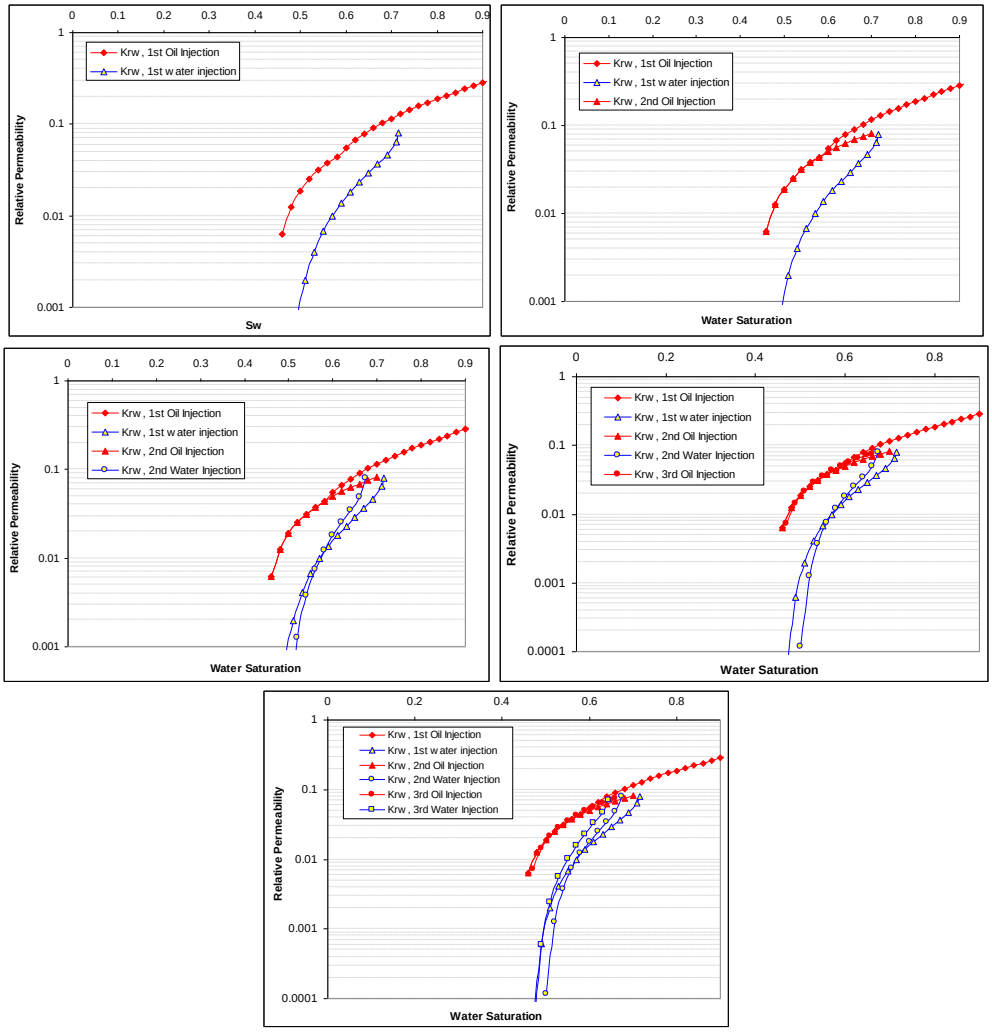

Figure 5-36: Hysteresis effect on water relative permeabilities (oil/water DIDIDI, 65 mD, mixed-wet).

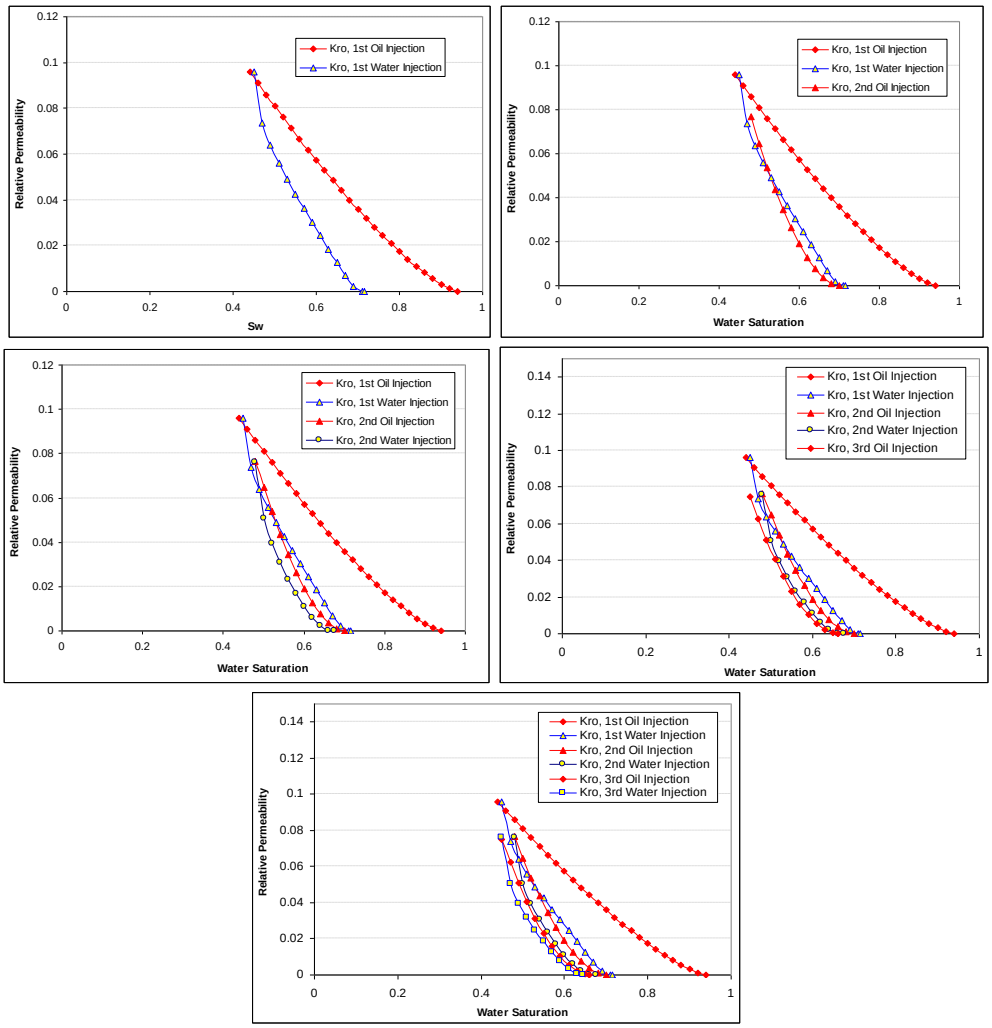

Figure 5-37: Hysteresis on oil relative permeabilities (oil/water DIDIDI, 65 mD, mixed-wet).

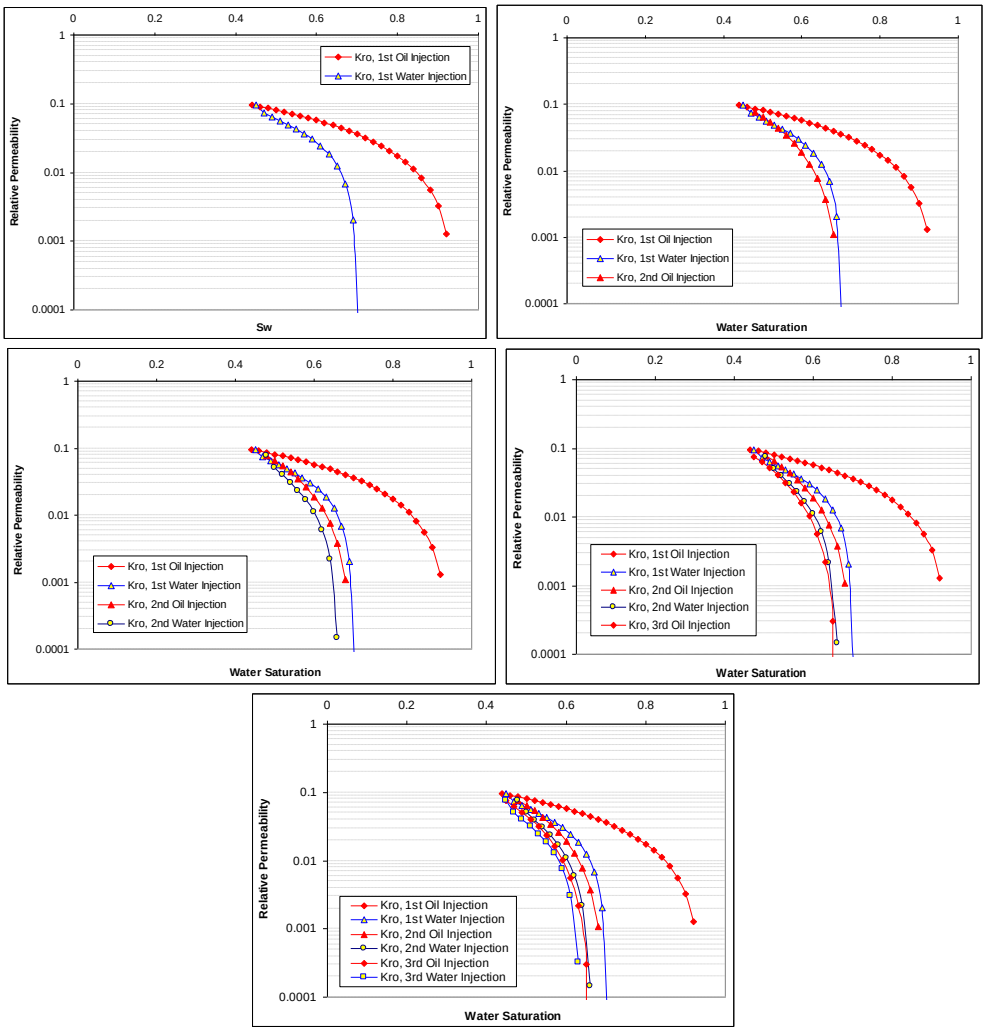

Figure 5-38: Hysteresis on oil relative permeabilities (oil/water DIDIDI, 65 mD, mixed-wet).

Assessment of Hysteresis Models:

In this section, predictions of well-known hysteresis models (Carlson and Killough models) have been evaluated in the case of oil-water two phase systems and mixed-wet core (Figure 5-39 through Figure 5-44). As discussed earlier, water does show considerable hysteresis for alternation of injection between imbibition and drainage periods. Contrary to this oil showed very less hysteresis for both imbibition and drainage periods after 1st water injection period. Regarding to the wetting phase relative permeabilities Carlson would not predict any hysteresis for water at all (assuming that water is wetting phase compared to oil, considering high degree of snap-off for water injection periods). Killough model would predict hysteresis just for the 1st imbibition period and experimental saturation path and model assumptions are in such a way that would be no hysteresis for wetting-phase afterwards. In the case of non-wetting phase both models would be fine since after the 1st imbibition period, no significant hysteresis was observed in k_{ro}. The same as gas-water system, it was assumed that for the 1st water

injection, Carlson and Killough models predictions regarding to the non-wetting phase, are exactly the same as relative permeabilities obtained from history matching. Regarding to the wetting-phase relative permeabilities for Carlson model it would be the same as those of 1st drainage period (Carlson model does not consider hysteresis for wetting-phase), but for Killough model it would be the same as the 1st water injection (Killough assumes hysteresis for wetting phase in imbibition direction). This would be again a bonus to the both models since obtaining scanning curve from bounding curve (as is the case in the original models) would result larger errors. The saturation path that has been followed in the experiments and assumptions of the models regarding to the hysteresis would result that predicted relative permeabilities for both models in the case of successive drainage and imbibition cycles, be the same as the 1st water injection. This means that there would be no hysteresis after 1st water injection period, which is not the case in the presented experiments. As the alternation between cycles continues deviation of the predicted relative permeabilities from those of history matching becomes larger. Generally Carlson model predictions are better for drainage periods (since for drainage periods actual k_{rw} are close to those of 1st drainage). Regarding to the imbibition periods the predicted oil recoveries for both models were the same (both overestimated oil recovery since the k_{ro} curves are the same for these two models and higher than experimental results), but Killough model predictions are better in terms of injectivities for imbibition periods (since actual k_{rw} values are close to those of 1st imbibition period).

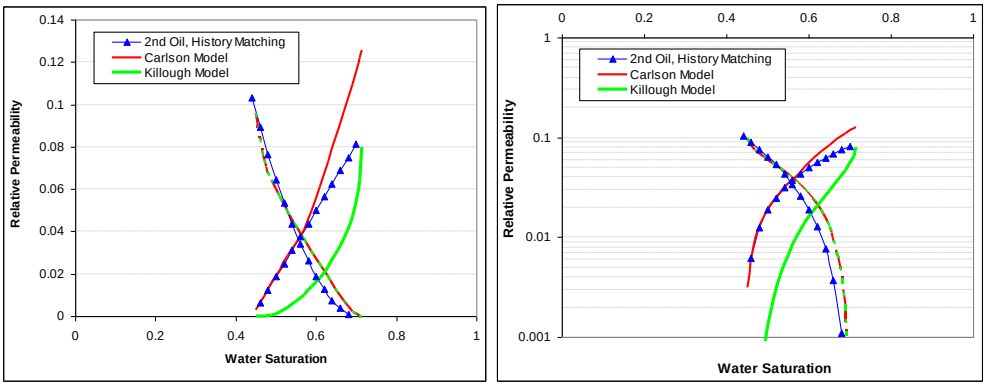

Figure 5-39: Experimental and predicted oil and water relative permeabilities (oil/water DIDIDI, 2nd oil injection, 65 mD, mixed-wet).

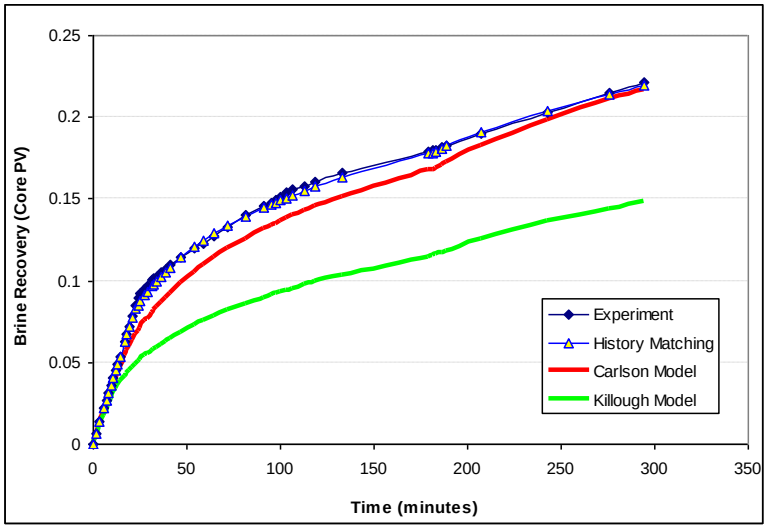

Figure 5-40: Experimental and predicted brine recovery (oil/water DIDIDI, 2nd oil injection, 65 mD, mixed-wet).

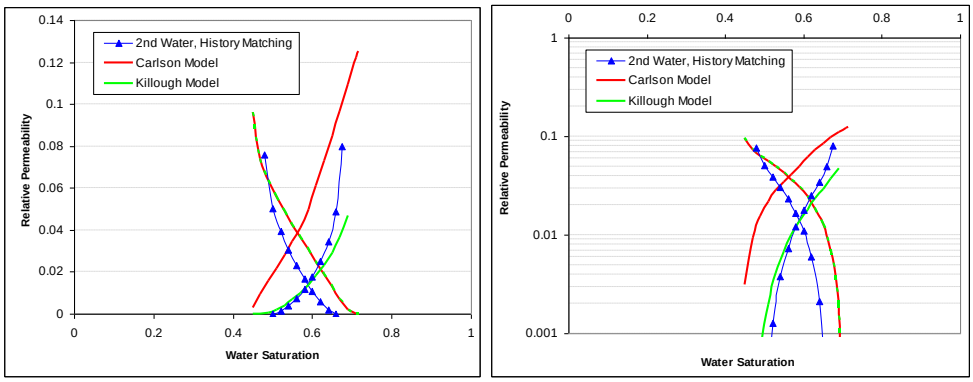

Figure 5-41: Experimental and predicted oil and water relative permeabilities (oil/water DIDIDI, 2nd water injection, 65 mD, mixed-wet).

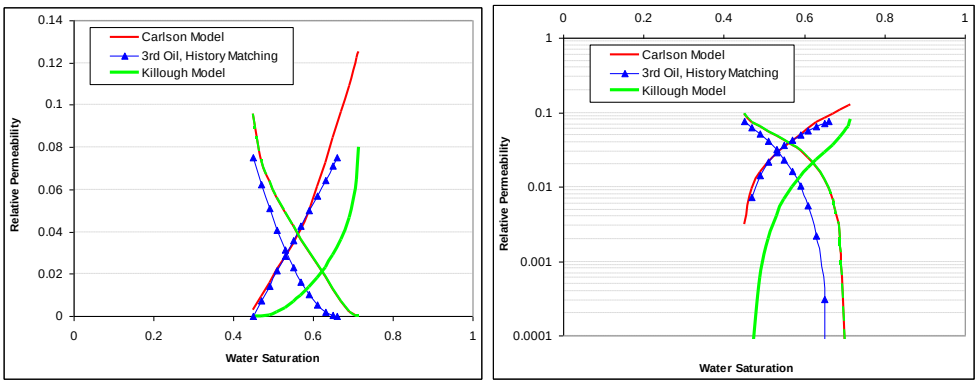

Figure 5-42: Experimental and predicted oil and water relative permeabilities (oil/water DIDIDI, 3rd oil injection, 65 mD, mixed-wet).

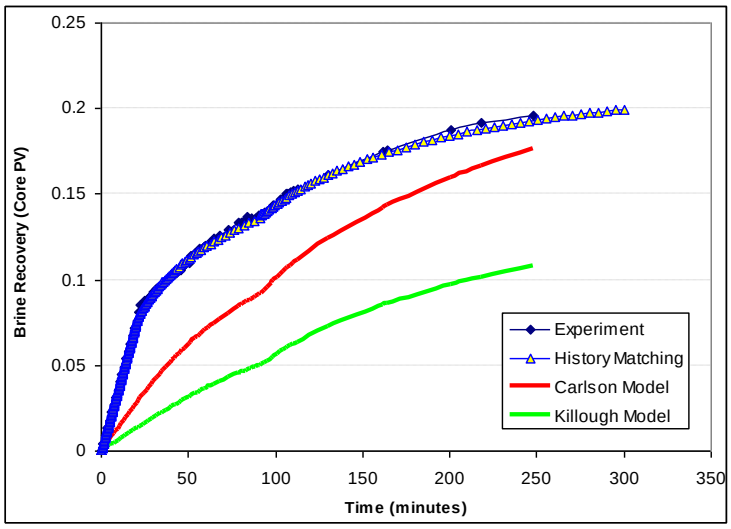

Figure 5-43: Experimental and predicted brine recovery (oil/water DIDIDI, 3rd oil injection, 65 mD, mixed-wet).

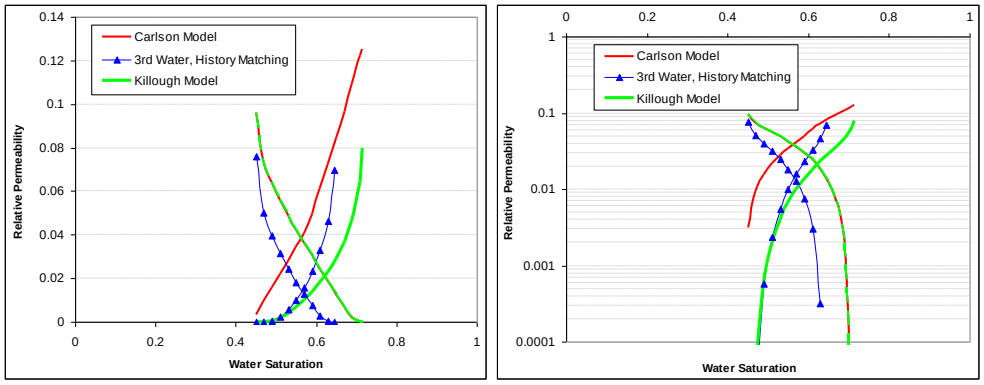

Figure 5-44: Experimental and predicted oil and water relative permeabilities (oil/water DIDIDI, 3rd water injection, 65 mD, mixed-wet).

5.4.3 Conclusions (Oil/Water System)

1) Although end point relative permeability to oil is as low as 0.1, it shows good mobility considering its much less viscosity (0.04 cp.) compare to water (0.68 cp.).

2) Water relative permeabilities show hysteresis for alternation between imbibition and drainage periods. Contrary to the usual behaviour of the wetting-phase in the water-wet system, in the case of the mixed-wet rock, it was observed that water relative permeabilities in imbibition direction are less than those of former drainage period. In addition the current assumption in the literature (such as Carlson and Killough models) which assumes the relative permeability for scanning drainages would follow the values of the former imbibition period isn't validated for water phase in oil-water system.

3) Oil relative permeability shows significant hysteresis for the 1st imbibition cycle compared to the 1st drainage period. Although after that, the oil relative permeability is generally decreasing with the alternation between imbibition and drainage periods, but still in the range of experimental accuracy it is fair to claim that there is no significant hysteresis after 1st imbibition period. This means that the current assumption in the hysteresis models (such as Carlson and Killough) that assumes the relative permeability for scanning drainage cycles would follow the values of the former imbibition periods, is validated for oil phase in oil-water system.

4) Water relative permeabilities do not show significant difference for drainage periods. This means that k_{rw} are on top of each for different drainage periods. This is true especially for lower water saturations.

5) Between Carlson and Killough models (due to their assumptions) predictions of Carlson is better for drainage periods. For imbibition periods, Killough model predictions are better than Carlson.

6) As the cyclic injection of imbibition and drainage periods continues, the effect of hysteresis on water relative permeabilities becomes less.

7) For the mixed-wet rock, although relative permeabilities of oil/water and gas/water systems are very close to each other for the 1st drainage periods (1st oil injection compare to 1st gas injection), the difference between their behavior respect to hysteresis (alternation of imbibition and drainage displacements) makes relative permeabilities very different for the later cycles. This means that current approach in industry to use oil-water relative permeabilities set instead of gas-water set might be fine for the 1st drainage period, but for cases with cyclic imbibition and drainage displacements (such as WAG process) it would cause significant errors on the predicted three-phase relative permeabilities and predicted recoveries.

5.5 Appendix A

5.5.1 Two-phase Hysteresis Models' Mathematical Formulation

In this section, mathematical formulation of some of the widely-used hysteresis models, i.e., Land, Carlson and Killough as well as Beattie et al. model will be reviewed and discussed.

Land (1968) Formulation:

Land trapping model was originally developed for predicting trapped gas saturation as a function of the initial gas saturation based on published experimental data from water-wet sandstone cores. In order to develop equations for relative permeability with the saturation change in the imbibition direction, it was first necessary to be able to predict the saturation of the non-wetting phase that remains mobile at any saturation. Land found that the difference in the reciprocals of initial and residual non-wetting saturation are approximately constant for a given porous media. When the initial gas saturation is unity, the residual gas saturation is the maximum residual saturation, $S^*_{gr,max}$ (Figure A-1).

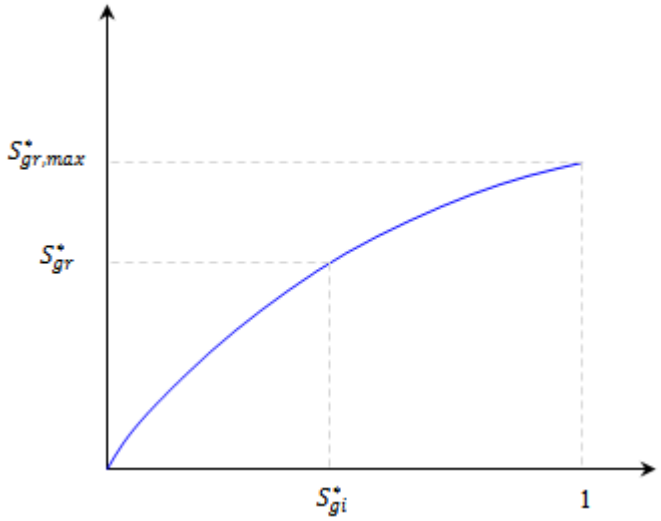

Figure A-1: schematic representation of residual gas saturation vs. initial gas saturation for imbibition (Land Model).

As a result he proposed the following equation:

$$\frac{1}{S^*_{gr}} - \frac{1}{S^*_{gi}} = \frac{1}{S^*_{gr,\max}} - 1 \qquad \text{(Eq. A-1)}$$

or

$$S^*_{gr} = \frac{S^*_{gi}}{1+CS^*_{gi}} \qquad \text{(Eq. A-2)}$$

where *C*, known as Land coefficient, is:

$$C = \frac{1}{S^*_{gr,max}} - 1 \qquad \text{(Eq. A-3)}$$

Consider a porous medium that initially contains a gas saturation S^*_{gi} which was established by withdrawal of wetting phase (drainage). If the wetting phase saturation is now increased from its initial value S^*_{wi} to its maximum value,$1 - S^*_{gr}$, the non-wetting phase saturation, S^*_g, assumes every value between S^*_{gi} and S^*_{gr} and the saturation $S^*_{gi} - S^*_{gr}$, would be replaced with wetting phase. During such a displacement the saturation of the gas which has been trapped inside the porous media, S^*_{gt}, increases. At any gas saturation, S^*_g, the trapped gas saturation so far, S^*_{gt}, would not contribute to gas flow. The other part of gas saturation that has remained mobile and is free to contribute to the flow is, S^*_{gf}, so that: $S^*_g = S^*_{gt} + S^*_{gf}$ in which:

$$S^*_{gf} = 0.5\left[\left(S^*_g - S^*_{gr}\right) + \sqrt{\left(S^*_g - S^*_{gr}\right)^2 + \frac{4}{C}\left(S^*_g - S^*_{gr}\right)}\right] \qquad \text{(Eq. A-4)}$$

and

$$S^*_{gt} = S^*_{gr} - \frac{S^*_{gf}}{1+CS^*_{gf}} \qquad \text{(Eq. A-5)}$$

By solving the general Corey-Burdine equation, the gas relative permeability would be:

$$k_{rg}(S^*_g) = {S^*_{gf}}^2\left[1 - \left(1 - S^*_{gf}\right)^{\in-2}\right] \qquad \text{(Eq. A-6)}$$

where $\in = 2/\lambda + 3$ and λ is a pore-size distribution factor;

Regarding the wetting phase relative permeability Land proposed the following equation:

$$k_{rw} = S_w^{*2}\left[\left(S_w^* + S_{gt}^*\right)^2 - 2/C^2\left(ln\frac{1-\{1-S_{gr,max}^*\}(S_w^*+S_{gt}^*)}{1-\{1-S_{gr,max}^*\}S_{wi}^*} + \frac{1}{1-(1-S_{gr,max}^*)(S_w^*+S_{gt}^*)} - \frac{1}{1-(1-S_{gr,max}^*)S_{wi}^*}\right)\right] \quad \text{(Eq. A-7)}$$

Land sensitivity study on the effect of initial saturation (based on the experimental data that he considered) showed very minor hysteresis for wetting-phase relative permeability. As a result, in his later work (Land, 1971) he didn't compare his wetting phase model versus experimentally measured relative permeabilities. In Land formulation, S^*, is effective saturation, fraction of effective pore space, defined by:

$$S_w^* = \frac{S_w - S_{wc}}{1 - S_{wc}} \quad \text{(Eq. A-8)}$$

$$S_g^* = \frac{S_g}{1 - S_{wc}} \quad \text{(Eq. A-9)}$$

What is very important in the accuracy of prediction of Land's model is the correct pore size distribution, λ, and *C*, Land coefficient value. λ can be obtained by capillary pressure measurement or by fitting non-wetting phase relative permeability curve for bounding imbibition through the formulation which is presented above.

Killough (1976) Hysteresis Model

According to the Killough (1976), relative permeability hysteresis is based on the entrapment of the non-wetting phase, and imbibition and drainage bounding curves. As long as the non-wetting phase saturation continues to increase, drainage, k_{rN}, is calculated from given experimental curves. Assume that a process of primary drainage (bounding curve) would be stopped at a certain non-wetting phase saturation S_N^{Hyst} (Figure A-2) and an imbibition displacement started. Residual gas saturation for such an imbibition displacement would be calculated as given by the same equation as Land (1968):

$$S_{Nr} = \frac{S_N^{Hyst}}{1 + C S_N^{Hyst}} \quad \text{(Eq. A-10)}$$

where

$$C = \frac{1}{S_{Nr}^{max}} - \frac{1}{S_N^{max}} \quad \text{(Eq. A-11)}$$

Once a decrease takes place, the amount of S_N which might be trapped (S_{Nr}), would be calculated from above equation. Once the location of the end point of scanning imbibition curve is obtained ($S_N = S_{Nr}$ and $k_{rN}^{imb}(S_{Nr}) = 0$, imbibition non-wetting relative permeability for intermediate saturations, k_{rN}^{imb} should be calculated and used for all saturations, S_N, between S_N^{Hyst} and S_{Nr}. Two methods of calculating of scanning k_{rN}^{imb} are proposed by Killough. These methods are parametric interpolation and normalized experimental data. For parametric interpolation method, the following equation is proposed: (where λ is a given parameter)

$$k_{rN}^{imb}(S_N) = k_{rN}^{Dr}(S_N^{Hsyt}).\left(\frac{S_N - S_{Nr}}{S_N^{Hyst} - S_{Nr}}\right)^{\lambda} \quad \text{(Eq. A-12)}$$

In which $k_{rN}^{Dr}(S_N^{Hsyt})$, is the non-wetting phase relative permeability value for bounding drainage curve at turning point, S_N^{Hyst}. λ in this formulation is a given parameter which can be obtained by curve fitting of the non-wetting phase bounding imbibition curve. For the normalized experimental data formulation:

$$k_{rN}^{imb}(S_N) = k_{rN}^{Dr}(S_N^{Hyst}).\left[\frac{k_{rN}^{exp}(S_N^{norm}) - k_{rN}^{exp}(S_{Nr}^{max})}{k_{rN}^{exp}(S_N^{max}) - k_{rN}^{exp}(S_{Nr}^{max})}\right] \quad \text{(Eq. A-13)}$$

Where

$$S_N^{norm} = S_{Nr}^{max} + \frac{(S_N - S_{Nr}).(S_N^{max} - S_{Nr}^{max})}{S_N^{Hyst} - S_{Nr}} \quad \text{(Eq. A-14)}$$

It is assumed that the experimental imbibition k_{rN}^{exp} curve (bounding imbibition curve) lies between the maximum possible non-wetting saturation, S_N^{max}, and the maximum residual non-wetting saturation, S_{Nr}^{max}.

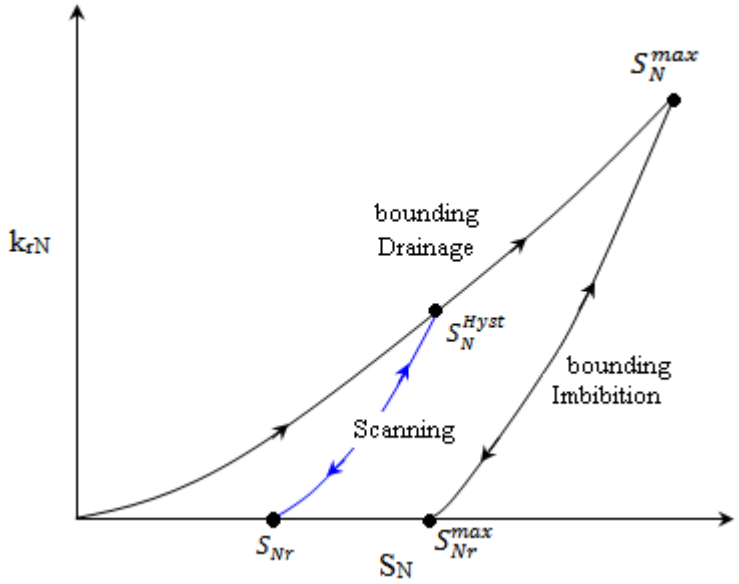

Figure A-2: Killough's hysteretic relative permeability characteristics for non-wetting phase (after Killough, 1976).

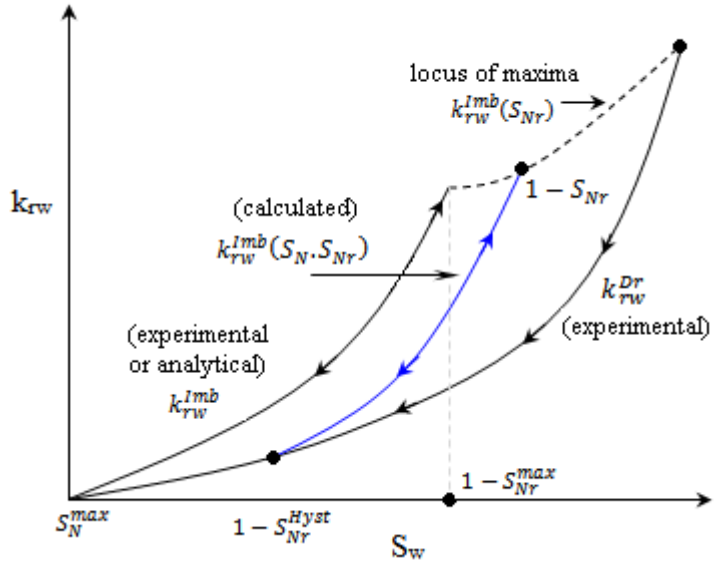

Figure A-3: Killough's hysteretic relative permeability characteristics for wetting phase (after Killough, 1976).

Regarding the wetting phase relative permeability, as long as non-wetting phase saturation increases drainage functions will be used (k_{rw}^{Dr}). A decrease in non-wetting phase saturation at S_N^{Hyst} (which is equivalent to $S_w = 1 - S_N^{Hyst}$) results in following an imbibition k_{rw} curve that falls between $k_{rw}^{Dr}(S_N^{Hyst})$ and a maximum attainable relative permeability, $k_{rw}^{imb,max}$, at a given S_{Nr} (in which $S_{N\ r}$ has been calculated through Land type trapping equation). $k_{rw}^{imb,max}$ will be approximated using the following equation: (see the locus of maxima in Figure A-3).

$$k_{rw}^{imb,max}(S_{Nr}) = k_{rw}^{Dr}(S_{Nr}) + \Delta k_{rw}.\left(\frac{S_{Nr}}{S_{Nr}^{max}}\right)^{a_2} \quad \text{(Eq. A-15)}$$

Where

$$\Delta k_{rw} = k_{rw}^{*imb.}(S_{Nr}^{max}) - k_{rw}^{Dr}(S_{Nr}^{max}) \quad \text{(Eq. A-16)}$$

In which a_2 is a given curvature parameter (that can be obtained through curve fitting if data for scanning curve exist) and $k_{rw}^{*imb.}$ is experimentally measured or analytically obtained (for example through Land formulation) bounding curve. Once the location of the end point of the imbibition scanning curve has been fixed ($S_{Nr}, k_{rw}^{imb,max}$), the intermediate imbibition relative permeability values k_{rw}^{imb} for a given S_N (between S_N^{Hyst} and S_{Nr}) are then calculated using the following formula:

$$k_{rw}^{imb}(S_N) = k_{rw}^{Dr}(S_N^{Hyst}) + \left[\frac{k_{rw}^{*imb}(S_N^{norm}) - k_{rw}^{*imb}(S_N^{max})}{k_{rw}^{*imb}(S_{Nr}^{max}) - k_{rw}^{*imb}(S_{Nr}^{max})}\right].\left[k_{rw}^{imb}(S_{Nr}) - k_{rw}^{Dr}(S_N^{Hyst})\right] \quad \text{(Eq. A-17)}$$

Carlson (1981) Hysteresis model

A simplified hysteresis and trapping model was developed by Carlson (1981) that similarly to Killough model requires the bounding drainage and imbibition curves. Assume that a process of primary drainage (bounding curve) would be stopped at a certain non-wetting phase saturation S_{gi} (Figure A-4) and an imbibition displacement starts. The mathematical formula for the non-wetting phase trapping is:

$$S_{gt} = S_{gt}^{max} - \Delta S_{gi} \quad \text{(Eq. A-18)}$$

where ΔS_{gi}, is the difference between S_g^{imb} and S_{gi} (turning point). S_g^{imb} is the gas saturation on the non-wetting phase relative permeability for bounding imbibition curve, in which $k_{rg}^{imb} = k_{rg}^{Dr}(S_{gi})$. Flowing gas saturation can be calculated from the fact that at each gas saturation value, S_g:

$$S_{gf} = S_g - S_{gt} \quad \text{(Eq. A-19)}$$

Once the end point of this imbibition curve has been fixed ($S_g = S_{gt}$ and $k_{rg}^{imb}(S_{gt}) = 0$), the imbibition relative permeability for the scanning curve would be obtained from $k_{rg}^{imb}(S_g) = k_{rg}^{Dr}(S_{gf})$. In fact, Carlson's method produces scanning curves that are parallel to the imbibition curve. The same as in Killough's model, in Carlson's model the scanning imbibition curve is assumed to represent any subsequent drainage process.

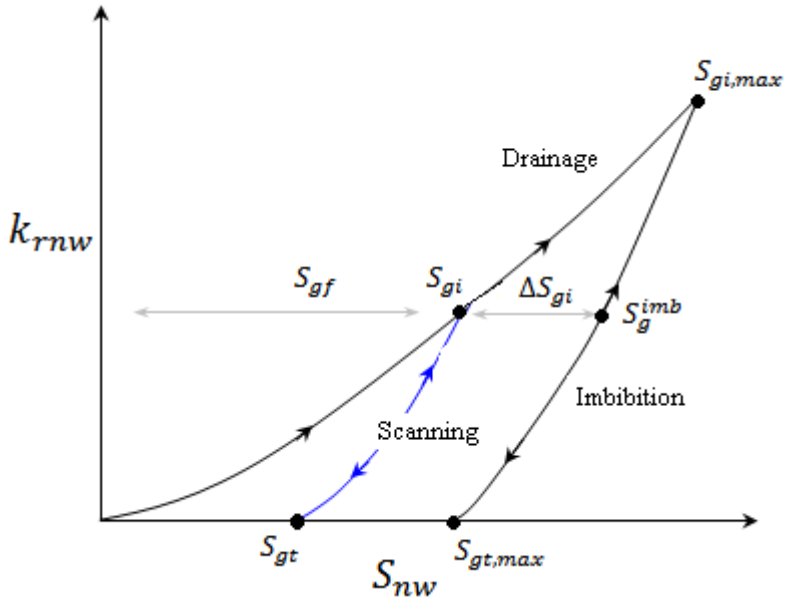

Figure A-4: Carlson's hysteretic relative permeability characteristics for non-wetting phase.

Beattie et al. (1991) Hysteresis model

Figure A-5 shows a pair of normalized water relative permeability bounding curves (for imbibition and drainage). The normalized relative permeability and water saturations are defined by:

$$k_{rw}^{*} = k_{rw}/(k_{rw})_{ro} \qquad \text{(Eq. A-20)}$$

$$S_w^{*} = \left[\frac{S_w - S_{wir}}{S_{wro} - S_{wir}}\right] \qquad \text{(Eq. A-21)}$$

In which $(k_{rw})_{ro}$ is water relative permeability at residual oil saturation. Assume that point P (Figure A-5) is a point of displacement path turning after some successive alternation. As the water saturation increases, the water relative permeability at point P will move toward the imbibition bounding curve. Beattie et al. defined a ratio such as *K*, that compares the distance between each point relative permeability (k_{rw}^{*}) and this

bounding curve (k^*_{rwi}) with the total distance between bounding imbibition (k^*_{rwi}) and drainage (k^*_{rwd}) relative permeability values at that saturation.

$$K = \frac{k^*_{rwi} - k^*_{rw}}{k^*_{rwi} - k^*_{rwd}} \qquad \text{(Eq. A-22)}$$

To be able to calculate k^*_{rw} from above equation, Beattie et al. assumed a saturation dependant correlation for K, which in the case of imbibition $K = A + B(1 - S^*_w)^n$. In which *A*, *B* and *n* are constants. For the case of drainage $K = A + B(S^*_w)^n$. As a result, Beattie et al. came up with the following equations (in which $n \geq 1$ and is a matching parameter if such as data for scanning curve exist).

For water relative permeability in imbibition:

$$k^*_{rw} = k^*_{rwi} - \left[\frac{k^*_{rwi,P} - k^*_{rw,P}}{k^*_{rwi,P} - k^*_{rwd,P}}\right]\left[\frac{1 - S^*_w}{1 - S^*_{w,P}}\right]^n (k^*_{rwi} - k^*_{rwd}) \qquad \text{(Eq. A-23)}$$

In the case of drainage:

$$k^*_{rw} = k^*_{rwd} + \left[\frac{k^*_{rw,P} - k^*_{rwd,P}}{k^*_{rwi,P} - k^*_{rwd,P}}\right]\left[\frac{S^*_w}{S^*_{w,P}}\right]^n (k^*_{rwi} - k^*_{rwd}) \qquad \text{(Eq. A-24)}$$

Normalized oil relative permeability ($k^*_{ro} = k_{ro}/k_{ro,ir}$) will be calculated from the following equations:

For imbibition:

$$k^*_{ro} = k^*_{roi} - \left[\frac{k^*_{ro,P} - k^*_{roi,P}}{k^*_{rod,P} - k^*_{roi,P}}\right]\left[\frac{1 - S^*_w}{1 - S^*_{w,P}}\right]^n (k^*_{rod} - k^*_{roi}) \qquad \text{(Eq. A-25)}$$

And for drainage:

$$k^*_{ro} = k^*_{rod} - \left[\frac{k^*_{rod,P} - k^*_{ro,P}}{k^*_{rod,P} - k^*_{roi,P}}\right]\left[\frac{S^*_w}{S^*_{w,P}}\right]^n (k^*_{rod} - k^*_{roi}) \qquad \text{(Eq. A-26)}$$

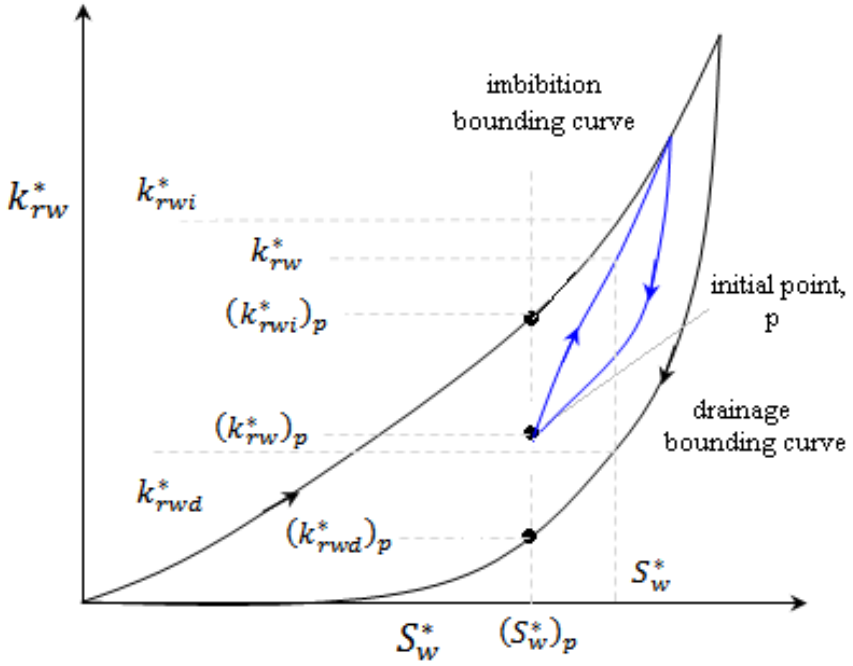

Figure A-5: normalized water relative permeability for Beattie et al. model.

5.6 References

Awan A.R., Teigland R., and Kleppe J., (2008): A Survey of North Sea Enhanced-Oil-Recovery Projects Initiated During the Years 1975 to 2005, SPE Reservoir Evaluation & Engineering, Volume 11, Number 3, pp. 497-512.

Bardon C., Longeron D.G., (1980): Influence of Very Low Interfacial Tensions on Relative Permeability, SPE Journal, Volume 20, Number 5, pp. 391-401.

Beattie, C.I., Boberg, T.C., and McNab, G.S., (1991): Reservoir Simulation of Cyclic Steam Stimulation in the Cold Lake Oil Sands, SPE Reservoir Engineering, Volume 6, Number 2, pp. 200-206.

Braun, E.M., and Holland, R.F., (1995): Relative Permeability Hysteresis: Laboratory Measurements and a Conceptual Model, SPE Reservoir Engineering, Volume 10, Number 3, pp. 222-228.

Carlson F.M, (1981): Simulation of Relative Permeability Hysteresis to the Nonwetting Phase, presented at SPE Annual Technical Conference and Exhibition, 4-7 October, San Antonio, Texas.

Colonna J., Brissard F, and Millet J.L., (1972): Evolution of Capillarity and Relative Permeability Hysteresis, SPE Journal, Volume 12, Number 1, pp. 28-38.

Delshad M., Lenhard R.J., Oostrom M., and Pope G.A., (2003): A Mixed-Wet Hysteretic Relative Permeability and Capillary Pressure Model for Reservoir Simulations, SPE Reservoir Evaluation & Engineering, Volume 6, Number 5, pp. 328-334.

Dixit A.B., McDougall S.R., Sorbie K.S., (1998): A Pore-Level Investigation of Relative Permeability Hysteresis in Water-Wet Systems, SPE Journal, Volume 3, Number 2, pp. 115-123.

Evrenos, A.I., and Comer, A.G., (1969): Numerical Simulation of Hysteretic Flow in Porous Media; presented at Fall Meeting of the Society of Petroleum Engineers of AIME, 28 September-1 October, Denver, Colorado.

Geffen T.M., Owens W.W., Parrish D.R., and Morse R.A., (1951): Experimental Investigation of Factors Affecting Laboratory Relative Permeability Measurements, Petroleum Transactions, AIME, Volume 192, pp. 99-110.

Jerauld G.R., (1997a): Prudhoe Bay Gas/Oil Relative Permeability, SPE Reservoir Engineering, SPE-35718 Volume 12, Number 1, pp. 66-73.

Jerauld G.R., (1997b): General Three-Phase Relative Permeability Model for Prudhoe Bay, SPE-36178, SPE Reservoir Engineering, Volume 12, Number 4, pp. 255-263.

Jerauld G.R. and Rathmell J.J., (1997): Wettability and Relative Permeability of Prudhoe Bay: A Case Study in Mixed-Wet Reservoirs, SPE Reservoir Engineering, Volume 12, Number 1, pp. 58-65.

Killough J.E., (1976): Reservoir Simulation with History-Dependent Saturation Functions, SPE Journal, Volume 16, Number 1, pp. 37-48.

Kjosavik A., Ringen J.K., and Skjaeveland S.M., (2002): Relative Permeability Correlation for Mixed-Wet Reservoirs, SPE Journal, Volume 7, Number 1, pp. 49-58.

Kleppe J., Delaplace P., Lenormand R., Hamon G., Chaput E., (1997): Representation of Capillary Pressure Hysteresis in Reservoir Simulation, SPE- 38899, SPE Annual Technical Conference and Exhibition, 5-8 October, San Antonio, Texas.

Land C.S., (1968): Calculation of Imbibition Relative Permeability for Two- and Three-Phase Flow From Rock Properties, SPE Journal, Volume 8, Number 2, pp. 149 – 156.

Land C.S., (1971): Comparison of Calculated with Experimental Imbibition Relative Permeability, SPE Journal, Volume 11, Number 4, pp. 419-425.

Morrow N.R., (1990): Wettability and Its Effect on Oil Recovery, Journal of Petroleum Technology, Volume 42, Number 12, pp. 1476-1484.

Osoba J.S., Richardson J.G., Kerver J.K., Hafford J.A. and Blair P.M., (1951): Laboratory Measurements of Relative Permeability, Petroleum Transactions, AIME, Volume 192, pp. 47-56.

Rao D. N., Girard M., and Sayegh S. G., (1992): The Influence Of Reservoir Wettability On Waterflood And Miscible Flood Performance, Journal of Canadian Petroleum Technology, Volume 31, Number 6, pp. 47-51.

Salathiel, R.A., (1973): Oil Recovery by Surface Film Drainage in Mixed-Wettability Rocks, Journal of Petroleum Technology, Volume 25, Number 10, pp. 1216-1224.

Skjaeveland S. M., Siqveland L. M., Kjosavik A., Hammervold W. L., Virnovsky G. A., (2000): Capillary Pressure Correlation for Mixed-Wet Reservoirs, SPE Reservoir Evaluation & Engineering, Volume 3, Number 1, pp. 60-67

Shahverdi H., Sohrabi M., Fatemi S.M., Jamiolahmady M., Ireland S., Robertson G., (2011): Evaluation of Three-Phase Relative Permeability Models for WAG Injection Using Water-Wet and Mixed-Wet Core Flood Experiments, presented at SPE EUROPEC/EAGE Annual Conference and Exhibition, 23-26 May, Vienna, Austria.

Sohrabi M., Tehrani D.H., Danesh A., Henderson G.D., (2004): Visualization of Oil Recovery by Water-Alternating-Gas Injection Using High-Pressure Micromodels, SPE-89000, SPE Journal, Volume 9, Number 3, pp. 290-301.

Sohrabi M., Danesh A., Tehrani, D. and Jamiolahmady M., (2008a): Microscopic Mechanisms of Oil Recovery by Near-Miscible Gas Injection; Transport in Porous Media, Volume 72, Number 3, pp. 351-367.

Sohrabi M., Danesh A., and Jamiolahmady M., (2008b): Visualisation of Residual Oil Recovery by Near-Miscible Gas and SWAG Injection Using High-Pressure Micromodels, Transport in Porous Media, Volume 74, Number 2, pp. 239-257.

Spiteri E.J., and Juanes R., (2006): Impact of relative permeability hysteresis on the numerical simulation of WAG injection, Journal of Petroleum Science and Engineering, Volume 50, Issue 2, pp. 115-139.

Suzanne K.; Hamon G.; Billiotte J.; V. Trocme, (2003): Experimental relationships between residual gas saturation and initial gas saturation in heterogeneous sandstone reservoirs, presented at SPE Annual Technical Conference and Exhibition, 5-8 October, Denver, Colorado, USA.

6. Investigation of Different Injection Scenarios for Water-Wet and Mixed-Wet Systems

Water flooding and gas injection are two widely used improved oil recovery techniques that can be applied individually or combined as water alternating gas (WAG) or simultaneous gas and water (SWAG) injections. Laboratory data on WAG and SWAG injections for non-water-wet systems are very limited especially for near-miscible (very low IFT) gas-oil systems, which represents injection scenarios involving high-pressure hydrocarbon gas and CO_2 injections. Simulation of these processes requires three-phase relative permeability (k_r) data. Most of the existing three-phase relative permeability correlations have been developed for water-wet conditions and are unable to adequately account for all the complex multi-phase and multi-physics processes involved in these oil recovery techniques. Majority of oil reservoirs are believed to be mixed-wet and hence, prediction of the performance of WAG injection in these reservoirs is associated with significant uncertainties. Performing reliable laboratory experiments is the key to evaluating the performance of these oil recovery techniques under reservoir conditions. The experimental data can be also used for assessment of different relative permeability and hysteresis models, and developing new methodologies for reliable simulation of WAG and SWAG injections.

This chapter, first reports the results of a comprehensive series of coreflood experiments carried out in a core under natural water-wet conditions. These included water injection, gas injection and also WAG injection. Then, to investigate the impact of wettability on the performance of the above injection strategies, the wettability of the same core was changed to mixed-wet (by aging the core in an appropriate crude oil) and a similar set of experiments were performed. WAG experiments under both wettability conditions started with water injection (I) followed by gas injection (D) and this cyclic injection of water and gas was repeated (IDIDID).

The results show that in both the water-wet and mixed-wet cores, the performance of WAG injection is better than water injection and gas injection alone. Changing the rock wettability from water-wet to mixed-wet, significantly improve the performance of

water injection. Ultimate oil recovery by gas injection is considerably higher than that obtained by water injection in the water-wet system, while in the mixed-wet system gas injection recovered considerably less oil. WAG oil recovery was observed to be higher for mixed-wet system compared to water-wet state.

To further investigate the performance of different injection scenarios for mixed-wet system, another series of WAG tests, and two series of SWAG injections have been also performed. The difference between the two WAG experiments was the order in which gas and water injections were carried out. The first WAG test started with water injection (IDIDID) whereas the second WAG experiment started with gas injection (DIDIDIDI). The difference between the two SWAG experiments was the gas/water (SWAG) ratio, which was 0.25 for the first one and 1.0 for the second SWAG test.

The results show that in mixed-wet core (under very-low oil/gas IFT condition), oil recovery by the WAG test which had started with water injection was higher than the WAG test started with gas injection. WAG injections had superior performance over SWAG injections. SWAG injection performed better compare to primary gas injection. However, surprisingly, SWAG injection resulted in lower oil recovery compared to primary waterflood in the mixed-wet system. It was observed that increasing the gas/water ratio in SWAG injection, leads to faster gas breakthrough, higher produced gas/oil ratio and further reduction in the oil recovery. Compared to the other injection strategies, a very high pressure drop across the core was observed during SWAG injection indicating injectivity problems with the application of the process in mixed-wet rocks. The results show that for mixed-wet rocks (and very-low oil/gas IFT), amongst the studied injection strategies, SWAG is the worst and alternating injection of water and gas (WAG), starting with a water flood period, is the best injection strategy.

6.1 Introduction

Water injection is the most common method of oil recovery. Usually after waterflood, significant amount of oil remains in the reservoir (S_{orw}). Part of this remaining oil can be recovered by gas injection. Various types of gas have been used for injection in oil reservoirs including, CO_2 (mostly in USA), hydrocarbon gas, nitrogen and air. CO_2 and hydrocarbon gases are used in 90% of the gas injection projects worldwide (Kulkarni

and Rao, 2005). Injection of hydrocarbon gases is very common in the North Sea area (Awan et al., 2008).

For many oil reservoirs poor sweep efficiency has been a problem in gas injection processes. This happens due to the high gas mobility compared to the oil and water. Therefore, continuous gas injection may not result in economically significant additional oil recovery. To improve the sweep efficiency of gas injections, Water alternating gas (WAG) injection was originally (Caudle and Dyes, 1958) proposed as an Improved Oil Recovery (IOR) method by using alternating injection of water (with gas) to control the mobility ratio and to stabilize the propagating front (Christensen et al., 1998).

From another point of view, in some oil reservoirs a relatively small amount of produced gas and/or a rapidly falling gas rate makes it uneconomic to develop a gas export solution. In offshore oil fields, it is not usually economically viable to supply gas to these reservoirs for a continuous gas injection scenario (due to remoteness). In such reservoirs, re-injection of the produced gas together with water in a WAG or SWAG injection scheme may provide reservoir pressure support, better sweep and hence increased recovery.

WAG injection is a complex form of three-phase fluid flow through porous media. Although WAG flooding has been successfully applied to many oilfields worldwide (Christensen et al., 1998), there is still an incomplete understanding of the actual mechanisms underlying oil recovery by WAG injection especially in systems with non-uniform and non-water-wet wettability conditions (Suicmez et al., 2007) and the current understanding is even more limited where the oil/gas interfacial tension (IFT) is very low (near-miscible condition). Nevertheless, less experience has been gained in SWAG compared to WAG and hence the process is even less known (Skauge and Aarra (1993); Larsen and Skauge (1999); Christensen et al. (1998); Larsen et al. (2000); Christensen et al. (2001); Sohrabi et al. (2004)). WAG injection is already reviewed in Chapter 1, so a brief introduction to SWAG injection is provided in this Chapter.

The first simultaneous water and solvent injection study was carried out by Caudle and Dyes (1958). They found that one way to improve the miscible displacement sweep efficiency is to lower the mobility behind the flooding front by injecting water with the

miscible gas. Their laboratory studies have shown that the increase in the sweep efficiency for a five-spot pattern can reach 90% with SWAG, whereas, if continuous gas injection is implemented, only 60% of oil is recovered. It should be mentioned that in their original work, the wettability of the porous medium had not been identified.

Blackwell *et al.* (1960) showed that higher recoveries were obtained with water-solvent mixtures as compared to water or solvent injection alone. In their experiments hexane was used as the solvent and Lucite sand pack (with an absolute permeability of 190 D) was used as the porous medium. Although not mentioned in their original work but the wettability of the porous medium is believed to have been water-wet.

Field studies on miscible CO_2 flooding (Stephenson et al., 1993) shows that SWAG injection appears to provide better control of the gas mobility than WAG injection, resulting in improved sweep efficiency as well as more steady gas production and GOR (gas/oil ratio) response. Quale *et al.* (2000) and Berg *et al.* (2002) reported improved oil recovery for SWAG injection of the produced associated gas in Siri field. The main contributions to increased recovery came from improved sweep and oil swelling. It was also noticed that combined water and gas injection may result in lower injectivity than single-phase injection. Injectivity considerations should therefore be taken into account for field applications of SWAG injection. Sohrabi et al. (2008) performed micromodels visualization experiments of SWAG injection after waterflooding. The original work was performed on water-wet micromodels using hydrocarbon gas (for very low gas/oil IFT systems). They concluded that a significant oil recovery by SWAG injection can be achieved and that the ultimate oil recovery by SWAG is independent of the SWAG ratio.

A major problem in the evaluation of WAG injection behaviour are uncertainties associated with the prediction of the wettability and spreading conditions of the system as well as the relative permeabilities values of the three phases for different injection cycles. Empirical correlations are usually used for obtaining three-phase relative permeability. However, most of the widely used empirical correlations are developed with an assumption that the rock is strongly water-wet (Blunt, 2000). This has contributed to a poor performance by the existing empirical equations used for determination of three-phase relative permeabilities for non-water-wet conditions (Element *et al.*, 2003, Sohrabi *et al.* 2010).

Experimental data on the performance of near-miscible WAG and SWAG injections (using hydrocarbon gases) is very scarce and this lack of data becomes even more severe for mixed-wet systems. This chapter presents the results of coreflood experiments, for such conditions, performed on 65 mD core sample, including WAG injection, SWAG injection and SWAG-tail gas injection scenarios, as well as primary waterflooding and primary gas injection. The objective of the present chapter is two folds. First, to extend the pore-scale investigations reported by Sohrabi *et al.* (2004) to core-scale and investigate the effect of wettability conditions (in the presence of immobile water saturation) on the process performance and recovery mechanism of water injection, gas injection and WAG injection for near-miscible gas/oil systems. Secondly, to generate reliable experimental data for estimation of three-phase relative permeabilities (Chapter 7). These three-phase relative permeabilities are used for the assessment of the three-phase relative permeabilities correlations available in the literature and commercial simulators (Sohrabi *et al.* (2010); Shahverdi *et al.* (2011); Shahrokhi *et al.* (2014)). The experiments are continued with SWAG injections and investigation of the effect of SWAG ratio on oil recovery. Also the feasibility of enhancing oil recovery after water breakthrough in SWAG injection is investigated by performing SWAG tail gas injection and WAG injection. The effect of injection sequence in WAG process (starting with water or gas) is also investigated. Table 6-1 and Table 6-2 show the list of the performed coreflood experiments presented in this paper. For the sake of completeness some of the coreflood experiments (Table 6-3) which were previously performed in 1000 mD sample (Sohrabi *et al.*, 2007) are also presented. These tests were performed on the 1000 mD mixed-wet core but the same fluids (oil, gas and brine) that were used in the tests on the 65 mD core were used here as well. Other experimental conditions were also the same as those used in the tests on the 65 mD core sample (P = 1840 psia, T = 100ºF and IFT_{o-g} = 0.04 $mN.m^{-1}$).

6.2 Coreflood Experiments

6.2.1 Primary Waterfloodings (65 mD)

Water-injection experiments (for both wettability conditions) were carried out with immobile water in the core (S_{wi}= 18%) and 82% oil. Brine was injected through the core at 25 $cm^3.hr^{-1}$. During the brine-injection period, the rate of injection and production of fluids (±0.05 cm^3) as well as the inlet, outlet, and average core pressure were accurately

measured (±0.001 psi, ±0.0069 kpa) and monitored. Brine injection continued for some time after the breakthrough until the rate of oil production became practically zero.

6.2.2 Primary Gas Injections (65 mD)

Having performed this waterflood experiment, the immobile water saturation was established again. The value of irreducible water saturation (volumetric) and its distribution along the core (using x-ray facility) were examined, which were the same as the values of the previous tests. The gas injection experiments began with the core containing 82% oil and 18% immobile water. Gas injection was performed at the same injection rate as the water injection, which was equal to 25 $cm^3.hr^{-1}$ at the test pressure of 12.69 MPa (1840 psia) and temperature of 38ºC. During the gas-injection period, the rate of injection and production of fluids as well as the pressure of the inlet, outlet, and average core pressure were measured. The rate of oil production from the core slowed down after the breakthrough of gas. Although the oil-recovery rate decreased after the BT, it remained significant until the end of the experiment. In theory, if large volumes of gas are injected into the core, the ultimate oil recovery achievable would be around 100% (because of very-low IFT between gas/oil).

6.2.3 Water-Alternating-Gas (WAG) Injections (65 mD; IDIDID)

The WAG tests were carried out to evaluate the process of WAG injection using near-miscible gas. The core containing irreducible water (18%) was saturated with oil (82%) at the test pressure of 12.69 MPa (1840 psia) and temperature of 38ºC. Then, three periods of water injection (Imbibition, I), each followed by gas injection (Drainage, D) were carried out (three WAG cycles-IDIDID). The injection rate at different cycles of WAG was the same, equal to 25 $cm^3.hr^{-1}$.

Table 6-1: Coreflood experiments presented in Chapter-6 (**65 mD, water-wet**, oil/gas IFT = 0.04 $mN.m^{-1}$).

Exp. #	*Coreflooding*	*Direction*
1	Gas Injection	Drainage (D)
2	Water Injection	Imbibition (I)
3	WAG	IDIDID

Table 6-2: Summery of the coreflood experiments presented in Chapter-6 (**65 mD, mixed-wet**, oil/gas IFT = 0.04 $mN.m^{-1}$).

#	*Experiment*	*Direction*
4	Gas Injection	Drainage
5	Water Injection	Imbibition
6	WAG	IDIDID
7	WAG	DIDIDIDI
8	SWAG (Q_g/Q_w=0.25)	(So↓, Sw↑, Sg↑)
9	Gasflooding*	(So↓, Sw↓, Sg↑)
10	WAG **	ID
11	SWAG (Q_g/Q_w=1)	(So↓, Sw↑, Sg↑)

* performed at the end of the SWAG experiment (No. 8)

** performed after SWAG-Tail gasflooding (No. 9)

Table 6-3: Summery of the coreflood experiments presented in Chapter-6 (**1000 mD, mixed-wet**, oil/gas IFT = 0.04 $mN.m^{-1}$).

#	*Coreflooding*	*Direction*
12	Gas Injection	Drainage
13	Water Injection	Imbibition
14	WAG	IDID
15	SWAG (Q_g/Q_w=0.25)	(So↓, Sw↑, Sg↑)

6.2.4 WAG Injection (65mD, Mixed-Wet Core, DIDIDIDI)

This WAG injection experiment (coreflood 7) started with gas injection (D) in order to compare its performance with a previous WAG injection test that had been started with water injection (I) (experiment 6). Comparing the performance of these WAG tests would show the dependency of the oil recovery by WAG injection on the order of gas and water injection in mixed-wet rocks (under very-low oil/gas IFT). The results of this WAG experiment would also be applicable to those reservoirs which are already under gas injection and are being considered for WAG injection. Before the start of the test, the immobile water saturation was established at S_{wim}=18%. The core was then saturated with oil with an initial saturation of 82% and WAG injection started with a primary gas injection at the test pressure of 12.69 MPa (1840 psia) and temperature of 38ºC. Four cycles of gas injection followed by water injection (alternating injection of brine and gas) were carried out at the rate of 25 $cm^3.h^{-1}$.

6.2.5 SWAG Injection (65mD, Mixed-Wet Core, Q_g/Q_w=0.25)

This experiment (coreflood 8) was carried out using the same mixed-wet 65mD core and near-miscible gas-oil system used in the previous test. Having established an initial oil saturation of 82% and immobile water saturation of 18% at 1840 psia, water and gas were simultaneously injected through the core. Water was injected at the rate of 40 $cm^3.h^{-1}$ while gas was injected at 10 $cm^3.h^{-1}$ making a total fluid injection rate of 50 $cm^3.h^{-1}$ and a SWAG ratio of 0.25 (vol/vol both at 1840psia and 38^oC). SWAG injection continued until almost 1.2 PV of fluids had been injected. SWAG injection resulted in some additional oil recovery up until the water breakthrough (BT). However, after water BT, no significant additional oil recovery was observed.

6.2.6 SWAG-Tail Gas Injection (65mD, Mixed-Wet)

The effect of injecting gas (coreflood 9) at the end of the period of SWAG injection (after water BT in SWAG injection) is also investigated. SWAG injection stopped after around 1.2 PV, and then continuous gas injection started at the rate of 50 $cm^3.h^{-1}$. This gas injection continued until a total of 2.8 PV of gas was injected.

6.2.7 SWAG-Tail WAG Injection (65mD, Mixed-Wet)

This test (coreflood 10) was performed to investigate the effect of alternating injection of gas and water on the recovery of the remaining oil after SWAG injection. At the end of the gas injection period carried out after SWAG injection, injecting fluid was switched to brine which was injected into the core at the rate of 50 $cm^3.h^{-1}$. After 0.6 PV of water injections there was no change in the fluids' average saturations in the core (oil and gas been trapped in the core). At this stage, water injection stopped and injection of gas at the rate of 50 $cm^3.h^{-1}$ started to complete the WAG cycle. This gas injection continued until a total of 2.5 PV of gas was injected.

6.2.8 SWAG Injection (65mD, Mixed-Wet, Q_g/Q_w=1.0)

To examine the effect of gas/water (SWAG) ratio on the performance of SWAG injection in the mixed-wet system, another SWAG injection test (coreflood 11) was carried out but with the gas/water ratio of 1. As in the previous SWAG test (coreflood 8, with gas/water ratio of 0.25), the experiment was carried out with the same core and near-miscible gas-oil system. Having established an initial oil saturation of 82% and an immobile water saturation of 18% at 1840 psia, water and gas were simultaneously injected through the core. Each fluid (water and gas) was injected at the rate of 25 $cm^3.h^{-1}$ (i.e., a total fluid injection rate was 50$cm^3.h^{-1}$ and the SWAG ratio was 1.0).

SWAG injection continued until almost 1.65 core PV (pore volume) had been injected. Similarly to the previous SWAG injection test, there was no significant additional oil recovery after the water breakthrough.

6.2.9 Primary Waterflooding (1000 mD)

Waterflooding experiment was carried out with immobile water in the core (S_{wi}= 8%) and 92% oil. Brine was injected through the core at 200 $cm^3.hr^{-1}$. Brine injection continued for some time after the breakthrough until the rate of oil production became practically zero.

6.2.10 Primary Gas Injection (1000 mD)

The gas injection experiments began with the core containing 92% oil and 8% immobile water. Gas injection was performed at the same injection rate as the water injection, which was equal to 200 $cm^3.hr^{-1}$ at the test pressure of 12.69 MPa (1840 psia) and temperature of 38ºC. The rate of oil production from the core slowed down after the breakthrough of gas, but it remained significant until the end of the experiment.

6.2.11 Water-Alternating-Gas (WAG) Injections (1000 mD; IDID)

The core containing immobile water (S_w = 8%) was saturated with oil (92%) at the test pressure of 12.69 MPa (1840 psia) and temperature of 38ºC. Then, two cycles of water injection (Imbibition, I), each followed by gas injection (Drainage, D) were carried out. The injection rate at different cycles of WAG was the same, equal to 200 $cm^3.hr^{-1}$.

6.2.12 SWAG Injection (1000mD, Near-Miscible, Mixed-Wet, Q_g/Q_w=0.25)

Having established the initial saturation condition of S_{wim} = 8% and S_o = 92%, water and gas were simultaneously injected through the core. To achieve SWAG ratio of 0.25, gas and water were injected at 40 and 160 $cm^3.h^{-1}$ respectively (total fluid injection rate of 200 $cm^3.h^{-1}$). SWAG injection continued until almost 2 PV (gas and water) had been injected.

6.3 Results and Discussion

6.3.1 Effect of Wettability on Primary Water Injection (65mD core)

Figure 6-1 compares the amount of recovered oil during primary water injection experiments in the water-wet and the mixed-wet systems (65 mD). As can be seen, oil recovery during waterflooding of the mixed-wet case is considerably higher than its

water-wet counterpart. For both wetting conditions, there is no oil production after the water breakthrough, which is expected for water-wet system. For the mixed-wet system cease of the oil production after water breakthrough is due to large water/oil viscosity ratio (μ_w/μ_o = 16.8 for both water-wet and mixed-wet systems) in the performed experiments which results in high pore-scale displacement efficiency. Water breakthrough (BT) occurs later in the case of mixed-wet system. The observed increase in oil recovery in the mixed-wet core experiment can be explained by suppression of the "snap-off" mechanism. In the mixed-wet core, the water phase would be a non-wetting or a weakly-wetting phase (considering variations of the wettability from pore to pore or even inside some pores), and hence, displacement of the oil at the pore-scale would be more piston-like (rather than film flow which would be dominant in water-wet systems). This microscopic difference in displacement mechanism for these two different wettability conditions results in much less oil trapping taking place in waterflooding of mixed-wet rocks (see Figure 6-2). As a result, oil displacement and recovery from neutral-wet rocks would be higher. The higher oil recovery observed for the mixed-wet core is in agreement with the results reported by Jadhunandan and Morrow (1995) and Tiab and Donaldson (2004), in which it was concluded that oil recovery by waterflooding increased with change of wettability from strongly water-wet to a maximum at close to neutral-wet.

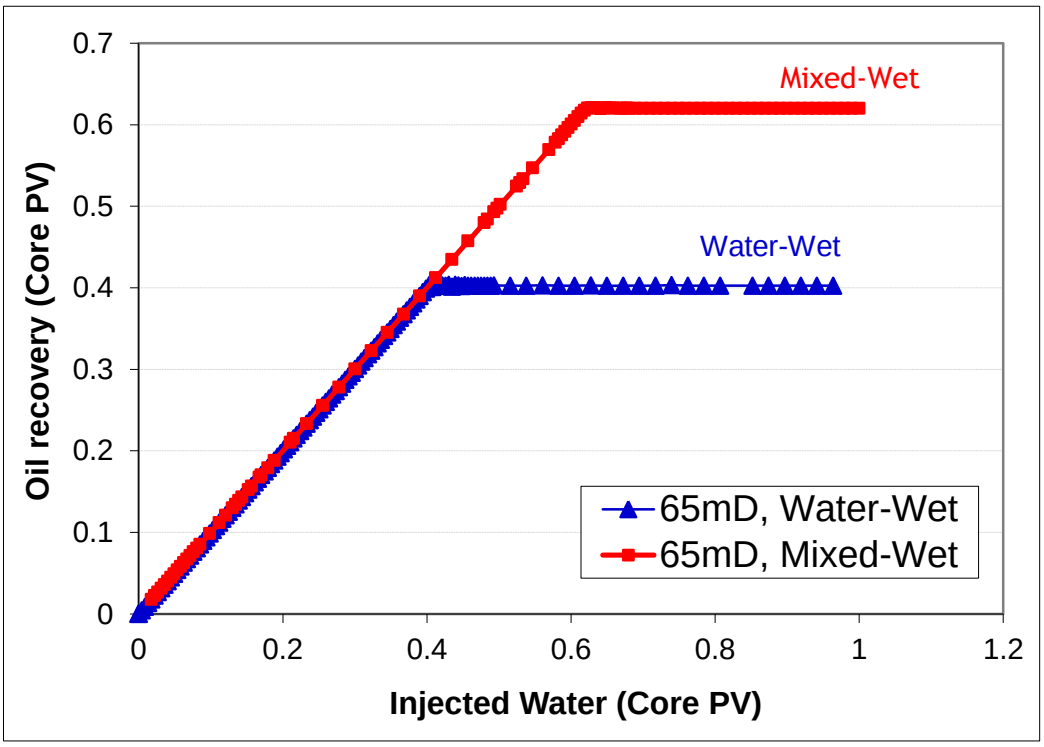

Figure 6-1: Effect of wettability on the performance of primary water injection (65 mD).

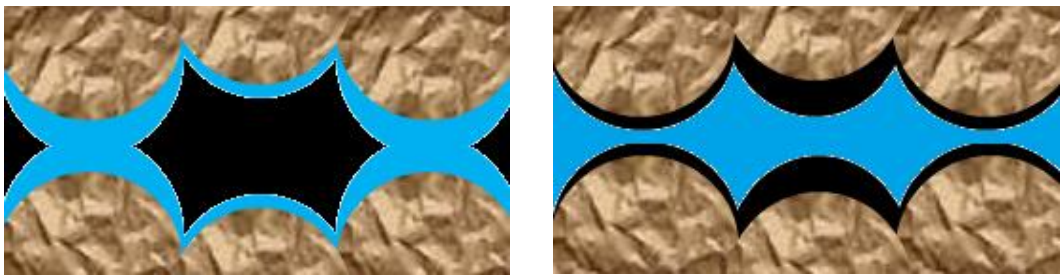

Figure 6-2: Pore-scale schematics of distribution of oil and water phases in water-wet (left) and non-water wet pores of mixed wet (right) system. (brown: grains; blue: water; black: oil)

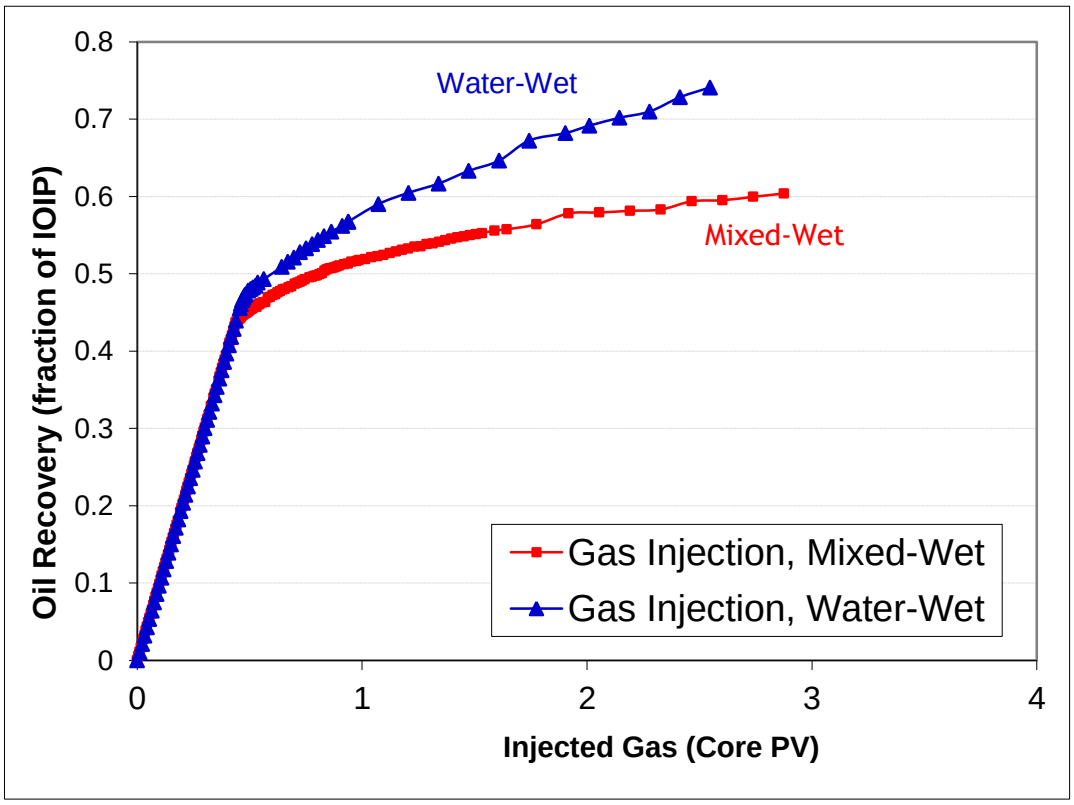

Figure 6-3: Effect of wettability on the performance of primary gas injection (65 mD).

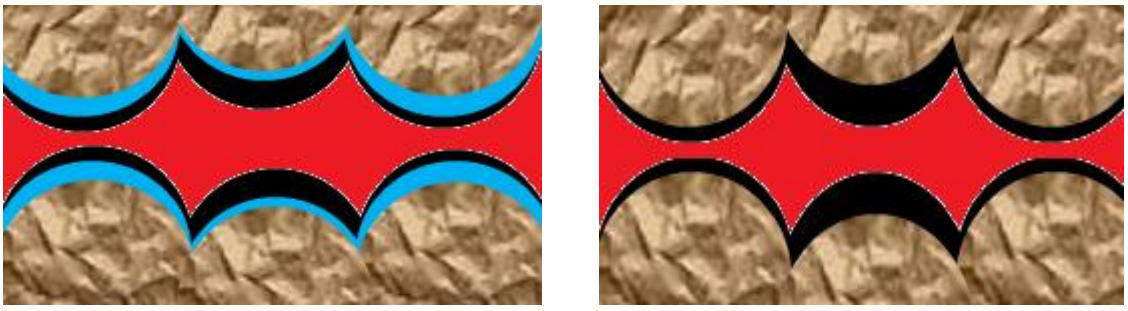

Figure 6-4: pore-scale schematics of distribution of gas, oil and water for gas injection in water-wet (left) and non-water wet pores of mixed-wet (right) systems. (brown: grains; blue: water; black: oil; red: gas)

6.3.2 Effect of Wettability on Primary Gas Injection (65mD core)

To investigate the effects of rock wettability on the performance of gas injection, the results of oil recovery from the water-wet and the mixed-wet cores were compared. Figure 6-3 shows that the gas BT in the water-wet rock happens slightly later than that in the mixed-wet core. The same graph also shows that the oil-production rate (slope of oil recovery curve) and the ultimate oil-recovery factor achieved in the case of the mixed-wet core is less compared to the case of water-wet core. These observations indicate that the performance of gas injection has been adversely affected in the mixed-wet core. This can be explained as follows. In the mixed-wet core, the pores can be

divided into two types: (1) partly water-wet (where there is a layer of immobile water covering the grains' surfaces) and (2) partly intermediate to oil-wet pores. The behaviour of the first group of the pores (water-wet) would be the same in both cores, but in the water-wet rock, the connected oil layers spreading on the films of immobile water (wetting layers) facilitate the oil flow and recovery during the near-miscible gas injection (Figure 6-4a). However, in the intermediate and oil-wet pores (in mixed-wet core), the oil layers are located on the surface of the grains (wetting layers) and hence are attached to the surfaces of the rock (Figure 6-4b), which make the recovery and flow of the oil more difficult compared with the water-wet rock.

6.3.3 Effect of Wettability on WAG Injections (65mD core)

Figure 6-5 shows ternary diagrams of the average saturation changes calculated from material balance for both water-wet and mixed-wet WAG experiments. As can be seen from this figure, oil saturation reduction is more for gas-injection periods (red lines) in the water-wet system compared to the mixed-wet system. This means that tertiary gas injections (three-phase) have higher oil recovery in the water-wet system than in the mixed-wet system. This is consistent with the results of primary gas injections (two-phase) explained earlier, in which oil recovery was less for the mixed-wet core compared to the water-wet rock.

Figure 6-6 compares the amount of oil recovery achieved in different cycles of the mixed-wet and the water-wet WAG experiments. As can be seen, although oil recovery by the first water injection is considerably higher for the mixed-wet compared with the water-wet case, the overall performances of the two WAG tests after alternating injections of 11 PV of water and gas are approximately the same, with a residual oil saturation of less than 5% IOIP. Figure 6-7 shows oil recovery for these two WAG processes as a fraction of residual oil saturation after the primary waterflooding. This figure shows that for both of these wettability conditions, WAG is very effective for further recovery of the trapped oil saturation after a primary waterflood. Figure 6-8 and Figure 6-9 show oil recovery performance of gas injection periods in the water-wet and mixed-wet WAG experiments, respectively. Comparison of these two figures reveals that alternation of gas injections with water periods significantly improves the recovery performance of the three-phase gas injections in the case of the water-wet system, but the effect is less for the mixed-wet sample.

Figure 6-10 and Figure 6-11 compare the performance of WAG injection with primary gas and primary water injection in the mixed-wet and water-wet systems, respectively. Oil recovery by WAG injection is higher than water injection for both wettability conditions (water-wet and mixed-wet). What is interesting is the lower performance of the primary gas injection compared to water injection in the mixed-wet system, while the performance of the primary gas injection is considerably higher than waterflooding for water-wet system. WAG injection has a superior performance over both water-only and gas-only injections for both wettability conditions tested (in terms of ultimate oil recovery achievable), but it seems that the performance of WAG will be further improved if the WAG process starts with a water-injection period for the mixed-wet rock and with a gas-injection period in the water-wet system.

It should be mentioned that the comparison of the performance of primary gas injection with that of WAG injection is not very straightforward in coreflood experiments. Although Figure 6-10 shows that at the small scale of cores in the laboratory, primary gas injection produces more oil (at least initially) compared with WAG injection, at the large scale of real reservoirs (where gravity and heterogeneity effects are present), it is expected that WAG performance would be much better than primary gas injection. Another point worth mentioning here in relation to comparison of gas and WAG injection is the additional cost of primary gas injection compared to WAG injection, giving WAG a more favourable economy than gas-only injection.

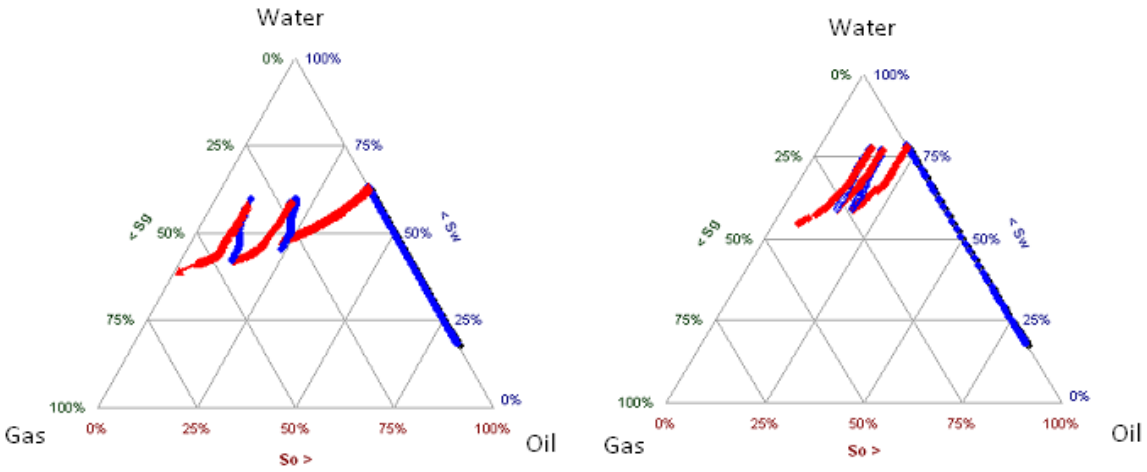

Figure 6-5: Effect of wettability on the ternary diagrams of saturation changes in WAG injection experiments; left: Water-Wet; right: Mixed-wet (65 mD; WAG injection, blue: water injection; red: gas injection)

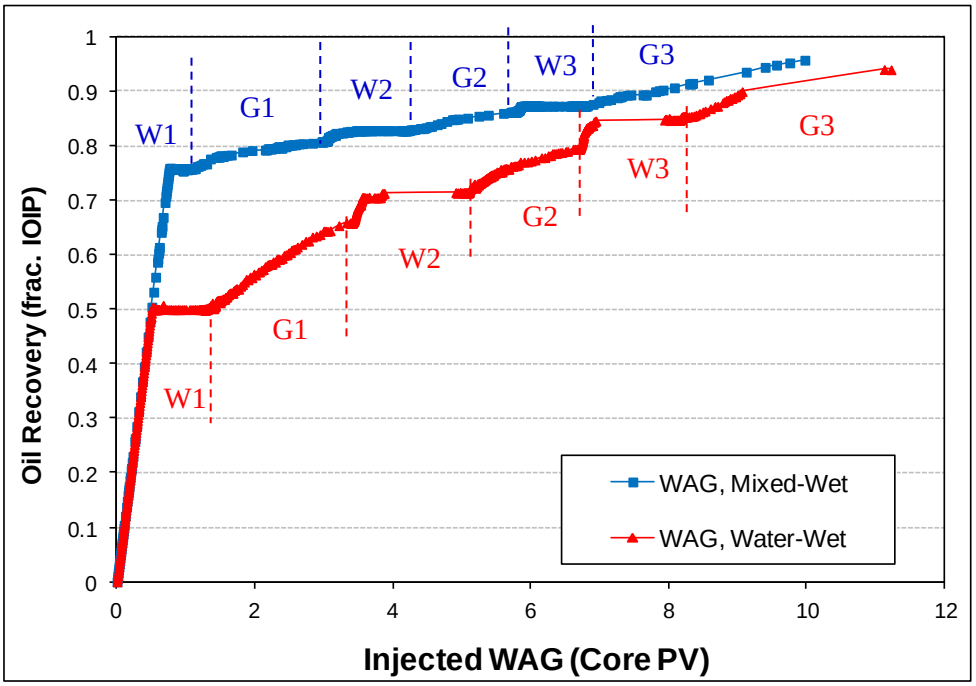

Figure 6-6: Effect of wettability on the performance of WAG injection (65 mD, IDIDID).

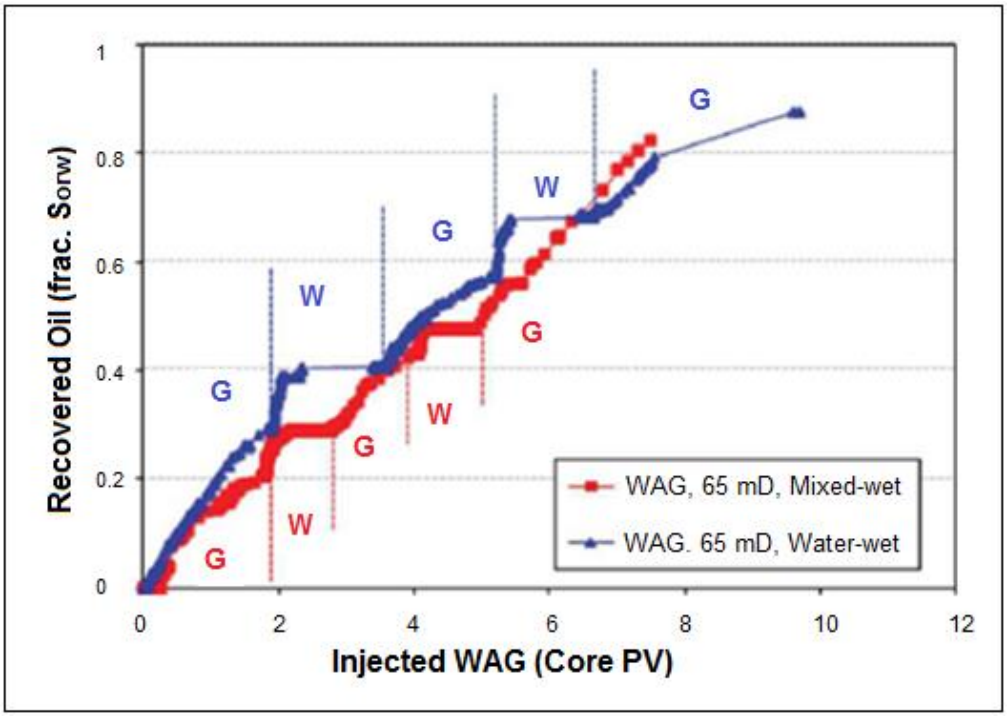

Figure 6-7: Oil recovery (fraction of the remained oil after primary waterflooding) vs. pore volume WAG injected (65 mD, IDIDID, Water-wet vs. Mixed-wet).

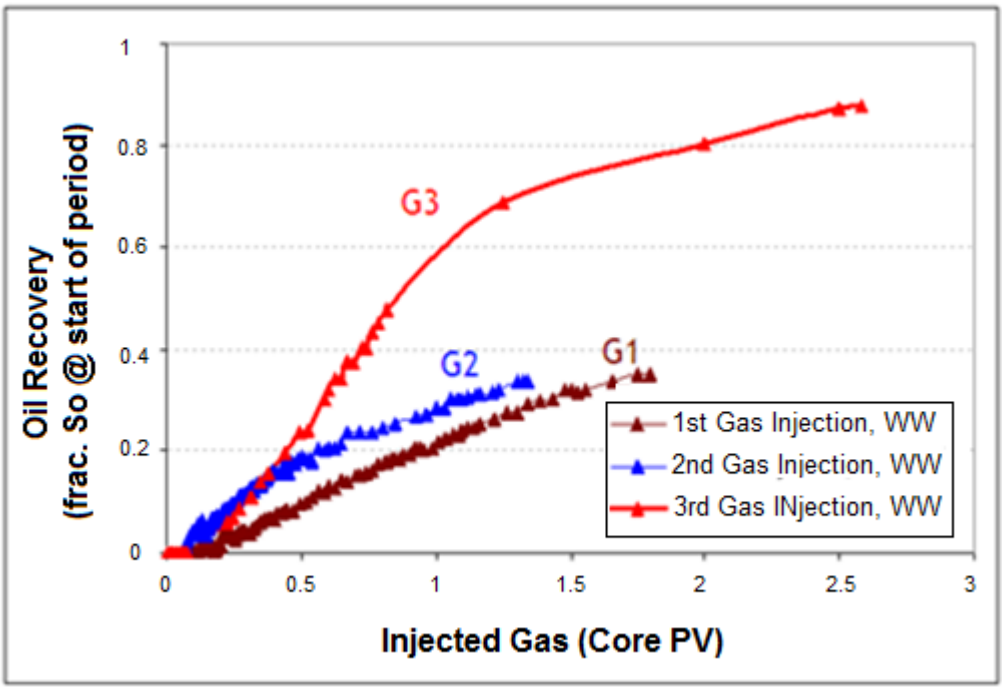

Figure 6-8: Oil recovery vs. pore volume gas injected for different three-phase gas injection periods (65 mD, WAG Injection, IDIDID, water-wet).

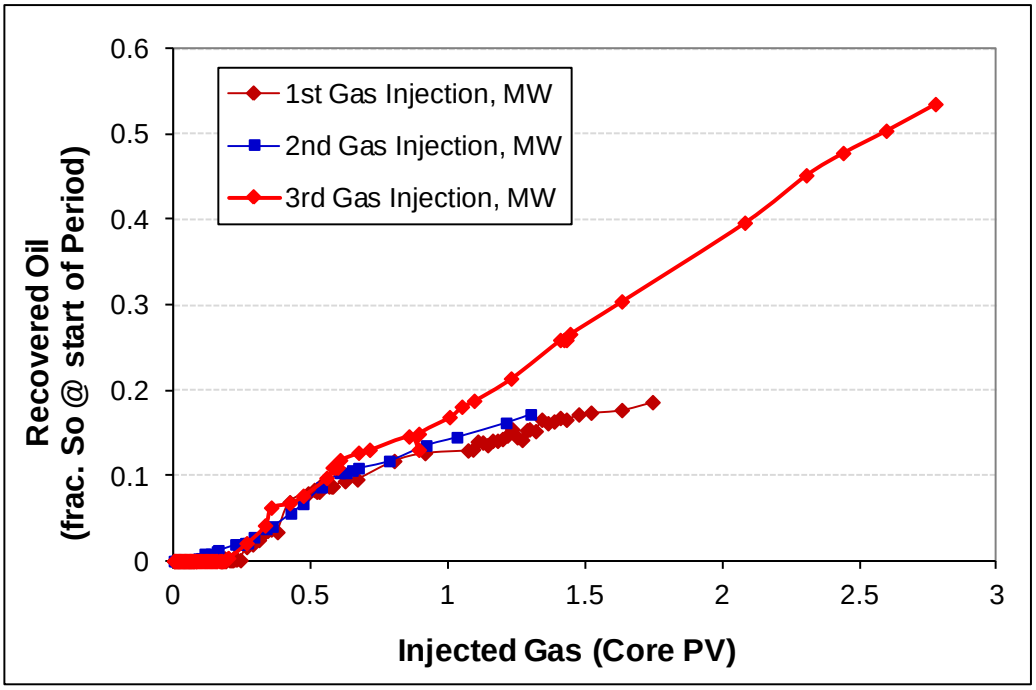

Figure 6-9: Oil recovery vs. pore volume gas injected for different three-phase gas injection periods (65 mD, WAG Injection, IDIDID, mixed-wet).

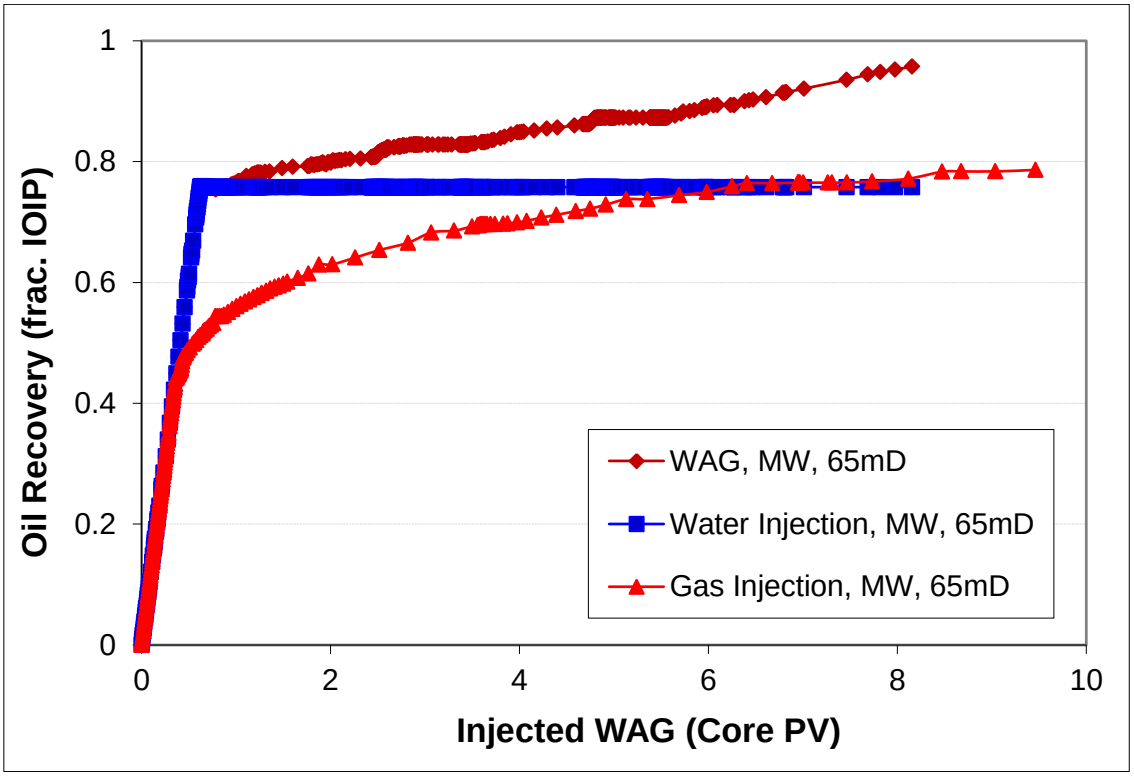

Figure 6-10: Oil recovery performance of WAG injection vs. primary gas injection and primary waterflooding (65 mD, mixed-wet).

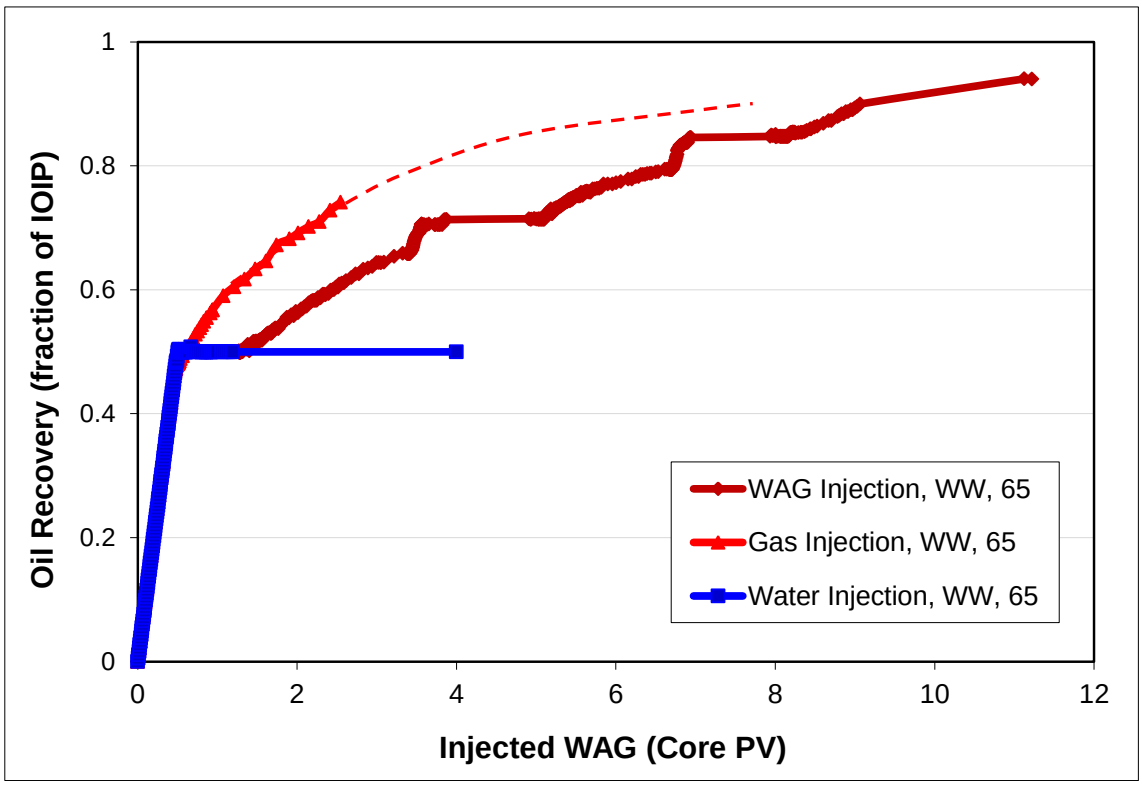

Figure 6-11: Oil recovery performance of WAG injection vs. primary gas injection and primary waterflooding (65 mD, water-wet).

6.3.4 Effect of Injection Sequence on WAG Process (65mD, Mixed-Wet)

Figure 6-12 compares the oil recovery of the two WAG tests performed on the 65mD mixed-wet core sample (experiments 6 and 7). As mentioned earlier, the difference between these two experiments was the order in which water and gas were injected into the core. This figure shows that the achieved oil recovery in the mixed-wet system is higher in the WAG injection starting with primary waterflooding. This is due to the very high efficiency of the first water injection compared to the first gas injection in mixed-wet systems. Figure 6-12 shows that, although for the 1st WAG cycle (1st water injection and gas injection cycle), more gas has been injected in the WAG test started with primary gas injection (WAG-DIDIDIDI), the ultimate oil recovery for this period is less for this WAG test compared to the WAG injection started with waterflooding (WAG-IDIDID). Aalthough in the performed experiments the order of injection of gas and water periods does not significantly influence the ultimate oil recovery achieved, but the rate of oil production and the amount of oil recovery for the same volume of injected WAG, is lower for the WAG started with gas. This is especially true for the early cycles of WAG which are more relevant to field applications. In addition, the injectivity during the WAG-DIDIDIDI injection scenario was considerably (almost three times) lower compared to the WAG-IDIDID. It is therefore recommended that in mixed-wet systems WAG injection begins with a water injection period.

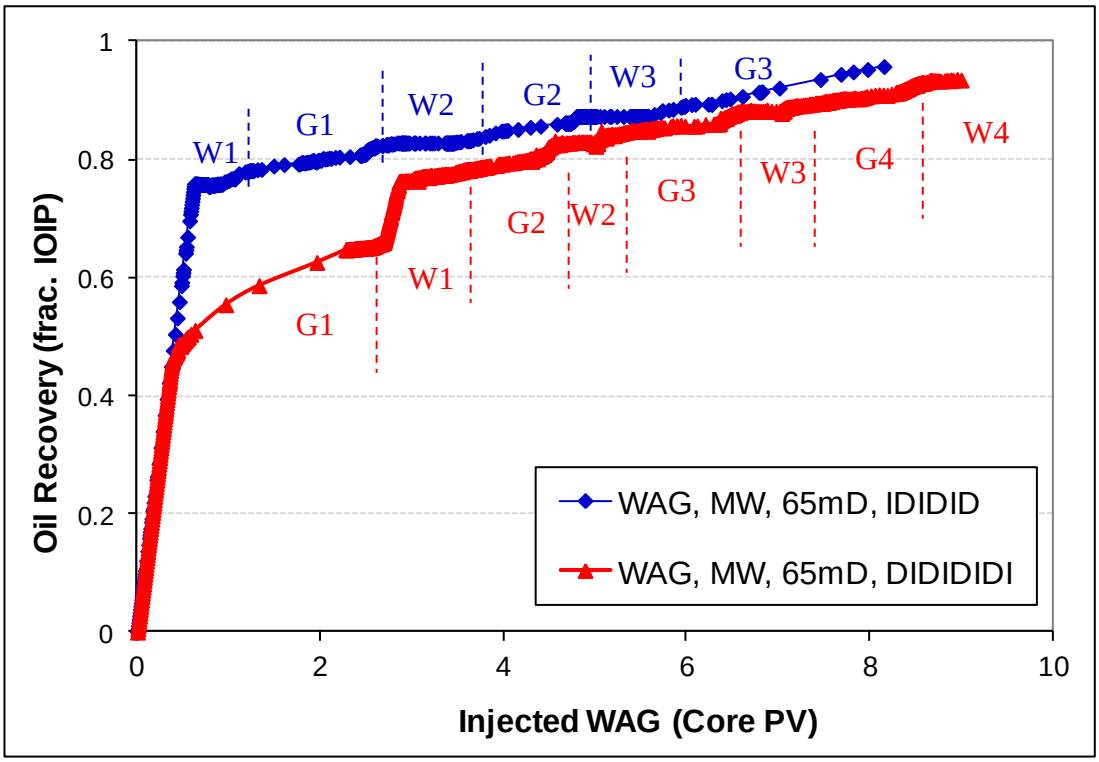

Figure 6-12: Comparison of oil recovery by two different WAG scenarios (DIDIDIDI and IDIDID); (65mD, mixed-wet).

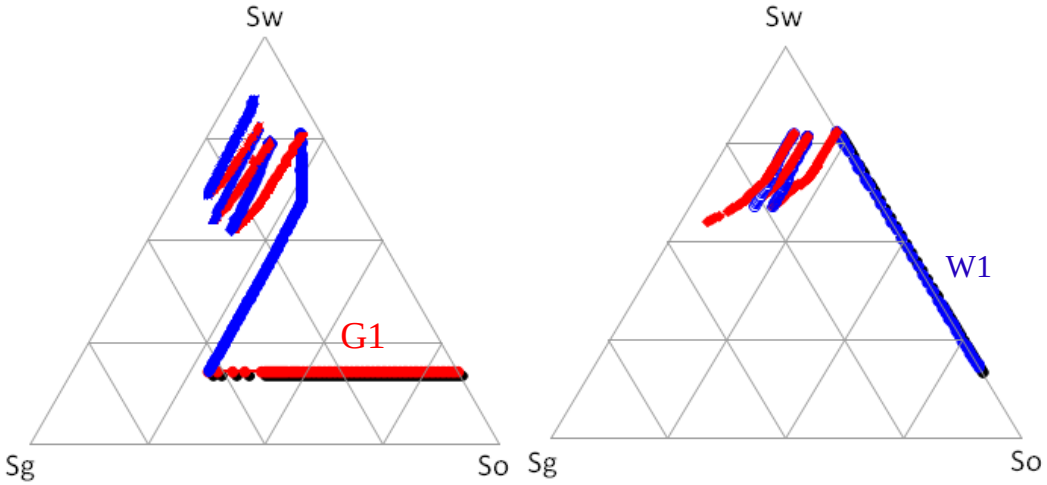

Figure 6-13: Ternary diagram of saturation changes for WAG injection tests on 65mD, mixed-wet system (left: DIDIDIDI, right: IDIDID; red: gas injection, blue: water injection).

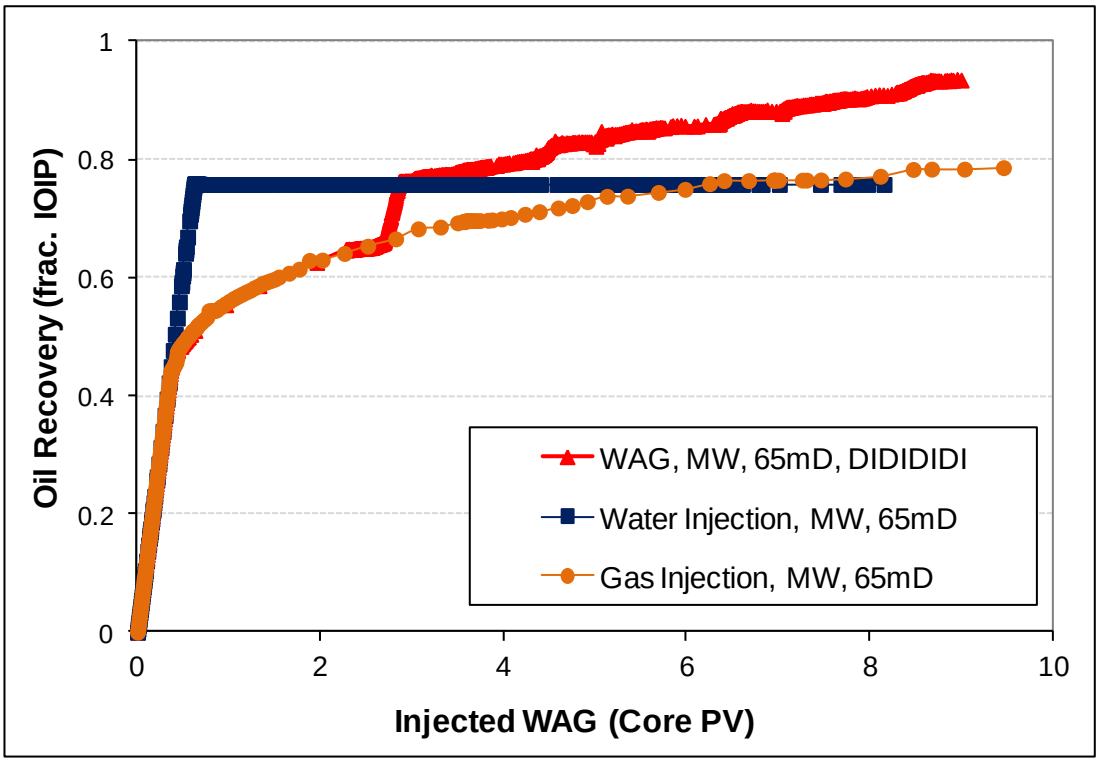

Figure 6-14: Comparison of oil recovery between WAG (DIDIDIDI) and primary waterflooding and primary gas injection; (65mD, mixed-wet).

Figure 6-13 shows ternary diagrams for saturations changes in these two WAG tests (DIDIDIDI and IDIDIDI). For DIDIDIDI injection scenario, test started with a gas injection coreflood (red line). Oil saturation decreases as the gas saturation increased, during which water saturation is constant and equal to the established immobile water saturation. During the 1st water injection period (blue line), at first there is no significant change in the oil saturation and, as the injection continues, water saturation increases while gas saturation decreases. As the injection continues further, and an oil bank is formed which is produced before the water front breakthroughs at the outlet (S_o starts to decrease suddenly). As the alternation between gas (red curves) and water (blue curves) injections continues, S_{or} decreases to 5%.

In the case of WAG test started with water (IDIDIDI), in the 1st water injection period, there is no gas in the system, and as the water injection continues, oil saturation decreases to the residual saturation with respect to water (S_{orw}). Further injection would not change the fluid saturations in the core. By switching to 1st gas injection (red curve), there will be no change in oil saturation up to breakthrough (gas saturation increases as the water saturation decreases). Just before the gas BT, there is a sudden decrease in S_o due to the oil bank formed ahead of gas front. Even after BT, the oil production continues (further reduction of S_o), although at low rates. Further alternation between

gas and water injections reduces the S_{or} to the 4%. Comparing the region of saturations after the primary injections (after 1st gas for DIDIDIDI test and after 1st water for IDIDID test) in these two WAG tests, shows the broader range of three-phase saturation area for the WAG test started with gas. Broader range of three-phase saturations means more confident three-phase k_r values could be estimated from this test.

Figure 6-14 compares the performance of $WAG_{DIDIDIDI}$ injection with those of primary gas injection and primary waterflooding for this mixed-wet core and fluid system. As is obvious from the figure, the recovery performance of the WAG injection at the end of 1st cycle (after 1st water injection) is slightly higher than the primary waterflooding and much higher than the primary gas injection. The same figure shows the repeatability of the experiments and stability of the wettability condition since the oil recovery performance of the WAG in the 1st gas injection period, matches with those of the primary gas injection quite well.

6.3.5 Effect of Gas/Water Ratio on SWAG Injection (65mD, Mixed-Wet)

Figure 6-15 shows the oil recovery results of the two SWAG injection experiments (experiments 8 and 11) performed at gas/water (SWAG) ratio of 0.25 and 1.0. For both tests gas breakthrough happened earlier than water breakthrough. The gas front moves ahead of water front since gas has much less viscosity compared to the water (and is also flowing through larger pores) its BT happens earlier than water. Water front moves behind and pushes out the oil (in smaller to medium pores) as well as part of the gas phase which has already entered to the small to medium pores due to the extra-low gas/oil IFT. Although one would expect that under near-miscible conditions, more injected gas yield more oil and delayed gas BT, but Figure 6-15 shows otherwise. In fact for SWAG injection in the mixed-wet system, at the higher gas/water ratio, the gas breakthrough happens earlier, and the oil production after gas BT is delayed. This can be due to the mixed-wet condition of the rock sample in which gas injection is less effective than waterflooding (Figure 6-10).

Although in this study no SWAG injection was performed in the water-wet system, but considering the higher efficacy of the gas injection compared to the waterflooding in that system (Figure 6-11) the author expect that larger fraction of the injected gas in water-wet system result to larger oil recoveries. It is also interesting to note that the ultimate oil recovery has stayed almost the same for both SWAG ratios. In other words, increasing the ratio of the injected gas (from 0.25 to 1.0) has not affected the ultimate

amount of oil recovery (after water breakthrough), but it has delayed its production by about 0.3 core PV. The observed independency of the ultimate oil recovery by SWAG injection, from gas/water ratio in these tests, is in line with previous findings on SWAG injection in micromodel experiments by Sohrabi *et al.* (2008b). However, those experiments had been carried out in a water-wet porous medium. Based on their micromodel studies, Sohrabi *et al.* concluded that in near-miscible SWAG injection, ultimate oil recovery was independent of SWAG ratio, in the range that they had investigated (SWAG ratio of 0.2 to 0.5).

Figure 6-16 presents the cumulative amount of produced gas versus cumulative amount of produced oil for the two SWAG injections. The Figure shows that, for the same amount of produced oil, much more gas was produced in test with SWAG ratio (Q_g/Q_w) of 1.0 compared to that produced in SWAG ratio of 0.25. This means that produced gas/oil ratio (GOR) is much higher in SWAG injection with gas/water ratio of 1.0 than with gas/water ratio of 0.25.

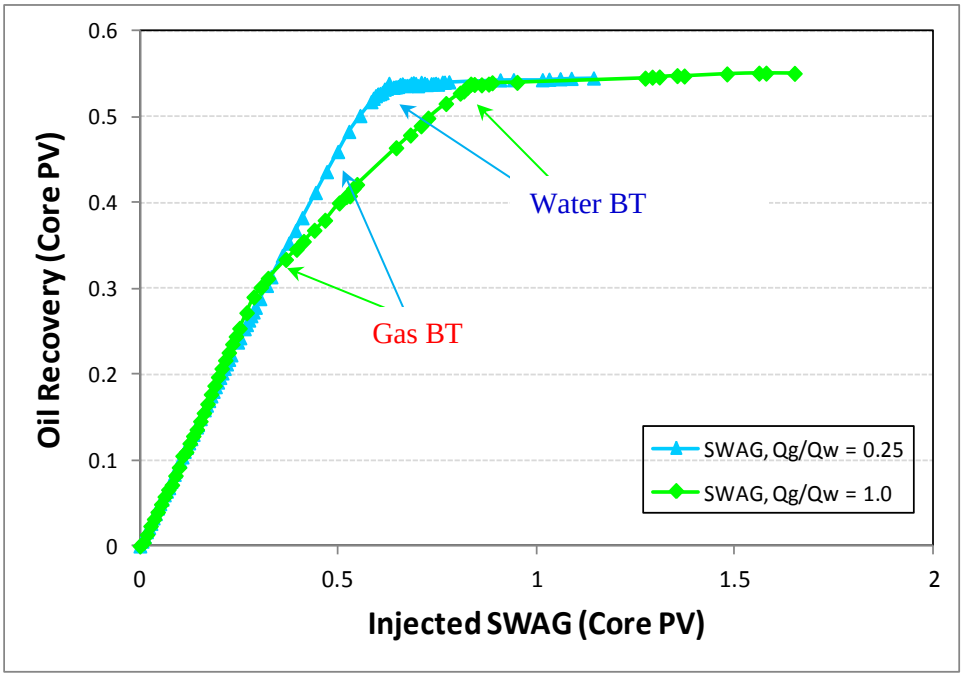

Figure 6-15: Effect of gas/water ratio on the recovery performance of the SWAG injection (65mD, Mixed-Wet).

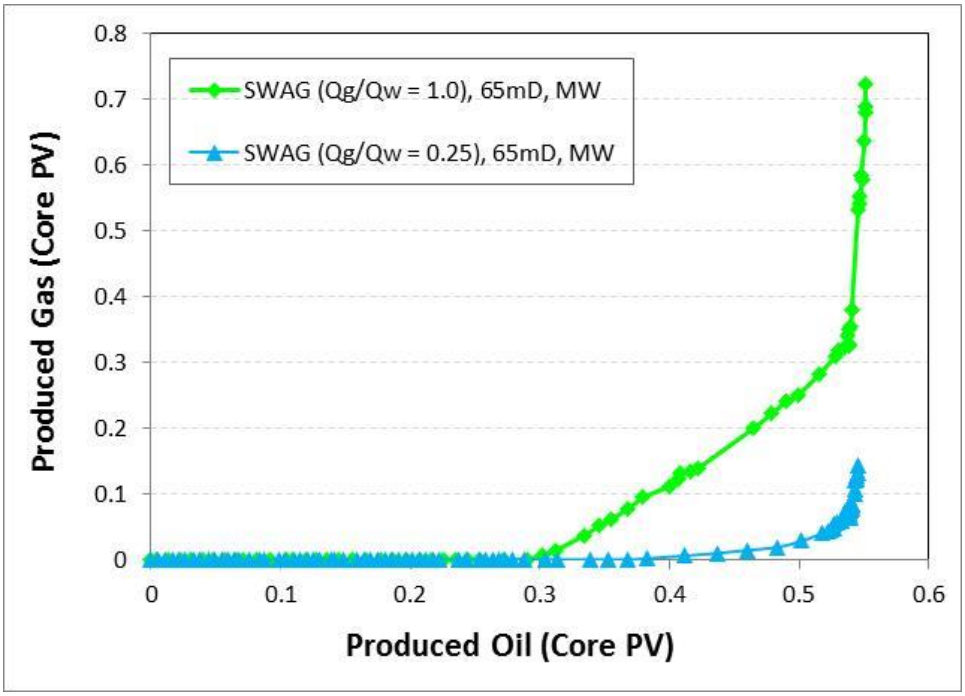

Figure 6-16: Comparison of the produced gas vs. recovered oil for two SWAG injections shows lower GOR for the case of Q_g/Q_w=0.25 (65mD, Mixed-Wet).

6.3.6 Different Injection Scenarios (65mD, Mixed-Wet)

Figure 6-17 compares the performance of the two SWAG injection tests with those of waterflooding and gas injection. It should be borne in mind that in these experiments the SWAG injections began from the start of oil production (not in tertiary mode after conventional waterflooding).

Figure 6-17 shows that (in the test performed in the 65mD mixed-wet rock) the oil recovery by the waterflooding is the highest, followed by SWAG injection with Q_g/Q_w = 0.25 and then by SWAG injection with Q_g/Q_w = 1.0. The lowest oil recovery in this series was obtained by the gas injection. Figure 6-18 shows the amount of cumulative produced gas versus cumulative produced oil, which confirms a lower GOR for SWAG injections compared to gas injection. It can be seen that with simultaneous injection of gas and water (SWAG), the amount of required gas for injection (and the produced GOR) is much less than that required in primary gas injection. But for a mixed-wet system, waterflooding gives the highest ultimate oil recovery, and as a result SWAG injection becomes much less attractive.

For comparison between the injectivity in SWAG injection and waterflooding, two options were possible. First, to keep the total injection rate the same in both SWAG and waterflooding (i.e., Q_w+Q_g for SWAG test = Q_w in waterflood test), or keep the water injection rate the same in both SWAG and waterflood experiments (since the pressure drop during primary gas injection is very small). Since previously for the $SWAG_{Qg/Qw}$ = 0.25 test in 1000mD sample (discussed in following section), the first option had been tried, in the 65mD core, the second option was applied. This means that in the case of gas and water flooding, the injection rate was $25cm^3.h^{-1}$, and for the SWAG test, water injection rate was kept at $25cm^3.h^{-1}$ (a total gas and water rate of 50 $cm^3.h^{-1}$). The experimental results show that although in two-phase flow, the gas injection has a negligible pressure drop compared to water injection, but its simultaneous injection with water dropped SWAG injection injectivity ($Q_{inj}/\Delta p$) almost half of the waterflooding. As will be discussed later in this chapter, the reduction of the SWAG injectivity compared to the waterflooding is also observed for the 1000 mD core sample, where the injection rate of water was also half of the waterflooding (keeping the total injection rate in SWAG the same as waterflooding injection rate).

Figure 6-19 compares the performance of the two SWAG injections with those of WAG_{IDIDID} and $WAG_{DIDIDIDI}$ injection scenarios. The performance of both WAG injections by the end of the 1st cycle was better than the SWAG injections. The water injection rate for all these experiments was 25 $cm^3.h^{-1}$. The observations in this study show that, in the $WAG_{DIDIDIDI}$ test, after each gas injection stage (drainage), the resistance to the flow of water in the next stage of injection (imbibition), is increased. Each stage of water injection exhibits even higher resistance (larger pressure drop across the core and less injectivity) to the flow than the previous stage. But this is not the case for the WAG_{IDIDID} since the pressure drop across the core for the 2nd and 3rd periods of imbibition remains almost the same. For 2nd water injection, the injectivity in $WAG_{DIDIDIDI}$ is almost half of that for 2nd water injection in WAG_{IDIDID}, which dropped to ¼ for the 3rd and 4th waterfloodings. Comparing the two WAG tests, it was concluded that the one started with drainage ($WAG_{DIDIDIDI}$) shows much higher injectivity problems than the WAG that starts with imbibition (WAG_{IDIDID}).

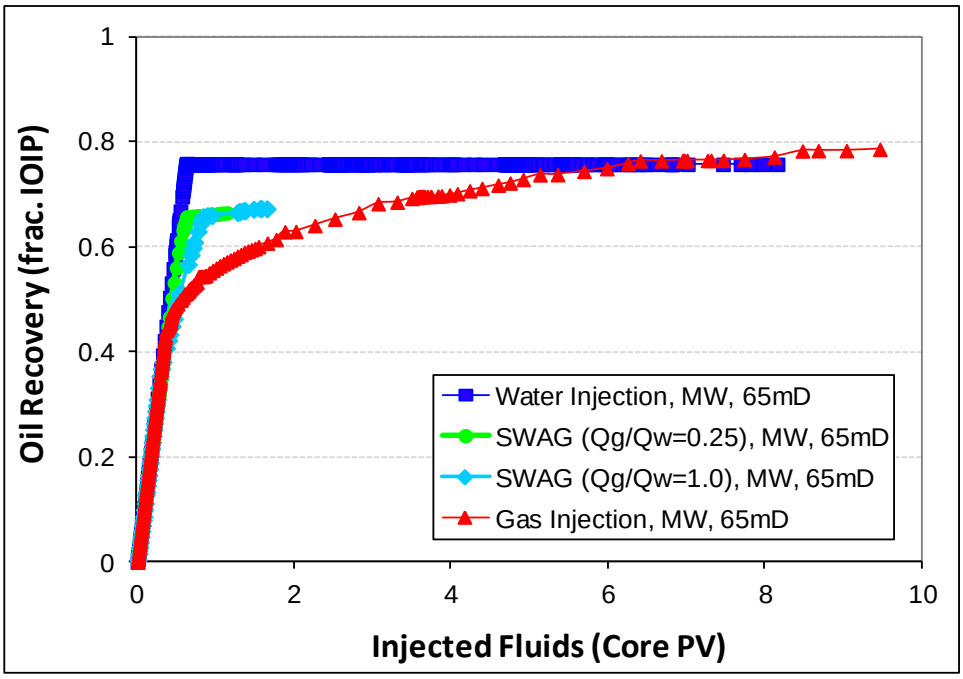

Figure 6-17: Comparison of the recovered oil for SWAG injections with primary gas injection and primary waterflooding (65mD, Mixed-Wet).

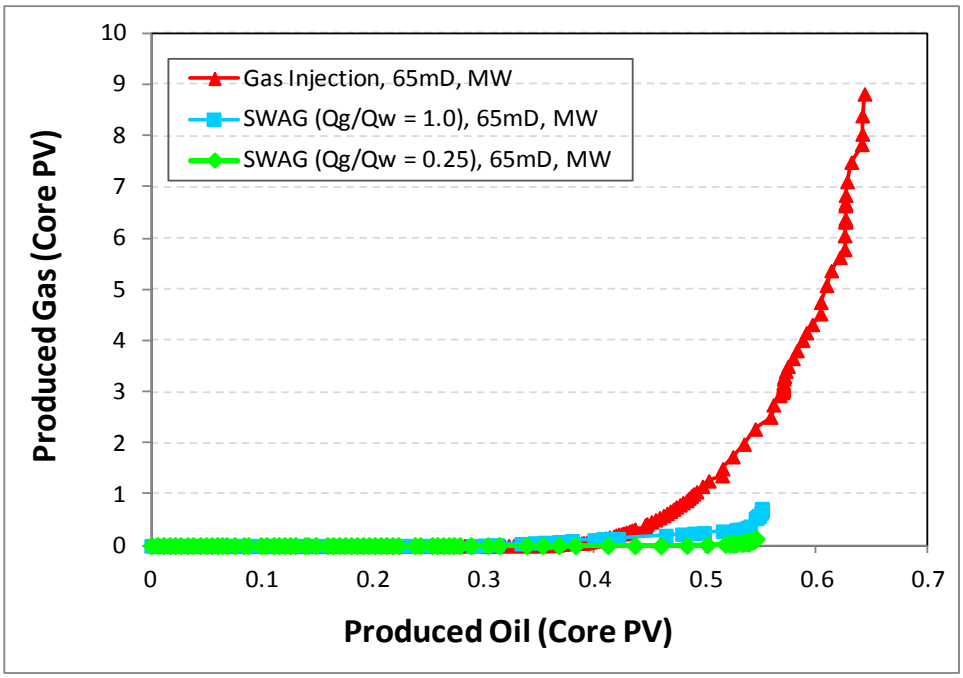

Figure 6-18: Produced gas vs. produced oil for gas injection and two SWAG injections (65mD, Mixed-Wet)

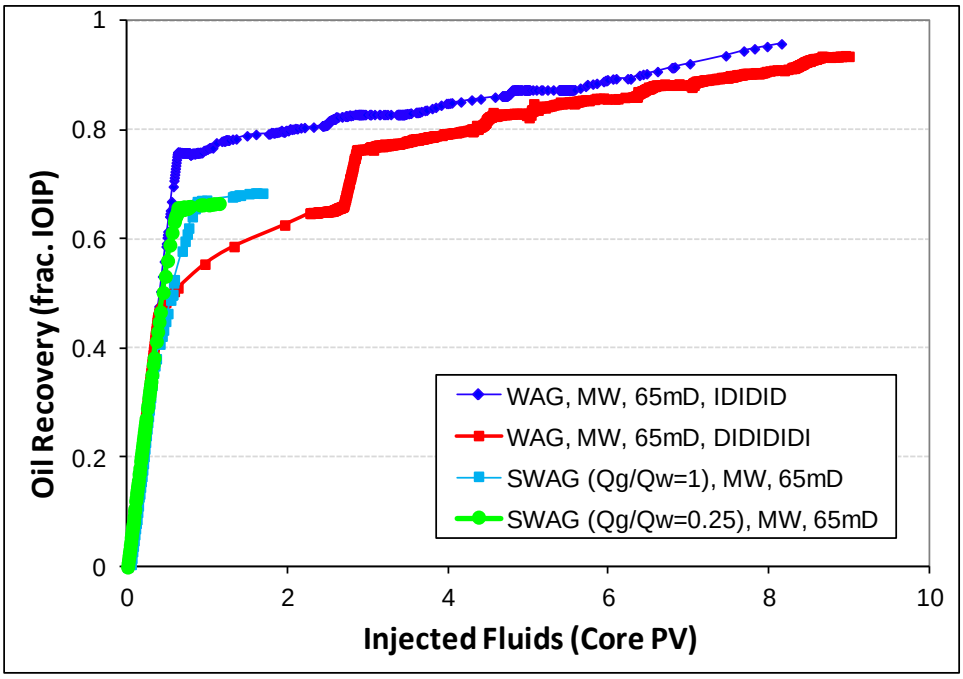

Figure 6-19: Comparison of the recovered oil for SWAG injections with two WAG injection scenarios (65mD, Mixed-Wet).

Figure 6-20 shows comparison of the injectivity indexes for different waterflooding stages of the WAG-IDIDID and WAG_DIDIDID injection scenarios as well as SWAG (Q_g/Q_w = 1) performed in the 65 mD mixed-wet sample at 1840 psia. The best injectivity response was observed for the WAG-IDIDID following by SWAG injection and the worst injection scenario in terms of injectivity was WAG-DIDIDIDI.

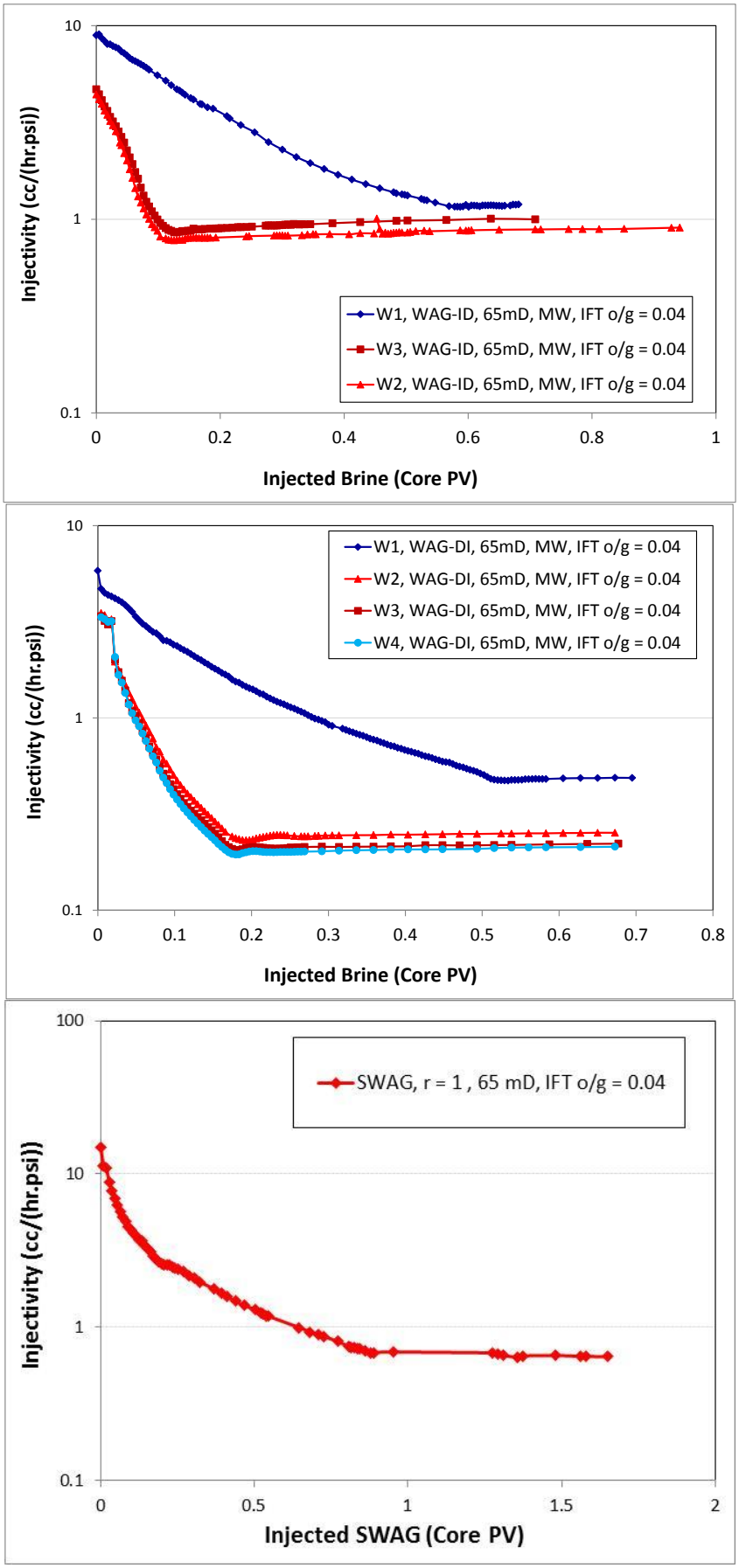

Figure 6-20: Fluids injectivity for different injection scenarios; from top to bottom, a) WAG-IDIDID, b) WAG-DIDIDIDI and c) SWAG (Q_g/Q_w) =1 (65mD, Mixed-Wet, gas/oil IFT = 0.04 $mN.m^{-1}$, 1840 psia).

6.3.7 SWAG-Tail Injection for additional Oil Recovery (65mD, Mixed-Wet)

Figure 6-21 shows saturation path during SWAG $_{Qg/Qw}$ = 0.25, as well as the extension of the experiment with a tertiary gas injection (experiment 9) and one cycle of WAG injection (experiment 10). As can be seen from this figure, there is not that much oil saturation change in the SWAG-Tail injection scenarios and the dominant flow is between gas and water by changing their positions during alternating injection of water and gas. Figure 6-22 shows the performance of the SWAG-Tail injection in which after a long injection period of 6.5 PV of gas and water injected, the additional oil recovery is just 2.52% of IOIP (0.85% during tertiary gas injection and 1.67% during the following WAG cycle). Figure 6-23 compares the performance of the extension of the SWAG $_{Qg/Qw}$ = 0.25 test (SWAG + Gas Injection +WAG) with those of primary waterflooding and primary gas injection. Figure 6-24 compares the performance of the same series of tests (SWAG + Gas Injection +WAG) with WAG_{IDIDID} and $WAG_{DIDIDIDI}$ injection scenarios. From these Figures it can be concluded that in addition to the observed poor performance of the SWAG injection test in the mixed-wet system, even the subsequent gas injection and/or WAG injection is not much beneficial for further oil recovery once the water breakthrough has happened in SWAG injection.

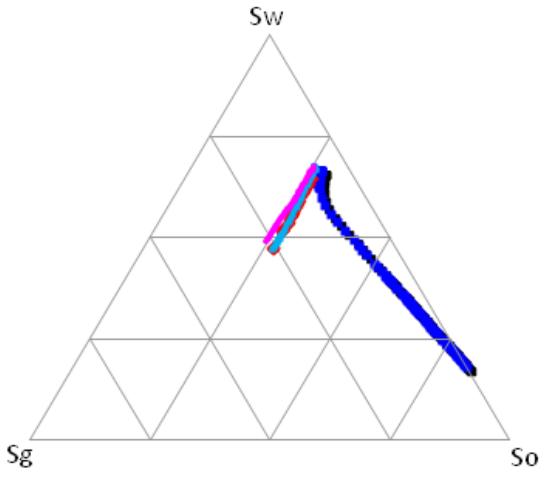

Figure 6-21: Ternary diagram of saturation path for SWAG-Tail gas injection of the WAG (65mD, Mixed-Wet, $SWAG_{Qg/Qw=0.25}$); dark blue: former SWAG; red: tertiary gas injection, light blue: water injection of subsequent WAG, pink: gas injection of subsequent WAG).

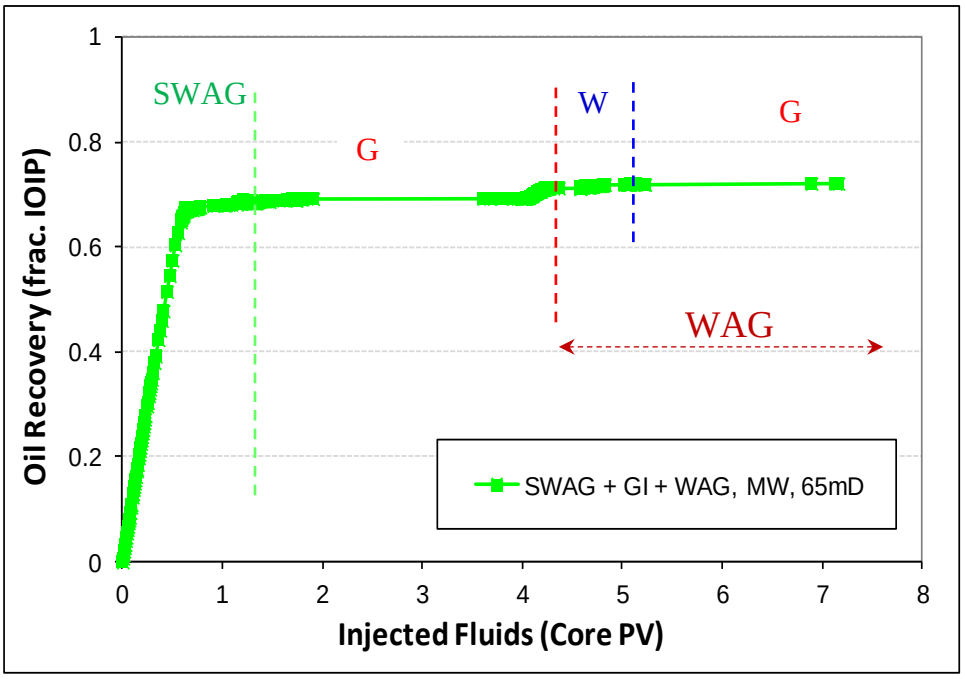

Figure 6-22: Recovered oil for the whole series of SWAG-Tail injection (SWAG + GI + WAG); (65mD, Mixed-Wet).

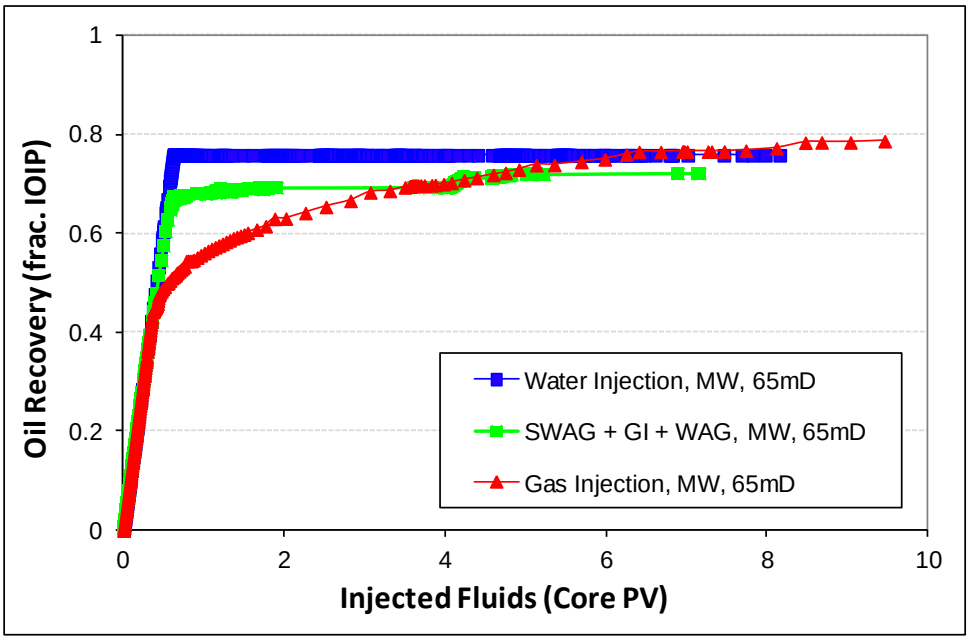

Figure 6-23: recovered oil for the case of gas injection, waterflood and the extension of the SWAG test (SWAG+GI+WAG); (65mD, Mixed-Wet).

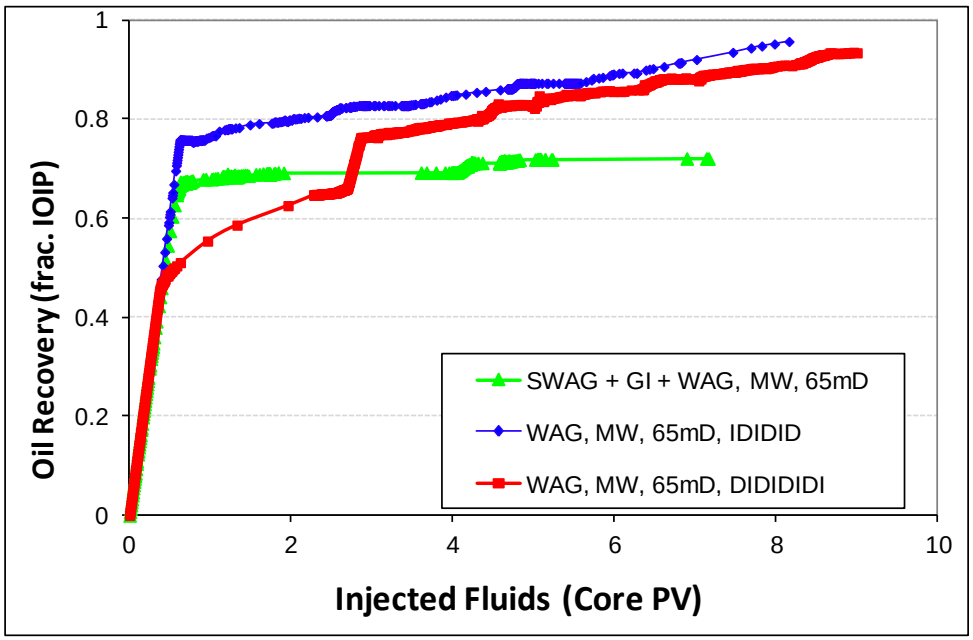

Figure 6-24: Recovered oil for the two WAG injection scenarios and the extension of the SWAG test (SWAG+GI+WAG); (65mD, Mixed-Wet)

6.3.8 Comparison of the two core samples (65mD vs. 1000mD)

As expected, oil recovery is higher for the 1000 mD core than it is for the 65 mD sample (Figure 6-25). This can be explained on the basis of pore throat size and pore size distribution. The average radii of the pores are smaller for the lower permeability core (65 mD) compared to the higher-permeability core (1000 mD). As a result, the retention of oil in the core would be higher in the 65 mD core compared with the 1000 mD one, and hence the lower oil recovery in the 65 mD core. Figure 6-26 compares the oil production performance of very-low IFT (nearly miscible) WAG injection for mixed-wet 65 mD core with that of the high-permeability core (1000 mD). As can be seen from this figure, the performance (fraction of the original oil recovered) of the first water-injection period is approximately the same in both tests. The same figure also shows that the ultimate oil recovery by low-IFT WAG injection in the 1000 mD core approaches 99% after two cycles of WAG (two water and two gas injections) at 5.2 PV of water and gas injections, while in the lower-permeability core (65 mD), after three WAG cycles and 10 PV of water and gas injection, the ultimate oil recovery is equal to 95% of the initial oil in place. Overall, the results show very high oil recovery was achieved by Low-IFT WAG injection in mixed-wet systems for both cores. Nevertheless, there are differences in the performance of WAG in a lower-permeability core compared to the higher permeability one. In both the low- and high-permeability cores, alternating injection of near-miscible (low-IFT) gas with water increased the

performance of gas injection periods. However, comparison of the first and second gas injections (with one water injection period in between) in both cores reveals that the positive effect of alternating injection has been more pronounced in the case of the 1000 mD core sample compared with the 65 mD rock (compare Figure 6-27 with Figure 6-9).

Figure 6-28 shows the comparison of oil recovery for primary waterflooding and primary gas injection with that of WAG injection for the mixed-wet 1000 mD core. The recovery trends and their qualitative position with respect to each other is the same as those already discussed for the 65 mD mixed-wet core (see Figure 6-10), which confirms the observed effect of wettability for the 65 mD core sample.

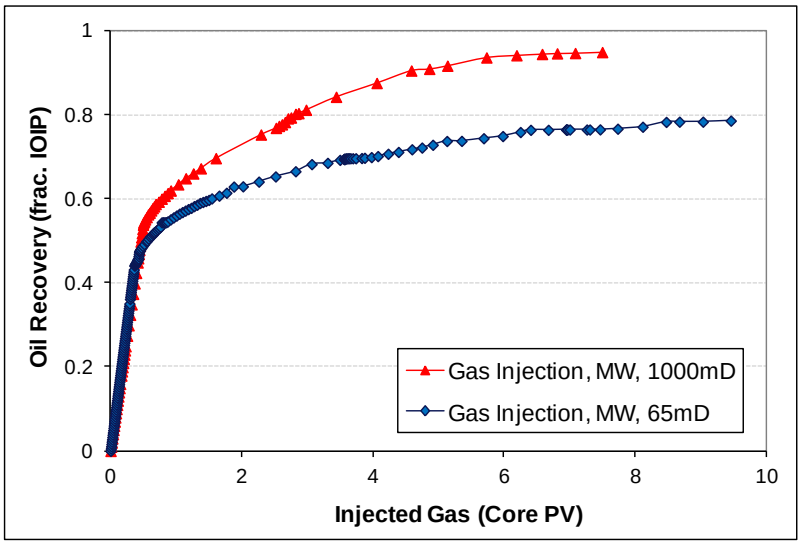

Figure 6-25: comparison of oil recovery by primary gas injections in the case of 1000mD and 65mD core samples (mixed-wet system).

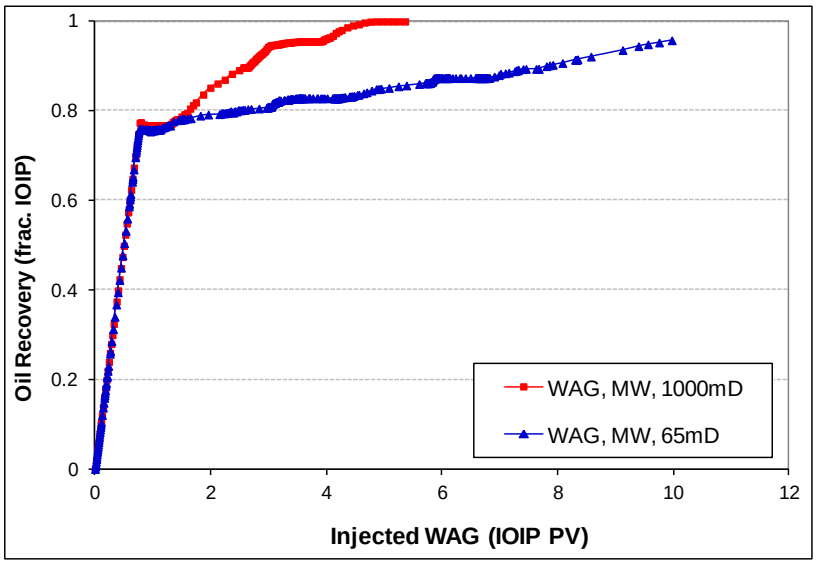

Figure 6-26: oil recovery vs. pore volume WAG injected in the case of mixed-wet cores (1000mD vs. 65mD)

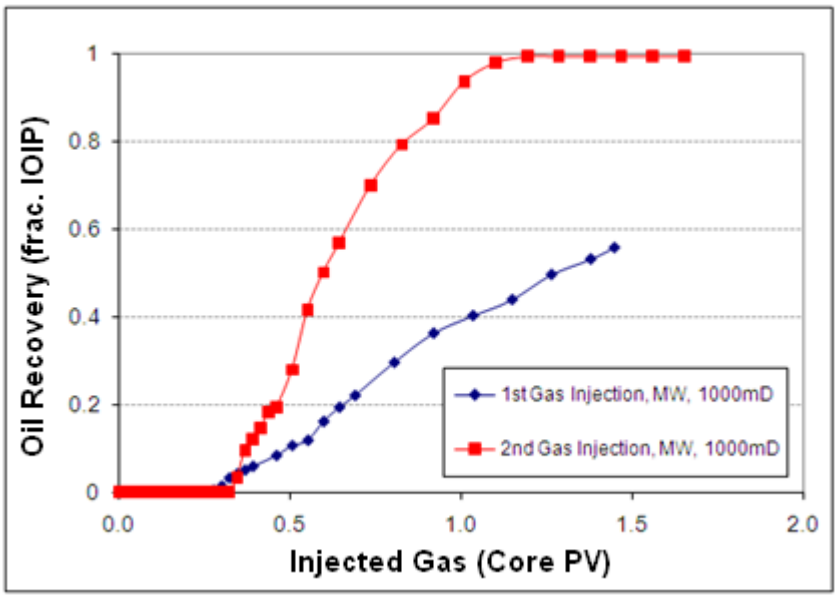

Figure 6-27: oil recovery vs. pore volume gas injected in the case of different gas injection periods (1000mD mixed-wet).

Figure 6-28 shows that SWAG injection recovered less oil compared to waterflood. The same figure also shows that SWAG injection recovery performance at initial times is higher than gas injection, but at later times (for 1000 mD after 2 PV injections) the recovery performance of the gas injection catches up with SWAG injection and goes higher afterwards. These are in agreement with the results obtained for the 65mD mixed-wet core. From these two series of tests performed on mixed-wet core samples (1000mD and 65mD), it is concluded that in the investigated mixed-wet system (under

very low oil/gas IFT), simultaneous injection of gas and water (SWAG) has lower recovery compared to conventional waterflood or WAG injection.

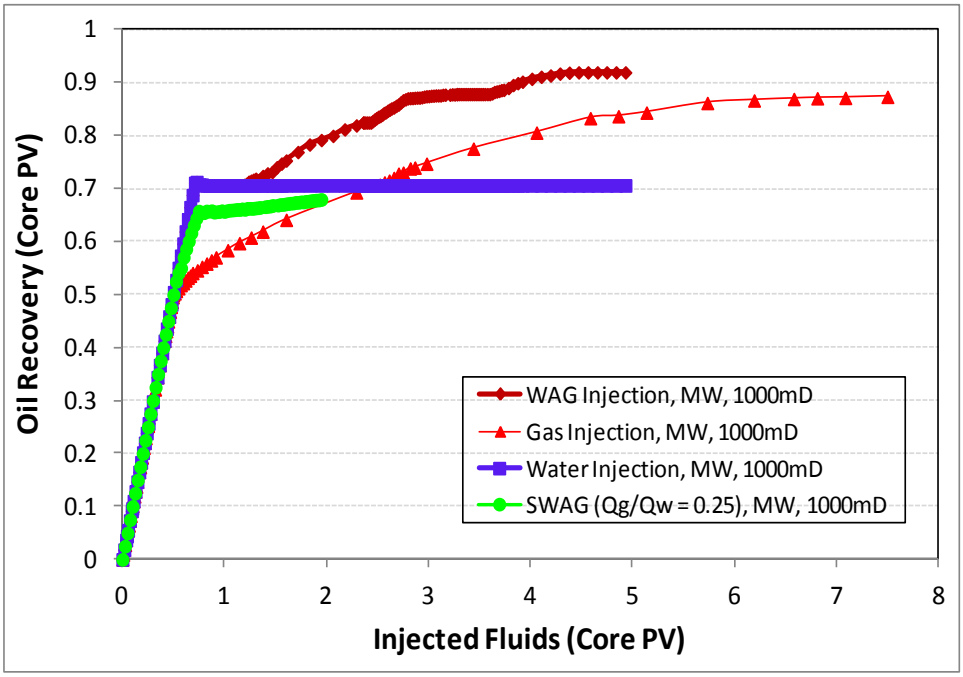

Figure 6-28: Oil recovery for different injection scenarios (1000mD, Mixed-Wet).

6.4 Conclusions

The results of a comprehensive series of coreflood experiments were presented and discussed in this chapter. The following conclusions can be drawn from the results.

1. Oil recovery by waterflood is much higher in the mixed-wet rock than in water-wet system. This is because of suppressed water-film flow and oil snap-off mechanisms under mixed-wet conditions. Contrarily, oil recovery by gas injection was higher for water-wet conditions compared to the mixed-wet system. This is attributed to higher tendency of the oil phase to adhere to the rock surfaces (and less conductivity of oil wetting layers) in mixed-wet rocks compared to the water-wet rocks (oil spreading layers).

2. In mixed-wet rocks, the performance of gas injection was lower compared with waterflood. In contrast, gas-injection performance was considerably higher than waterflood in water-wet systems. The new insights provided by these experiments clearly demonstrate the importance of wettability of the rock in the design of a field WAG injection process. The performance of water, gas, and

WAG injection are strongly affected by the state of wettability. It is therefore necessary to ensure a proper core-handling procedure in which the reservoir native state wettability is preserved. In cases where the wettability state of the core has changed, it is crucial to follow a suitable approach to reproduce the reservoir wettability before commencing coreflood experiments.

3. For water-wet systems, alternating injection of gas and water cycles increased the oil-recovery performance of each gas injection period compared with its preceding gas-injection period. This means that oil recovery, based on the fraction of oil at the beginning of the gas-injection period, is highest for the third gas-injection period and lowest in the first gas-injection period. Although the same trend is also observed for mixed-wet systems, this effect was considerably less profound in mixed-wet systems compared with water-wet systems. It should, however, be mentioned that in the mixed-wet system, most of the oil was produced in the primary stage of waterflooding and hence less oil remained for recovery in subsequent stages of WAG injection.

4. Comparison of the amount of oil recovered by WAG, SWAG, gas injections and waterflood reveals that, for the conditions of the presented experiments, WAG has a superior performance over other injection strategies tested in mixed-wet systems. In terms of oil recovery, the order of injection strategies from highest to lowest is; WAG, water flooding, SWAG and gas injection. The results also reveal that the performance of WAG injection (in mixed-wet rocks) would be adversely affected (lower oil recovery and injectivity) if WAG injection begins with a gas injection period (instead of water).

5. The results on the effects of SWAG (gas/water) ratio of 0.25 and 1.0 show that the rate of oil recovery in mixed-wet systems decreases by increasing the gas fraction. However, the ultimate oil recovery achieved remained almost the same for the two SWAG ratios tested.

6. In addition to the lower oil recovery obtained by SWAG injection in the mixed-wet systems, it was also noticed that SWAG injection results in considerably lower injectivity than what was observed for single-phase fluid injection. Although some degree of injectivity reduction is expected when water and gas injection is combined, yet the observed reduction in injectivity for SWAG

injection was disproportionate to the amount of additional oil recovery obtained from it. The injectivity index for SWAG injection was also lower compared to the WAG-IDIDID but still above the index for the WAG-DIDIDID injection sequence.

6.5 References

Agbalaka C., Dandekar A.Y., Patil S.L., Khataniar S., Hemsath J.R., (2008): The Effect of Wettability on Oil Recovery: A Review, SPE 114496-MS, SPE Asia Pacific Oil and Gas Conference and Exhibition, 20-22 October, Perth, Australia.

Awan A.R., Teigland R., and Kleppe J., (2008): A Survey of North Sea Enhanced-Oil-Recovery Projects Initiated During the Years 1975 to 2005, SPE Reservoir Evaluation & Engineering, Volume 11, Number 3, pp. 497-512.

Berg L.I., Stensen J.A., Crapez, B., Quale, A., (2002): "SWAG behaviour based on Siri field data", SPE-75126, presented at SPE/DOE IOR symposium, April 13–17, Tulsa, Oklahoma, USA.

Blackwell R.J., Terry W.M., Rayne J.R.; Lindley D.C.; Henderson J.R.; (1960): Recovery of Oil by Displacements with Water-Solvent Mixtures". *Petroleum Transactions*, 219, pp. 293-300.

Blunt M.J., (2000): An empirical model for three-phase relative permeability, SPE Journal, Volume 5, Issue 4, pp. 435–445.

Caudle, B. H. and Dyes, A. B.: 1958, Improving miscible displacement by gas–water injection, Petroleum Transactions, AIME, Volume 213, pp. 281-283.

Christensen J.R., Stenby E.H., Skauge A., (1998):"Compositional and relative permeability hysteresis effects on near miscible WAG", presented at SPE/DOE Improved oil recovery symposium, 19–22 April, Tulsa, Oklahoma, USA.

Christensen, J. R., Stenby, E. H., and Skauge, A., (2001): Review of WAG Field Experience, SPE Reservoir Evaluation & Engineering, Volume 4, Number 2, pp. 97-106.

DiCarlo D.A., Sahni A. and Blunt M.J., (2000a): Three-phase Relative Permeability of Water-wet, Oil-wet, and Mixed-wet Sand-packs, SPE Journal, Volume 5, Issue 1, pp. 82–91.

DiCarlo D.A., Sahni A. and Blunt M.J., (2000b): The Effect of Wettability on Three-phase Relative Permeability, Transport Porous Media, Volume 39, Issue 3, pp. 347–366.

Skauge A. and Aarra M., (1993): Effect of Wettability on the Oil Recovery by WAG, presented at the 7th European IOR Symposium, October 26-28, Moscow, Russia.

Element D.J., Masters J.H.K., Sargent N.C., Jayasekera A.J. and Goodyear S.G., (2003): Assessment of Three-phase Relative Permeability Models Using Laboratory Hysteresis Data, SPE 84903, Proceedings of the SPE International Improved Oil Recovery Conference in Asia Pacific, Kuala Lumpur, Malaysia.

Jadhunandan, P.P. and Morrow, N.R. 1995. Effect of Wettability on Waterflood Recovery for Crude-Oil/Brine/Rock Systems, SPE Formation Evaluation, Volume 10, Issue 1, pp. 40–46.

Kulkarni M.M. and Rao D.N.; (2005): Experimental investigation of miscible and immiscible Water-Alternating-Gas (WAG) process performance. Journal of Petroleum Science and Engineering, Volume 48, Issue 1-2, pp. 1-20.

Larsen J.K. and Skauge A., (1999):"Simulation of the immiscible WAG process using cycle-dependent three-phase relative permeabilities", SPE-56745, presented at SPE Annual Technical Conference and Exhibition, 3–6 October, Houston, Texas, USA.

Larsen J.K., Bech N., Winter A., (2000): "Three-phase immiscible WAG injection: Micromodel experiments and network models", presented at SPE/DOE Improved oil recovery symposium, 3–5 April, Tulsa, Oklahoma, USA.

Quale E.A., Crapez B., Stensen J.A., and Berge L.I., (2000):"SWAG Injection on the Siri Field - An Optimized Injection System for Less Cost", SPE-65165, presented at the SPE European Petroleum Conference, 24–25 October, Paris, France.

Skauge A. and Aarra M., (1993): "Effect of wettability on oil recovery by WAG", presented at 7th EAPG IOR Europe, 27–29 October, Moscow, Russia.

Shahverdi H., Sohrabi M. and Jamiolahmady M., (2010): A New Algorithm for Estimating Three-Phase Relative Permeability from Unsteady-state Core Experiments, International Symposium of the Society of Core Analysts, Halifax, Nova Scotia, Canada, 4-7 October.

Shahrokhi O., Fatemi S.M., Sohrabi M., Ireland S., Ahmed K., (2014): Assessment of Three Phase Relative Permeability and Hysteresis Models for Simulation of Water-Alternating-Gas (WAG) Injection in Water-wet and Mixed-wet Systems, SPE-169170, SPE Improved Oil Recovery Symposium held in Tulsa, Oklahoma, USA, 12–16 April.

Shahverdi H., Sohrabi M., Fatemi M., Jamiolahmady M., Ireland S., Robertson G., (2011): Evaluation of Three-Phase Relative Permeability Models for WAG Injection Using Water-Wet and Mixed-Wet Core Flood Experiments, presented at SPE EUROPEC/EAGE Annual Conference and Exhibition, 23-26 May, Vienna, Austria.

Sohrabi M., (2001): Water Alternating Gas Injection (WAG) Studies, PhD Thesis submitted to Institute of Petroleum Engineering at Heriot-Watt University, Edinburgh, Scotland.

Sohrabi M., Tehrani D.H., Danesh A., Henderson G.D., (2004): Visualisation of Oil Recovery by Water-Alternating-Gas Injection Using High-Pressure Micromodels, SPE J., Volume 9, Number 3, pp. 290-301.

Sohrabi, M., Tehrani, D. H. and Al-Abri, M., (2007): "Performance of Near-Miscible Gas and SWAG Injection in a Mixed-Wet Core", proceedings of the International Symposium of the Society of Core Analysts, 10-13 September, Calgary, Canada.

Sohrabi M., Danesh A., Tehrani, D. and Jamiolahmady M., (2008a): Microscopic Mechanisms of Oil Recovery By Near-Miscible Gas Injection, Transport in Porous Media, Volume 72, Number 3, pp. 351-367.

Sohrabi M., Danesh A., and Jamiolahmady M., (2008b): Visualisation of Residual Oil Recovery by Near-Miscible Gas and SWAG Injection Using High-Pressure Micromodels, Transport in Porous Media, Volume 74, Number 2, pp. 239-257.

Sohrabi M., Shahverdi H., Jamiolahmady M., Fatemi M., Ireland S., Robertson G., (2010): Experimental and Theoretical Three-phase Relative Permeability for WAG Injection in Mixed-Wet and Low IFT Systems, presented at International Symposium of the Society of Core Analysts, Halifax, Canada

Sohrabi M., Fatemi M., Shahverdi H., Jamiolahmady M., Ireland S., Robertson G., (2011): Reliable Prediction of Water Alternating Gas (WAG) Injection Performance, presented at 8th DEVEX, Aberdeen, UK, 11-12 May 2011.

Stephenson D.J., Graham A.G., Luhning R.W., (1993):"Mobility control experience in the Joffre Viking miscible carbon dioxide flood", *SPE Reservoir Engineering*, **11**, Number 3, pp.183–188.

Suicmez V.S., Piri M. and Blunt M.J., (2007): Pore-scale Simulation of Water Alternate Gas Injection, Transport in Porous Media, Volume 66, Number 3, pp. 259-286.

Tiab, D. and Donaldson, E.C., (2004), Petrophysics: Theory and Practices of Measuring Reservoir Rock and Fluid Transport Properties, second edition. Oxford, UK: Gulf Professional Publishing.

7. Hysteresis Effect on Three-Phase Relative Permeabilities

One major problem in the prediction of the performance of Water Alternating Gas (WAG) process is the uncertainty associated with the changes in three-phase relative permeability (k_r) values of oil, gas and water in different cycles, which is known as cyclic hysteresis. This chapter investigates the effect of cyclic injection on three-phase k_r of the presented WAG coreflood experiments under both water-wet and mixed-wet conditions. Three-phase relative permeabilities were obtained analytically from the coreflood data using an extension of Buckley-Leveret formula to three-phase flow. The investigation covers the effects of wettability, immobile water saturation, injection scenario and permeability on the cyclic hysteresis behaviour of k_r for each the three phases (gas, oil and water). The results show the importance of properly accounting for irreversible k_r hysteresis loops (especially for gas and oil) in the processes involving cyclic injection under three-phase flow conditions. Gas relative permeability (k_{rg}) dropped in successive cycles under both water-wet and mixed-wet conditions. k_{rg} hysteresis was larger in the water-wet system compared to the mixed-wet case. The results also reveal saturation history dependency for oil relative permeability (k_{ro}), which tends to increase in successive gas injection periods. The improvement in k_{ro} was larger in the water-wet system. For the IDIDID injection sequence and in water-wet system, it was found that k_{rg} shows larger hysteresis effect for the case with higher immobile water saturation. k_{rw} hysteresis was larger in the DIDIDIDI injection scenario compared to the IDIDID case. k_{rg} and k_{rw} hysteresis effects were larger for the 1000 mD core compared to the low permeability (65 mD) sample, which is due to the saturation history differences.

In both water-wet and mixed-wet systems, the largest k_{rw} hysteresis happens for the transition from two-phase (oil/water system) to three-phase system (from 1st water injection into 1st gas injection) and the subsequent WAG cycles does not show much hysteresis for k_{rw} in the presented experiments. This study also offers insights into and explanations for the observed cyclic hysteresis behaviour based on the pore-scale and core-scale displacement mechanisms involved in WAG injection. The results highlight

some serious shortcomings of the existing reservoir simulators for reliable simulation of oil recovery processes involving three-phase flow and flow reversal.

7.1 Introduction

The three-phase relative permeability (k_r) is an important parameter in understanding and modelling of a field performance undergoing processes involving multiphase flow. The most comprehensive sets of three-phase data reported in the literature have been measured by steady-state flow (Oak, 1990; Oak *et al.* 1991; Oak 1991; Baker 1995). Dria *et al.* 1990 and Skauge and Larsen (1994) argued that the most representative relative permeability data are those obtained by a saturation path similar to the real process that occur in the reservoir. Skauge and Larsen (1994) stated that unsteady-state experiments at reservoir condition and rates are the best representative of the force balances and process path of any three-phase displacement process in a reservoir.

Sarem (1966) published a theory for interpretation of three-phase displacement experiments. He assumed that each phase's relative permeability depends only on its own saturation. Grader and O'Meara (1988) presented their derivation of the three-phase extension of the method earlier presented by Welge (1949) for two-phase flow. Their derivation shows that Johnson, Bossler and Naumann (JBN) method (Johnson *et al.* 1959) can be extended to three-phase flow as well. The assumptions that have to be made in order to use their analytical solution are: the fluids are incompressible and immiscible, the flow is one-dimensional, isothermal and the capillary pressure is neglected.

Later, a solution was also presented by Virnovskii (1984). The expressions for calculating the relative permeability curves are similar to those of Grader and O'Meara (1988), but Virnovskii's expressions are valid from the start of the experiment, during two-phase flow intervals and across phases' discontinuities. The required data are the same as for the standard JBN method (Johnson *et al.*, 1959) i.e., pressure drop and produced volumes as a function of time. One, two or three phases may be injected at fixed ratios and the total rate may vary with time. Mejia *et al.* (1996) and Nordtvedt *et al.* (1997) described a novel methodology (based on history matching technique) for determination of three-phase relative permeability functions at reservoir conditions. They estimated the appropriate three-phase relative permeability and capillary pressure functions, through solution of a series of optimization problems, so that the calculated

quantities by the simulator (such as pressure drop, saturation profiles along the core, and fluids recovery curves) are consistent with the measured values.

Three-phase relative permeabilities measurement experiments (especially the steady-state method) are often time consuming and technically difficult to perform, especially under reservoir condition. As a result, empirical models (such as Stone-I, Stone-II, Baker and etc) are almost always used to estimate three-phase relative permeabilities from the more readily two-phase data. The empirical nature of these models limits the ability to accurately predict three-phase flow in the reservoir. There is a convincing body of theoretical and experimental evidence that relative permeabilities depend on many rock and fluid parameters (Avraam and Payatakes, 1995), including fluid viscosity, interfacial tension, flow rate, rock wettability, immobile water saturation, pore size distribution and of special interest to us, saturation history. Relative permeabilities are considered to be dependent on initial saturation and saturation history. This latter dependency is described in the literature as relative permeability hysteresis. The number of phases present in porous media is important when discussing hysteresis.

Several tertiary oil recovery processes have shown cycle-dependent hysteresis for relative permeability. This is especially important in Enhanced Oil Recovery (EOR) processes involving cyclic injection scenarios such as Water Alternating Gas (WAG) and Cyclic Steam Stimulation (CSS). Multiphase flow involving saturation path reversals should be modelled with history-dependent relative permeability functions. Earlier approaches are based on two-phase flow (such as Killough (1976) and Carlson (1981) models). The problem of k_r hysteresis becomes significantly more complicated when moving from two-phase to three-phase flow systems. It is now widely accepted that the cycle-dependent hysteresis in two-phase systems cannot be directly linked to three-phase flow. Larsen and Skauge (1998) showed that when saturation oscillations occur during three-phase flow such as WAG injection, the existing two-phase hysteresis models will generally not be able to describe relative permeabilities obtained from corefloods.

7.1.1 Three-Phase Relative Permeability Hysteresis: Simulation Studies

Guzmen *et al.* (1994) simulation results showed that there is a significant uncertainty associated with the selection of three-phase relative permeability models for field simulations of gas and WAG injections. Depending on the model, vastly different results were obtained in terms of the distribution of the fluids inside large volumes of

the reservoir, total oil recovery and fluids production rates. They concluded that accurate predictions of oil recovery in processes that exhibit three-phase flow need more rigorous models for three-phase relative permeability.

Using simulation analysis, Spiteri *et al.* (2005) demonstrated that accounting for trapping and relative permeability hysteresis of the non-wetting CO_2 phase is essential in order to correctly characterize the migration and final distribution of the injected CO_2. Trapping of the injected CO_2 is desirable for sequestration purposes. They showed that trapping of CO_2 can be enhanced by alternatively injecting water and CO_2 the same way as in classical WAG injection for enhanced oil recovery. Spiteri *et al*. (2006) full field simulations showed that the impact of the three-phase interpolation models (such as Stone-I, Stone-II, Baker etc.) is slightly less significant compared to laboratory scale because of the effects of gravity and heterogeneity. But the impact of relative permeability hysteresis is still very significant. They found that inclusion of the gas phase trapping in simulation model reduces the overall gas mobility, which results in better sweep efficiency, higher fluid production and lower gas/oil ratio.

Ghomian *et al.* (2008) simulations compared oil recovery for different simulation cases, with and without hysteresis and with different WAG ratios, but all at the same CO_2 slug size. Injection of water after each gas cycle caused gas to be trapped in the reservoir due to hysteresis, which reduced the gas mobility. Consequently, this can make barriers to the water phase resulting in lower water cut as well as lower gas-oil ratio. In addition, gas trapping helped achieving better sweep, which resulted in higher recovery compared to the simulations without the hysteresis effects.

7.1.2 Three-Phase Relative Permeability Hysteresis: Experimental Studies

Holmgren and Morse (1951) found that the relative permeability to oil was significantly reduced by the presence of a trapped gas phase in water-wet sandstone while water relative permeability was only slightly reduced. Schneider and Owens (1976) reported a reduction of water mobility in a three-phase flow situation compared to the two-phase flow in moderately oil-wet carbonates. This reduction resembles field evidence of reduced water injectivity. Low fluid mobility in field applications and injectivity decline during CO_2 tertiary floods have been also reported by Patel *et al*. (1987).

Little effort has been made to investigate cycle-dependent hysteresis (Hawkins and Bouchard, 1992; Beattie *et al.*, 1991). The data becomes even more scares for three-phase flow. Very few researchers have reported k_r hysteresis phenomena in multi-cyclic three-phase systems. Eikje *et al.* (1992) presented three-phase experimental data to demonstrate the hysteresis effects in micellar-flooding. They also investigated the validity of the Virnovskii's (1984) theory for interpreting three-phase displacement experiments when hysteresis is present. Eikje *et al.* concluded that for oil/water/micro-emulsion system, drainage water relative permeabilities only depend on water saturation. The imbibition curves were quite different, and the water phase clearly exhibited hysteresis. The results showed that the relative permeability curves were process dependent, even at the low interracial tension of 0.1 $mN.m^{-1}$ for micro-emulsion/water, and 0.005 $mN.m^{-1}$ for micro-emulsion/oil. Skauge and Matre (1989) and Kvanvik *et al*. (1992) reported similar experimental observations for the three-phase hysteresis in micellar-flooding. Delshad *et al.* (1985) found strong hysteresis in the water relative permeabilities, and a weak hysteresis for both the micro-emulsion (wetting-phase) and the oil (non-wetting phase) relative permeabilities.

Several experimental studies (Skauge and Aarra (1993); Skauge and Larsen (1994)) of three-phase flow have concluded that gas relative permeability may be strongly reduced from two-phase gas drainage (primary gas injection) to the case of drainage after waterflooding (secondary gas injection). The trapping of oil seemed to restrict the flow of gas. Larsen and Skauge (1995) experimental studies showed that trapping process in three-phase systems is non-reversible, thus the imbibition curve will not be retraced when gas saturation is increasing after an imbibition process. Water phase mobility reduction occurs between two imbibition processes separated with a gasflood. This is due to the fact that in the 1^{st} waterflood (assuming water-wet condition) oil is the non-wetting phase but in 2^{nd} waterflood, gas is the non-wetting phase and oil is the intermediate-wetting phase (assuming water-wet conditions).

Eleri *et al.* (1995) performed unsteady-state coreflood experiments in a water-wet Clashach core to calculate three-phase oil, water and gas relative permeabilities. From the experimental results they concluded that relative permeabilities to the oil and gas phase depend on more than one phase saturation. Hysteresis from increasing and decreasing saturations was most pronounced for the oil phase, but they could not conclude any systematic changes with saturation history. Their experimental results

showed that both water and oil relative permeabilities were reduced in the presence of an immobile gas phase.

Skauge *et al.* (1999) highlight that although, the three-phase reduction of gas relative permeability may seem little, but it has a significant effect on production and pressure profiles. Petersen et al. (2008) performed measurements on reservoir core material and under full reservoir conditions to ensure representative wettability and spreading conditions. They confirmed that phase saturation and saturation history are major factors in determining three-phase relative permeabilities.

7.1.3 Three-Phase Relative Permeability Hysteresis: Effect of Wettability

Generally, the wetting phase refers to water and is thought to have less drainage-imbibition hysteresis than the non-wetting phase because it cannot be trapped or disconnected in natural porous media. Studies of two-phase flow (Braun and Holland (1995); Wei, J.Z. and Lile, (1993)) have shown increased water-phase hysteresis at intermediate wettability. Wang (1988) reported trapping of water in a mixed-wet porous medium. In two-phase flow, trapping of water, and thereby reducing water mobility can occur in a non-water-wet reservoir.

Dicarlo *et al*. (2000) studied three-phase flow in water-wet, oil-wet, and fractionally-wet sand-packs under gravity drainage. In their experiments, the gas saturation increased while the oil and water saturations decreased. Their experiments did not include water injection, or WAG cycles of water and gas flooding and therefore hysteresis effect has not been investigated. Nevertheless, their results are valuable to understand the effect of wettability on three-phase relative permeabilities for different phases. They found that the gas relative permeability is lower in an oil-wet medium than in a water-wet medium at the same gas saturation. Dicarlo *et al.* found that water relative permeability in the oil-wet medium resembles the oil relative permeability in the water-wet medium for non-spreading oil. For the fractionally-wet sand, the oil, water and gas relative permeabilities were between the oil, water and gas relative permeabilities in the water-wet and oil-wet sands.

Skauge and Larsen (1994) summarized the results of three-phase relative permeability measurements at different wettability for water-wet, intermediate and oil-wet cores. Gas or water was the injected phase in these displacements. For water-wet system, water

relative permeability curves showed slight hysteresis. The oil relative permeabilities were all obtained from experiments where oil saturation was decreasing. Therefore, their study could not show the possible hysteresis in the oil relative permeability but they found k_{ro} to be saturation history dependent. The gas relative permeabilities showed a strong dependence on process path i.e. increasing or decreasing saturation change. For oil-wet system, they concluded that k_{rw} shows hysteresis especially when comparing secondary waterflood with tertiary gas injection. The more oil-wet cores generally showed stronger hysteresis in k_{rw}, and also showed a dependence on the saturation history. k_{ro} showed only minor changes with saturation history. k_{rg} showed large reduction for tertiary gas injection compared to primary gas injection. In the case of intermediate-wet system, secondary waterflood performed after gas injection showed much lower water relative permeability than primary water injection. k_{rg} showed strong variation with process and injection sequence, and it was history dependent. Skauge *et al.* (1999) highlighted that for mixed-wet rocks, the gas relative permeability was more affected by three-phase flow than in the case of water-wet rock. Generally, Skauge and his co-workers concluded that k_{rg} show strong hysteresis effects independent of the wetting state of the core, and k_{rg} values for decreasing gas saturation (waterflood) were lower than the k_{rg} data obtained in former increasing gas saturation direction (former gas injection). These experimental results were used as the basis of their three-phase hysteresis model (Larsen and Skauge, 1998).

Element *et al.* (2003) investigated secondary and tertiary immiscible WAG floods in both water-wet and intermediate-wet Berea cores. They found that after wettability, hysteresis is the most important phenomena affecting multi-cycle floods. They confirmed the irreversibility of the relative permeability hysteresis cycles. Relative permeabilities for the floods in water-wet core showed a more marked irreversibility than the intermediate-wet core data.

From the above literature, it is clear that incorporating hysteresis in relative permeability curves is essential in order to obtain accurate predictions of realistic immiscible WAG processes. Larsen and Skauge (1998) developed a new three-phase relative permeability model to account for hysteresis effects in immiscible WAG processes which involves: (1) Hysteresis in gas relative permeability; (2) Hysteresis in water relative permeability; (3) Modification of the residual oil saturation in the Stone-I model, and (4) Coupling of residual oil saturation to trapped gas (oil relative

permeability saturation history dependency). The Larsen and Skauge (1998) three-phase relative permeability model is currently the only available model in the literature which has been developed specifically to reproduce the observed cyclic hysteresis behaviour in WAG injections. There is insufficient published data to judge the quality of the model especially for different wettability conditions. Wettability is an important factor in gas relative permeability in three-phase flow and it determines the local distribution of the phases. A comparison with measurements from a variety of cores would be required to assess the validity of the model. In previous chapters, series of WAG experiments for both water-wet and mixed-wet systems were reported and compared with different injection scenarios including primary waterflooding and primary gas injection. This chapter reports the set of three-phase relative permeabilities obtained from those WAG tests for both wettability conditions.

The extension of Johnson et *al.* (1959) method to three-phase flow as stated separately by Virnovskii (1984) and Grader and O'Meara (1988) has been used to analytically derive the relative permeabilities as a function of their own saturations. As discussed earlier, the assumptions that have to be made in order to use these analytical solutions are: (1) fluids are incompressible, (2) immiscible, (3) the flow is one-dimensional, (4) isothermal and (5) the capillary pressure is neglected. All the above conditions are met in the experiments presented in this study but there were concerns over the effect of capillary pressure. However, capillary pressure measurements using water/oil system and converting them to oil/gas and oil/water systems at experimental conditions (using J-function) confirmed that capillary pressures are not significant in the performed experiments. This was particularly true for the oil/gas system with a very low oil/gas interfacial tension (IFTo-g = 0.04 $mN.m^{-1}$). In addition, Shahverdi (2012) three-phase simulations also showed that capillary pressure effects were minimal for the conditions of the experiments. Shahverdi (2012) also confirmed that the variation of fluid properties (viscosity and interfacial tension) alongside the core throughout the tertiary injections in insignificant.

The data presented here are applicable to WAG injections when oil and gas are in near-miscible conditions. Therefore, data presented here are considered relevant to real-life field applications of tertiary gas injections. The analysis of the laboratory data presented here only considered whether the existing hysteresis model can capture the key hysteresis features observed in the experimental data. No quantitative assessment has

been made of the accuracy with which the model could describe the data. Such quantitative study can be found elsewhere (Shahrokhi et al., 2014).

7.2 WAG Experiments

Previous Chapter, presented general experimental procedures applied during these WAG injection experiments. In this chapter, considering the fact that hysteresis effect and saturation history dependency of relative permeabilities are investigated, more details for each flood (each of gas or water injection periods) such as saturation variations and etc., are presented for each of these WAG injections. Two series of WAG tests started with a water injection into the core saturated with oil and immobile water (Table 7-1, experiments 1 and 2) are reported. These tests performed for both water-wet and mixed-wet systems. The water injection period (Imbibition, I) was followed by a gas injection period (Drainage, D) and the periods of water and gas injections were repeated and in total three water injections and three gas injection periods were carried out sequentially (IDIDID). In addition, three additional WAG experiments (Table 7-1, experiments 3 to 5) were presented which were performed to further investigate the effect of immobile water saturation, injection scenario and rock permeability. To investigate the effect of immobile water saturation on three-phase relative permeability hysteresis, the WAG Experiment-3 with S_{wim}=16% is performed on the 65mD water-wet system and compared with its water-wet counterpart (Experiment-1) which has a higher immobile water saturation (S_{wim}=18%). To study the possible effect of injection scenario, another WAG injection (Experiment-4) which is performed on the 65mD mixed-wet system, started with the primary gas injection and compared with the results of the WAG experiment performed with the same immobile water saturation and wettability condition but started with primary waterflooding (Experiment-2). And finally, to understand the possible effect of rock permeability (pore size distribution), the last WAG experiment presented (started with primary waterflooding) is performed on the 1000mD mixed-wet system (Experiment-5) and compared to its counterpart performed on the 65mD mixed-wet system (Experiment-2, with the same wettability and injection sequence).

Table 7-1: Coreflood experiments used in chapter-7.

Exp. #	*Core*	*Coreflooding*	*Direction*	*Wettability*	S_{wim}
1	65 mD	WAG Injection	IDIDID	Water-Wet	18%
2	65 mD	Water Injection	IDIDID	Mixed-Wet	18%
3	65 mD	WAG Injection	IDID	Water-Wet	16%
4	65 mD	WAG Injection	DIDIDIDI	Mixed-Wet	18%
5	1000 mD	WAG Injection	IDID	Mixed-Wet	8%

7.2.1 WAG Injection (65mD, Water-Wet, IDIDID, S_{wim} = 18%):

1st Water Injection

The 1st water injection was carried out with immobile water in the core (S_{wim}= 18%) and 82% oil. Brine was injected through the core at 25 $cm^3.hr^{-1}$. When water broke through at the production end of the core, oil production stopped almost immediately and no more oil was produced. Just over 40% pore volume (PV) of oil was produced during this waterflooding with significant amount of oil still trapped in the core (S_{otw}). Brine injection continued after the breakthrough and in total 1 PV (pore volume) of brine was injected.

1st Gas Injection

After the first water injection period as described above, the first gas injection period through the core was started at a rate of 25 $cm^3.hr^{-1}$and with the core contained S_{wi}=58% and S_{otw}=42%. Since initially there is high water saturation in the core, the differential pressure across the core jumped to around 40 psi immediately and then declined continuously to reflect the displacement of the higher viscosity water and oil with the lower viscosity gas. With the start of the gas injection, the only producing phase was water. This is due to the high water saturation within the core, which was due to the previous water injection period (oil is already at its residual saturation respect to water, S_{orw}). Oil recovery did not begin until the gas breakthrough happened. After the gas breakthrough, rate of water production become very small, and oil recovery took place gradually alongside the flowing gas. The injection of gas continued for 1 PV at which time gas injection stopped (water/gas ratio = 1).

2nd Water Injection

The second cycle of this WAG injection began with a 2nd water injection period at the rate of 25 $cm^3.hr^{-1}$ with the fluid saturations in the core being S_{org}=29%, S_{wrg}=47%, and S_{gi}=24%. During this period of water injection, initially only gas and, to a much lesser extent, oil was produced. The oil recovery started slowly with gas production and increased steadily until the water broke through. The highest rate of oil recovery was

observed just before water breakthrough indicating formation of an oil bank ahead of the water front. When water broke through, the gas and oil recovery stopped. This is consistent with previous micromodel experiments by Sohrabi *et al.* (2004) that showed fragmentation and snap-off of the continuous gas paths during water injection, which results in cessation of oil flow.

2nd Gas Injection

The WAG experiment continued by the 2nd period of gas injection at the same injection rate of 25 $cm^3.hr^{-1}$. At the start of the 2nd gas injection period, the saturations of the fluid in the core were, S_{otw}=25%, S_{wi}=57%, and S_{gtw}=18%. In the 1st gas injection, since the saturation of the oil is still relatively high inside the core, the gas preferentially displaces the oil due to a much lower gas/oil IFT compared to gas/water IFT and hence the flowing gas would be more in contact with oil rather than water. This gas would be trapped inside the core due to the successive brine injection periods. Considering the high value of capillary entry pressure for these pores, in the later gas injection period, gas would follow a new path (compared to the former gas injection period), which are occupied by brine (and trapped oil). Sohrabi *et al.* (2004) micro-model experiments confirmed this theory. They showed that when gas was injected subsequent to WAG (gas and water) cycles, it would not follow the same path as the previous gas did. This redistribution of the fluids within the porous medium improves sweep efficiency and hence oil recovery.

3rd Brine Injection

The third cycle of WAG injection began with the 3rd water injection period at the rate of 25 $cm^3.hr^{-1}$ and with S_{org}=19%, S_{wrg}=40%, S_{gi}=41%. Similarly to the 2nd water injection period, initially only gas was produced. The oil recovery started slowly with gas production and increased steadily until water broke through. A difference in the trend of gas recovery profile was observed in the 3rd water injection period compared to the 2nd one. In the 2nd brine injection period, the production of the gas ceased after water breakthrough but in the 3rd period of brine injection the gas recovery was observed to take place in an extended time period (albeit at a very low rate) even after water breakthrough.

3rd Gas Injection

The experiment was completed by performing another period of gas injection. The 3rd gas injection period was again started with an injection rate of 25 $cm^3.hr^{-1}$ with S_{org}=15%, S_{wrg}=56%, and S_{gi}=29%. Since prior to this gas injection period, water was

being injected through the core (3rd water injection period), the water saturation in the core was high and at the same time the gas and oil were discontinuous and immobile and hence, at the beginning of the 3rd gas injection period, only water was produced from the core. However, the injected gas quickly reconnects parts of the fragmented gas in the core and starts to be produced. Comparison of the 2nd and 3rd gas injection periods shows that the gas breakthrough happens faster (in terms of PV injections) in the latter one. Gas injection continued after the breakthrough until the rate of the oil production became practically zero at which time the core contained; S_{org}=6%, S_{wrg}=38%, and S_g=56%.

7.2.2 WAG Injection (65mD, Mixed-Wet, IDIDID, S_{wim} = 18%):

1st Water Injection

Similarly to the water-wet WAG experiment, this WAG injection also started with a period of waterflooding. The 1st water injection was carried out with immobile water in the core (S_{wim}= 18%) and 82% oil. Brine was injected through the core at the rate of 25 $cm^3.hr^{-1}$. When water broke through to the production end of the core (after 0.62 PV injections), the oil production stopped almost immediately and the differential pressure across the core stabilised. The trapped oil inside the core could not be recovered by water injection which was continued for 1 PV.

1st Gas Injection

After the 1st water injection period, the experiment was continued by 1st gas injection period in the core with water and oil saturations of S_{wi}=80% and S_{otw}=20%. The gas injection period started with a rate of 25 $cm^3.hr^{-1}$ and continued for around 1 PV. With the start of the gas injection, the only producing fluid was brine until the gas breakthrough (BT). Compared to the 1st gas injection in the water-wet experiment, brine production continues at higher rates after the gas breakthrough. Once the gas breakthrough happened, oil starts to produce slowly alongside with the gas. This can be explained by the wettability differences between these two systems and the difference in the distributions of the fluids inside the pores. In the water-wet system, water is the wetting phase, oil is the intermediate phase and gas would be the non-wetting phase. As a result, during the 1st water injection period water tends to occupy the smaller pores (by film flow), driving the oil outside. As the water injection continues, water enters increasingly into larger pores, until it breaks through at the outlet. At this stage, part of the oil is trapped inside the pores and would not be produced due to capillary forces. Considering the relatively high residual oil saturation trapped in the core at the end of

the 1st waterflood, one can argue that the amount of water present in those larger pores would not be much. Once the subsequent gas injection starts (1st gas injection), the gas would prefer to enter these larger pores, where the oil saturation is much higher in each pore compared to the water saturation. In contrast to this, in the mixed-wet system, in larger pores, oil is the wetting phase, while water and gas are non-wetting phases. Oil displacement during the 1st water injection would be in the form of piston-like movement of water in the centre of the pores, and oil drainage through wetting layers. Considering the very low oil saturation at the end of this stage (for the mixed-wet), one can argue that the amount of water saturation in those larger pores is high. Also, this water is in the body of the pores (not on the pore walls) Once the subsequent gas injection starts (1st gas injection), the gas would prefer to enter the larger pores, where compared to the water-wet system, it should first displace continuous water clusters from the body of the pores, before being in contact with the oil phase on the surface of the grains. This explains why during gas injection periods, water production in mixed-wet system (compared to water-wet system) is higher, while less oil has been recovered.

2nd Water Injection

The 2nd WAG cycle began by another water injection period at the rate of 25 $cm^3.hr^{-1}$ and fluid saturations of S_{org}=16%, S_{wrg}=60%, S_{gi}=24%. With the start of the brine injection, initially, only gas was being produced at the core outlet, with very little oil starting to produce along with the gas. As brine injection continued, at 0.17 PV of injection, the brine breakthrough happened. Contrary to the water-wet system, for this 2nd water injection, the production of hydrocarbons (oil and gas) continued even after the brine breakthrough (albeit at slower rates). This production is consistent with the observed decrease in pressure drop data after BT. This difference between the water-wet and mixed-wet systems can be explained by the snap-off mechanism in water-wet system which traps the gas and oil inside the pore bodies. After around 0.5 PV of brine injection, the recovery of oil and gas ceased, and as a result, the pressure drop across the core stabilized.

2nd Gas Injection

Following the 2nd water injection period, the test continued by performing the 2nd period of gas injection at the rate of 25 $cm^3.hr^{-1}$ with the fluid saturations of S_{orw}=14%, S_{wi}=78%, and S_{grw}=8%. As the gas injection started, before the BT of the gas, only brine was produced. However, after the gas BT, oil recovery began too. Similarly to the 1st gas injection period, brine production continues even after the gas breakthrough.

3rd Water Injection

The final WAG cycle in this test began with the 3rd water injection period in the core (S_{org}=12%, S_{wi}=60%, S_{grw}=28%) at the rate of 25 $cm^3.hr^{-1}$. The brine injection continued until the oil and gas production rates were practically zero. As the gas saturation in the core was relatively high and mobile, with the start of brine injection, only gas was produced at the core outlet, with a very little amount of oil being produced along with the gas. The water broke through at 0.13 PV of brine injection (earlier than the previous water injection period). The production of gas continued even after the brine breakthrough (although at the very low rates) but the oil recovery ceased after water breakthrough. After around 0.72 PV of brine injection, gas production ceased as well and the pressure drop across the core stabilized (which took place around 0.22 PV later compared to the 2nd water injection period).

3rd Gas Injection

This mixed-wet WAG test was completed with the 3rd gas injection period in the core at the same injection rate of 25 $cm^3.hr^{-1}$ (S_{orw}=11% S_{wi}=79%, and S_{grw}=10%). There was no evidence of oil recovery before the gas breakthrough. Brine production continued with the oil and gas production (at very low rates) even after the gas breakthrough. The average saturations of the oil and brine remaining in the core at the end of this 3rd gas injection period were 6% and 54%, respectively.

7.2.3 WAG Injection (65mD, Water-Wet Core, IDID, S_{wim}=16%):

To perform this core flood experiment, first, immobile water saturation was established to be 16%. Then the core was saturated with the pre-equilibrated oil at 1840 psia and 100°F. Two successive cycles of water injection (Imbibition, I) each followed by a gas injection (Drainage, D) were carried out (IDID).

1st Water Injection (primary waterflooding)

Brine was injected through the core at a rate of 50 $cm^3.hr^{-1}$. Water injection continued until no further oil production was taking place. As the initial water saturation in the core was immobile, before the water breakthrough (around 0.4 PV of water injection) only oil was produced from the core. When water broke through at the production end of the core, the oil production stopped almost immediately (due to the water-wet nature of the rock and trapping of the oil phase due to snap-off mechanism). After 1 PV (pore volume) of injection, the trapped oil saturation in the core was around 40%. This 40% represent significant amount of the original oil in place that cannot be recovered by

water injection alone. Hence water injection was stopped and gas injection began as explained below.

1st Gas Injection

The 1st gas injection period (tertiary gas injection) began through the core at the same rate as the preceding water injection (50 $cm^3.hr^{-1}$). The water and oil saturations at the beginning of this injection period were S_{wi}=60% and S_{otw}=40%. Due to the high mobile water saturation in the core and the fact that oil has already reached its residual saturation with respect to the water, oil recovery does not begin until just before the gas breakthrough happens. Oil and water production continues after gas breakthrough along with the flow of gas. To be able to investigate the effect of cyclic injection of water and gas on three-phase k_r values, the gas injection period stopped after injecting around 1.0 pore volume of gas.

2nd Brine Injection

The second cycle of WAG injection began with the 2nd water injection period in which almost 1.0 PV of water (brine) was injected through the core. The saturation of fluids in the core at the beginning of this water injection period were; S_{wrg} = 48%, S_{org} = 34%, and S_{gi} =18%. Water injection was performed at 50 $cm^3.hr^{-1}$ and continued until the gas and oil production rates became practically zero. Initially, only gas was produced from the core. The recovery of the oil started slowly with the gas production and increased steadily until the water broke through. When the water broke through, the gas production as well as oil recovery stopped. Trapped oil and gas saturations were around 30% and 9% respectively, at the end of this 2nd water injection period.

2nd Gas Injection

This WAG experiment was completed by another period of gas injection. The 2nd gas injection period was again performed at 50 $cm^3.hr^{-1}$ and continued for around 1 PV. The same as the 1st gas injection period, oil recovery did not begin until just slightly before the gas breakthrough. Gas breakthrough happened faster in the case of 2nd gas injection compared to the 1st gas injection period. The brine production continued with oil and gas production after the gas breakthrough and the slope of the brine production curve remained almost constant. The oil and brine residual saturations at the end of the 2nd gas injection period were equal to 25% and 52%, respectively.

7.2.4 WAG Injection (65mD, Mixed-Wet, DIDIDIDI, S_{wim} = 18%):

This WAG experiment started with gas injection (Drainage, D). Comparing k_r values obtained from this experiment with those of the WAG test started with water injection (Experiment-2) would show the possible effect of injection scenario on relative permeability of each of the three phases and their hysteresis behaviour. The results of this WAG experiment (started with gas injection) would also be applicable to those reservoirs which are already under later stages of primary gas injection (Zhou *et al.*, 2012) and their oil production rates has decreased.

Skauge and Aarra (1993) reported that for non-strongly water-wet system (intermediate-wet) their oil recovery curves showed no difference due to the sequence of the injected phases. The results (see chapter 6) for the system under investigation here (near-miscible gas/oil condition), showed that for the mixed-wet system, the general performance of the WAG started with primary waterflooding is higher than the WAG injection started with primary gasflooding. This is mostly due to the higher recovery factor of waterflooding compared to the primary gas injection in the mixed-wet system. Before start of the test, immobile water saturation was established (S_{wim}=18%). The core was saturated with equilibrated oil (82%) in the presence of immobile water saturation and the WAG test started with primary gas injection at the test pressure of 12.69 MPa (1840 psia) and temperature of 38 ºC (100 ºF). Four periods of gas injection each followed by a water injection (four WAG cycles) were carried out.

1st Gas Injection (primary gasflooding)

This WAG test was started by 1st gas injection period in the core with water and oil saturation of S_{wim}=18% and S_{oi}=82%. The gas injection was performed at 25 $cm^3.hr^{-1}$. The production of oil continues after the gas breakthrough (although at lower rates). As mentioned before, this is due to the near-miscible (very low IFT, 0.04 $mN.m^{-1}$) condition between oil and gas. To avoid further reduction of the oil saturation (to be able to observe the hysteresis effect on oil recovery and to be able to investigate three-phase k_r values on the broader saturation range), the gas injection stopped after 2.3 PV injections.

1st Water Injection

The WAG experiment continued with a period of water injection immediately after the 1st gas injection at which time the saturation of water, oil and gas in the core were S_{wim}=18%, S_{org}=53% and S_{gi}=29%, respectively. Brine injection through the core was

carried out at a rate of 25 $cm^3.hr^{-1}$ and continued until the oil and gas production rates were practically zero. With the start of the brine injection, initially only gas was being produced at the outlet, with a very little oil started to be produce along with the flow of gas (Figure 7-1). The rate of recovery of the oil slightly increased as the injection continued. After around 0.42 PV of brine injection there was a reduction in gas production rate while a significant increase in oil recovery was observed. Oil recovery at these high rates continued up to 0.6 PV brine injections where brine breakthrough happened and practically there was no oil or gas production afterwards and these two phases were trapped inside the pores by water. The high recovery rates of the oil between 0.41-0.6 PV injections can be attributed to the oil bank formed ahead of the water front. Brine injection stopped after 1.0 PV injection.

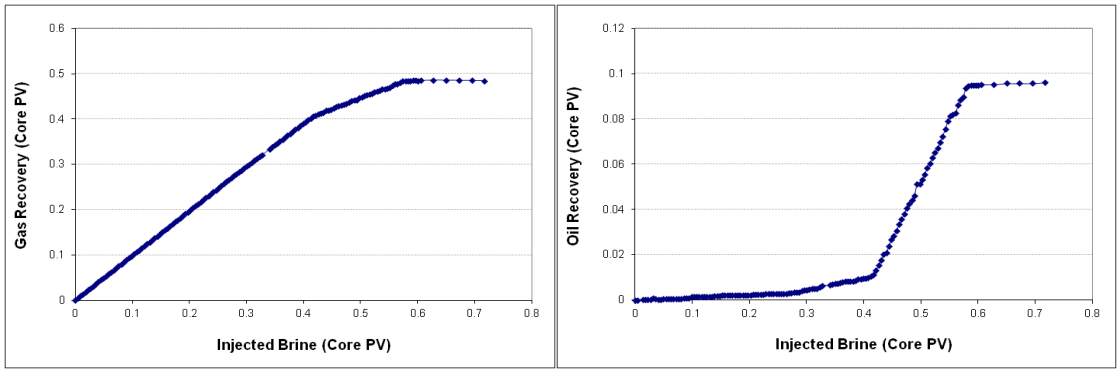

Figure 7-1: Gas recovery (left) and oil recovery (right) vs. PV brine injected (WAG, 65mD, mixed-wet, DIDIDIDI, 1st water injection).

2nd Gas Injection

The 2nd cycle of this WAG experiment started with another period of gas injection immediately after the 1st water injection (end of 1st WAG cycle) at which time the saturation of water, oil and gas in the core were S_{wi}=76%, S_{gtw}=5% and S_{otw}=19% respectively. Gas injection through the core was carried out at a rate of 25 $cm^3.hr^{-1}$. With the start of the gas injection, initially only brine was being produced at the outlet (due to the fact that oil had already reached its residual saturation in respect to water). Oil production starts just before gas breakthrough (oil bank). After 0.11 PV injections, gas broke through and thereafter the brine production continued at lower rates. Oil production also continued after gas breakthrough. Gas injection stopped after 1.35 PV injections in which 3% additional oil recovery (fraction of PV) obtained during this gas injection period.

2nd Water Injection

To complete the 2nd cycle of the WAG experiment, the test continued with another period of water injection after the 2nd gas injection at which time the saturation of water, oil and gas in the core were S_{wrg}=52%, S_{org}=16% and S_{gi}=32% respectively. Brine injection through the core was carried out at a rate of 25 $cm^3.hr^{-1}$. With the start of the brine injection, initially only gas was being produced at the outlet, with a very little oil starting to produce along with the gas. As brine injection continued, the rate of recovery of the oil slightly increased, until water broke through (at 0.21 PV injections). The high recovery rates of the oil between 0.1-0.2 PV injections can be attributed to the oil bank formed ahead of water front. Although at very small rates but production of oil and gas continues even after water breakthrough. This is in contrary to the tertiary water injection results in water-wet system and confirms the idea that in mixed-wet systems the snap-off mechanism and trapping of oil and gas is less than the water-wet condition. After 0.7 PV of brine injection, 2% additional pore volume of oil has been recovered in this period of injection.

3rd Gas Injection

3rd cycle of WAG, started with a period of gas injection immediately after the 2nd water injection (end of 2nd WAG cycle) at which time the saturation of water, oil and gas in the core were S_{wi}=74%, S_{gtw}=12% and S_{otw}=14% respectively. Gas injection through the core was carried out at a rate of 25 $cm^3.hr^{-1}$. With the start of the gas injection, initially only brine was being produced at the core outlet, with no oil production. As the process continues, at 0.05 PV injections there is a sudden increase in the oil recovery (oil bank). Gas breakthrough happens after 0.1 PV injections. With the gas BT, brine recovery continues at very lower rates. Due to the coupled flow of oil and gas (at very low IFT) oil production continues after gas BT, towards the end of injection period. After 1.35 PV gas injections, 3% additional oil (fraction of PV) has been recovered in this period.

3rd Water Injection

To complete the 3rd cycle of this WAG experiment, the test continued with another period of water injection at which time the saturation of water, oil and gas in the core were S_{wrg}=55%, S_{org}=11% and S_{gi}=34% respectively. Brine injection through the core was carried out at a rate of 25 $cm^3.hr^{-1}$. With the start of the brine injection, initially only gas was observed to be produced at the core outlet, with a very little oil starting to be produced along with the gas. Oil production (due to the coupled displacement with gas) continues, and as brine injection continued, the rate of recovery of the oil slightly

increases (an oil bank formed ahead of the water front), until water breakthrough (at 0.21 PV injections). Although at very small rates, oil recovery continues after BT up to 0.25PV brine injections where it becomes practically zero. After 1.0 PV brine injections, 1.5% additional oil (fraction of PV) had been recovered in this period.

4th Gas Injection

Last cycle of this WAG experiment started with another period of gas injection at which time the saturation of water, oil and gas in the core were S_{wi}=78%, S_{gtw}=12.5% and S_{otw}=9.5% respectively. Gas injection through the core was carried out at a rate of 25 $cm^3.hr^{-1}$. The same as the 2nd and 3rd gas injection periods, with the start of the gas injection, initially only brine was being produced at the outlet, with no oil production. As the process continues, at 0.03 PV injections there is an increase in the oil recovery (oil bank coming through). The gas breakthrough (BT) happens at the outlet after 0.08 PV injections. With the gas BT, brine recovery rate decreases but production continues at very lower rates. Oil production continues after the gas BT, towards the end of injection period. After 1.3 PV injections of gas, 1.5% additional oil (fraction of PV) was recovered during this gas injection period.

4th Water Injection

The test was finished with another period of water injection at which time the saturation of water, oil and gas in the core were S_{wrg}=61%, S_{org}=7% and S_{gi}=32% respectively. Brine injection was carried out at the same injection rate as the previous injection period (i.e., 25 $cm^3.hr^{-1}$). With the start of the brine injection, initially only gas was being produced at the outlet. As brine injection continued, the rate of recovery of the oil slightly increased (oil bank ahead of water front). Water breakthrough took place at 0.21 PV injections. Unlike the previous water injection periods, oil recovery (although at small rates) continues even after water BT (Figure 7-2a). There is also some gas production after BT but at very small rates). After 0.68 PV injections of brine, trapped gas and oil saturations are 10% and 5% respectively which shows 2% additional oil recovery during this period of water injection.

Figure 7-2a shows oil recovery for different water injection stages as a fraction of S_o at the start of that waterflooding stage. From this figure it can be seen that the oil recovery profile for the 1st water injection is totally different with those of the 2nd, 3rd and 4th water injection periods. For the 1st water injection, there is no mobile water in the core. At the start of this injection period, water saturation is equal to S_{wim}, while for the subsequent water injection periods, there is a S_{wrg} due to a previous gas injection period

(which is mobile). Putting aside the 1st water injection, as the alternation of water and gas injection continues the oil recovery increases for successive water injection periods. This means that in terms of fraction of the S_o at the start of that injection period, the recoverable oil and also the rate of production (slope of curves) is larger for the later stages of water injections compared to the earlier ones. Figure 7-2b shows the produced oil in 2nd, 3rd and 4th water injection periods in terms of the fraction of PV. It is obvious that from this point of view the oil production has decreased for later stages of the water injection compared to the former ones. Figure 7-2c shows produced gas for different water injection periods (in terms of fraction of the gas at the start of that injection period). Again, there is a substantial difference between the observed profile for the 1st water injection and those of subsequent water injection periods. Putting aside the gas recovery profile of the 1st water injection period, the gas recovery performance of the 2nd, 3rd and 4th water injection are almost identical.

Figure 7-3a shows oil recovery for different three-phase gas injection periods of the recent WAG test (as a fraction of the initial oil in place at the start of that gas injection). As can be seen from this figure, in terms of the fraction of the S_{or} at the start of each gas injection, by the alternation of injection between water and gas, oil recovery and also production rate (slope of the curves) improved for the later gas injection periods compared to the earlier ones. From another point of view, Figure 7-3b compares produced oil in these three gas injections as fraction of core PV. There is a slight improvement for 3rd gas injection period compared to the 2nd gas injection; nevertheless the produced oil during the 4th gas injection is less than oil production 3rd gas injection. Figure 7-3c shows that the brine recovery has decreased for later stages of gas injection.

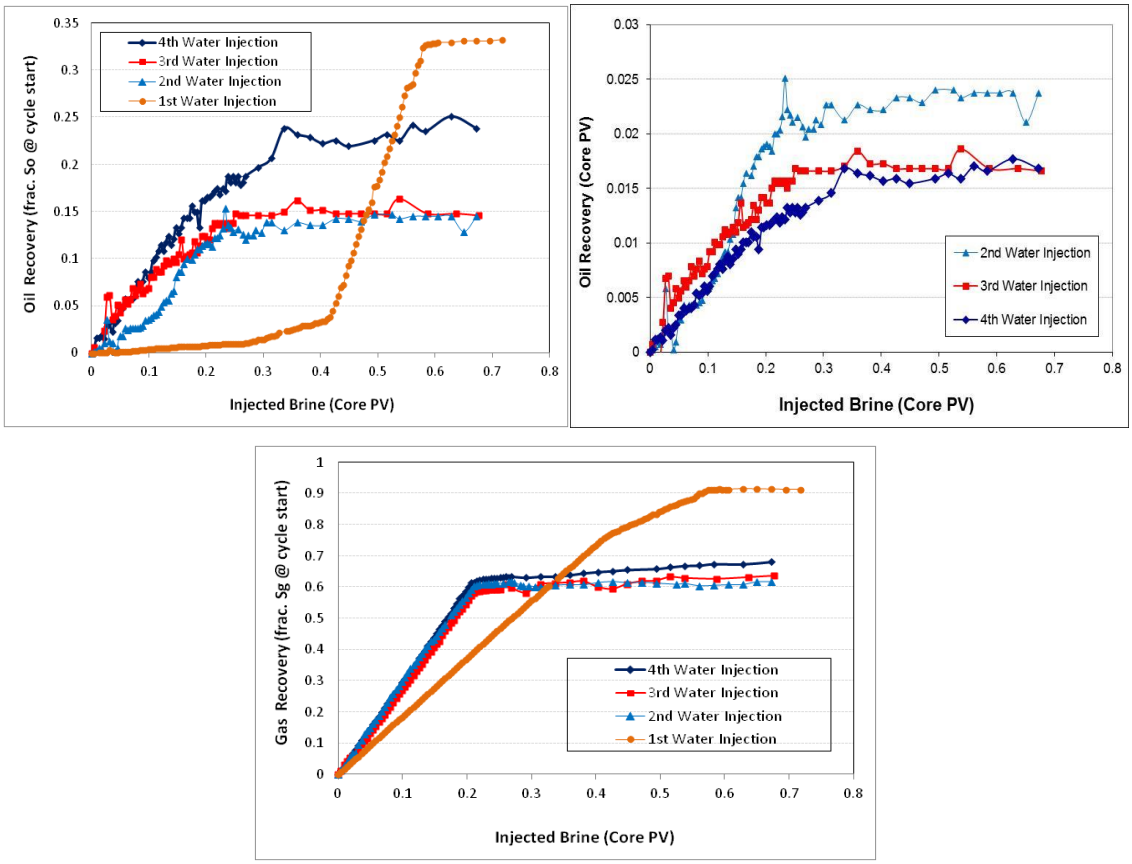

Figure 7-2: a) Top-left: oil recovery (fraction of S_o @ start of cycle); b) Top-right: oil recovery (fraction of core PV) c) Bottom: gas recovery (fraction of S_g @ start of cycle; right) vs. PV brine injected (WAG, 65mD, mixed-wet, DIDIDIDI).

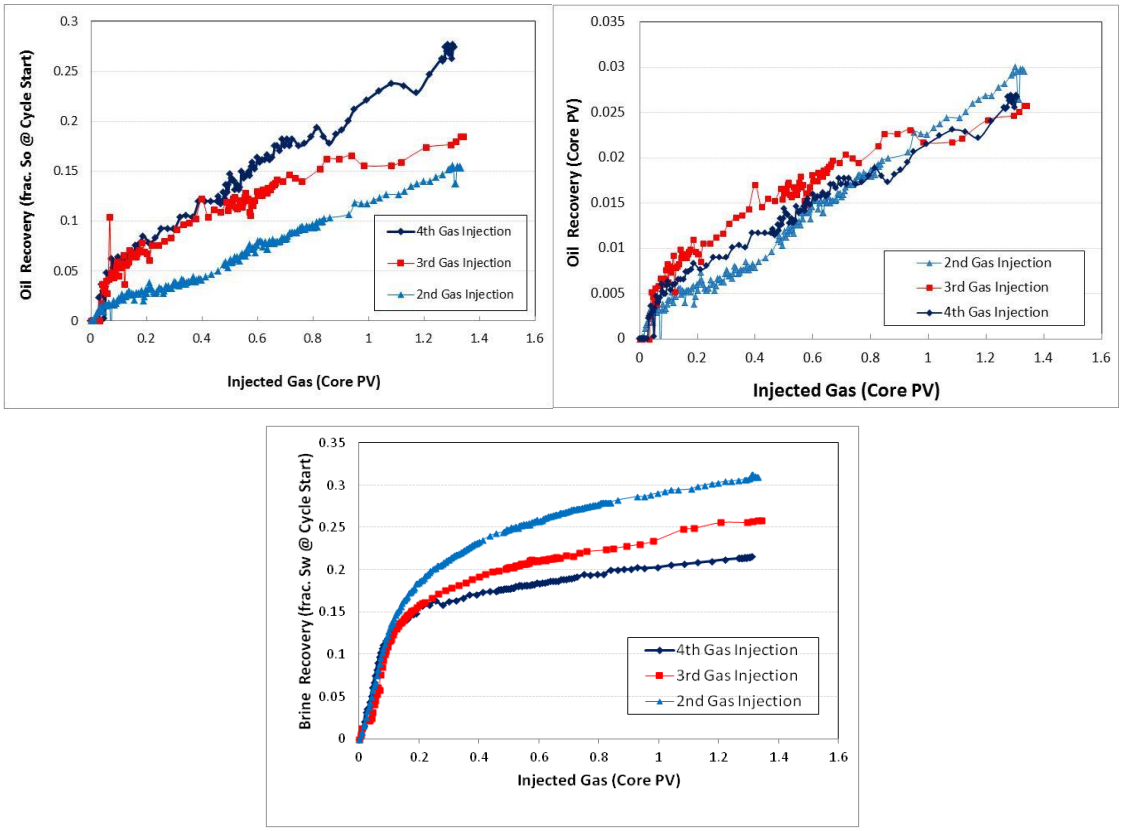

Figure 7-3: a) Top-left: oil recovery (fraction of S_o @ start of cycle); a) Top-right: oil recovery (fraction of core PV); c) Bottom: brine recovery (fraction of S_w @ start of cycle; right) vs. PV gas injected (WAG, 65mD, mixed-wet, DIDIDIDI).

7.2.5 1000mD, Mixed-Wet Core, IDID Injection Scenario, S_{wim}=8%:

This WAG injection test was carried out to evaluate the effect of rock permeability on cyclic hysteresis behaviour of different fluid phases. The core containing immobile water was saturated with oil at 1840 psia. Then two periods of water injection each followed by a gas injection (two WAG cycles) were carried out.

1st Water Injection (primary waterflooding)

In the first water injection period, brine was injected through the core (S_{wim} = 8%, S_{oi} = 92%) at a rate of 200 $cm^3.hr^{-1}$. Water injection continued until no further oil production was taking place. Before the water breakthrough (around 0.70 PV of injection) only oil was produced from the core. When water broke through at the production end of the core, the oil production stopped almost immediately and no more oil was produced. After 1 PV (pore volume) of injection, the trapped oil saturation in the core at the end of this 1st water injection was around 22%.

1st Gas Injection

Having performed a water injection period (S_{otw} = 22%, S_{wi} = 78%), gas was injected through the core at the same rate as the preceding water injection (200 $cm^3.hr^{-1}$). Initially (before the gas breakthrough) there was no oil or gas production and the only producing phase was water (due to high water saturation within the core). Oil recovery does not begin until gas phase breaks through. The injection was continued until almost 1.5 PV of gas had been injected.

2nd Water Injection

The second cycle of this WAG injection test began with the 2nd water injection period, at which time S_{org} = 10%, S_{wrg}= 42% and S_{gi} = 48%. Almost 1 PV of water (brine) was injected through the core (at 200 $cm^3.hr^{-1}$). The oil recovery graph reveals that the recovery of oil started slowly with gas production and increased steadily until the water broke through. When water broke through, the oil and gas recovery stopped.

2nd Gas Injection

The test was completed by another period of gas injection at which time S_{org} = 4%, S_{wrg}= 82% and S_{gi} = 14%. The second gas injection period was again carried out at 200 $cm^3.hr^{-1}$ and continued for around 1.5 PV. At the end of the second WAG cycle, the oil saturation dropped to 0.5% of the core pore volume.

7.3 Results

In this section the effects of cyclic hysteresis will be examined, saturation history and wettability by investigating the three-phase relative permeabilities of different phases obtained from the coreflood experiments described in the previous section.

7.3.1 Cyclic Hysteresis Effect in Water-Wet System:

Figure 7-4 shows the (three-phase) gas relative permeabilities (k_{rg}) obtained for different gas injection stages of the water-wet WAG experiment (S_{wi} = 18%). The results are shown on both linear and semi-log scales. As can be seen, gas relative permeability decreases with increasing the number of WAG cycles. This means that for the 1st gas injection period, k_{rg} is higher than the 2nd gas injection period and likewise k_{rg} for the 2nd gas injection is higher than the 3rd one. This confirms the saturation history dependency for k_{rg} in water-wet systems. This means that k_{rg} values for the same process (drainage) are different due to the differences between the saturation histories of the rock at the start of each gas injection stage. The same graph shows that the end point

relative permeabilities of the gas have been decreasing continuously during WAG injection as the number of WAG cycles increased. This is attributed to the effect of water slugs which were injected in between the gas injection periods. Water would trap the free gas, and since this trapping process is not reversible, as the alternation of injection between imbibition (water) and drainage (gas) stages continues the cumulative trapped gas saturation inside the core increases. Trapped gas restricts the flow of fluids in the later stages of the gas injection and k_{rg} decreases.

Water relative permeabilities presented in Figure 7-5, show much less hysteresis dependency compared to k_{rg}. This is especially true for the 1st and 2nd gas injection cycles in which practically no hysteresis has been observed. For the last gas injection period (3rd gas injection) it was observed that k_{rw} dropped by around 30% compared to the two preceding gas injections. Comparison of oil relative permeabilities of different gas injection cycles (Figure 7-6) reveals significant saturation history dependency for oil. Figure 7-6 shows that alternation between imbibitions (water) and drainages (gas), significantly improved oil relative permeability and reduced residual oil saturations.

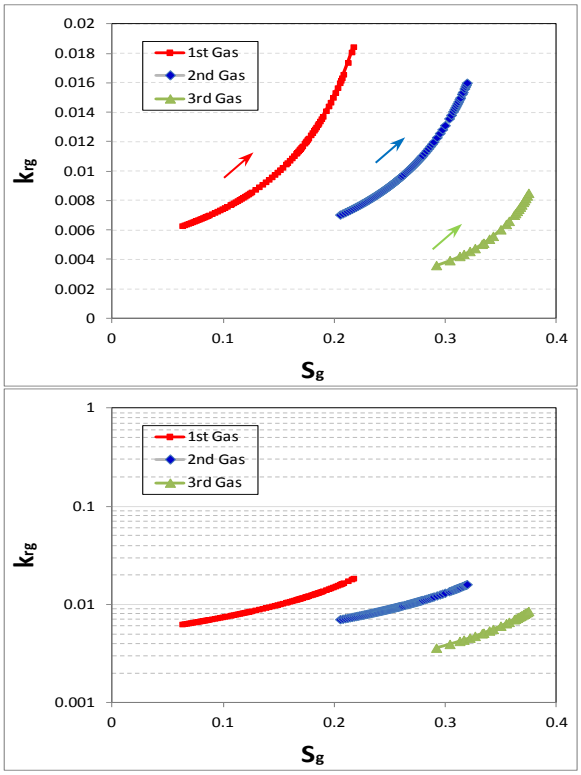

Figure 7-4: Gas three-phase relative permeabilities obtained in gas injection stages in the water-wet WAG experiment (65mD, IDIDID, experiment-1).

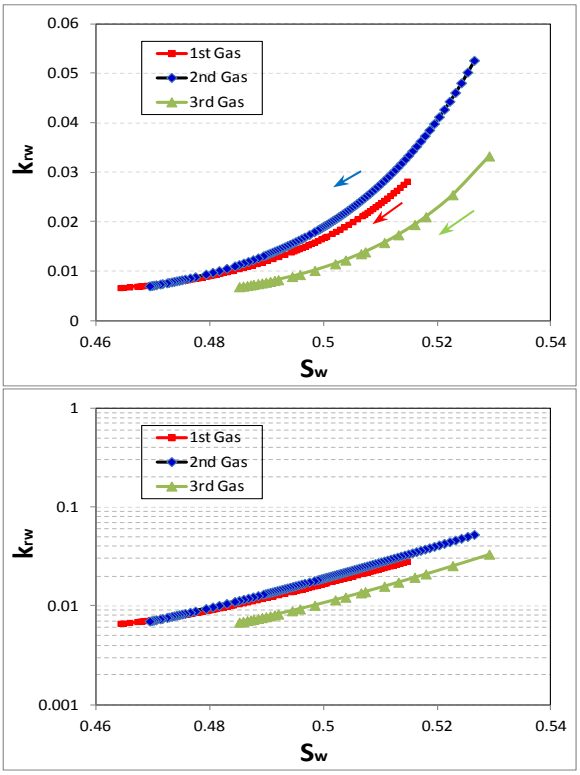

Figure 7-5: Water three-phase relative permeabilities obtained in gas injection stages in the water-wet WAG experiment (65mD, IDIDID, experiment-1).

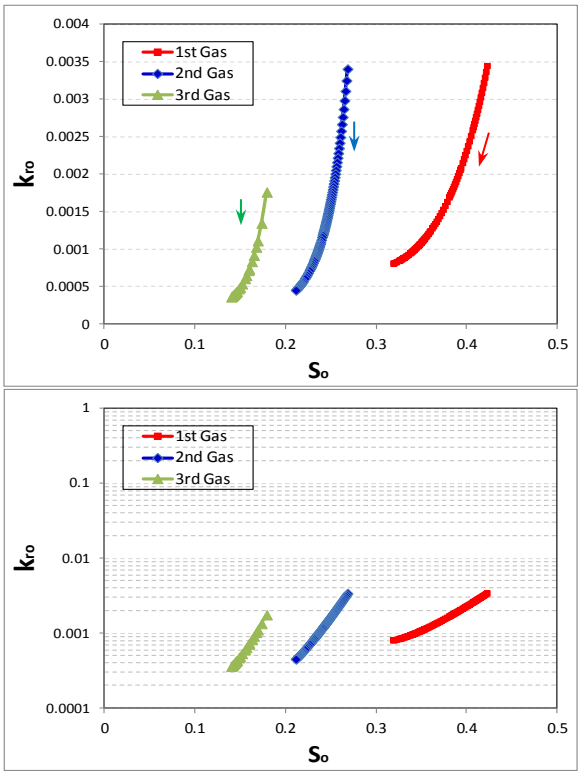

Figure 7-6: Oil three-phase relative permeabilities obtained in gas injection stages in the water-wet WAG experiment (65mD, IDIDID, experiment-1).

In water injection periods of the WAG core flood experiments, after the water break through (BT), production of oil (and gas) tends to cease rapidly and hence there is little multiphase flow after the BT. As a result, limited reliable k_r points can be obtained for water injections. This is not the case for gas injections in which typically there is an extended period of time (after the gas BT) where multiphase flow takes place. Nevertheless the calculated k_r data helps to better understand the saturation history dependency in the imbibition (water injection) stages and how the alternation of water and gas affects trapped oil and gas saturations and oil/gas/water relative permeabilities. The oil and gas relative permeabilities for the 2nd and 3rd water injection periods which are presented in Figure 7-7 and Figure 7-8 show that after the water breakthrough, the relative permeabilities of both gas and oil phases drop significantly. This is especially true in the case of gas relative permeabilities (Figure 7-7), in which the gas saturation change after water breakthrough is practically negligible.

As can be seen in Figure 7-7, the trapped gas saturation at the end of the 3rd water injection period is larger than the 2nd water injection period. This can be explained by irreversibility of the trapping process and also by the higher initial gas saturation at the start of the 3rd water injection compare to the 2nd water stage. In the case of oil relative permeabilities (Figure 7-8), formation of the small oil bank ahead of water front (see previous section) and its production result in a slightly larger saturation range at which oil relative permeabilities have been obtained (compared to the gas relative permeabilities). Oil relative permeabilities show that alternation of gas and water injections (WAG) has improved the oil relative permeability values of the 3rd water injection period compared to the 2nd waterflooding, especially at lower oil saturations. The same Figure shows that residual (trapped) oil saturation at the end of the 3rd water injection period has also been reduced compared to the previous water injection. Figure 7-9 shows that end-point k_{rw} have not changed much between the 2nd and the 3rd water injection stages (although it is slightly smaller for 3rd water injection compared to the 2nd water injection period).

To investigate the effect cycle-dependent hysteresis, relative permeabilities from successive drainage (gas injection) and imbibition (water injection) cycles are compared in Figure 7-7 through Figure 7-9. To highlight the differences for low saturation and k_r values, semi-log plots are provided as well. Figure 7-7 shows calculated gas relative permeabilities (marker points) in which the dashed lines show possible trends of k_r values from drainage into imbibition and vice versa. For each drainage period, k_{rg}

values are higher compare to the subsequent imbibition period. In addition, for each imbibition stage, k_{rg} values are also higher compared to the succeeding drainage stage. This means that gas relative permeabilities are not reversible, neither for the change of displacement from drainage into imbibition and nor for the change of displacement from imbibition into drainage. The result is that k_{rg} hysteresis loops are not closed. Comparing the 1st hysteresis loop (1st drainage and 2nd imbibition) with the 2nd hysteresis loop (2nd drainage and 3rd imbibition) show that as the cyclic injection of water and gas continues, the effect of hysteresis would be still important.

Figure 7-8 shows oil relative permeabilities of the drainage and imbibition stages of the water-wet WAG experiment. From the trend of k_{ro} curves (especially in semi-log plot) one can conclude that residual oil saturation is larger for the waterflooding stage compared to the preceding drainage stage (if it was continued). Yet, WAG process works since alternating injection of gas and water, would reduce the gas relative permeability and improve oil relative permeability in the successive gas injection (drainage) periods. Since water relative permeabilities (Figure 7-9) are not in the same saturation range, no conclusion can be made regarding the k_{rw} process dependency. In Figure 7-7 through Figure 7-9, the saturation ranges for which the k_r values have been obtained during water injections are very narrow compared to the gas injections. As is mentioned earlier, this is due to the quick cessation of gas and oil flow after water BT during water injection stages.

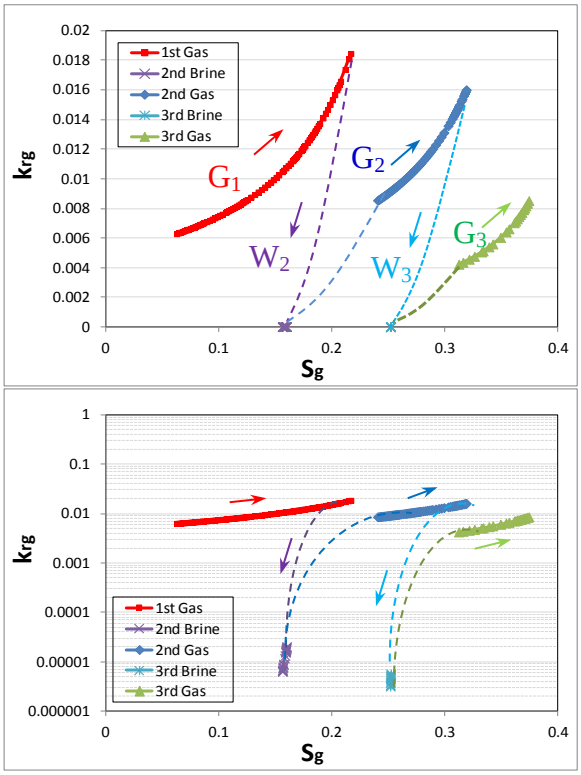

Figure 7-7: Gas (three-phase) relative permeabilities for different stages of gas and water injections during WAG injection (65 mD, water-wet, IDIDID, experiment-1).

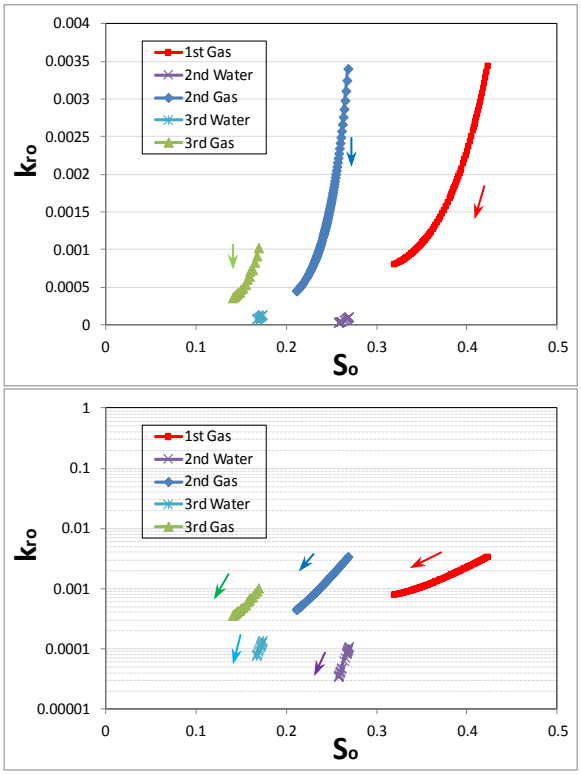

Figure 7-8: Oil (three-phase) relative permeabilities for different stages of gas and water injections during WAG injection (65 mD, water-wet, IDIDID, experiment-1).

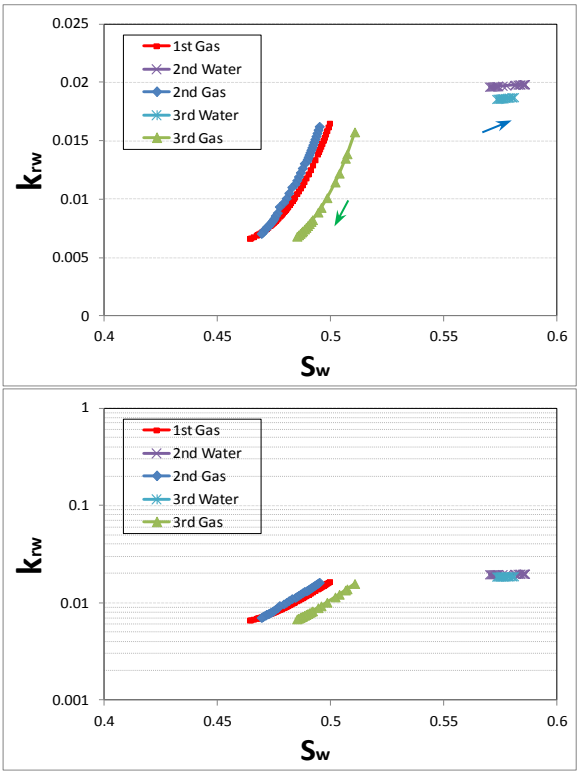

Figure 7-9: Water (three-phase) relative permeabilities for different stages of gas and water injections during WAG injection (65 mD, water-wet, IDIDID, experiment-1).

7.3.2 Cyclic Hysteresis Effect in Mixed-Wet System

Figure 7-10 through Figure 7-12 show relative permeabilities obtained for different phases during the gas injection periods of the mixed-wet experiment. The corresponding semi-log plots are provided as well. Similarly to the water-wet system, the gas relative permeability (Figure 7-10) decreases as the number of WAG cycles increases. This confirms cycle-dependent hysteresis k_{rg} in mixed-wet system. The same graph shows that end-point relative permeability of gas has decreased for the 2nd gas injection stage compared to the 1st gas injection (when the same volume of the gas has been injected in these two processes).

In the 3rd gas injection period, end-point relative permeability has improved compared to the former drainage stages. This can be due to the fact that the last drainage stage (3rd gas injection) had been extended to longer PV injections compared to the other two gas injections, to produce as much oil as possible at the end of the WAG experiment. As a result the total volume of the injected gas is almost twice of the volume injected in the previous ones and the end-point k_{rg} value is higher (yet, the trend of the data shows that for the same S_g values, k_{rg} for the 3rd gas injection cycle are below those of the 1st and 2nd stages of drainage). Comparing the results of Figure 7-10 with those of its water-wet

counterpart (Figure 7-4), shows that cycle-dependent hysteresis for gas relative permeabilities is larger in water-wet system compared to the mixed-wet sample. This is attributed to the fact that gas trapping by snap-off mechanism (due to water injection) is more likely to happen and also more effective in water-wet systems than in mixed-wet systems.

Figure 7-11 shows water relative permeability saturation-history dependency. Generally, the difference between the k_{rw} values for these gas injection stages is negligible. Comparison of oil relative permeabilities of different gas injections (Figure 7-12) confirms saturation history dependency for this phase as well. Alternation of injection between imbibition and drainage improved oil relative permeability at lower oil saturations. Although in the 1st and 2nd gas injection periods the trend of relative permeabilities does not show much improvement in the residual oil saturation, the S_{org} significantly reduced in the 3rd gas injection period.

Due to the mixed-wet nature of the rock in this experiment, the oil and gas production after water breakthrough continued for a longer time compared to the water-wet experiment and hence, the relative permeabilities for water injections were obtained for a wider saturation range compared to their water-wet counterparts (Figure 7-13 through Figure 7-15). The oil and gas relative permeabilities show that, after water breakthrough, relative permeabilities for both phases drop. The gas relative permeabilities show that trapped gas saturation at the end of the 3rd water injection increased compared to the 2nd water injection period. This is attributed to larger initial gas saturation at the beginning of this stage.

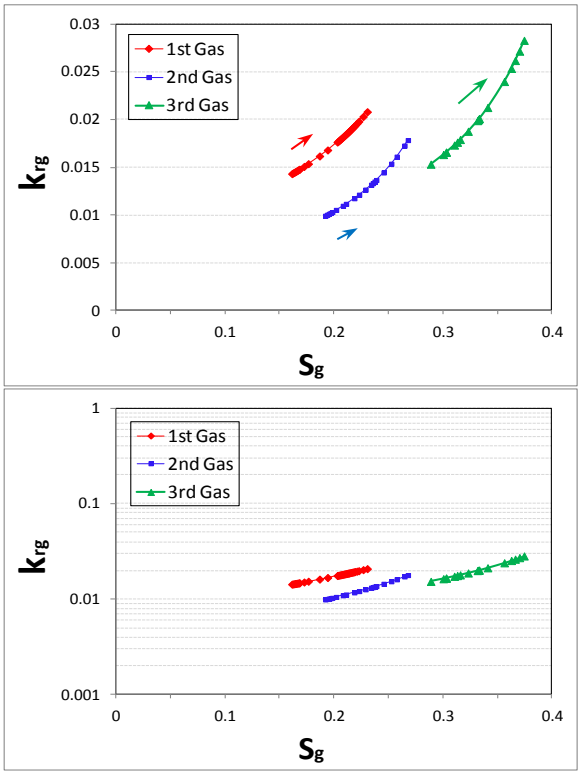

Figure 7-10: Gas (three-phase) relative permeabilities for different stages of gas injection during WAG experiment (65 mD, mixed-wet, IDIDID).

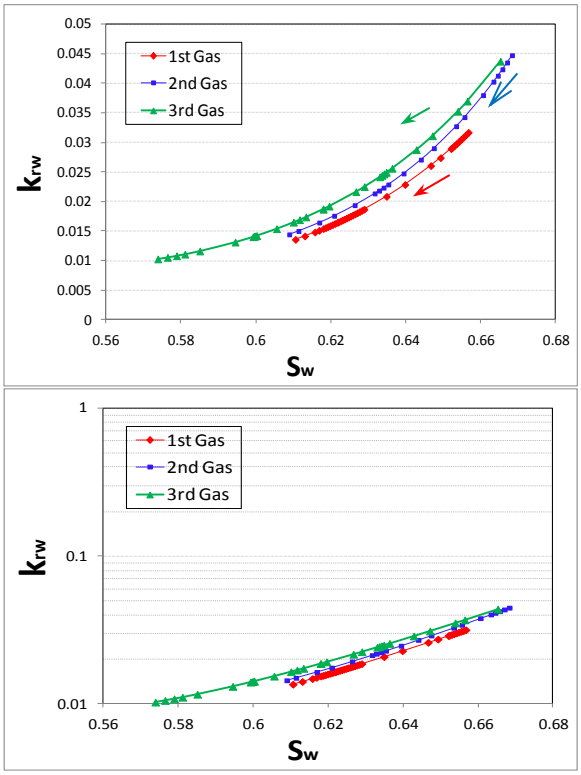

Figure 7-11: Water (three-phase) relative permeabilities for different stages of gas injection during WAG experiment (65 mD, mixed-wet, IDIDID).

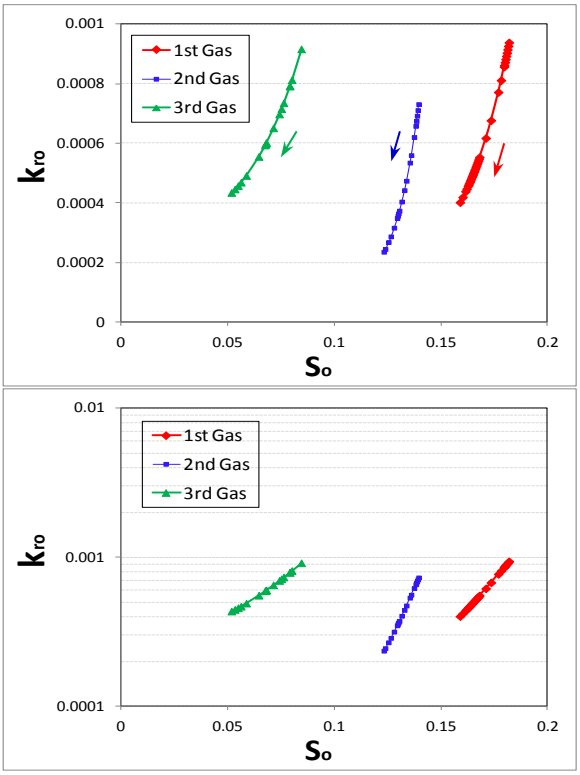

Figure 7-12: Oil (three-phase) relative permeabilities for different stages of gas injection during WAG experiment (65 mD, mixed-wet, IDIDID).

Oil relative permeabilities (Figure 7-14) show that alternation of water and gas injection has improved the relative permeability values in the 3rd water injection period compared to the 2nd water flood. The same Figure shows that residual (trapped) oil saturation reduced as the number of water injection cycles increased. Figure 7-15 shows that water end-point relative permeability has slightly improved in the 3rd water injection compared to the 2nd one. Yet, the difference between the k_{rw} is negligible. To investigate the effect of cycle-dependent hysteresis, the relative permeabilities obtained from successive drainage and imbibition cycles are also compared in Figure 7-13 through Figure 7-15. Figure 7-13 shows gas relative permeabilities and the dashed lines show the trend of k_r values when switching from drainage to imbibition and vice versa. For the gas relative permeabilities, the qualitative nature of the hysteresis in the mixed-wet experiment is the same as that in the water-wet system. This means that gas relative permeabilities curves are not reversible, neither for the change of displacement from drainage into imbibition and nor for the change of displacement from imbibition into drainage. The outcome is that the k_{rg} hysteresis loops are not closed. Generally, the gas relative permeability cyclic hysteresis effect is larger in the water-wet system (Figure 7-7) compared to the mixed-wet system. Comparing 1st hysteresis loop (1st drainage and

2^{nd} imbibition) with the 2^{nd} hysteresis loop (2^{nd} drainage and 3^{rd} imbibition) shows that as the cyclic injection of water and gas continues, the effect of hysteresis would be less.

Figure 7-14 shows the oil relative permeabilities of different drainage and imbibition stages. From the trend of the k_{ro} curves (especially in semi-log) one can conclude that residual oil saturation is higher for the water injection period compared to the preceding drainage (gas injection) stage (if it had continued). Similarly to the water-wet system, water injection periods would reduce the gas relative permeability and improve oil relative permeability in the successive gas injections (drainage) periods. One of the main assumptions in the literature is that in a water-wet system, water relative permeabilities for two- and three-phase are equal to each other. This means that water phase relative permeabilities are independent of the presence of the third phase (gas). The obtained results invalidate this assumption. Figure 7-16 shows that in the performed experiments, for both water-wet and mixed-wet systems, water relative permeability of water/oil two-phase system (1^{st} water injection period, shown by marker points) are significantly higher than those of three-phase systems obtained during WAG experiments (continues blue lines for water-wet and continues red lines for mixed-wet system). The brown dashed lines show the possible trend of k_{rw} values from drainage into imbibition and vice versa.

As was discussed earlier, conventional approaches for simulation of WAG process is based on two-phase flow hysteresis models such as Killough and Carlson. The main assumption is that the imbibition process is reversible. In the WAG experiments reported here, the process is started with an imbibition (water injection) period. As a result neither Killough nor Carlson model would take into account any k_{rw} hysteresis in the subsequent gas injection period. This is not valid since k_{rw} for the 1^{st} gas injection is much lower than k_{rw} for the 1^{st} water injection (Figure 7-16). Contrary to this conventional approach (using two-phase hysteresis such as Carlson and Killough), Larsen and Skauge (1998) three-phase hysteresis model (WAG hysteresis model in Eclipse software), has the flexibility that different water relative permeability curves for two-phase (1^{st} water injection) and for three-phase (2^{nd} water injection) can be defined. The model includes an interpolation for later cycles of the WAG process and also includes a transition regime between two-phase and three phase zones. As a result their approach generates more accurate k_{rw} compared to the conventional two-phase hysteresis models. Nevertheless numerical simulations show that even this model is not

able to capture the observed coreflood data and estimated relative permeabilities, especially for mixed-wet system (Shahrokhi et al., 2014). Figure 7-16 shows in both water-wet and mixed-wet systems, the largest k_{rw} hysteresis happens for the transition from two-phase (oil/water system) to three-phase system (from 1st water injection into 1st gas injection) and also for the transition of injection from 1st gas injection into 2nd water injection. The subsequent WAG cycles afterwards, do not show much hysteresis for k_{rw} in the performed experiments. For the sake of completeness, Figure 7-17 shows comparison of the two-phase oil relative permeability obtained from the 1st water injection with those obtained from three-phase displacements during WAG injection. For both wettability conditions, WAG process improved the two-phase relative permeability of the oil (especially at very low oil saturations).

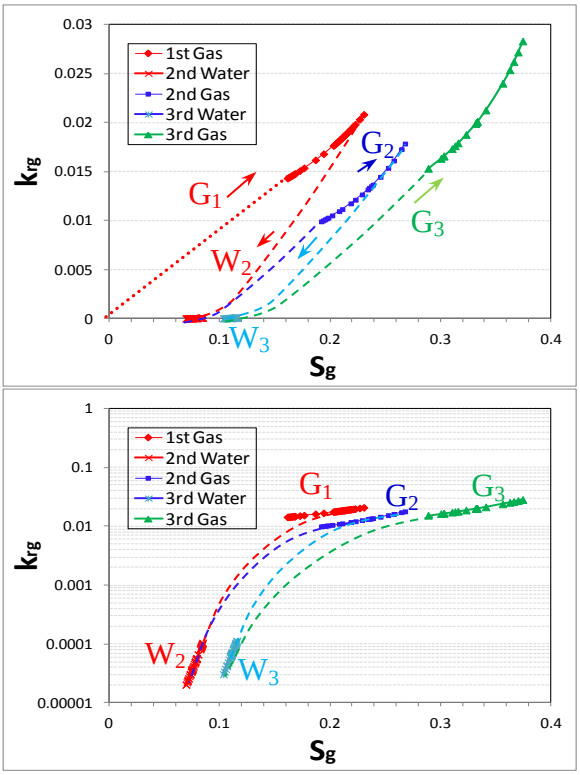

Figure 7-13: Gas (three-phase) relative permeabilities for different stages of gas and water injection during WAG experiment (65mD, mixed-wet, IDIDID).

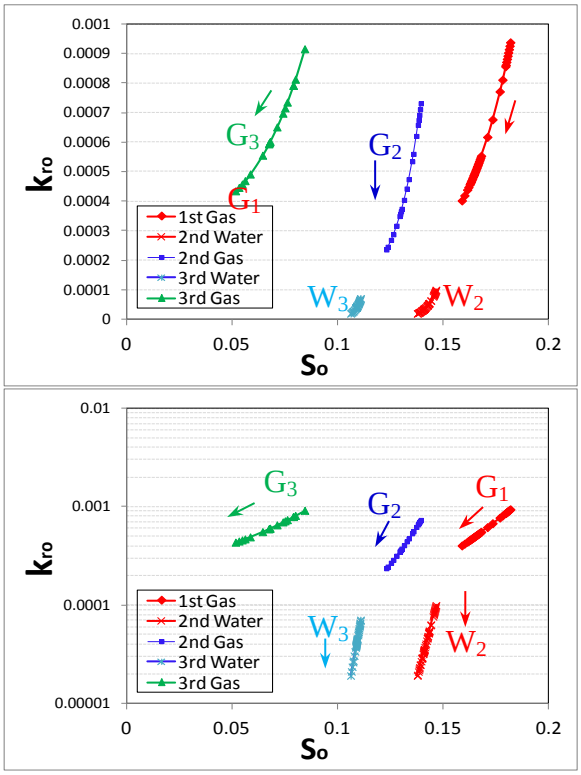

Figure 7-14: Oil (three-phase) relative permeabilities for different stages of gas and water injections during WAG experiment (65mD, mixed-wet, IDIDID).

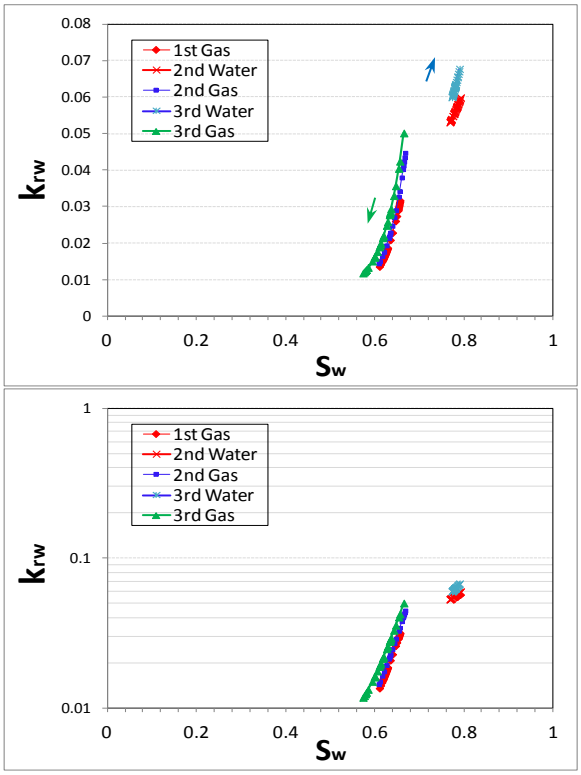

Figure 7-15: Water three-phase relative permeabilities for different stages of gas and water injection during WAG experiment (65mD, mixed-wet, IDIDID).

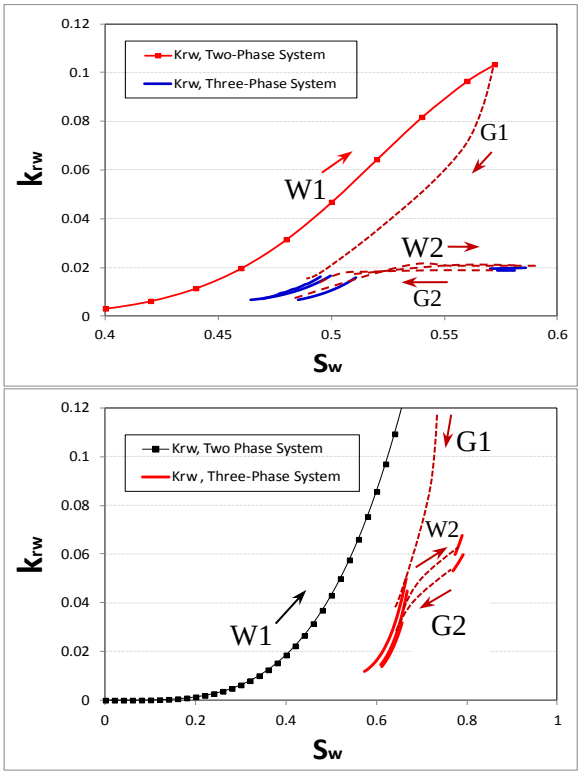

Figure 7-16: Water two- and three-phase relative permeabilities for water-wet (top) and mixed-wet (bottom) systems (65mD, IDIDID), (for individual three-phase k_{rw} values during WAG refer to Figure 7-9 and Figure 7-15).

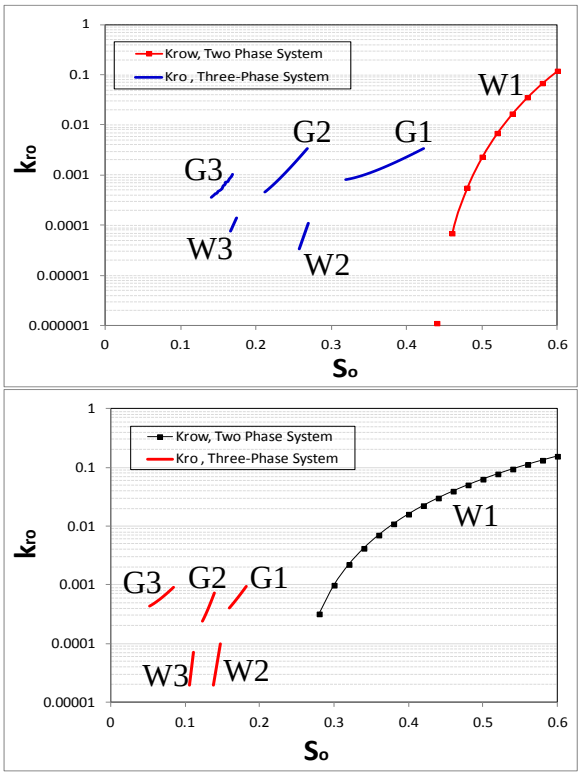

Figure 7-17: Oil two- and three-phase relative permeabilities for water-wet (top) and mixed-wet (bottom) systems (65mD, IDIDID), (for individual three-phase k_{ro} values during WAG refer to Figure 7-8 and Figure 7-14).

7.3.3 Effect of S_{wim} on Cyclic Hysteresis in Water-Wet System

Figure 7-18 shows the (three-phase) gas relative permeabilities (k_{rg}) obtained for different gas injection stages of this water-wet WAG, Experiment-3. The results are shown on both linear and semi-log scales. As can be seen, for the 1st gas injection period, k_{rg} is higher than the 2nd gas injection period. This confirms the saturation history dependency for k_{rg} in water-wet systems. This means that k_{rg} values for the same process (drainage) are different due to the differences between the saturation histories of the rock at the start of each gas injection stage. The same graph shows that the end point relative permeability of the gas in the 2nd drainage period decreased compared to the 1st gas injection. These are attributed to the effect of water slug which is injected in between the gas injection periods. Water traps the free gas, and since this trapping process is not reversible. The trapped gas restricts the flow of fluids in the later stages of the gas injection and the k_{rg} decreases.

Water relative permeabilities for the two gas injection periods which are presented in Figure 7-19, show the same hysteresis dependency as k_{rg}. This means that k_{rw} for the 2nd gas injection period is decreased compare to the 1st drainage period. Comparison of oil relative permeabilities of different gas injection periods (Figure 7-20) reveals significant cycle dependency for oil. Figure 7-20 shows that alternation between imbibitions (water) and drainages (gas), significantly improved oil relative permeability and reduced residual oil saturations.

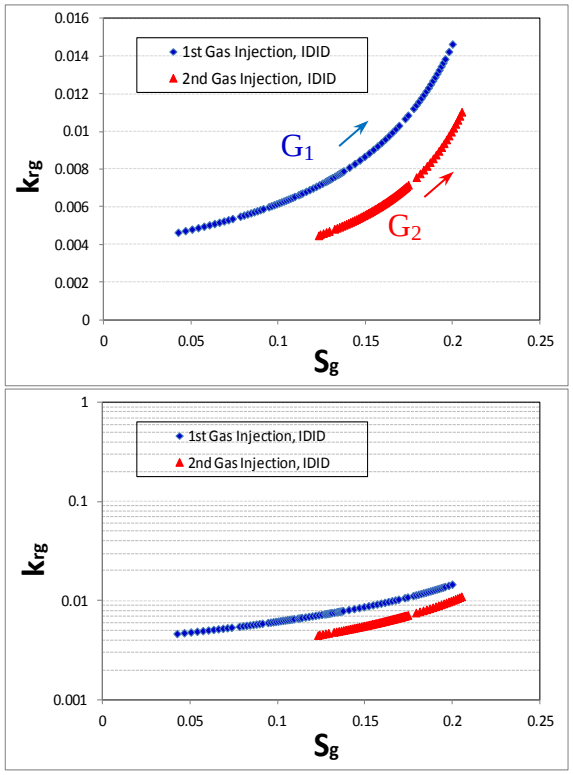

Figure 7-18: Three-phase gas relative permeabilities obtained from gas injection periods of the water-wet WAG injection (experiment-3; 65 mD, water-wet, IDID, S_{wim}= 16%).

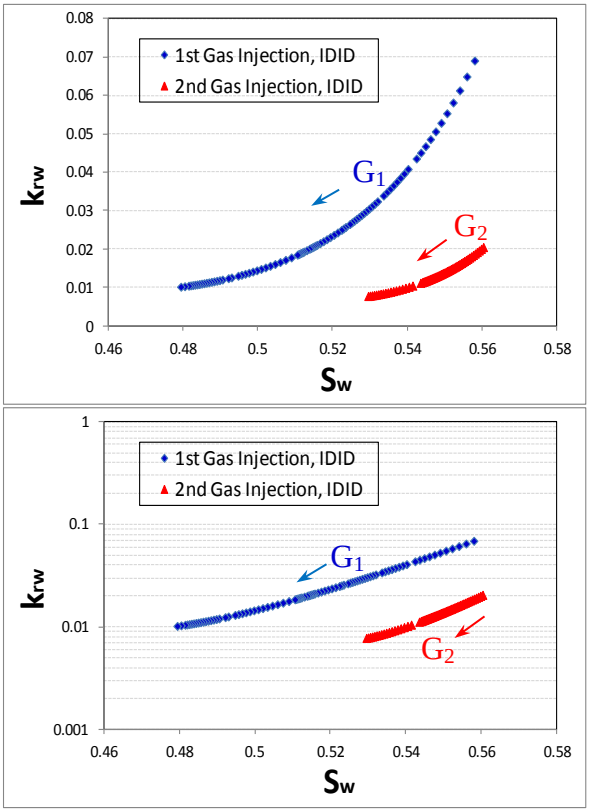

Figure 7-19: Three-phase water relative permeabilities obtained from gas injection periods of the water-wet WAG injection (experiment-3; 65 mD, water-wet, IDID, S_{wim}= 16%).

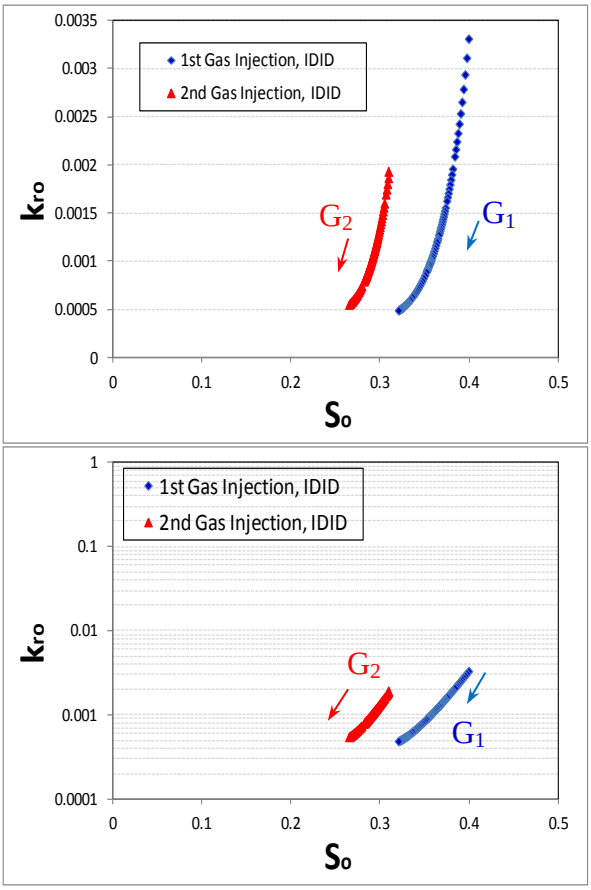

Figure 7-20: Three-phase oil relative permeabilities obtained from gas injection periods of the water-wet WAG injection (experiment-3; 65 mD, water-wet, IDID, S_{wim}= 16%).

To investigate the effect of cycle-dependent hysteresis, relative permeabilities from successive drainage (gas injection) and imbibition stages (water injections) are compared in Figure 7-21 through Figure 7-23. To highlight the differences for low saturation and k_r values, semi-log plots are provided as well. Figure 7-21 through Figure 7-23 show that after the water breakthrough, the relative permeabilities of both gas and oil phases drop significantly. This is especially true in the case of oil relative permeabilities (Figure 7-21), in which the gas saturation change after water breakthrough is practically negligible.

Figure 7-21 also shows calculated gas relative permeabilities (marker points) in which the dashed lines show possible trends of k_r values from drainage into imbibition and vice versa. For 1st drainage period, k_{rg} values are higher compared to the subsequent imbibition period (2nd water injection). In addition, for 2nd imbibition stage, k_{rg} values are also higher compared to the succeeding drainage stage (2nd gas injection). This means that gas relative permeabilities are not reversible, neither for the change of displacement from drainage into imbibition and nor for the change of displacement from

imbibition into drainage. The result is that k_{rg} hysteresis loops are not closed. Figure 7-24 compares the trend of measured three-phase gas relative permeabilities for this test (water-wet, S_{wim}=16%) with those of its water-wet counterpart but with higher immobile water saturation (Experiment-1). From this figure it can be concluded that for both conditions, the same trend of hysteresis behavior has been observed. Yet, the hysteresis effect is more significant for the core with higher immobile water saturation. This can be explained according to the trapped gas saturations. The same graph shows that trapped gas saturation at the end of 2nd water injection period is larger (S_{gtw} = 17%) for the core with higher immobile water saturation, compared to the other core (S_{gtw} = 8%). Higher trapped gas saturation in the former case would further decrease the k_{rg} in the subsequent gas injection period (compared to the 1st gas injection period).

Figure 7-23 shows oil relative permeabilities of the drainage and imbibition stages of this water-wet WAG experiment. From the trend of k_{ro} curves (especially in semi-log plot) one can conclude that residual oil saturation is larger for the waterflooding stage compared to the preceding drainage stage (if it was continued). Yet, the WAG process works since alternating injection of gas and water would reduce the gas relative permeability and improve oil relative permeability in the successive gas injection (drainage) stages.

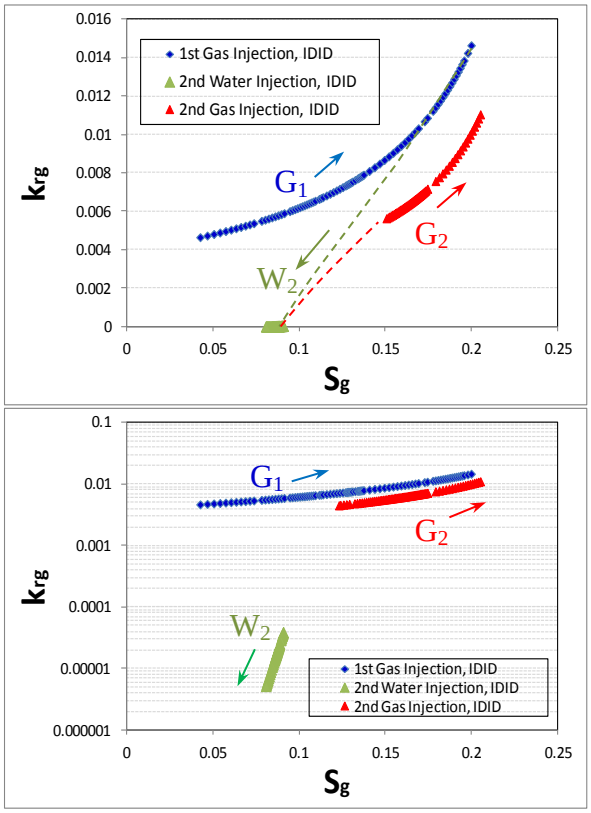

Figure 7-21: Three-phase gas relative permeabilities for different periods of gas and water injections during WAG experiment-3 (65mD, water-wet system).

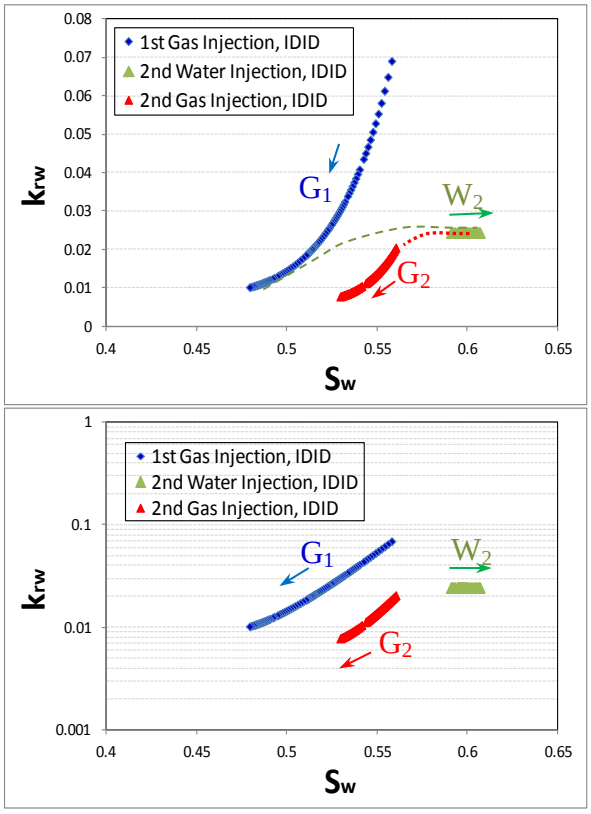

Figure 7-22: Three-phase water relative permeabilities for different periods of gas and water injections during WAG experiment-3 (65 mD, water-wet system).

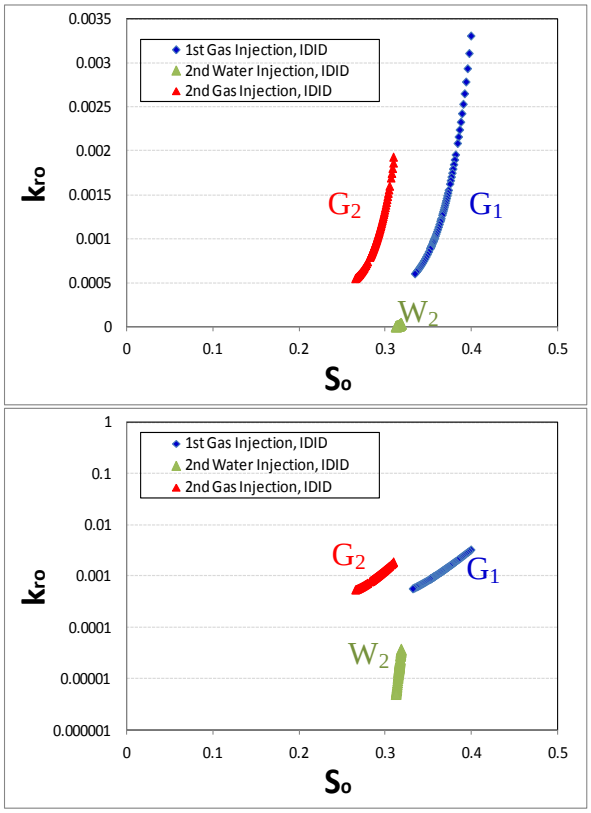

Figure 7-23: Three-phase oil relative permeabilities for different periods of gas and water injections during WAG experiment-3 (65 mD, water-wet system).

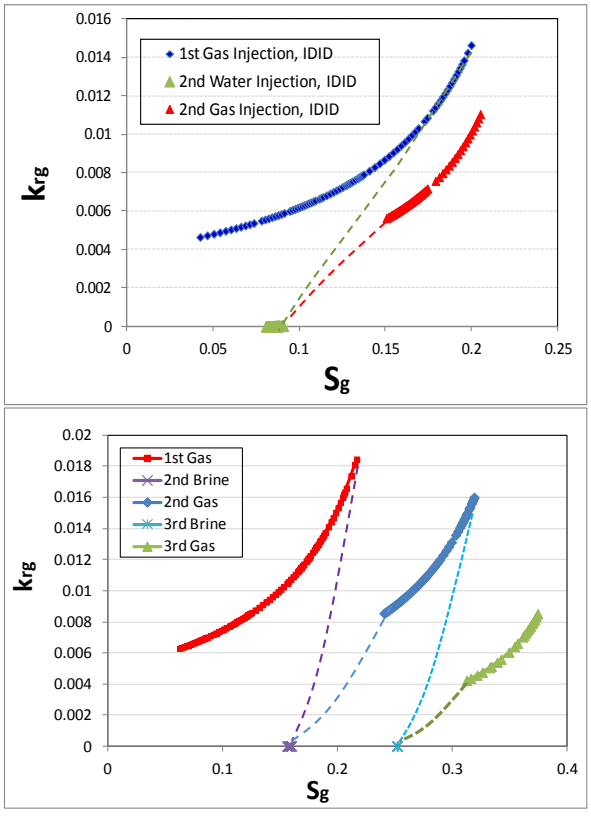

Figure 7-24: Comparison of measured three-phase gas relative permeabilities for the case of experiment-3 (top) with those of experiment-1 (bottom), revealing the effect of immobile water saturation for the case of water-wet samples.

7.3.4 Effect of Injection Scenario on Cyclic Hysteresis in Mixed-Wet System

Figure 7-25 through Figure 7-27 show relative permeabilities obtained for different phases during the gas injection periods of this mixed-wet WAG, Experiment-4. The corresponding semi-log plots are provided as well. Similarly to the previous WAG tests, the gas relative permeability (Figure 7-25) decreases as the number of WAG cycles increases. This confirms cycle-dependent hysteresis k_{rg} in mixed-wet system. Figure 7-28 compares the results of Experiment-4 (DIDIDIDI injection sequence) with those of its IDIDID injection sequence counterpart (Experiment-2), which shows the same trend of hysteresis behavior for k_{rg}.

Figure 7-26 shows the observed water relative permeability saturation-history dependency. k_{rw} values decreased systematically as the number of WAG cycles increased. Water relative permeabilities dropped in the later gas injection periods compared to the earlier ones. The same behavior has been observed for the water injection periods in which k_{rw} of the later water flood periods are lower than those of former water injection periods. As a result k_{rw} curves are not reversible not for the change of direction from drainage into imbibition nor for the change of direction from imbibition into drainage. The result is that k_{rw} hysteresis loops are not closed. Figure 7-29 compares the k_{rw} hysteresis for this test (DIDIDIDI injection sequence) with those of the IDIDID injection scenario. For the latter case, the effect of hysteresis is minimal, which is especially true for gas injection periods (considering percentage change of the k_{rw} values). Decreasing the k_{rw} values in successive stages of DIDIDIDI injection sequence can be responsible for much lower water injectivity in later stages of this experiment compared to the IDIDIDI injection scenario.

Comparison of oil relative permeabilities of different gas injections (Figure 7-27) confirms saturation history dependency for this phase as well. Alternation of saturation direction between imbibition and drainage improved oil relative permeability at lower oil saturations.

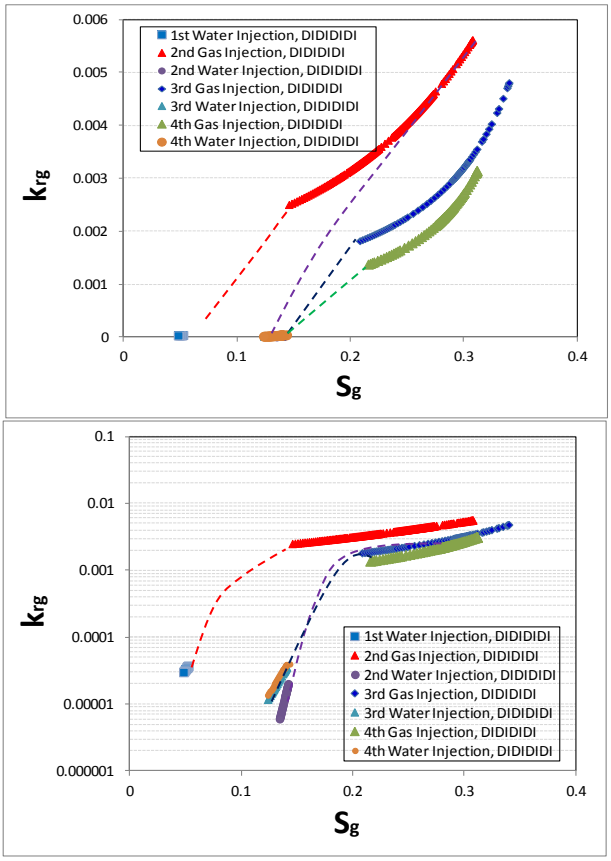

Figure 7-25: Three-phase gas relative permeabilities for different periods of gas and water injections during WAG experiment-4 (65mD, mixed-wet system, DIDIDIDI).

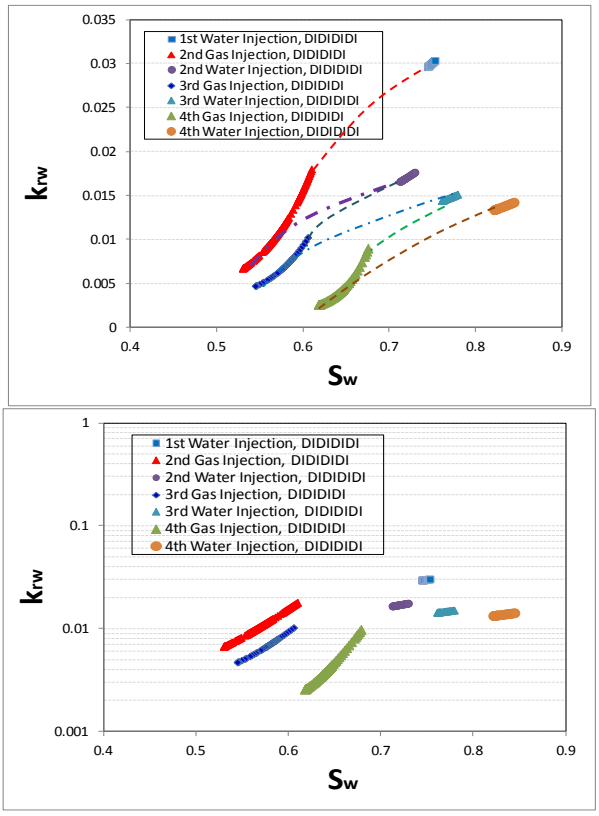

Figure 7-26: Three-phase water relative permeabilities for different periods of gas and water injections during WAG experiment-4 (65mD, mixed-wet system, DIDIDIDI).

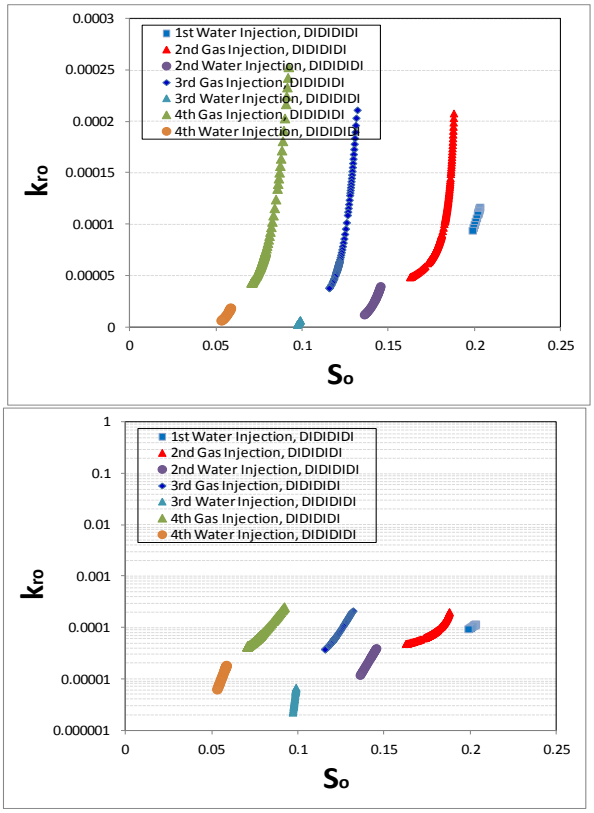

Figure 7-27: Three-phase oil relative permeabilities for different periods of gas and water injections during WAG experiment-4 (65mD, mixed-wet system, DIDIDIDI).

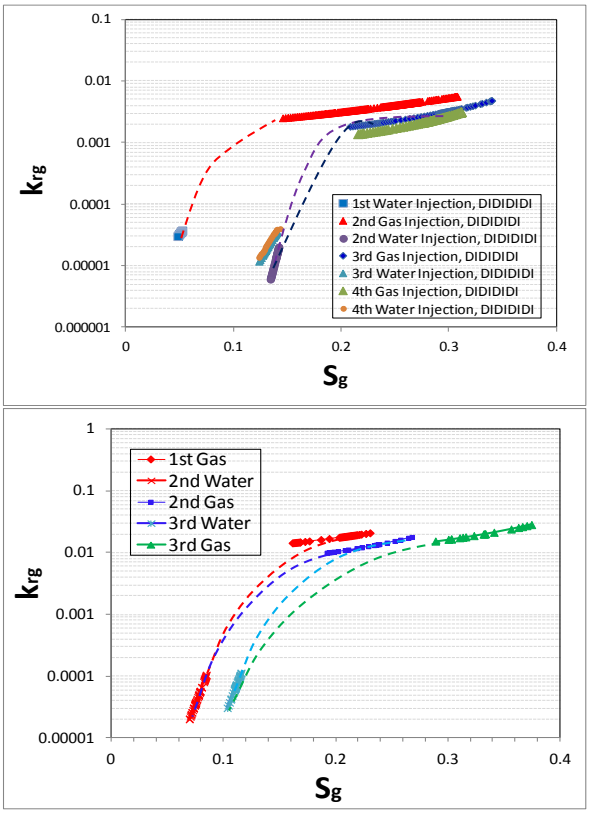

Figure 7-28: Comparison of three-phase gas relative permeabilities for DIDIDID (top) and IDIDID (bottom) injection scenarios in mixed-wet core (65 mD).

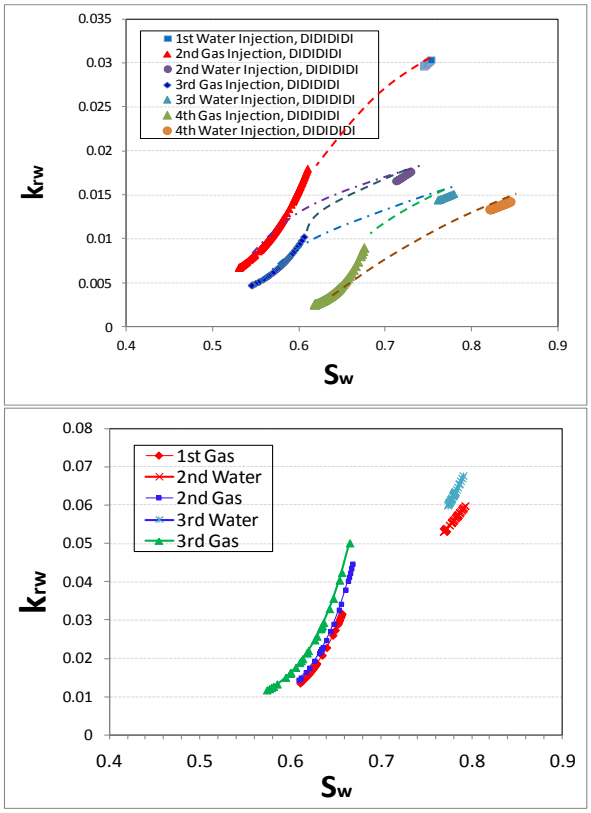

Figure 7-29: Comparison of three-phase water relative permeabilities for DIDIDID (top) and IDIDID (bottom) injection scenarios in mixed-wet core (65 mD).

7.3.5 Effect of Permeability on Cyclic Hysteresis in Mixed-Wet System

Figure 7-30 shows the (three-phase) gas relative permeabilities (k_{rg}) obtained for different gas injection stages of this WAG injection (experiment-5). The same as other WAG experiments, for the 1st gas injection period, k_{rg} is higher than the 2nd gas injection period. The same graph shows that the end point relative permeability of the gas in 2nd drainage period decreased compared to the 1st gas injection (gas trapping due to snap-off by water layers). As discussed earlier, trapped gas restricts the flow of fluids in the later stages of the gas injection and therefore k_{rg} decreases. Comparison of oil relative permeabilities during different gas injection periods (Figure 7-31) reveals that, unlike the other three-phase k_{ro} reported in this chapter, k_{ro} for the 2nd gas injection period does not show improvement over those of 1st gas injection period (for low oil saturations). In fact, k_{ro} in 2nd gas injection period does follow the trend of k_{ro} in 1st gas injection period for low oil saturations (if the 1st gas injection had been extended). Water relative permeabilities presented in Figure 7-32, show the same hysteresis dependency as k_{rg}. This means that k_{rw} for the 2nd gas injection period has decreased compare to the 1st drainage period. Figure 7-33 and Figure 7-34 compare three-phase gas and water relative permeability measured for the 1000 mD core sample with its counterparts measured on the 65 mD (same wettability, injection sequence and

immobile water establishment process). Although the general k_{rg} hysteresis behavior is the same for the two core samples, the hysteresis effect is more significant for the higher permeability core. The same is true for the k_{rw} values, in which high permeability core (1000 mD) shows stronger hysteresis compared to the 65 mD sample. This can be explained according to the trapped gas saturations. The 1st gas injection performance is much higher in the 1000 mD sample compared to the 65 mD sample. The gas saturation at the end of the 1st gas injection is around 48% for the 1000 mD core while for the 65 mD it is just 22%. This means higher initial gas saturation in the subsequent water injection period in the case of the 1000 mD sample, which results in higher trapped gas saturation (14% for 1000 mD compared to 7% for 65 mD sample). This higher trapped gas saturation restricts the flow of water and gas in 2nd gas injection and as a result the subsequent relative permeabilities show more reduction for the 1000 mD compared to the 65 mD sample.

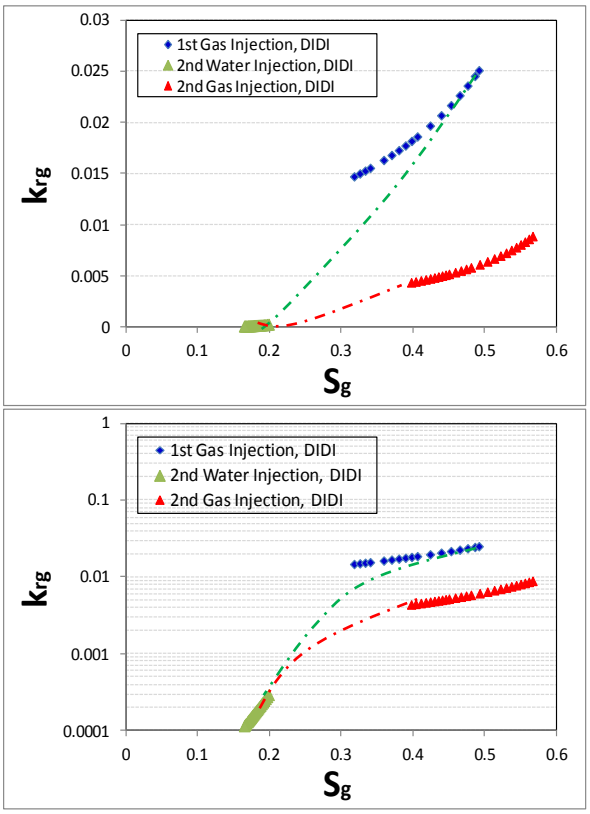

Figure 7-30: Three-phase gas relative permeabilities for different periods of gas and water injection during WAG experiment-5 (1000mD, mixed-wet, IDID).

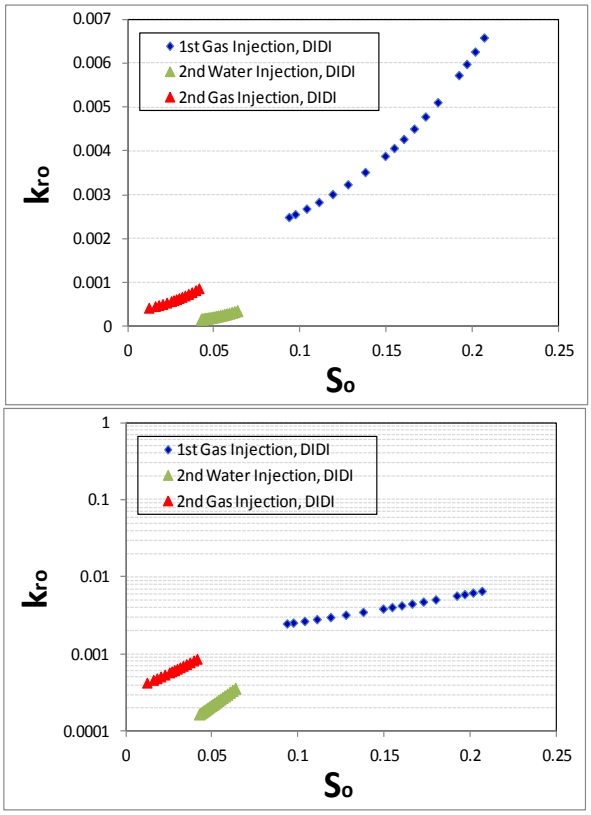

Figure 7-31: Three-phase oil relative permeabilities for different gas and water injections during WAG experiment-5 (1000mD, mixed-wet, IDID).

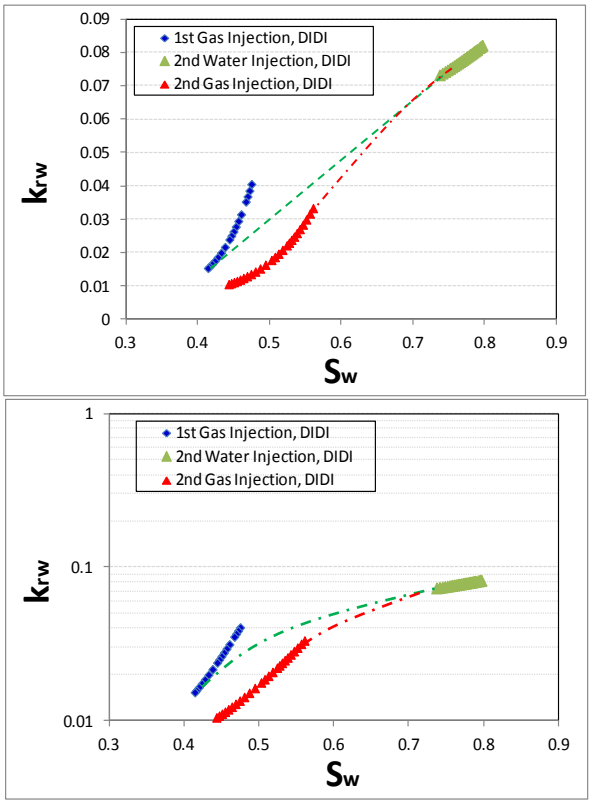

Figure 7-32: Three-phase water relative permeabilities for different periods of gas and water injection during WAG experiment-5 (1000mD, mixed-wet, IDID).

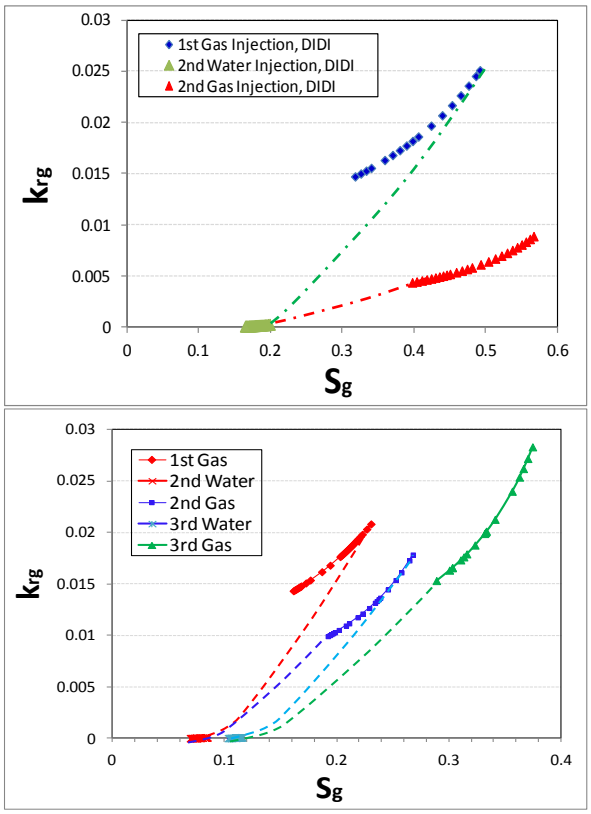

Figure 7-33: Three-phase gas relative permeabilities for 1000 mD (top) and 65 mD (bottom) systems (mixed-wet system and same injection sequence).

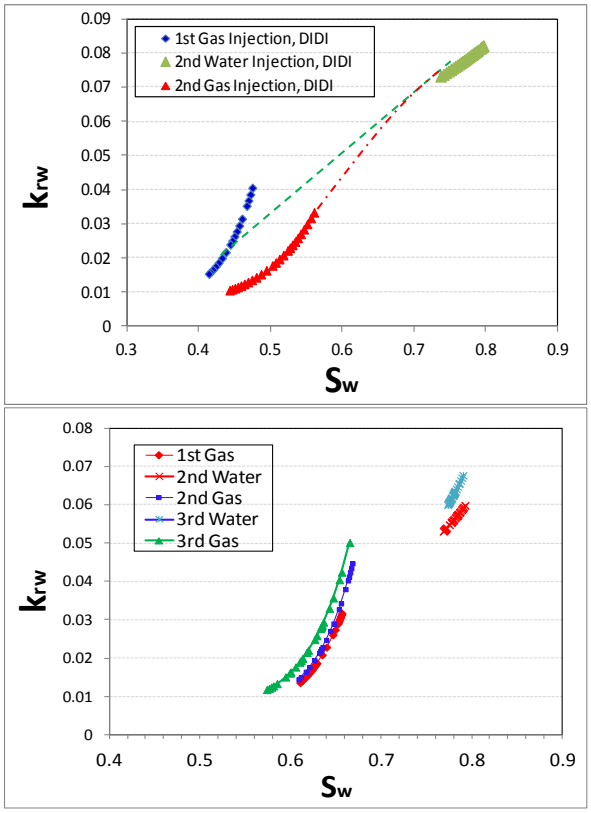

Figure 7-34: Three-phase water relative permeabilities for 1000 mD (top) and 65 mD (bottom) systems (mixed-wet system and same injection sequence).

7.4 Conclusions

In this chapter, the effect of cyclic injection of water and gas (water-alternating-gas) on the three-phase k_r of water, gas and oil under both water-wet and mixed-wet conditions was investigated. The results show irreversible k_r hysteresis loops for gas under three-phase flow conditions. Gas relative permeability (k_{rg}) dropped in successive WAG cycles under both water-wet and mixed-wet conditions. k_{rg} cycle-dependent hysteresis was found to be larger in the water-wet system compared to the mixed-wet one. The results also reveal cycle-dependent hysteresis for oil relative permeability (k_{ro}) curves in which k_{ro} increased in successive gas injection periods separated by water injection periods. k_{ro} improvement was larger for water-wet systems compared to mixed-wet conditions. In both water-wet and mixed-wet systems, for WAG_{IDIDID}, the largest k_{rw} hysteresis happens for the transition from two-phase (primary waterflooding) to three-phase system. For both WAG_{IDIDID} and $WAG_{DIDIDIDI}$ injection scenarios the hysteresis for water phase becomes minimal after the 2nd three-phase displacement (2nd water injection in IDIDID and 2nd gas injection in DIDIDIDI injection sequences).

Conventional approaches for simulation of WAG injection are based on two-phase flow hysteresis models such as Killough and Carlson. The main assumption in these hysteresis models is that the imbibition process is reversible. In some of the WAG experiments reported here, the processes are started with an imbibition (water injection) period. As a result neither Killough nor Carlson model would take into account any k_{rw} hysteresis in the subsequent gas injection period. This is clearly not valid since the measured data shows that k_{rw} obtained during the 1st gas injection (three-phase) is much lower than k_{rw} obtained in the 1st water injection (two-phase). For the WAG test started with primary gas injection (DIDIDIDI), Killough hysteresis model predicts that k_{rw} for the 2nd water injection should be above that of previous drainage curve and Carlson model does not consider any hysteresis for k_{rw}, which is against the experimental results in this study. With regards to the k_{rg} curves, these models assume that drainage relative permeability curves are always above those of the former imbibition period, which is again not supported by the experimental results. Contrary to the conventional approach (using two-phase hysteresis such as Carlson and Killough), Larsen and Skauge (1998) three-phase hysteresis (WAG) hysteresis model assumes that three-phase k_{rw} values for later periods of the WAG injection lies between those of primary waterflooding and 2nd water injection. This assumption is not supported by the performed coreflood results in the mixed-wet core, since k_{rw} continually dropped in the later stages of $WAG_{DIDIDIDI}$

injection test. The presented results show that the importance of cyclic hysteresis of each phase depends on reservoir and operational parameters such as wettability, immobile water saturation, rock permeability and injection scenario. The results presented here points out the need for development of more accurate three-phase hysteresis formulations especially for mixed-wet systems.

7.5 References

Awan A.R., Teigland R., and Kleppe J., (2008): A Survey of North Sea Enhanced-Oil-Recovery Projects Initiated During the Years 1975 to 2005, SPE Reservoir Evaluation & Engineering, Volume 11, Number 3, pp. 497-512.

Avraam and Payatakes, (1999): Flow Mechanisms, Relative Permeabilities, and Coupling Effects in Steady-State Two-Phase Flow through Porous Media. The Case of Strong Wettability, Industrial and Engineering Chemistry Research, Volume 38, Issue 3, pp. 778–786.

Baker, L.E.: (1988): Three-Phase Relative Permeability Correlations, SPE-17369, presented at the 1988 SPE/DOE Enhanced Oil Recovery Symposium, Tulsa, Oklahoma, 17–20 April.

Baker L.E., (1995): Three-phase relative permeability of water-wet, intermediate-wet and oil-wet sandstone, *from* De Haan H.J. *(ed.)*, New Developments in Improved Oil Recovery, Geological Society Special Publication, Volume 84, pp. 51-61.

Beattie, C.I., Boberg, T.C., and McNab, G.S., (1991): Reservoir Simulation of Cyclic Steam Stimulation in the Cold Lake Oil Sands, SPE Reservoir Engineering, Volume 6, Number 2, pp. 200-206.

Braun, E.M. and Holland, R.F., (1995): "Relative Permeability Hysteresis: Laboratory Measurements and a Conceptual Model, SPE Reservoir Engineering, Volume 10, Number 3, pp.222-228.

Carlson F.M, (1981): Simulation of Relative Permeability Hysteresis to the Non-wetting Phase, presented at SPE Annual Technical Conference and Exhibition, 4-7 October, San Antonio, Texas, USA.

Delshad M., MacAllister D.J., Pope G.A., Rouse B.A., (1985): Multiphase Dispersion and Relative Permeability Experiments, SPE Journal, Volume 25, Number 4, pp. 524-534.

Delshad, M., Pope, G.A., (1989): Comparison of the three-phase oil relative permeability models, Transport in Porous Media, Volume 4, issue 1, pp. 59– 83.

DiCarlo D.A., Sahni A., Blunt M.J., (2000): Three-Phase Relative Permeability of Water-Wet, Oil-Wet, and Mixed-Wet Sandpacks, SPE-60767, SPE Journal, Volume 5, Number 1, pp. 82-91.

Dria, D.E., Pope, G.A. and Sepehrnoori, K., (1990): Three-phase gas/oil/brine relative permeabilities measured under carbon dioxide flooding conditions, SPE-20184, presented at the Symposium on Enhanced Oil Recovery, April 22-25, Tulsa, Oklahoma, , USA.

Egermann P., Vizika O., Dallet L., Requin C., Sonier F., (2000): Hysteresis in Three-Phase Flow: Experiments, Modelling and Reservoir Simulations, SPE-65127, presented at SPE European Petroleum Conference, 24-25 October, Paris, France.

Eikje E., Jakobsen S.R., Lohne A., Skjæveland S.M.,1992: Relative permeability hysteresis in micellar flooding, Journal of Petroleum Science and Engineering, Volume 7, Issues 1–2, , pp. 91–103.

Element D.J., Masters J.H.K., Sargent N.C., Jayasekera A.J., Goodyear S.G., (2003): Assessment of Three-Phase Relative Permeability Models Using Laboratory Hysteresis Data, SPE International Improved Oil Recovery Conference in Asia Pacific, 20-21 October, Kuala Lumpur, Malaysia.

Eleri O.O., Graue A., Skauge A., and Larsen J.A., (1995): Calculation of Three-phase Relative Permeabilities from Displacement Experiments with Measurements of In-situ Saturation, SCA-9509, International Symposium of the Society of Core Analysts, San Francisco, CA, USA.

Ghomian Y., Pope G.A., and Sepehrnoori K., (2008): Hysteresis and Field-Scale Optimization of WAG Injection for Coupled CO_2-EOR and Sequestration, SPE-110639, presented at the SPE/DOE Improved Oil Recovery Symposium, 19–23 April, Tulsa, Oklahoma, USA.

Grader A.S. and O'Meara D.J., (1988): Dynamic displacement measurements of three-phase relative permeabilities using three immiscible liquids, SPE-18293, presented at SPE Annual Technical Conference and Exhibition, 2-5 October, Houston, Texas, USA.

Guzman R.E., Giordano D; Fayers F.J., Aziz K., Godi A., (1994): Three-Phase Flow in Field-Scale Simulations of Gas and WAG Injections, SPE-28897, European Petroleum Conference , 25-27 October , London, United Kingdom.

Hawkins, J.T. and Bouchard, A.J., (1992): "Reservoir-Engineering Implications of Capillary-Pressure and Relative-Permeability Hysteresis," The Log Analysts, Volume 33, Number 4, pp. 415-420.

Holmgren C.R. and R.A. Morse; (1951): SPE-951135-G, Effect of Free Gas Saturation on Oil Recovery by Water Flooding, , Journal of Petroleum Technology, Volume 3, Number 5, pp. 135-140.

Johnson, E.F., Bossler, D.P. and Naumann, V.O., (1959): Calculation of relative permeability from displacement experiments, SPE- 1023-G, Petroleum Transactions, AIME, Volume 216, pp. 370-372.

Killough, J.E., 1976. Reservoir simulation with history dependent saturation functions. SPE J. (Feb.): 37-48.

Kvanvik B.A.; Skauge A., Matrea B., Kolltveita K., (1992): Three-phase micro-emulsion relative permeabilities: Experimental and theoretical consideration , Journal of Petroleum Science and Engineering, Volume 7, Issues 1–2, April, pp. 105–116.

Land C.S., (1968): Calculation of Imbibition Relative Permeability for Two- and Three-Phase Flow From Rock Properties, SPE Journal, Volume 8, Number 2, pp. 149 – 156.

Larsen J.A. and Skauge A., (1995): Comparing Hysteresis Models for Relative Permeability in WAG Studies, Society of Core Analysts International Symposium, SCA-9506, San Francisco, CA, USA.

Larsen J.A. and Skauge A. (1998): Methodology for Numerical Simulation with Cycle-Dependent Relative Permeabilities, SPE Journal, Volume3, Number 2, pp.163-173.

Mejia G.M., Watson A.T., Nordtvedt J.E., (1996): Estimation of three-phase flow functions in porous media, AIChE Journal, Volume 42, Issue 7, pp. 1957–1967.

Nordtvedt J.E., Ebeltoft E., Iversen J.E., Sylte A., Urkedal H., Vatne K.O., Watson A.T., (1997): Determination of Three-Phase Relative Permeabilities from Displacement Experiments, SPE-36683, SPE Formation Evaluation, Volume 12, Number 4, pp. 221-226

Oak, M.J., (1990): Three-Phase Relative Permeability of Water-wet Berea, SPE-20183, presented at the SPE/DOE Enhanced Oil Recovery Symposium, 22-25 April, Tulsa, Oklahoma, USA.

Oak, M.J., (1991): Three-Phase Relative Permeability of Intermediate-Wet Berea Sandstone, SPE-22599, presented at SPE Annual Technical Conference and Exhibition, 6-9 October, Dallas, Texas, USA.

Oak M.J., Baker L.E. and Thomas D.C.; (1990): Three-Phase Relative Permeability of Berea Sandstone, SPE-17370, Journal of Petroleum Technology, Volume 42, Number 8, pp. 1054-1061.

Sarem, A.M., (1966): Three-Phase Relative Permeability Measurements by Unsteady-State Method, SPE-1225, SPE Journal, Volume 6, Number 3, pp. 199–205.

Patel, P.D., Christman, P.G., and Gardner, J.W., (1987): "An Investigation of Unexpectedly Low Field-Observed Fluid Mobilities During Some CO2 Tertiary Floods," SPE Reservoir Engineering, Volume 2, Number 4, pp. 507-513.

Petersen E.B., Lohne A., Vatne K.O., Helland J.O., Virnovsky G. and Øren P.E., Relative Permeabilities for Two- and Three-phase Flow Processes Relevant to the Depressurization of the Stafjord Field, SCA2008-23, presented at the International Symposium of the Society of Core Analysts, 29 October-2 November, Abu-Dhabi, UAE.

Schneider, F.N. and Owens, W.W., (1976): "Relative Permeability Studies of Gas-Water Flow Following Solvent Injection in Carbonate Rocks," SPE Journal, Volume 16, Number 1, pp. 23-30.

Shahrokhi O., Fatemi S.M., Sohrabi M., Ireland S., Ahmed K.; (2014): "Assessment of Three Relative Permeability and Hysteresis Models for Simulation of Water-Alternating-Gas (WAG) Injection in Water-wet and Mixed-wet Systems", SPE-169170-MS, accepted for presentation at 2014 SPE Improved Oil Recovery Symposium to be held 12 -16 April, in Tulsa, OK, USA.

Shahverdi H., (2012): Characterization of Three-phase Flow and WAG injection in Oil Reservoirs, PhD Thesis, submitted to the Institute of Petroleum Engineering, Heriot-Watt University, Edinburgh, UK.

Skauge, A. and Aarra M.: "Effect of Wettability on the Oil Recovery by WAG," presented at the 1993 7th IOR Symposium, 26–28 October, Moscow, Russia.

Skauge A. and Larsen J.A., (1994): Three-phase Relative Permeabilities and Trapped Gas Measurements Related to WAG Processes, Society of Core Analysts International Symposium, SCA-9421, September, Stavanger, Norway.

Skauge, A. and Matre, B., (1989): Three phase relative permeabilities in brine-oil-microemulsion systems, Presented at the 5th European Symposium on Improved Oil Recovery, 25-27 April, Budapest, Hungary.

Skauge A., Veland I., and Larsen J.A., (1999): Factors Influencing Three-phase Flow Parameters in WAG Experiments, Society of Core Analysts International Symposium, Golden, Colorado, USA

Sohrabi M., Danesh A., Tehrani, D. and Jamiolahmady M., (2008a): Microscopic Mechanisms of Oil Recovery By Near-Miscible Gas Injection, Transport in Porous Media, Volume 72, Number 3, pp. 351-367.

Sohrabi M., Danesh A., and Jamiolahmady M., (2008b): Visualisation of Residual Oil Recovery by Near-Miscible Gas and SWAG Injection Using High-Pressure Micromodels, Transport in Porous Media, Volume 74, Number 2, pp. 239-257.

Sohrabi M., Tehrani D.H., Danesh A., Henderson G.D., (2004): Visualization of Oil Recovery by Water-Alternating-Gas Injection Using High-Pressure Micromodels, SPE-89000, SPE Journal, Volume 9, Number 3, pp. 290-301.

Spiteri E.J., Juanes R., (2006): Impact of relative permeability hysteresis on the numerical simulation of WAG injection, Journal of Petroleum Science and Engineering, Volume 50, Issue 2, pp. 115– 139.

Spiteri E.J., Juanes R., Blunt M.J., and Orr F.M., (2005): Relative Permeability Hysteresis: Trapping Models and Application to Geological CO_2 Sequestration, SPE-96448, SPE Annual Technical Conference and Exhibition, 9 – 12 October, Dallas, Texas, USA.

Stone, H.L. (1970): Probability Model for Estimating Three-Phase Relative Permeability, Journal of Petroleum Technology, Volume 22, Number 2, pp. 214-218.

Stone, H.L., (1973): Estimation of Three-Phase Relative Permeability and Residual Oil Data, Journal of Canadian Petroleum Technology, Volume 12, Number 4, pp. 51-61.

Virnovskii, G.A., (1984): Determination of relative permeabilities in a three-phase flow in a porous medium, Fluid Dynamics, Volume 19, Number 5, pp. 835-837.

Wang, F.H.L., (1988): Effect of Wettability Alteration on Water/Oil Relative Permeability, Dispersion, and Flowable Saturation in Porous Media, SPE Reservoir Engineering, Volume 3, Number 2, pp.617-628.

Wei, J.Z. and Lile, O.B., (1993): "Influence of Wettability and Saturation Sequence on Relative Permeability Hysteresis in Unconsolidated Porous Media," SPE-25282, available from Onepetro eLibrary.

Welge H.J., (1949): Displacement of Oil from Porous Media by Water or Gas, Transactions of the AIME, Volume 179, Number 1, pp. 133-145.

Zhou D., Yan M., Calvin W.M., (2012): Optimization of a Mature CO2 Flood - from Continuous Injection to WAG, SPE-154181, SPE Improved Oil Recovery Symposium, 14-18 April, Tulsa, Oklahoma, USA.

8. Trapped Oil and Gas Saturations

Relative permeability, hysteresis effects, and trapped phase saturations are key parameters for reliable simulation of processes involved in oil recovery including WAG injection. Although hydrocarbon gas and CO_2, which are widely used in WAG schemes, are likely to be injected at very low IFT (near-miscible) conditions into reservoir rocks with mixed wettability, current models are based on high IFT two-phase flow conditions and water-wet systems.

This chapter investigates the characteristic properties of rock/fluids systems (wettability, immobile water saturation, permeability, saturation history and oil/gas IFT) that influence the entrapment of gas and oil in petroleum reservoirs. In both water-wet and mixed-wet cores, trapped gas saturation obtained for two-phase water-gas systems (S_{gtw}) are higher than those obtained for two-phase gas-oil systems (S_{gto}) under low gas-oil IFT. The differences of measured trapped gas saturations during three-phase and two-phase water/gas systems, especially for small S_{gi} values, were not significant. Both three-phase trapped gas and trapped oil saturations were larger in water-wet systems compared to what was obtained in mixed-wet systems. Measured three-phase trapped oil and gas saturations for lower permeability rock (65mD) were larger than those of the 1000 mD core sample.

The effect of trapped gas saturation (S_{gt}) on the amount of residual oil saturation at the end of water injection periods (S_{orw}) of WAG injection is also investigated. It is found that the S_{orw} increases linearly by decreasing the S_{gt}, and approaches to the two-phase S_{orw} (after primary waterflooding) at its limit where $S_{gt} = 0$. S_{orw} vs. S_{gt} curve of the water-wet system lies above that of the mixed-wet system. This means that the amount of oil that is trapped by water in the presence of gas increases as the porous medium becomes more water-wet. From the different parameters studied here, injection scenario, permeability and oil/gas IFT have the largest effect on the slope of the S_{orw} vs. S_{gt} curve. For both water-wet and mixed-wet systems it was found that total trapped hydrocarbon saturations (for different water injections of WAG injection) remained close to the residual oil saturation at the end of primary waterflooding.

The above experimental results are discussed and explained based on pore-scale and core-scale displacement mechanisms of multiphase flow and cyclic injections (especially WAG injection) in porous media. Using the experimental results, it will be demonstrated that although some previously developed empirical trap models are able to capture the trends of trapped gas and trapped oil saturations for two-phase systems, but the observed trends in three-phase (especially for mixed-wet system) cannot be captured using available models. This further emphasises the need for developing more reliable models for fluid displacements in three-phase flow regime.

8.1 Introduction

Trapped gas saturation is recognized to be a key factor in evaluating gas recovery from a gas reservoir invaded by water (Crowell and Loomis, 1966; Suzanne et al., 2003). It is also important during CO_2 injection into underground aquifers for sequestration purposes as it will reduce the risk of relying on sealing cap-rock (Al-Mansoori et al., 2010). In this case, CO_2 bubbles will be immobilized in pore-space surrounded by water layers. Gas entrapment occurs at the trailing edge of a CO_2 plume as it migrates upwards, when it is displaced by natural groundwater flow or by the injection of chase brine (Kumar et al., 2005; Juanes et al., 2006; Qi et al., 2009)

Trapped gas saturation is also a major parameter in enhanced oil recovery processes such as water-alternating-gas (WAG) injection (Sohrabi et al., 2004), which is the subject of the present work. Gas trapping during water injection periods of WAG, reduces the mobility of the gas and also redistributes the flow paths of the gas in successive gas injection periods and hence improves the sweep efficiency of the process. In Chapter 7, the effect of cyclic injection of water and gas on the three-phase k_r of water, gas and oil (under both water-wet and mixed-wet conditions) was investigated. It was found that, due to the gas entrapment during water injection periods, the gas relative permeability (k_{rg}) drops in WAG cycles under both water-wet and mixed-wet conditions. The results also revealed saturation history dependency for oil relative permeability (k_{ro}), which tends to increase in successive gas injection periods. The improvement in k_{ro} was higher for water-wet systems, where the gas entrapment was larger due to stronger snap-off mechanism.

To account for the reduction of S_{or} during gas injection performed after water injection, Larsen and Skauge (1998) proposed a linear relationship between residual oil and trapped gas saturation as defined below:

$$S_{or} = S_{orw} - \alpha S_{gt} \quad \text{(Eq 8-1)}$$

Where S_{or} and S_{gt} are residual oil and trapped gas saturations in the three-phase flow (after water injection periods), S_{orw} is the residual oil under the two-phase flow process, achieved by primary waterflooding and α is a tuning parameter, to be determined by matching experimental data.

Suzanne et al. (2001, 2003) and Hamon et al. (2001) experimental results showed that porosity (or permeability) and the amount of micro-porosity along with the initial gas saturation control S_{gt} values. Using data from mixed-wet Prudhoe Bay sandstone core samples, Jerauld (1997a) also suggested that pores structures play an important role in determining the trapped gas saturation. He showed that the trapped gas saturation decreases with increasing porosity for sandstones. He proposed that lower porosity samples have larger pore/throat aspect ratios which in turn results in more snap-off displacements disconnecting gas clusters. Jerauld (1997b) suggested that the total hydrocarbon (oil and gas) trapped in a three-phase system would be up to 20% greater than the water-flood residual oil saturation during two-phase flow. He concluded that unless the system is strongly water-wet, the trapped gas and residual oil saturations should be approximately independent since they are not necessarily competing to occupy the same pores.

Kralik et al. (2000), Skauge and Ottesen (2002) and Skauge and Larsen (1994) demonstrated experimentally that the three-phase residual gas saturation is lower than the two-phase residual gas saturation. It is assumed that gas and oil are both trapped in a fixed number of larger pore spaces and, in three-phase flow, they compete for these spaces and hence the amount of oil or gas trapping is reduced from an equivalent two-phase (oil/water or gas/water) displacement. Contrary to this, Maloney and Zornes (2003), Jerauld (1997b) and Caubit et al. (2004) suggested that the two- and three-phase residual gas saturations are equal.

Trapping in three-phase flow has been also studied using pore-scale modelling by Suicmez et al. (2008). They simulated gas invasion into oil and water, followed by waterflooding. They found that the total amount of gas and oil trapped was larger than the maximum trapped non-wetting phase saturation found during two-phase flow. Suicmez et al. (2008) showed that the amount of oil that is trapped by water in the presence of gas increases as the medium becomes more oil-wet, which is opposite from that seen for two-phase flow.

Kralik et al (2000) used their comprehensive set of experimental data from preserved reservoir sandstone to demonstrate important trapping features for oil-wet systems. They found that unlike water-wet systems, the three-phase trapped gas saturation depends on the relative amounts of oil and water. While two-phase trapped gas values were consistent with values in the literature for similar sandstones, three-phase trapped gas levels were approximately a factor of two lower. Contrary to Kralik et al (2000), Caubit et al. (2004) showed that three-phase trapped gas saturation is independent of wettability and is similar to the two-phase values. Skauge and Larsen (1994) found that trapped gas saturation is strongly dependent on the maximum gas saturation during the displacement process and is independent of the wettability.

Blunt (2000) developed a three-phase trapping model by extending Land (1968) two-phase model to three-phase systems. He assumed that the total trapped hydrocarbon saturation in a strongly water-wet system can be estimated by using a similar approach to Land. According to his model, the total trapped hydrocarbon saturation in a three-phase system should be the same as the trapped non-wetting phase saturation in a two-phase flow. However, Suzanne et al. 2003 have questioned the validity of applying Land's trapping model to rock/fluid systems other than those analyzed by Land (consolidated rock with strongly water-wet condition).

In general, trapped gas saturation is a function of interfacial tension, spreading conditions, pore morphology, displacement mechanism (coreflood or spontaneous imbibition), saturation history and wettability. The objective of the present chapter is to study reliable trapped oil and gas saturations applicable to the WAG injection process. Although hydrocarbon gases and CO_2 are usually the gases that are injected in oil reservoirs and are likely to be injected under near-miscible (very low IFT) conditions

and into reservoir rocks with mixed wettability, current trapping models are based on two-phase experiments under high IFT conditions and water-wet systems. For this reason the focus of the current study is the systems in which oil and gas are at near-miscible condition (IFT = 0.04 $mN.m^{-1}$). The characteristic properties of rock/fluid system (wettability, immobile water saturation, saturation history, permeability and oil/gas IFT) that influence the entrapment of gas and oil in oil reservoirs are investigated.

8.2 Coreflood Experiments

The experiments, which their results are used in this chapter, include both two-phase (oil/water, oil/gas and water/gas systems) and three-phase (WAG) displacements. Table 8-1 through Table 8-3, show the list of coreflood experiments which are used in this study. Detailed discussion of these corefloods can be found in previous chapters. Figure 8-1 shows the change in average saturation of oil and gas during two-phase cyclic injection of oil and gas as DIDID. Figure 8-2 shows the change in average saturations of oil and gas during two-phase cyclic injection of oil and gas as IDIDI. In these two series of experiments oil injections are referred to as imbibition (I) and gas injection are presented by drainage (D). Therefore, IDIDI represents a series of coreflood displacements started with an oil injection into the core saturated by gas and immobile water followed by cyclic injection of gas and oil performed in the order of oil-gas-oil-gas-oil. Figure 8-3 shows the change in the average saturations of water and gas during two-phase cyclic injection of water and gas in DIDIDI order. Figure 8-4 shows the change in the average saturations of water and gas during two-phase cyclic injection of water and gas in IDIDI order. In these two series of corefloods, "I" stands for water injection (imbibition) and gas injection (drainage) is presented by "D". Figure 8-5 shows the change in average saturations of water and oil during two-phase cyclic injection of water and oil in DIDIDI order. In these two series of corefloods, "I" stands for water injection (imbibition) and oil injection (drainage) is presented by "D". Figure 8-6 shows ternary diagrams of average saturations changes (saturation path) during different WAG experiments on both 65 mD and 1000 mD core samples. For WAG injections, "I" stands for water injection (imbibition) and gas injection (drainage) is presented by "D".

Table 8-1: 65mD, Coreflood experiments at 1840 psia and 100ºF used in Chapter-8 (Oil/Gas IFT = 0.04 $mN.m^{-1}$).

Exp. #	*Mobile Fluids*	*Coreflooding*	*Direction*	*Wettability*	S_{wim}
1	Oil/Gas	Oil Injection	Imbibition (I)	Water-Wet	✓
2	Water/Oil	Water Injection	Imbibition (I)	Water-Wet	✓
3	Water/Oil	Water Injection	Imbibition (I)	Mixed-Wet	✓
4	Oil/Gas	2 phase Hysteresis	DIDID	Mixed-Wet	✓
5	Oil/Gas	2 phase Hysteresis	IDIDI	Mixed-Wet	✓
6	Water/Gas	2 phase Hysteresis	DIDIDI	Mixed-Wet	✓
7	Water/Gas	2 phase Hysteresis	IDIDI	Mixed-Wet	✓
8	Water/Oil	2 phase Hysteresis	DIDIDI	Mixed-Wet	✓
9	Water/Oil/Gas	WAG Injection*	IDID	Water-Wet	✓
10	Water/Oil/Gas	WAG Injection	IDIDID	Water-Wet	✓
11	Water/Oil/Gas	WAG Injection	IDIDID	Mixed-Wet	✓
12	Water/Oil/Gas	WAG Injection	DIDIDIDI	Mixed-Wet	✓

* with different S_{wi} = 16%

Table 8-2: 1000mD, Coreflood experiments at 1840 psia and 100ºF used in Chapter-8 (Oil/Gas IFT = 0.04 $mN.m^{-1}$).

Exp. #	*Mobile Fluids*	*Coreflooding*	*Direction*	*Wettability*	S_{wim}
13	Oil/Gas	Oil Injection	Imbibition (I)	Mixed-Wet	✓
14	Water/Oil/Gas	WAG Injection	IDID	Mixed-Wet	✓

Table 8-3: 65mD, Coreflood experiments at 1200 psia and 100ºF used in Chapter-8 (Oil/Gas IFT = 2.70 $mN.m^{-1}$).

Exp. #	*Mobile Fluids*	*Coreflooding*	*Direction*	*Wettability*	S_{wim}
15	Water/Oil/Gas	WAG Injection	IDIDIDID	Mixed-Wet	✓

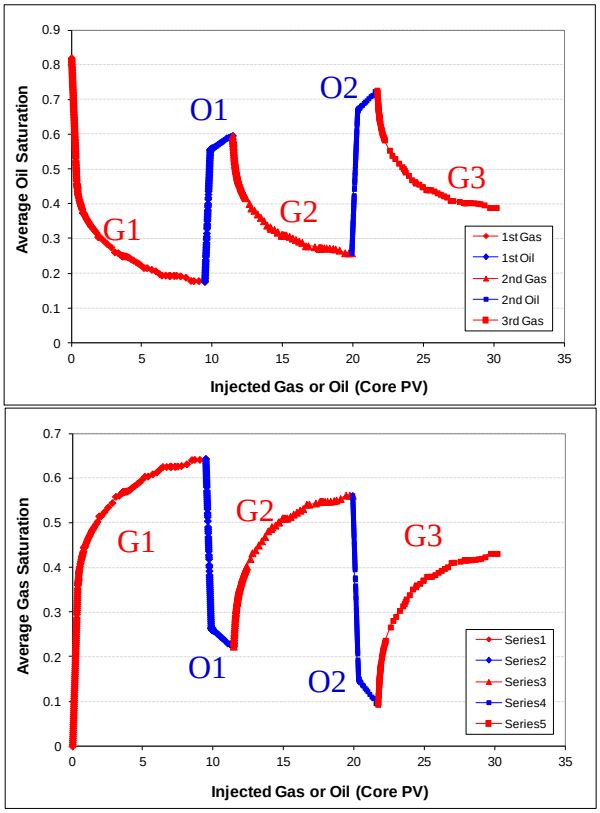

Figure 8-1: Average oil (top) and gas (bottom) saturations inside the core during different cycles of two-phase oil/gas DIDID hysteresis test (experiment 4).

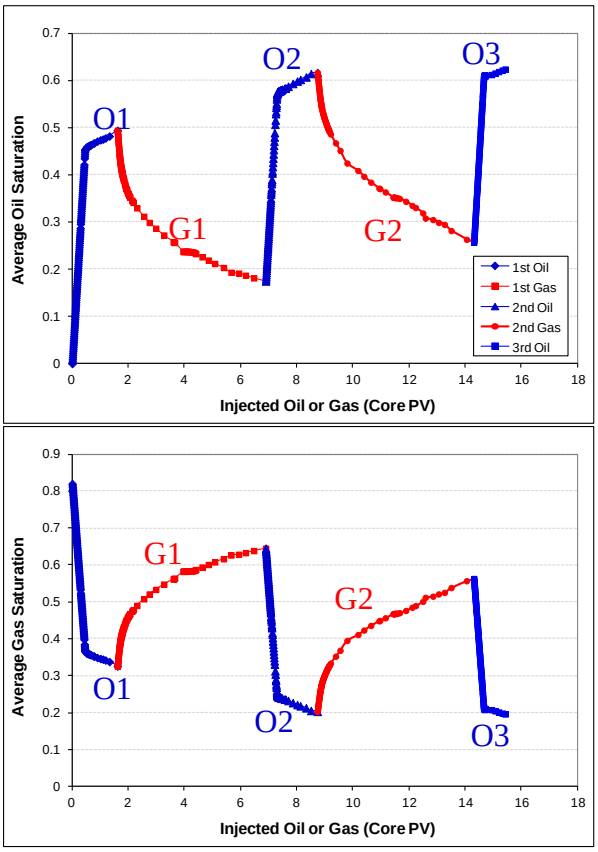

Figure 8-2: Average oil (top) and gas (bottom) saturations inside the core during different cycles of two-phase oil/gas IDIDI hysteresis test (experiment 5).

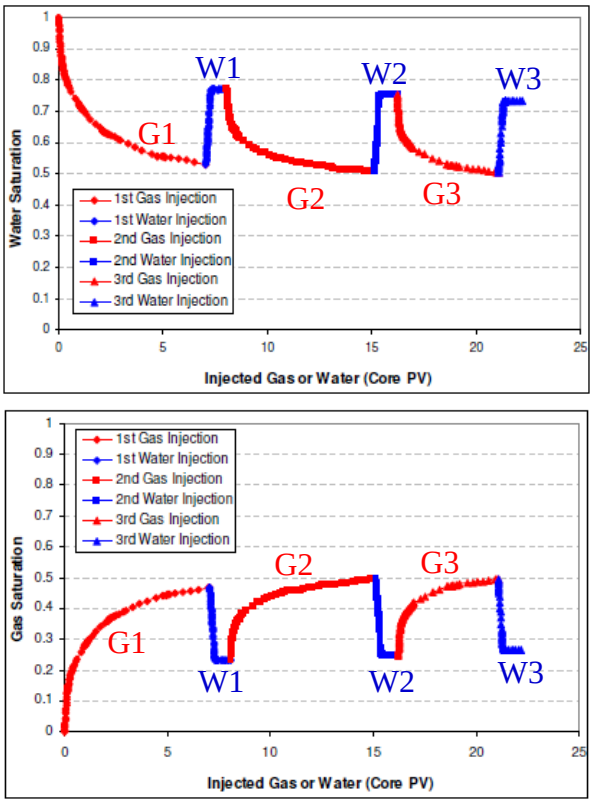

Figure 8-3: Average brine (top) and gas (bottom) saturations inside the core during different cycles of two-phase water/gas DIDIDI hysteresis test (experiment 6).

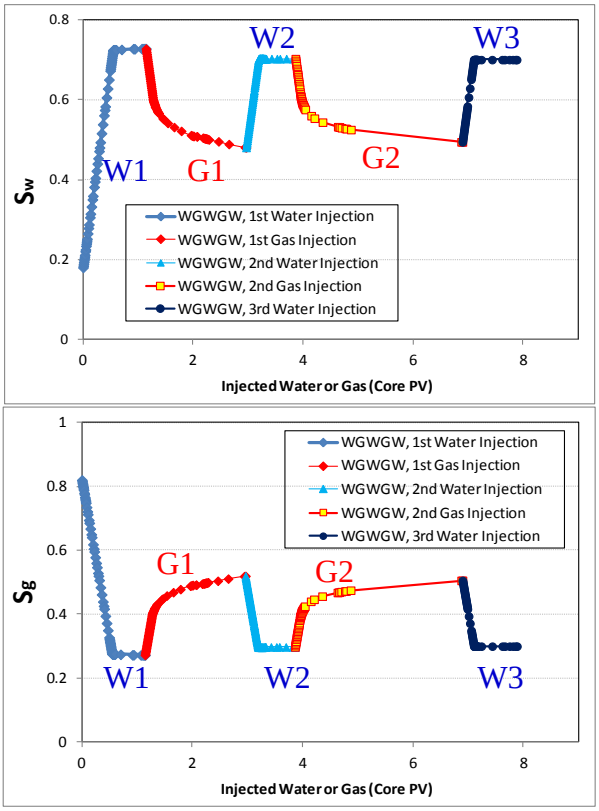

Figure 8-4: Average water (top) and gas (bottom) saturations inside the core during different cycles of two-phase water/gas IDIDI hysteresis test (experiment 7).

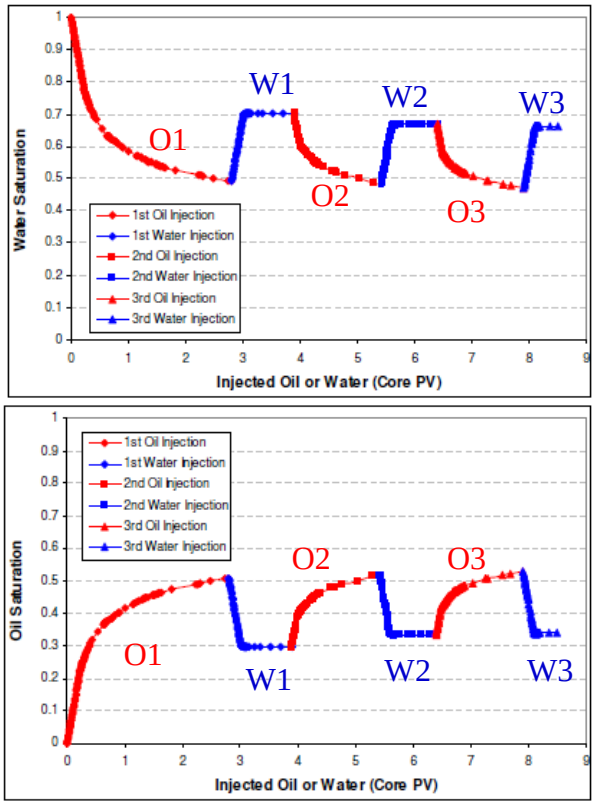

Figure 8-5: water (top) and oil (bottom) average saturations' change inside the core during different cycles of two-phase water/oil DIDIDI hysteresis test (experiment 8).

8.3 Results and Discussion

8.3.1 Two-Phase Systems:

Gas-Oil System:

Figure 8-7 shows measured residual gas saturations as a function of initial gas saturation during oil injection periods of the two-phase oil/gas cyclic injections (in the presence of immobile water). Trapped gas saturation is a strong function of initial gas saturation and increases with the increase in it. The same figure also compares the performance of the existing non-wetting phase trapping models such as Land, Carlson, Jerauld 1st and Jerauld 2nd models against the experimentally obtained residual gas saturations. Carlson and Jerauld 2nd models have the closest prediction of the trapped gas saturations. Considering the fact that Jerauld 2nd model requires two measured data (compared to the other three models that need only one measured point), the best method for predicting residual gas in the two-phase gas-oil system appears to be the Carlson model. Both Land and Jerauld 1st models overestimate the residual gas saturation resulting in a very poor prediction.

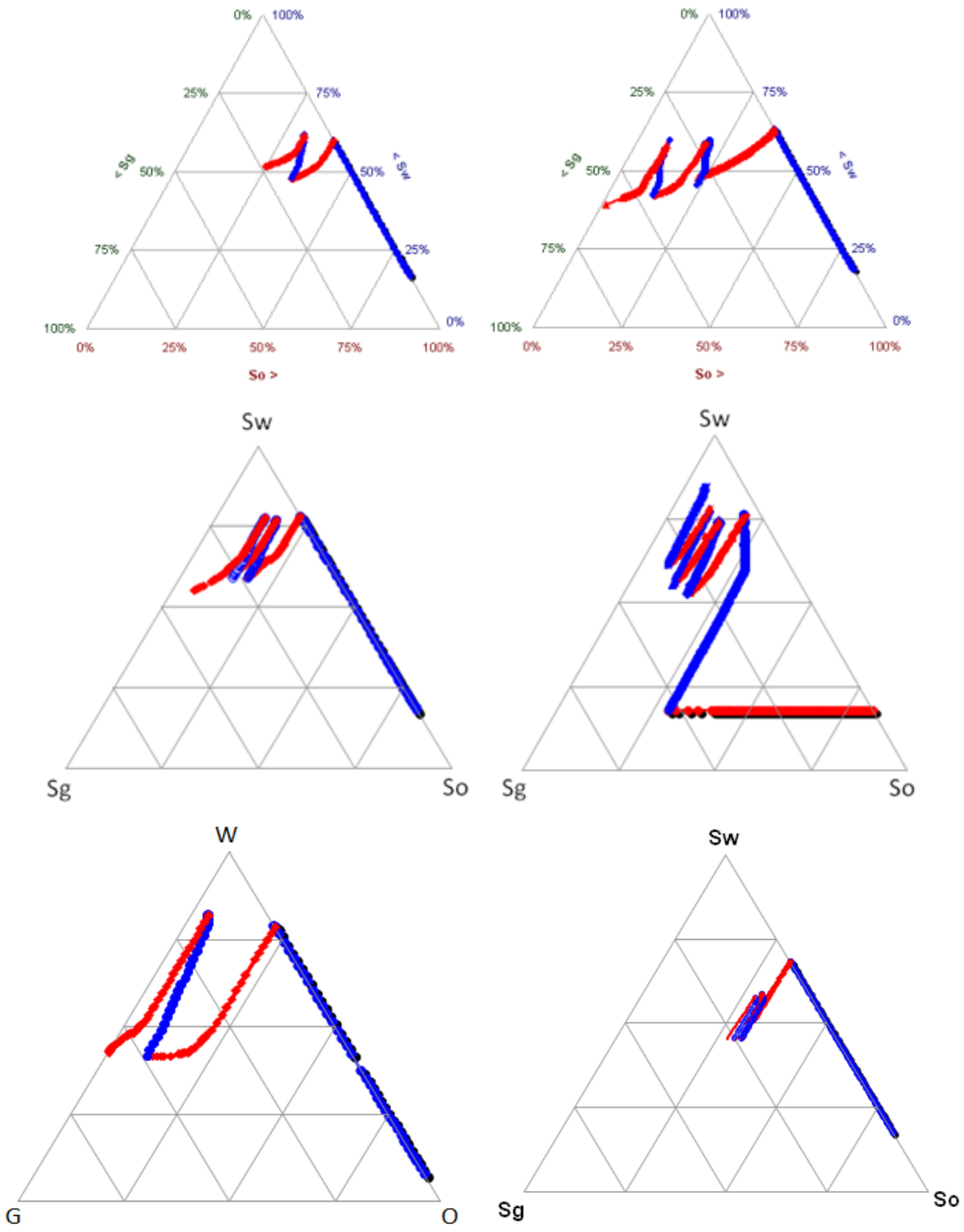

Figure 8-6: Ternary diagram of saturation changes for WAG tests. From left to right and top to bottom: a) experiment 9; b) experiment 10; c) experiment 11; d) experiment 12; e) experiment 14.; f) experiment 15, (blue: water injection; red: gas injection).

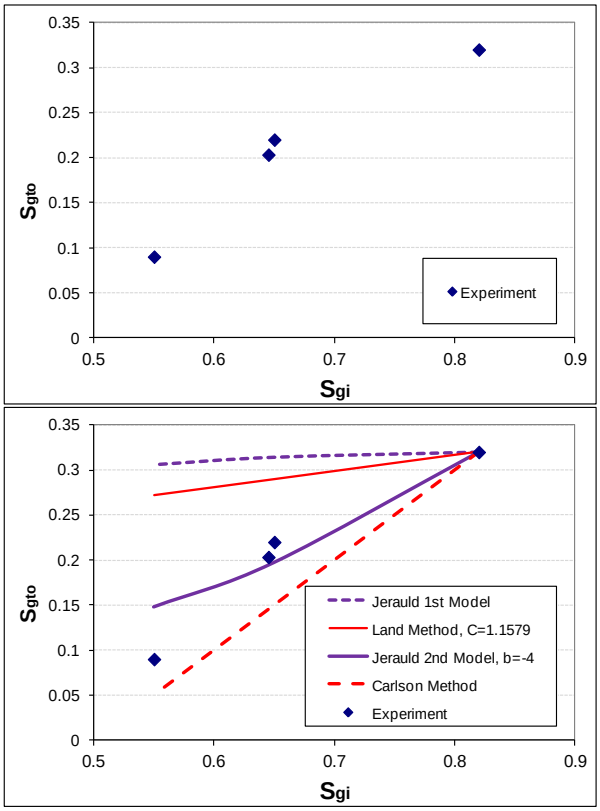

Figure 8-7: Assessment of different trapping models for oil/gas system (65mD, mixed-wet, DIDID and IDIDI tests).

Gas-Water System:

Figure 8-8a, shows an example of the profile of initial and trapped gas saturation along the core obtained from x-ray during the two-phase water-gas cyclic injection tests. This particular Figure shows gas saturation in the core before and after 1st water injection in the DIDIDI gas/water injection series. Similar data obtained from x-ray during 2nd and 3rd water injections were used to plot the relationship between initial and final gas saturation which is shown in Figure 8-8b. This Figure also shows average gas saturations (average initial and trapped gas saturations for each water injection period) obtained by material balance (production data). Although the x-ray data is scattered but it can be seen that the trapped gas saturation points obtained during the first water injection are located under the average saturations line (red points) whereas the points obtained from the 3rd water injection are located above the average saturation line. This suggests that trapped gas saturation in two-phase gas-water system is not only a function of initial saturation but also seem to show cyclic dependency. This cyclic dependency of trapped gas saturation is not currently accounted for in models available for trapped phase saturation calculation, e.g., Land, Carlson, etc.

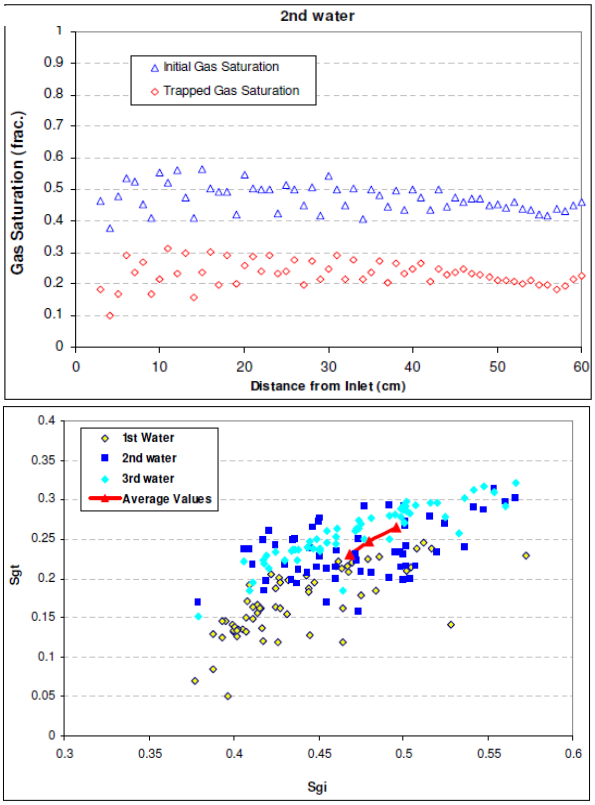

Figure 8-8: a) Initial and trapped gas saturation along the core length (from x-ray data) for the 1st water injection of DIDIDI injection series; b) local trapped gas vs. local initial gas saturations (from x-ray data analysis) for three water injections along with average saturations from material balance (65 mD, mixed-wet, gas/water system, DIDIDI).

Figure 8-9a, shows trapped gas saturation (average values obtained from material balance calculation) measured from water injection stages of gas/water hysteresis experiments (DIDIDI and IDIDI). This graph shows that in the system under investigation here, for high initial gas saturations, the value of the trapped gas saturation remains constant as the initial gas saturation decreases. This means that up to a critical value ($S_{gi\text{-}crit}$= 0.52), trapped gas saturation remains independent of the initial gas saturation. Further reduction of the initial gas saturation below that critical value would cause dependency of the S_{gt} to S_{gi}, as the trapped gas saturation would be lower for lower initial gas saturation. Figure 8-9b compares the trend of trapped gas saturation (as a function of initial gas saturation) for gas/oil (near-miscible, $IFT_{o\text{-}g}$=0.04 $mN.m^{-1}$) and the gas/water systems. As it is obvious from this Figure, the trends of the trapped gas saturation for these two systems are completely different. For the gas/oil system there is no critical $S_{gi\text{-}crit}$ value and the higher the value of S_{gi} the higher will be the value of S_{gt} and vice versa (at least within the range of the tests). As a result, for near-miscible oil/gas system (contrary to the current approach for high oil/gas IFT systems), S_{gt}-S_{gi}

measured for oil/gas systems and water/gas systems should not be used instead of one another.

Figure 8-10a shows assessment made of the well-known published trapped gas saturation models such as Land, Carlson and Jerauld's (see Appendix for mathematical formulation). This Figure shows that none of these models are able to capture the observed trend for trapped gas saturation. Figure 8-10b shows assessment of some less known trapping models such as Spiteri *et al.,* Aissaoui and Kleppe *et al* (see Appendix for mathematical formulation). The only model which is able to capture the observed trend for the trapped gas saturation is the model proposed by Aissaoui. In Figure 8-11 the scattered data obtained from x-ray scans analysis are also included. This Figure shows that Aissaoui's model is able to capture the values of trapped gas saturation data obtained by volumetric balance and x-ray scanning within the range of experimental errors. It should be mentioned that in the original model proposed by Aissaoui the critical saturation (for the measured porosity value in this study which is greater than 0.1) is a function of porosity and $0.6 < S_{g\text{-}cr} < 0.7$. But in this study $S_{g\text{-}cr} = 0.52$ has been used in the evaluation of the model. To be able to apply Aissaoui model, one should perform relevant experiments to obtain such a $S_{g\text{-}cr}$ for their own system.

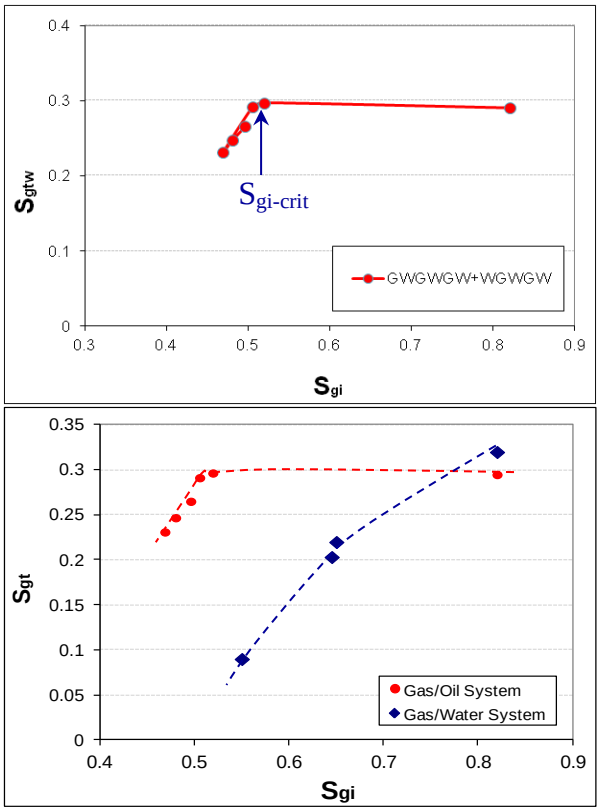

Figure 8-9: a) Trapped gas saturation vs. initial gas saturation for water/gas hysteresis tests (65mD, mixed-wet, DIDID and IDIDI). b) Comparison between trapped gas saturation trend for gas/oil and gas/water systems (65mD, mixed-wet).

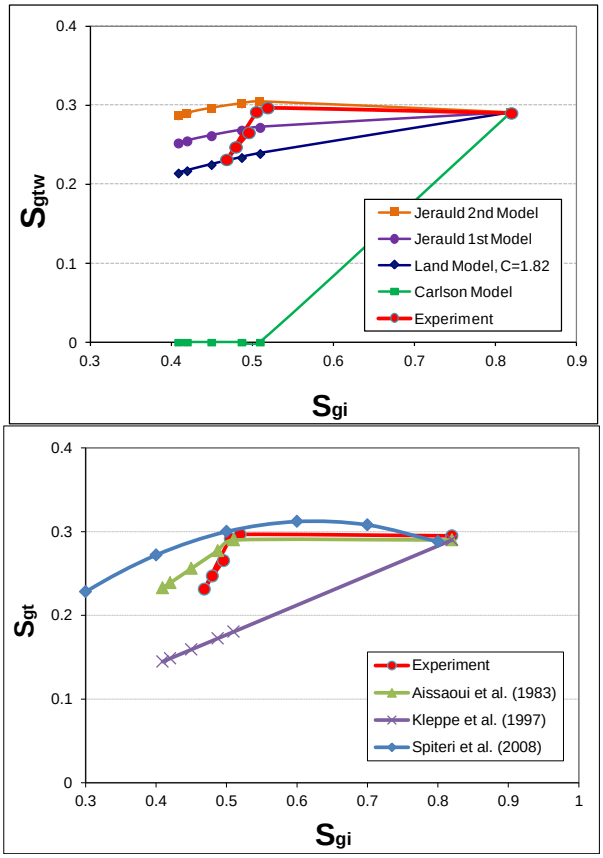

Figure 8-10: Assessment of different trapping models for the gas/water hysteresis experiments (65mD, mixed-wet, DIDID and IDIDI).

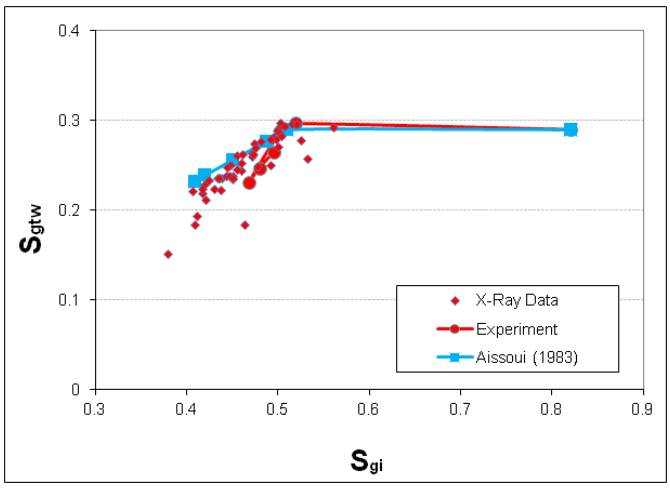

Figure 8-11: Comparison of Aissaoui trapping model predictions with the experimental results (average values and x-ray results), (65mD, mixed-wet, gas/water system, DIDID and IDIDI).

Oil-Water System:

Oil-trapping predictions are important for estimating reserves in transition zones. For strongly water-wet rocks, the oil-trapping relationship should be identical to the gas-trapping relationship. Indeed, because of this analogy and because it is easier to measure gas-trapping relationships, few oil-trapping relationships have been measured. Figure 8-12a compares the trend of trapped oil (from oil/water two-phase displacement tests) with those of trapped gas saturation (from water/gas two-phase displacement tests), both measured in the 65 mD mixed-wet rock. It should be mentioned that for oil/water system, the first point on the right hand side (with highest S_{oi}) is taken from the primary waterflooding (experiment 3), while the rest of the data are obtained from water injection periods of DIDIDI series of injection (experiment 8).

This Figure shows that trapping behaviour of oil and gas in the presence of water may not be in line with each other. For very high initial oil saturations, trapped oil saturation increases with decreasing the initial oil saturation. This happens up to a critical oil saturation value ($S_{oi\text{-}crit}$=62%), where further reduction of the initial saturation would cause reduction of the trapped oil saturation. On the other hand, as discussed above, for gas/water system, for high initial gas saturations, trapped gas saturation remains independent of the initial gas saturation and it would start decreasing with further reduction of the initial gas saturation after the critical value ($S_{gi\text{-}crit}$= 52%). This shows that in addition to gas/water and gas/oil systems, in gas/water and oil/water systems as well, trapped saturations cannot be used instead of one another.

The observed trend in mixed-wet system is in contrast to the known trend for water-wet systems, in which trapped saturations increase as the initial saturations increase. The discrepancy can be explained by the differences in displacement mechanisms. For water-wet media, trapping during waterflooding is controlled by the snap-off mechanism. As the contact angle increases (moving from strong water-wet condition to intermediate and oil-wetness), there is a crossover from trapping by snap-off in water-wet systems to trapping by bypassing in mixed-wet or oil-wet systems (Spiteri et al. (2008)). For water-wet system, the amount of trapped oil increases monotonically with increasing initial oil saturation since there is more oil to be trapped. For the mixed-wet and oil-wet systems, trapping (due to bypassing) is dependent on the presence of water clusters in the core sample. For the case with high initial oil saturation, there are few water clusters and little chance for bypassing which results in lower trapping. As the oil saturation decreases and presence of water clusters increases, the chance of oil to become trapped between these clusters increases. For lower initial oil saturations (here below 0.62), again monotonic decrease in trapped oil saturation with a decrease of the initial oil saturation will be observed, since there is less oil to be trapped in the first place. For more discussion regarding to the differences of trapping mechanisms in water-wet and oil-wet systems, refer to Spiteri et al. (2008).

The observed behaviour for trapped oil saturations is in line with those of Spiteri et al. (2008) trends obtained from pore-network modelling in the case of intermediate or oil-wet systems. Figure 8-12b shows different trapped oil saturation profiles from Spiteri et al. pore scale modelling for different contact angles, π, (or wettability conditions). The closest match obtained with experimental data corresponds to the contact angle of 90^{o}, which means intermediate wettability. It should be mentioned that Spiteri et al. model is based on pore-network modelling not coreflood experiments. This model is developed for oil/water system but for a homogeneous porous media, which means that contact angle of the fluids and rock is a constant value for the whole system. This is contrary to what is expected for the rock system under investigation in this study, in which there are some pores (small pores) which are water-wet, and others (larger pores) which are non-water wet (oil-wet or neutral-wet). In addition, for the mixed-wet system the contact angles might be different in some parts of the same pore (partly water-wet and partly oil-wet). This makes the investigated system in this study more complex and that may explain the observed quantitative discrepancy between the experimental trapped oil data and those obtained by the Spiteri et al. model. Another issue is the pore size distribution

and pore-network structure. Spiteri et al. pore network model represents Berea sandstone which its pore size distribution and pore-network structure is not the same as the Clashach sandstone used in this study. This highlights the need for generalization of Spiteri et al. model parameters (a and b, see the Appendix) for different rock types.

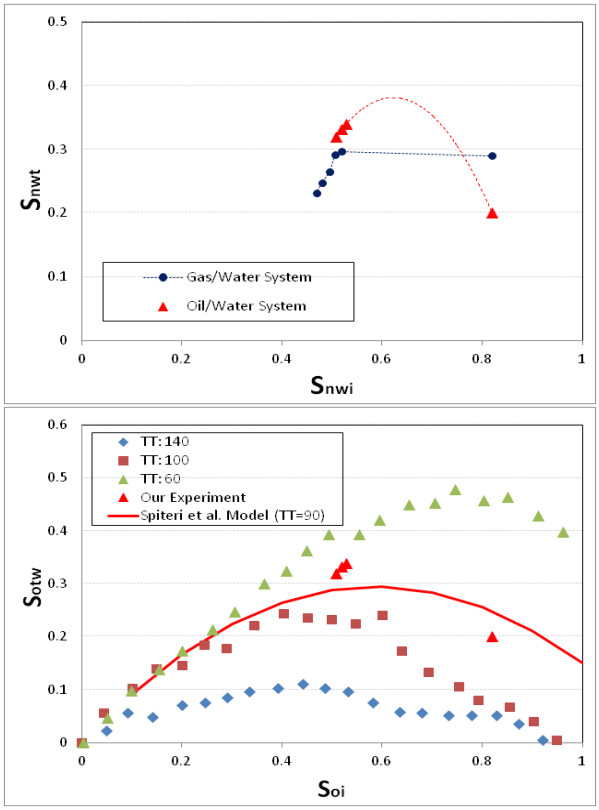

Figure 8-12: a) comparison between trapped gas saturation and trapped oil saturation obtained from gas/water and oil/water two-phase hysteresis experiments (65mD, Mixed-wet). b) comparison of the trapped oil saturation (oil/water two-phase hysteresis test) with predictions of Spiteri et al. model for different wettability conditions (different contact angles, π).

8.3.2 Three-Phase Systems:

S_{ot}: Effect of Wettability

Figure 8-13a compares three-phase trapped oil saturation values for water-wet and mixed-wet systems which are obtained from water injection stages of the WAG tests (both WAG injections started with primary waterflooding). It should be mentioned that for both systems the trapped oil saturation corresponding to the highest initial oil saturation point (S_{oi}=82%) is in fact the two-phase trapped oil saturation obtained in presence of immobile water saturation. This point can be assumed as a limit of three-phase trapped oil saturation at which initial gas saturation approaches zero (since in the presence of immobile water saturation (S_{wi}=18%) and S_{oi}=82% there will be no gas in the system). The Figure shows that for both two-phase and three-phase conditions, the trapped oil saturation is larger in the water-wet system compared to the mixed-wet

system. This is attributed to the snap-off mechanism that traps oil inside the water wetting layers and the fact that this effect is stronger for water-wet systems compared to mixed-wet. The difference between the two systems is more pronounced for high initial oil saturations. As the initial oil saturation approaches zero, the trends and values of trapped oil saturations for both systems approach each other. It should be mentioned that trend of the trapped oil results (also see Figure 8-15a) are in contrast with those obtained by pore-network simulations reported by Suicmez et al. (2008), in which they found that three-phase trapped oil saturations for water-wet system were lower than those obtained for oil-wet and weakly water-wet conditions (for two-phase system they observed the opposite trend, which is in line with the trend that was observed for two-phase data). Zero slope for the S_{ot}-S_{oi} curve at high initial oil saturations for the mixed-wet system, is in line with the results published by Jerauld (1997a,b) for Prudhoe Bay mixed-wet cores.

S_{ot}: Assessment of Models

Figure 8-13b assesses the Spiteri *et al.* trap model against the measured 3-phase trapped oil saturations for both wettability conditions (for water-wet system $\theta = 0^o$ and for mixed-wet $\theta = 90^o$). The Figure shows that the model is not able to predict the exact values (especially for higher initial S_{oi} values). Once again it should be mentioned that Spiteri *et al.* model is based on homogenous wettability through the porous media which is not necessarily the case in the mixed-wet rock. Also the rock pore size distribution is probably different from Berea sandstone which is the basis of the pore-network structure used by Spiteri et al. In addition, the original model has been developed for two phase oil/water system rather than three phase system.

Figure 8-14a compares the results of trapped oil saturations obtained from WAG injection in water-wet system, with the predictions of Land and Jerauld 1st and Jerauld 2nd models. As can be seen from this Figure, none of these models are able to accurately capture the measured data. The fact is that although these models are for strongly water-wet rocks, which is the condition of the experiment, but these are based on two-phase flow while the results were obtained under three-phase flow. This shows the importance of developing new trap phase models for three-phase systems (even for water-wet rocks). Figure 8-14b shows the predictions of these models for the mixed-wet system. The best predictions are obtained by Jerauld 2nd model. It should be mentioned that this model requires two experimental points to adjust the curvature of the prediction curve

("b" in the formulation, see Appendix), while other evaluated models are just based on one experimental point (maximum initial oil saturation).

Figure 8-15 shows residual oil saturation as a function of trapped gas (at the end of water injections) obtained in the water-wet and mixed-wet WAG experiments. In all the WAG injections, as the trapped gas saturation increases the residual oil saturation decreases linearly. The linear relationship between trapped oil saturation and trapped gas saturation in studied system is in line with the proposed formulation by Larsen and Skauge (the slope of the line is "α" parameter). Figure 8-15 shows that from different parameters investigated here (wettability, injection scenario, immobile water saturation and permeability) the most important parameters that affect the "α" value are injection scenario (either IDIDID or DIDIDID) and permeability. Nevertheless, even for the case with different wettability and immobile water saturation (which have approximately identical slope, "α" parameter), to be able to apply the formulation proposed by Larsen and Skauge, one should have the residual oil saturation to the primary waterflooding (ideally from coreflood) under the new condition. It should be mentioned that since Larsen and Skauge WAG hysteresis model uses Land trap model to predict S_{gt} from S_{gi}, and since Land model, as discussed before, is unable to capture the experimental results, the predicted S_{gt} will not be correct (even if you use a correct value for α from experimental results).

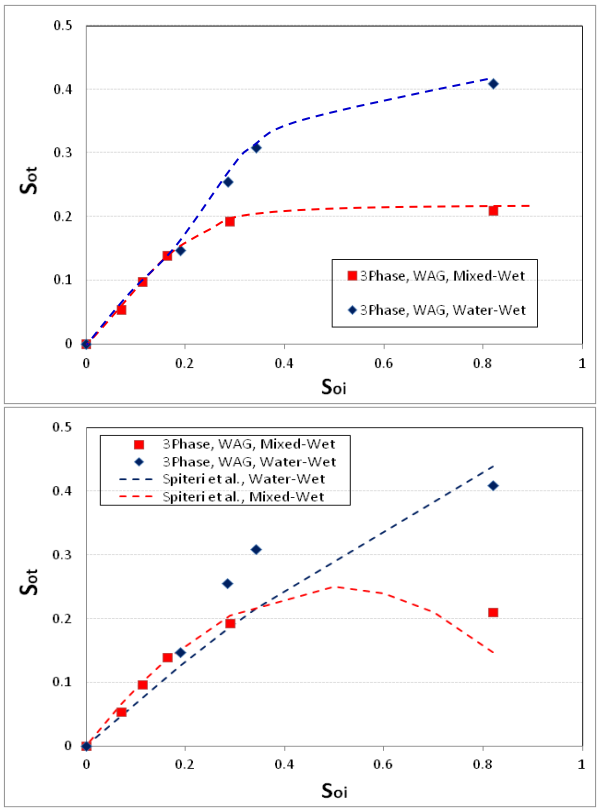

Figure 8-13: a) Comparison of the trend of trapped oil saturation for water-wet and mixed-wet systems (65mD, water injection periods of WAG tests). b) Assessment of Spiteri et al. trapping model for the three-phase measured values under water-wet and mixed-wet conditions.

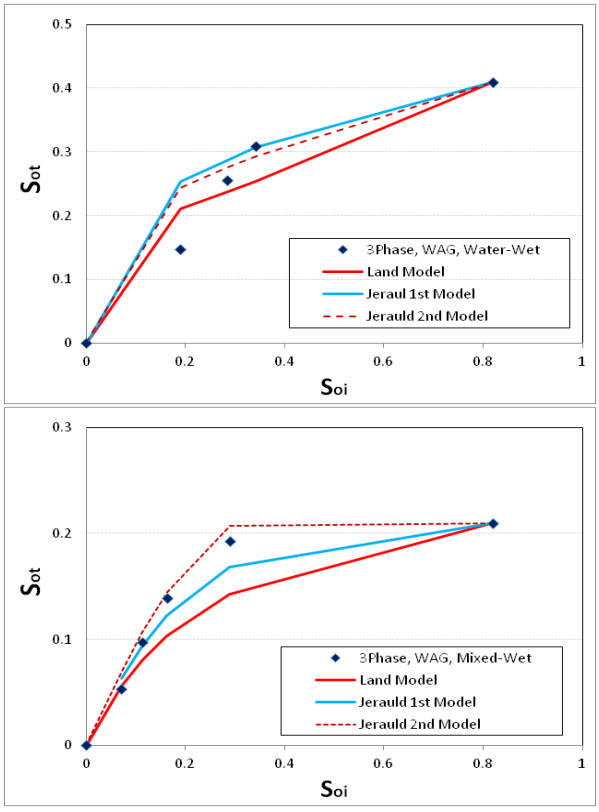

Figure 8-14: a) assessment of trapping models to predict measured three-phase trapped oil saturation (65mD, left: water-wet; right: mixed-wet).

S_{gt}: Effect of Wettability

Comparison of the trapped gas saturation (obtained from water injection periods of WAG tests) in the mixed-wet and water-wet systems (for the 65 mD core) shows that trapped gas saturation is higher for the water-wet system, probably due to the stronger snap-off mechanism in this system (Figure 8-16). This indicates the importance of obtaining trap parameters (such as C in the Land's model) for the rock samples with wettability that is representative of the wettability of the actual reservoir under consideration.

Figure 8-17 demonstrates the effect of wettability on gas productions during the 2nd water injection periods of the water-wet and mixed-wet WAG experiments carried out on the 65mD (both started with primary waterflooding). As can be seen, for water-wet system, the gas production ceased after the water breakthrough. However, for the mixed-wet system the production of gas continues even after water breakthrough (although at very small rates). This can be explained by the effect of snap-off mechanism which is much more effective in water-wet system compared to mixed-wet condition. It should be mentioned that the results for trapped gas are in line with the pore-network simulations by Suicmez et al. (2008), in which they found that three-phase trapped gas saturations for water-wet system are larger than those of oil-wet and weakly water-wet systems.

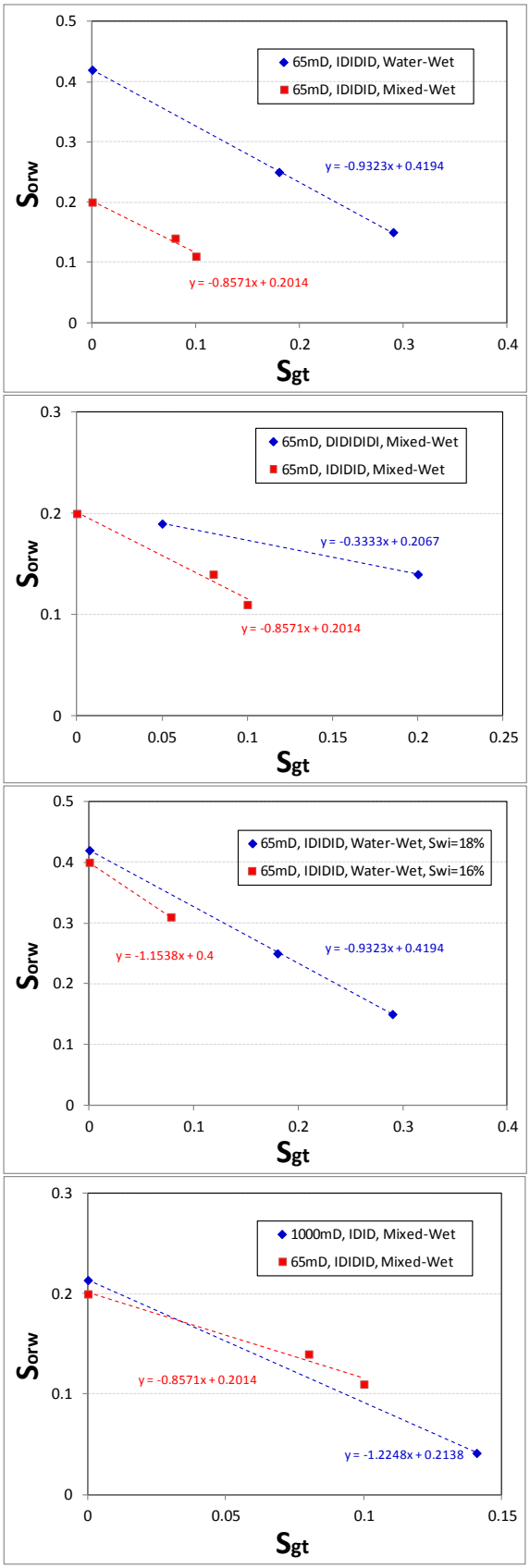

Figure 8-15: Trend of residual oil saturation at the end of water injection periods of WAG injection as a function of trapped gas saturation (from top to bottom: a) effect of wettability; b) effect of injection scenario; c) effect of immobile water saturation; d) effect of permeability).

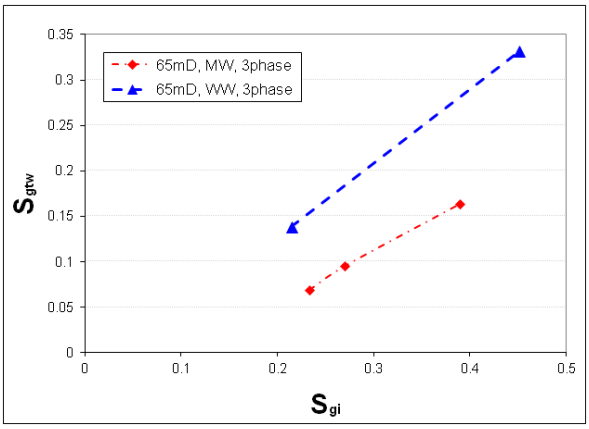

Figure 8-16: Trapped gas saturation vs. initial gas saturation for water-wet and mixed-wet systems obtained during water injection periods of WAG injection experiments carried out in the 65mD core sample.

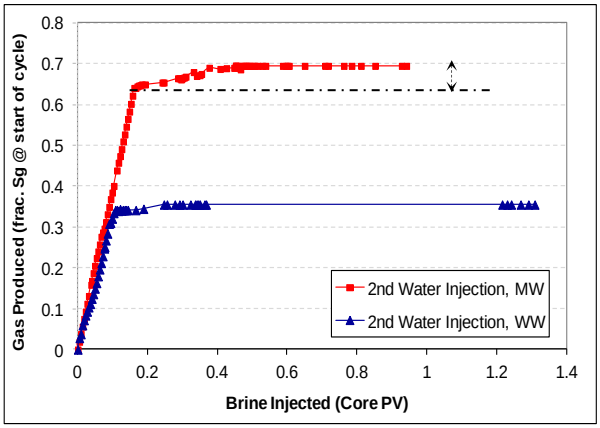

Figure 8-17: Comparison of the produced gas vs. pore volume injected brine during the 2nd water injection of the water-wet and mixed-wet WAG experiments (65 mD, IDIDID).

S_{gt}: Effect of Rock Permeability

Comparison of the three-phase trapped-gas saturation values (obtained from the three-phase water injection periods of WAG injections started with primary waterflooding) in the 1000 mD and 65 mD mixed-wet cores, shows that, as expected, trapped gas saturation is higher in the 65 mD than that in the 1000 mD core. This is attributed to the effect of different pore size distribution; and due to smaller throat sizes of the 65 mD core, see Figure 8-18.

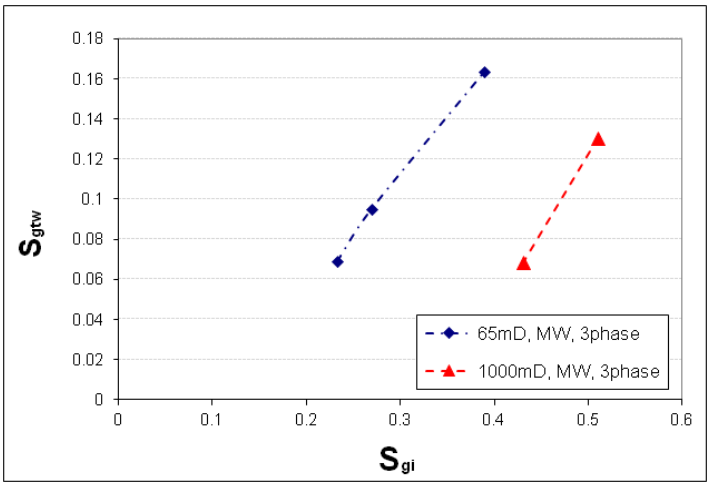

Figure 8-18: Trapped gas saturation vs. initial gas saturation obtained during water injection periods of WAG injection experiments carried out on the 1000 mD and 65 mD mixed-wet core samples.

S_{gt}: 2-phase vs. 3-phase

Figure 8-19 compares trapped gas saturations obtained from two-phase gas-water as well as those obtained from three-phase experiments of WAG. The results show that the trend of trapped gas saturation (for small S_{gi}) seems to be the same for two-phase and three-phase systems. This may suggest that two-phase trapped gas saturation of gas-water system might be alternatively used for three-phase trapped gas saturation for the purpose of prediction and modelling. However, it should be mentioned that in this particular mixed-wet WAG experiment the recovery factor of the initial water flood was so high that little oil (less than 20%) was left during tertiary injection periods of WAG injection and as a result the system was close to a two-phase gas-water system. In any case, since this is based on one example, more measured data are required to verify and generalize this observation.

S_{gt} vs. S_{ot}: 3-phase

Figure 8-20a compares trapped gas and trapped oil saturations as a function of their own initial saturations obtained from water injection periods of a WAG experiment in the water-wet 65 mD core started with water injection (IDIDID). Figure 8-20b shows the same information for the WAG experiment started with water injection in the mixed-wet system. As can be seen from this figure, for the water-wet case, trapped gas and trapped oil saturations follow the same trend. However, for the mixed-wet system, trapped oil saturation values are above those of the trapped gas saturation. This can be explained by the fact that in the mixed-wet system water is not complete wetting-phase anymore, and the distribution of fluids in the pore network is such that water and gas should share the body of the pore for flow (while in the water-wet system, water is

separated from gas by the oil spreading layers). The different distribution of the three phases in the mixed-wet system reduces the chance of water to trap the gas by snap-off mechanism. The main mechanism of gas trapping in the mixed-wet system would be through bypassing, which is less effective. From a different point of view, considering the oil-wet nature of some pores, the stronger adhesion forces from grains' surfaces towards the oil wetting layers, increases the residual oil saturation compared to the trapped gas phase.

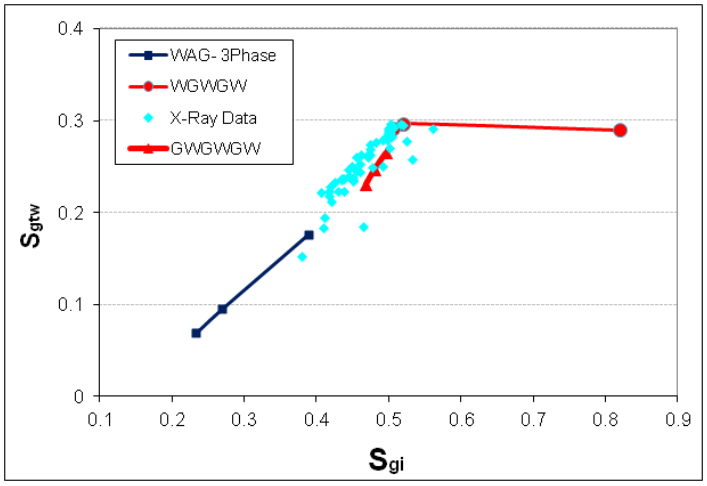

Figure 8-19: Comparison of the trend of trapped gas saturation obtained from two-phase gas/water hysteresis (by volumetric balance and by x-ray) with those of three-phase water injections of WAG test (by volumetric balance).

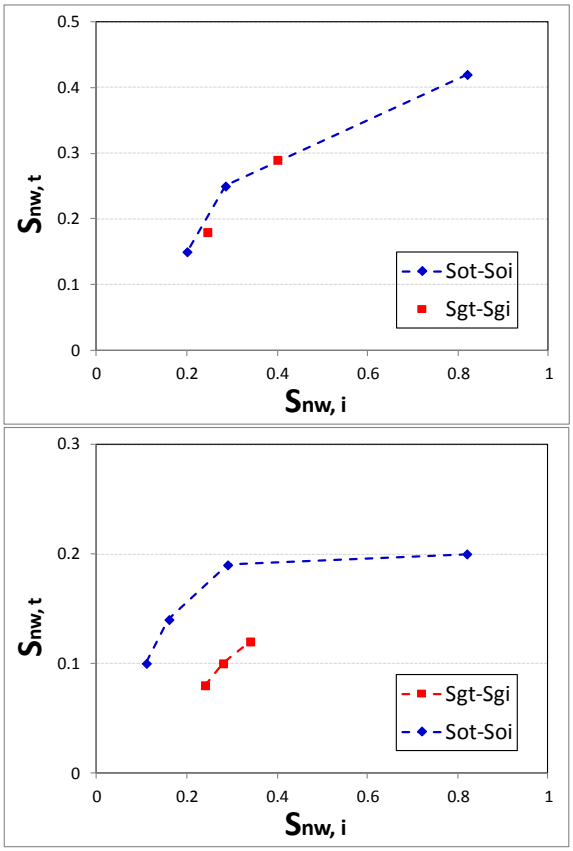

Figure 8-20: Three-phase trapped oil and gas saturations as a function of their own initial saturations along with residual oil saturation to primary waterflooding ($S_{nw,i}$ = 0.82); (top: water-wet; bottom: mixed-wet).

S_{ht} (3-phase) vs. S_{orw} (2-phase):

Figure 8-21 shows trapped hydrocarbon saturations (S_{ht}) as a function of initial hydrocarbon in place for different waterflooding periods of the two WAG injections (water-wet and mixed-wet system) performed in 65 mD core (both started with primary waterflooding, IDIDID). The point with S_{hi}= 0.82 represent primary waterflooding which is the limit of the three-phase condition at which S_{gi} = 0 and S_{hi} = S_{oi}. From this figure, during these two WAG experiments, the total amount of trapped hydrocarbon in three-phase system, is just slightly larger than those of trapped oil saturation in two-phase. This is in line with the assumption made in Blunt (2000) model, in which he assumed the total trapped hydrocarbon saturation in a three-phase system would be the same as the trapped non-wetting phase saturation in a two-phase flow.

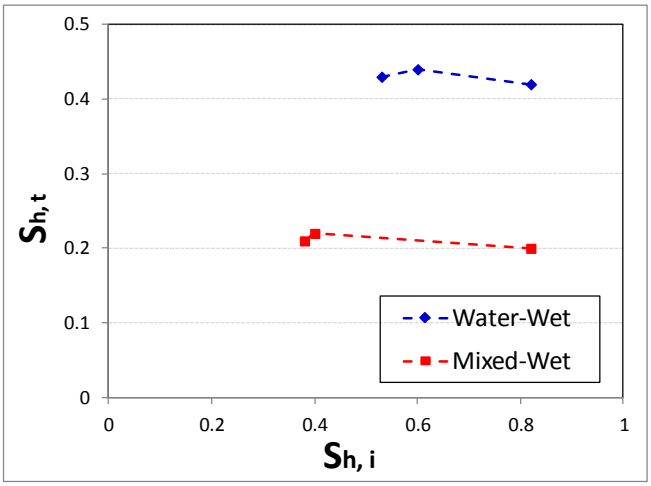

Figure 8-21: Three-phase trapped hydrocarbon saturation (oil+gas) as a function of its own initial saturation, compared with the trapped oil saturation after primary waterflooding (S_{hi} = 0.82).

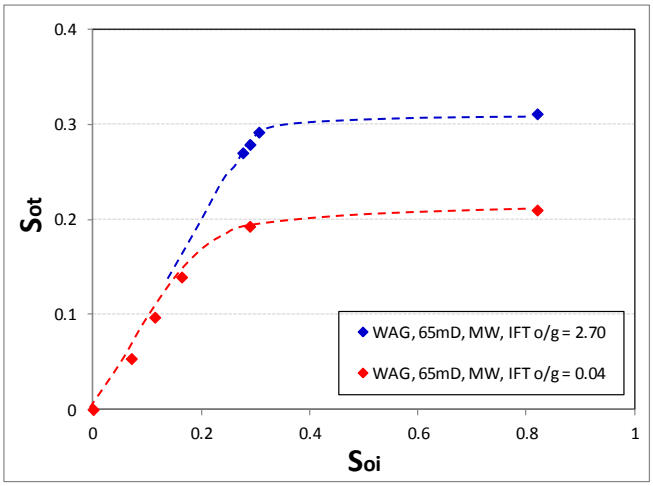

Figure 8-22: Comparison of the trapped oil saturation vs. initial oil saturation during waterflooding periods of the WAG injections performed at 1840 psia and 1200 psia (65mD, WAG, mixed-wet).

S_{orw} and S_{gtw}: Effect of Oil/Gas IFT

Figure 8-22 compares three-phase trapped oil saturations obtained from water injection stages of the WAG tests performed on the 65 mD mixed-wet system, which highlights the effect of the interfacial tension between oil and gas phases (which is 2.70 for experiment-15 compared to the near-miscible condition which is 0.04 $mN.m^{-1}$). In addition to the oil/gas IFT, the viscosity ratios for the two experiments are different. For experiment-15, μ_o/μ_g = 5.62 while for the near-miscible conditions, μ_o/μ_g = 1.62. The dashed lines in this Figure show the trend of data points. It should be mentioned that for both systems the trapped oil saturation corresponding to the highest initial oil saturation (S_{oi} = 82 %) is in fact the two-phase trapped oil saturation obtained in the presence of immobile water (primary waterflooding). As discussed before, this point can be assumed to be the limit of the three-phase trapped oil saturation as the initial gas

saturation approaches zero. Flat trend of these curves at higher S_{oi} shows the mixed-wet nature of the core for both gas/oil IFTs (also see Figure 8-13 for the same results for water-wet condition). The Figure shows that trapped oil saturation is larger in immiscible WAG injection (1200 psia) compared to the near-miscible WAG injection (1840 psia). This shows that snap-off mechanism which traps oil inside the water wetting layers, are stronger for the WAG injection performed at 1200 psia (more viscous oil). Figure 8-23 compares the three-phase trapped gas saturations obtained from water injection stages of the two WAG tests. The Figure shows that trapped gas saturation is larger in the immiscible WAG injection (1200 psia) compared to the near-miscible WAG injection (1840 psia). This shows that larger trapped gas saturations do not necessarily mean higher efficiency in WAG injection.

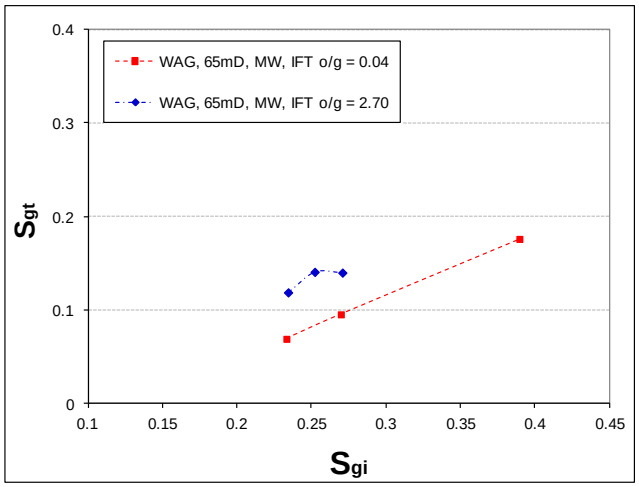

Figure 8-23: Comparison of the trapped gas saturation vs. initial gas saturation during tertiary waterflooding of the two WAG injections performed at 1840 psia and 1200 psia (65mD, WAG, mixed-wet).

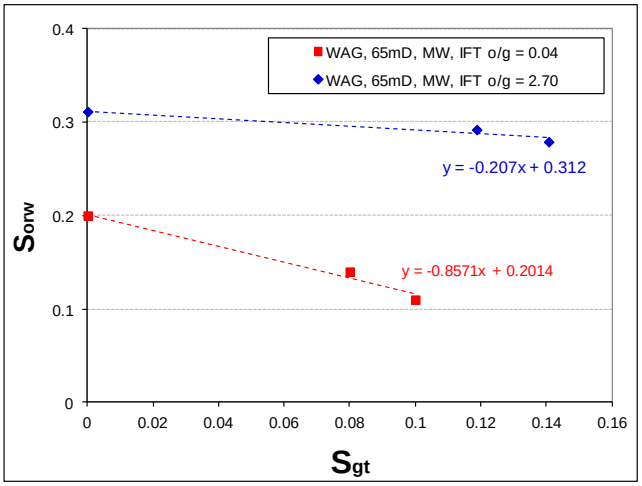

Figure 8-24: Effect of gas/oil IFT on the trend of residual oil saturation at the end of water injection periods as a function of trapped gas saturation (65 mD, mixed-wet, IDIDID).

Figure 8-24 shows residual oil saturation as a function of trapped gas (at the end of water injections) for these two WAG experiments. Similar to the previous WAG experiments (see Figure 8-15), for immiscible WAG injection, as trapped gas saturation increases the residual oil saturation is decreased linearly. Figure 8-24 highlights the effect of oil/gas IFT (and viscosity ratio) on the "α" parameter in WAG hysteresis model (proposed by Larsen and Skauge, 1998).

S_{gt} and S_{ot}: Comparing the Experimental Results with Literature

Skauge and Ottesen (2002) provide a summery on the experimentally derived non-wetting phase residual saturations for some North-Sea cores. Figure 8-25a, shows the comparison of the measured two-phase trapped gas saturation (for gas/water system) with those reported by Skauge and Ottesen. The Figure shows a relatively good agreement between the two data sets. The same has been observed for three-phase trapped gas saturations (Figure 8-25b). For both datasets, for low initial gas saturation, the trend of trapped gas saturation vs. initial gas saturation for the three-phase system is the same as those measured for two-phase gas/water system (Figure 8-26), which means that presence of the third phase (oil) has little or no effect on the trapped gas saturation (for low initial gas saturation). Skauge and Ottesen have provided a correlation to relate end-point relative permeability of water (at the end of primary waterflooding; $krw_{(Sorw)}\times(1-S_{orw})$) to the Amott-Harvey wettability index (Figure 8-27a). In the case of 65 mD core sample, for water-wet condition the Amott-Harvey wettability index is equal to 1. Calculating the vertical axis function ($krw_{(Sorw)}\times(1-S_{orw})$) from primary water injection, the water-wet point (which is shown by a red rectangle on the right hand side of the graph) was obtained. Using the lower amount of $krw_{(Sorw)}\times(1-S_{orw})$ obtained for the water-wet core compared to the North-Sea cores' correlation (dashed blue line as proposed by Skauge and Ottesen), a line parallel (red dashed line) to the North-Sea cores correlation was draw passing from 65 mD, water-wet point. Calculation of $krw_{(Sorw)}\times(1-S_{orw})$ function for 65 mD mixed-wet core (from primary water flooding) shows that for the estimated correlation (red dashed line), Amott-Harvey wettability index is equal to 0 for the 65 mD mixed-wet core, which is the same as the one previously measured for the 1000 mD mixed-wet rock (Sohrabi et al., 2007).

Figure 8-24b shows the Skauge and Ottesen correlation between S_{orw} and the Amott-Harvey index. Calculating the vertical axis function (S_{orw}) from primary water injection, the water-wet point was obtained. Using the higher amount of S_{orw} obtained for the

water-wet core compared to Skauge and Ottesen correlation (dashed blue curve), a curve parallel (red dashed line) to the North-Sea cores' correlation was draw passing through the 65 mD, water-wet point. Calculation of S_{orw} for 65 mD mixed-wet core (from primary water flooding) shows that for the estimated correlation (red dashed curve), Amott-Harvey wettability index is equal to 0 for the 65 mD, mixed-wet core, which is in line with the value obtained from Figure 8-27a. Although the measured residual oil saturation is higher, the residual oil saturation for the mixed-wet system makes the same trend as those of North-Sea cores at the Amott-Harvey index of zero. Skauge and Ottesen have also correlated the measured oil recovery to the initial water saturation. Figure 8-28a, shows a comparison between their correlation and the measured values, which are in good agreement.

Mixed-wet systems are divided into three different wettability types (Skauge and Ottesen, 2002), known as: MWS type (with smaller pores to be oil-wet or non-water wet), MWL (with large pores to be non-water wet) and finally FW in which a fraction of the pores is water-wet and the rest is non-water wet. For FW definition different wettability conditions can occur in the pores with different pore sizes and even a type in which a pore might be partly water-wet and partly non-water wet. The measured USBM and Amott-Harvey indexes for the 1000 mD core (Sohrabi et al., 2007) shows that the mixed-wet system under investigation in this study would be classified as Fractional Wet (FW) type (Figure 8-28b).

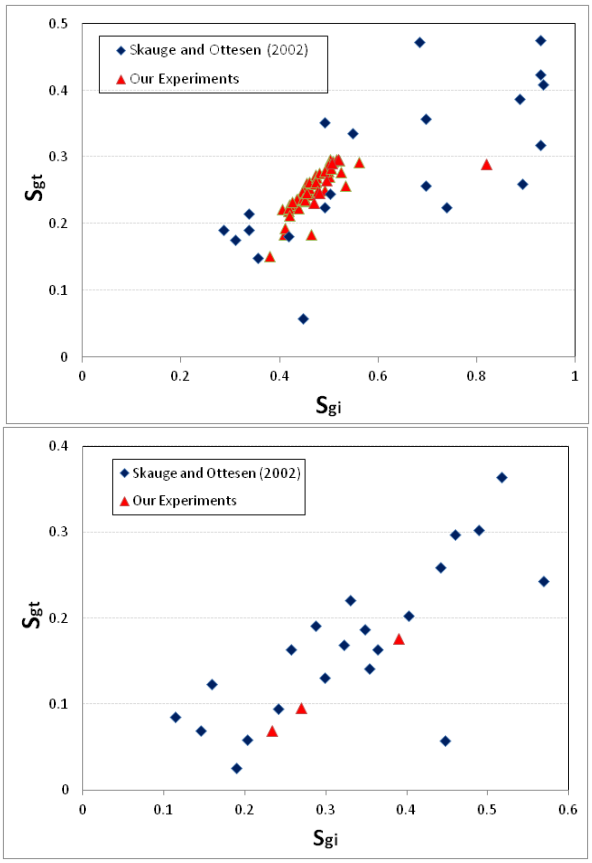

Figure 8-25: a) Comparison of the measured trapped gas saturations (water/gas two-phase hysteresis test, 65 mD, mixed-wet) with two-phase average values obtained from North-Sea core samples (Skauge and Ottesen, 2002). b) Comparison of the measured three-phase trapped gas saturation (water injection stages of WAG test, 65mD, mixed-wet) with average three-phase values obtained from North-Sea core samples (Skauge and Ottesen, 2002).

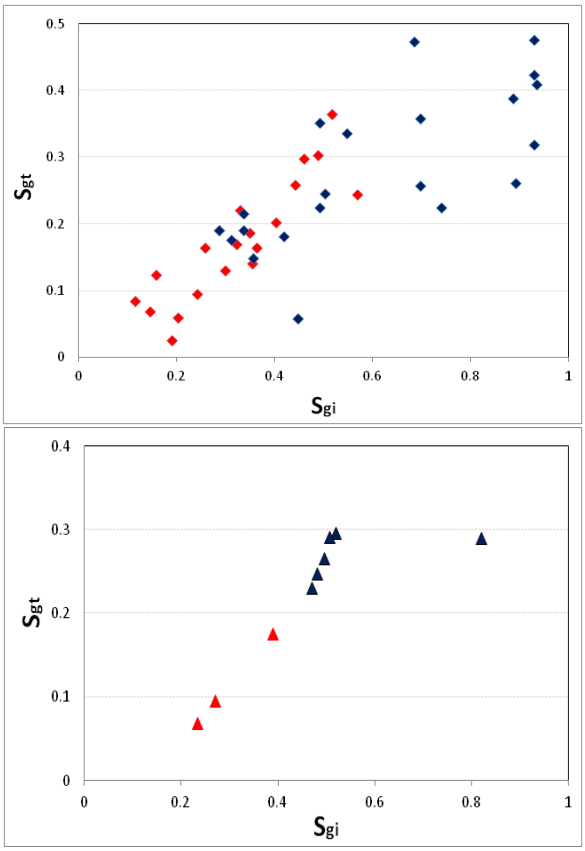

Figure 8-26: a) Comparison of the two-phase (blue) and three-phase (red) trapped gas saturation measured on some North-Sea core samples (Skauge and Ottesen, 2002). b) Comparison of the measured two-phase (blue) and three-phase (red) trapped gas saturations in this study (gas/water two-phase hysteresis and water injection stages of WAG, 65mD, mixed-wet).

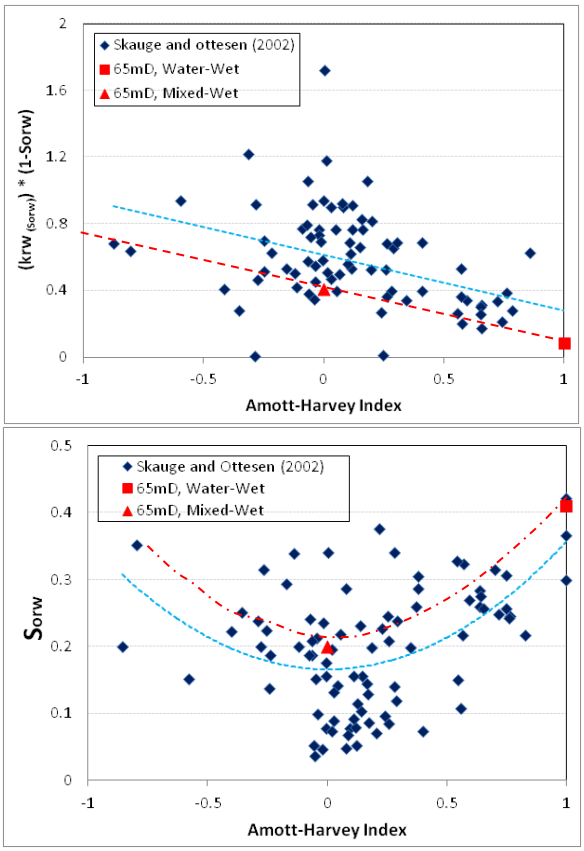

Figure 8-27: a) Obtaining Amott-Harvey index of the 65mD mixed-wet core samples from correlation proposed for North-Sea sandstones by Skauge and Ottesen (2002). b) Comparison of the measured residual oil saturation values (for primary water injection in water-wet and mixed-wet rocks) with average trends of North-Sea core samples (from Skauge and Ottesen, 2002).

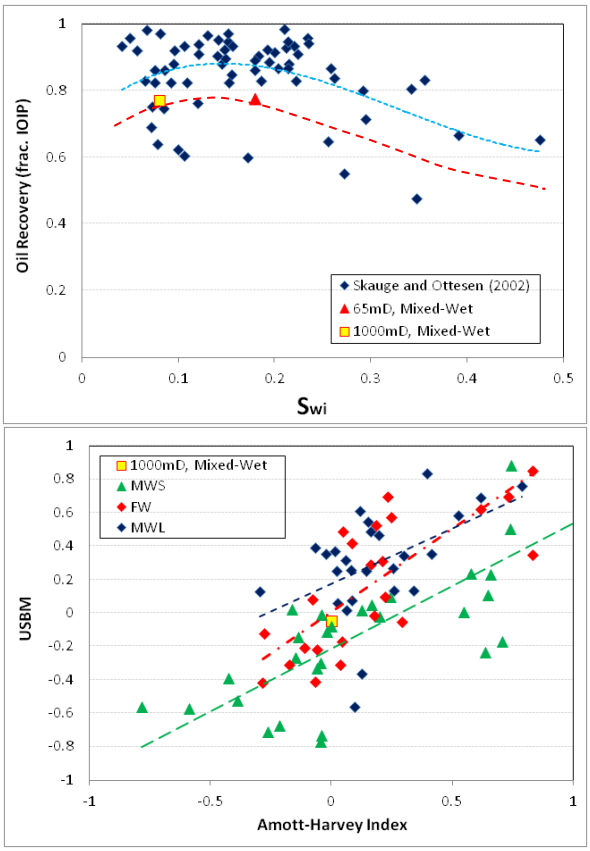

Figure 8-28: a) Comparison of the measured recovery factors as a function of immobile water saturation, with average values obtained from North-Sea core samples (Skauge and Ottesen, 2002). b) Obtaining the type of mixed-wet system for the rock samples used in this study, based on the correlations provided by Skauge and Ottesen (2002) for North-Sea samples.

8.4 Conclusion

- The experimental results show that for low IFT (near-miscible) oil/gas systems, trapped gas saturations obtained from oil/gas and water/gas systems should not be used instead of the other. The same is true for trapped saturations obtained from gas/water and oil/water systems.
- It is found that for three-phase systems under WAG injection, the S_{orw} increases linearly by decreasing the S_{gt}, and approaches to the two-phase S_{orw} (obtained after primary waterflooding) for the limit case with $S_{gt} = 0$.
- From different parameters studied here, injection scenario, permeability and oil/gas IFT had the largest effect on the slope of the S_{orw} vs. S_{gt} curve.
- Investigation of the effect of oil/gas IFT showed that for immiscible WAG injection, residual oil saturation to the waterflooding periods of the WAG injection, are minimally affected by the presence of trapped gas (although trapped gas saturations were higher than those of near-miscible WAG injection).

As a result immiscible WAG injection, unlike near-miscible WAG injection, is not effective in increasing the oil recovery (reducing the residual oil saturation).

8.5 Appendix B

8.5.1 Trapping Models:

Land model:

Land trap model was originally developed for predicting trapped gas saturation as a function of the initial gas saturation based on published experimental data from water-wet sandstone cores. Land found that the difference in the reciprocals of initial and residual non-wetting saturation are approximately constant for a given porous media. When the initial gas saturation is unity, the residual gas saturation is the maximum residual saturation, $S^*_{gr,max}$ (Figure B-1). As a result he proposed the following equation:

$$\frac{1}{S^*_{gr}} - \frac{1}{S^*_{gi}} = \frac{1}{S^*_{gr,\max}} - 1 \qquad \text{(Eq. B-1)}$$

or

$$S^*_{gr} = \frac{S^*_{gi}}{1+CS^*_{gi}} \qquad \text{(Eq. B-2)}$$

Where *C*, known as Land coefficient, is:

$$C = \frac{1}{S^*_{gr,max}} - 1 \qquad \text{(Eq. B-3)}$$

Carlson model:

A simplified trapping model was developed by Carlson (1981). Assume that a process of primary drainage (bounding curve) would be stopped at a certain non-wetting phase saturation S_{gi} (Figure B-2) and an imbibition displacement starts. The mathematical formula for the non-wetting phase trapping is:

$$S_{gt} = S^{max}_{gt} - \Delta S_{gi} \qquad \text{(Eq. B-4)}$$

where ΔS_{gi}, is the difference between S_g^{imb} and S_{gi} (turning point).

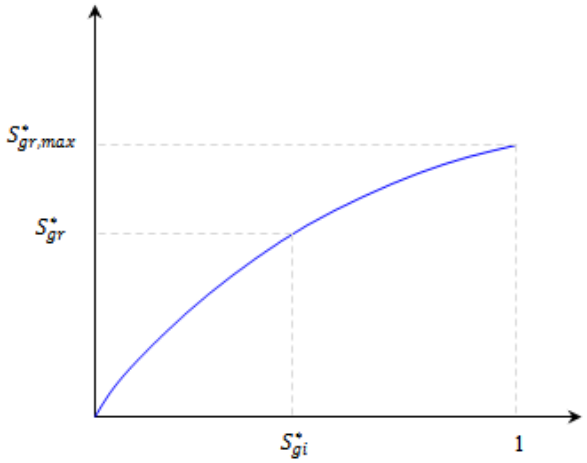

Figure B-1: schematic representation of residual gas saturation vs. initial gas saturation for imbibition (Land Model).

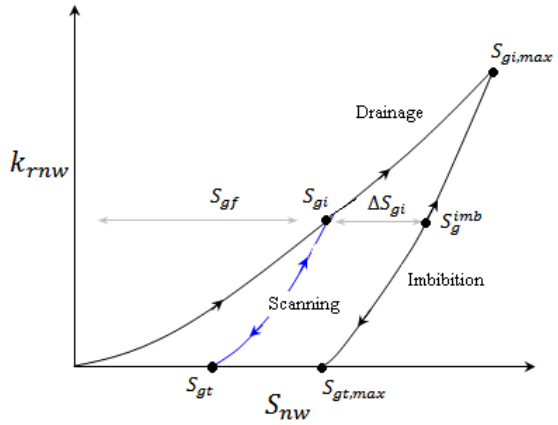

Figure B-2: Carlson's hysteretic relative permeability characteristics for non-wetting phase.

Aissaoui Model:

Aissaoui (1983) proposed a piecewise linear formulation, characterized by two parameters: the maximum residual gas saturation, $S_{gr,max}$, and the saturation corresponding to the intersection of the two segments, S_{gc} (Figure B-3). Based on this model, initially S_{gr} increases linearly with S_{gi} before becoming flat at $S_{gr,\,max}$.

If $S_{gi} < S_{gc}$ then: (S_{gc} corresponds to the critical gas saturation where the maximum trapped saturation is reached)

$$S_{gr} = \frac{S_{gr,max}}{S_{gc}} S_{gi} \qquad \text{(Eq. B-5)}$$

Else $S_{gr} = S_{gr,max}$.

Aissaoui studied only Fontainebleau sandstones and according to his studies:

- If $\Phi < 0.1$, $S_{gc} = 1 - S_{w,im}$
- If $\Phi > 0.13$, $0.60 < S_{gc} < 0.70$

Suzanne et al. (2003) found that S_{gc} is dependent on the amount of microporosity. The constant S_{gr} region confirms that the microporosity does not trap gas. The linear S_{gr}/S_{gi} region corresponds to gas trapped in the macroporosity.

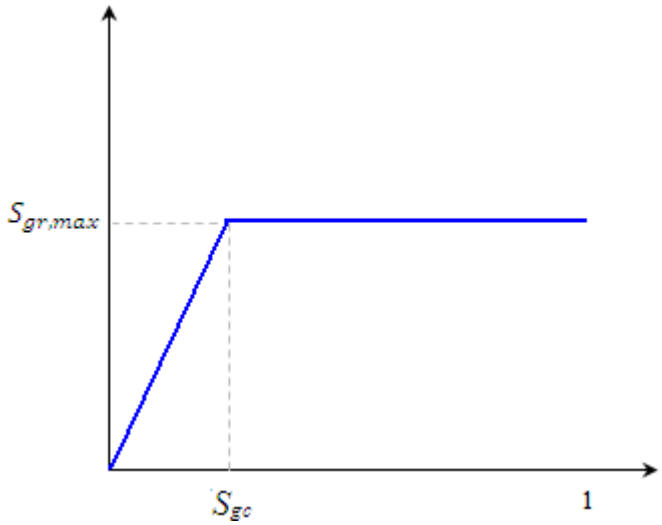

Figure B-3: schematic representation of residual gas saturation vs. initial gas saturation (Aissaoui Model).

Jerauld 1st and 2nd Models:

Jerauld (1997a) extended Land's formulation to be able to match the observed trapped gas saturations for the mixed-wet rock samples from Prudhoe Bay oil field.

$$S^*_{gr} = \frac{S^*_{gi}}{1+\left(\frac{1}{S^*_{gr,max}}-1\right)S^{*\,\frac{1}{1-S^*_{gr,max}}}_{gi}} \qquad \text{(Eq. B-6)}$$

Jerauld (1997b) extended his formulation as follows:

$$S^*_{gr} = \frac{S^*_{gi}}{1+\left(\frac{1}{S^*_{gr,max}}-1\right)S^{*\,1+\frac{bS^*_{gr,max}}{1-S^*_{gr,max}}}_{gi}} \qquad \text{(Eq. B-7)}$$

"b" is an empirically derived constant and is equal or less than 1.

Kleppe et al. Model:

Kleppe et al. (1997) proposed the following linear relationship to match trapped gas saturations obtained from an artificial core.

$$S_{gr} = \frac{S_{gi}}{S_{gi,max}} S_{gr,max} \quad \text{(Eq. B-8)}$$

Spiteri et al. Model:

Spiteri et al. (2008) used pore-network modelling and developed the following quadratic formulation to predict the trapped oil saturations.

$$S_{or} = aS_{oi} - bS_{oi}^2 \quad \text{(Eq. B-9)}$$

where "a" and "b" are contact angle dependant coefficients which are obtained by Spiteri et al. for their pore structure.

8.6 References

Aissaoui A., (1983): "Etude théorique et expérimentale de l'hystérésis des pressions capillaires et des perméabilités relatives en vue du stockage souterrain de gaz", PhD Thesis submitted to Ecole des Mines de Paris, 223 p.

Al-Mansoori S.K., Iglauer S., Pentland C.H. and Blunt M.J; (2009): Three-phase measurements of oil and gas trapping in sand packs, Advances in Water Resources, Volume 32, Issue 10, pp. 1535–1542.

Al-Mansoori S.K., Itsekiri E., Iglauer S., Pentland C.H., Bijeljic B., Blunt M.J., (2010): Measurements of non-wetting phase trapping applied to carbon dioxide storage, International Journal of Greenhouse Gas Control, Volume 4, Issue 2, pp. 283–288.

Blunt M.J., (2000): An empirical model for three-phase relative permeability, SPE Journal, Volume 5, Number 4, pp. 435–445.

Carlson F.M, (1981): Simulation of Relative Permeability Hysteresis to the Nonwetting Phase, presented at SPE Annual Technical Conference and Exhibition, 4-7 October, San Antonio, Texas.

Caubit C., Bertin H., Hamon G.; (2004): Three-phase flow in porous media: wettability effect on residual saturations during gravity drainage and tertiary waterflood, SPE 90099, proceedings of the SPE annual technical conference and exhibition, 26–29 September, Houston, Texas, USA.

Crowell D.C., Dean G.W., Loomis A.G., "Efficiency of gas displacement from a water-drive reservoir", Report of investigations 6735 USBM, (1966), pp 1- 29.

Hamon G., Suzanne K., Billiotte J., Trocme V; (2001): "Field-wide variations of trapped gas saturation in heterogeneous sandstone"; SPE 71524, presented at SPE Annual Technical Conference and Exhibition, 30 September – 3 October 20, New Orleans, Louisiana.

Jerauld G.R., (1997a): Prudhoe Bay gas–oil relative permeability, SPE-35718, SPE Reservoir Engineering, Volume 12, Number 1, pp. 66–73.

Jerauld G.R., (1997b): General three-phase relative permeability model for Prudhoe Bay, SPE 36178, SPE Reservoir Engineering, Volume 12, Number 4, pp. 255–263.

Juanes R., Spiteri E.J., Orr F.M., Blunt M.J., (2006): Impact of relative permeability hysteresis on geological CO2 storage, Water Resources Research, Volume 42, Issue 12, p. W12418.

Kleppe, J., Delaplace, P., Lenormand, R., Hamon, G., Chaput, E., (1997): Representation of Capillary Pressure Hysteresis in Reservoir Simulation, SPE-38899, SPE Annual Technical Conference and Exhibition, 5-8 October, San Antonio, Texas, USA.

Kralik J.G., Manak L.J., Jerauld G.R., and Spence A.P., (2000): Effect of Trapped Gas on Relative Permeability and Residual Oil Saturation in an Oil-Wet Sandstone, SPE 62997, presented at the 2000 SPE Annual Technical Conference and Exhibition, 1-4 October, Dallas, Texas, USA.

Kumar A., Ozah R., Noh M., Pope G.A., Bryant S., Sepehrnoori K., Lake L.W., (2005): Reservoir simulation of CO2 storage in deep saline aquifers, SPE Journal, Volume 10, Issue 3, pp. 336–348.

Land C.S., (1968): Calculation of Imbibition Relative Permeability for Two- and Three-Phase Flow From Rock Properties, SPE Journal, Volume 8, Number 2, pp. 149 – 156.

Larsen A. and Skauge A., (1998): Methodology for Numerical Simulation with Cycle-Dependent Relative Permeabilities, SPE- 38456, SPE Journal, Volume 3, Number 2, pp. 163-173.

Maloney D., Zornes D.; (2003): Trapped versus initial gas saturation trends from a single core test, SCA2003-22, proceedings of the international symposium of the society of core analysts, 21–24 September, Pau, France.

Pentland C.H., Itsekiri E., Al Mansoori S.K., Iglauer S., Bijeljic B., and Blunt M.J., (2010): Measurement of Nonwetting-Phase Trapping in Sandpacks, SPE-115697, SPE Journal, Volume 15, Number 2, pp. 274-281.

Qi R., LaForce T., Blunt M.J., (2009): Design of carbon dioxide storage in aquifers, International Journal of Greenhouse Gas Control, 3 (2), pp. 195–205.

Skauge A. and Larsen J.A., (1994): Three-phase Relative Permeabilities and Trapped Gas Measurements Related to WAG Processes, SCA-9421, presented at International Symposium of the Society of Core Analysts, Stavanger, Norway.

Skauge A. and Ottesen B.; (2002): A summary of experimentally derived relative permeability and residual saturation on North Sea reservoir cores, SCA2002-12, proceedings of the international symposium of the society of core analysts, 22–25 September, Monterey, California, USA.

Sohrabi, M., Tehrani, D. H. and Al-Abri, M., (2007): "Performance of Near-Miscible Gas and SWAG Injection in a Mixed-Wet Core", proceedings of the International Symposium of the Society of Core Analysts, 10-13 September, Calgary, Canada.

Sohrabi M., Tehrani D.H., Danesh A., Henderson G.D., (2004): Visualization of Oil Recovery by Water-Alternating-Gas Injection Using High-Pressure Micromodels, SPE-89000, SPE Journal, Volume 9, Number 3, pp. 290-301.

Spiteri E.J., Juanes R., Blunt M.J., Orr F.M.; (2008): A New Model of Trapping and Relative Permeability Hysteresis for All Wettability Characteristics, SPE Journal, Volume 13, Number 3, pp. 277-288.

Suzanne K.; Hamon G.; Billiotte J.; Trocme V., (2003): Experimental relationships between residual gas saturation and initial gas saturation in heterogeneous sandstone reservoirs, SPE-84038, SPE Annual Technical Conference and Exhibition, 5-8 October, Denver, Colorado, USA.

Suzanne K., Hamon G., Billiotte J., Trocme V., (2001): "Distribution of trapped gas saturation in heterogeneous sandstone reservoirs", Proceedings, 2001 International Symposium of the Society of Core Analysts, 17-19 September, Edinburgh, UK.

Suicmez V.S., Piri M., Blunt M.J., (2008): Effects of wettability and pore-level displacement on hydrocarbon trapping, Advances in Water Resources, Volume 31, Issue 3, pp. 503–512.

9. Conclusions and Recommendations

Waterflooding and gas injection are two widely used improved oil recovery techniques that can be applied individually or combined as water alternating gas (WAG) or simultaneous gas and water (SWAG) injection. Laboratory data on WAG and SWAG injections for non-water-wet systems are very limited especially for near-miscible (very low IFT) gas-oil systems (which represents a number of processes of great importance to reservoir engineers including high pressure hydrocarbon gas injection and CO_2 flooding). Simulation of WAG injections requires three-phase relative permeability (k_r) data as well as taking to account for hysteresis. The current approach in the industry (except hysteresis model proposed by Larsen and Skauge) is to use two-phase bounding imbibition and drainage relative permeabilities along with a two-phase hysteresis model (Land, Carlson or Killough) and input the result to a three-phase correlation to simulate hysteresis in WAG injection. The other approach in the industry to account for hysteresis in WAG injection is the WAG-hysteresis model (proposed by Larsen and Skauge) along with Stone-I correlation. These models and approaches are developed based on high oil/gas IFT and water-wet systems. However, the majority of oil reservoirs are believed to be mixed-wet and hence, prediction of the performance of WAG injection in these reservoirs is associated with significant uncertainties.

Accurate determination of relative permeability values and their hysteresis behavior is crucial for obtaining a reliable prediction of the performance of water-alternating-gas (WAG) injection in oil reservoirs. Performing reliable laboratory experiments is the key to evaluating the performance of these oil recovery techniques under reservoir conditions. The experimental data can be also used for assessment of different relative permeability and hysteresis models, and developing new methodologies for reliable simulation of WAG and SWAG injections.

This chapter presents the main conclusions drawn from the experimental and theoretical studies in this work followed by some recommendations for future studies.

Chapter 4: Gas-Oil Two-Phase Flow at Very-low IFT

- Current assumptions in the literature suggest that as a fluid system approaches miscibility, relative permeabilities of both phases (wetting and non-wetting phases), as a function of wetting-phase saturation, show linear behaviour and become diagonal lines. The results of this study show that only for non-wetting phase (gas), in drainage direction, this assumption is valid. However, for the two rocks tested in this work, the wetting phase relative permeability (oil), in both imbibition and drainage directions, and also the non-wetting-phase (gas) k_r in imbibitions direction, show significant deviation from this assumption even at the very low IFT of 0.04 $mN.m^{-1}$.

- Based on the current assumptions in the literature, in the vicinity of miscibility, non-wetting phase relative permeabilities hysteresis diminishes and normally no hysteresis is assumed for the wetting-phase. The results presented here show that even at near-miscible conditions (IFT=0.04 $mN.m^{-1}$), significant hysteresis was observed for both the non-wetting-phase (gas) and the wetting-phase (oil), in both the high permeability (1000mD) and the low permeability (65mD) rocks. Although, hysteresis for both the wetting- and non-wetting phases were less in the highly permeable core (1000mD) compared to the 65mD core sample. In agreement with literature the hysteresis effect was larger for non-wetting phase (gas) compared to the wetting phase (oil).

- Current assumptions in the literature also suggest that as long as connate water is immobile it does not influence the relative permeability of the phases. Presented investigations in this study show that the effect of immobile water on wetting-phase relative permeability (oil) is not significant if the k_r data is presented based on the oil (wetting phase) saturation. However, the effect of immobile water saturation on the non-wetting phase (gas) relative permeability was significant and should not be ignored. This effect was more profound in gas injection (drainage) compared to oil injection (imbibitions). These observations show the importance of performing SCAL (k_r) tests with representative connate water saturation (for near-miscible conditions).

- Relative permeability of both the wetting and non-wetting phases (oil and gas) in the mixed-wet systems reduced compared to the water-wet systems. The reduction was observed for both imbibition and drainage directions. This shows the importance of performing SCAL tests under representative wettability of the reservoir rock (for near-miscible conditions and in the presence of immobile water saturation).

- Based on presented results low IFT liquid/liquid systems should not be used as an analogue for low IFT gas/liquid (oil) systems. The behaviour of these two systems and the involved displacement mechanisms are different and that explains why in the present study significant k_r hysteresis was observed at low gas/oil IFT but other researchers using a low IFT liquid/liquid system as an analogue for low IFT gas/oil systems have not reported k_r hysteresis.

Chapter 5: Hysteresis in Different Two-Phase Systems (Mixed-Wet)

Gas-Oil Two-phase System (in the presence of immobile water):

- Despite a very low IFT (0.04 $mN.m^{-1}$) between the oil and gas, the k_r curves show significant hysteresis. Cyclic Hysteresis is much less for wetting phase (oil) compared to the non-wetting phase (gas). This is consistent with the observations available in the literature. As the alternation of imbibition and drainage cycles continues, the hysteresis effects on oil relative permeabilities diminish. However the hysteresis effect on gas relative permeabilities stays significant.

- Although Carlson model predictions for the magnitude of trapped gas saturations were fair, its predictions for non-wetting phase relative permeability (in imbibition direction) were poor. This is attributed to the oversimplifying assumption in the model that the curvature of scanning imbibition curves should be exactly the same as that of the bounding imbibition curve.

- Killough model predictions underestimate gas relative permeability as the oil saturation increases (especially near trapped gas saturation).

- Killough model overestimates the wetting phase relative permeability, especially as the value of residual (trapped) gas saturation is approached. This could be because the Killough hysteresis model uses Land's model to estimate trapped gas saturation and Land's model overestimates trapped gas saturation based on the experimental results.

- Oil and gas k_r curves showed hysteresis in drainage direction compared to the preceding imbibition cycle. Neither Carlson nor Killough model predicts such behaviour (neither for wetting phase nor for non-wetting phase).

- Beattie *et al.* hysteresis model does consider hysteresis for wetting and non-wetting phases, and for both imbibition and drainage stages. Although qualitatively this model is able to capture the oil/gas relative permeability hysteresis behavior that was observed in this study, but it is still unable to accurately predict the observed hysteresis quantitatively (which results in poor fluid recovery predictions), especially for the later cycles of imbibition and drainage.

- Based on the results, more flexible hysteresis models such as that of Beattie *et al.* should be considered and included in commercial simulators.

Gas-Water Two-phase System:

General Observations

- It is observed that for the non-wetting phase (gas), relative permeability of the scanning drainage periods would not follow those of the former imbibitions. This is against the assumptions in Carlson, Land and Killough hysteresis models and shows the importance of including non-reversible hysteresis loops models such as Beattie *et al*. and Kjosavik *et al.* in commercial simulators.

- Contrary to the prediction of existing k_r hysteresis models, it was observed that although the same saturation as the former imbibition turning point is achieved in drainage periods, end-point relative permeability of gas would be less than the previous drainage period. This means that at the end of the 2nd gas injection (which is at the same saturation as that of the end of the 1st gas injection), k_{rg} for the 2nd gas injection is less than that of the 1st gas injection. Current two-phase hysteresis models (except Beattie *et al.*) assume they are the same.

- For both wetting (water) and non-wetting (gas) phases, the cyclic hysteresis effect is less important for the later cycles.

Gas-Water System: (IDIDI)

- Water (wetting phase) relative permeability shows hysteresis in alternating imbibition and drainage periods. The results show that k_{rw} values drop in successive change of injection from imbibition to drainage and vice versa. The hysteresis in k_{rw} becomes less as the number of alternation increases (later cycles).

- As the alternation between imbibition and drainage cycles continues, gas relative permeability for drainage and imbibition periods keeps decreasing. In three-cycle water and gas injections, k_{rg} was higher for the 1st water injection and was lowest for the 3rd water injection. Generally k_{rg} cyclic hysteresis for this series of experiments was not significant. All of the scanning k_{rg} curves fall below bounding imbibition k_{rg} curve.

Gas-Water System: (DIDIDI)

- Generally, water (wetting phase) relative permeability does not show much hysteresis during alternation between imbibitions and drainages (especially for higher water saturations). Compared to the k_{rw}, cyclic hysteresis is more pronounced for k_{rg}. The k_{rg} scanning curves lie between bounding drainage and bounding imbibition curves. As the cyclic injection continues, the k_{rg} from each drainage period is larger than its subsequent imbibition k_{rg} and gas relative permeabilities approach to those of bounding imbibition curve.

Oil-Water Two-phase System: (DIDIDI)

- Water relative permeabilities show hysteresis for alternation between imbibition and drainage periods. Contrary to the usual behaviour of the wetting-phase in the water-wet system, in the case of the mixed-wet rock, it was observed that water imbibition relative permeabilities are less than former drainage period. In addition the current assumption in the literature (such as Carlson and Killough models) which assumes the relative permeability for scanning drainages would follow the values of the former imbibition period isn't validated for water phase in oil-water system studied here.

- As the cyclic injection of imbibition and drainage periods continues, the effect of hysteresis on water relative permeabilities becomes less.

- Oil relative permeability shows significant hysteresis for the 1^{st} imbibition compare to the 1^{st} drainage period. Although after that with the alternation between imbibition and drainage periods the oil relative permeability is generally decreasing, but still in the range of experimental accuracy it is fair to claim that there is no significant hysteresis after 1^{st} imbibition period. This means that the current assumption in the hysteresis models (such as Carlson and Killough) that assumes the relative permeability for scanning drainages would follows the values of the former imbibition periods, is somehow validated for oil phase in oil-water system studied here.

- Water relative permeabilities do not show significant difference for drainage periods. This means that k_{rw} are on top of each for different drainage periods. This is especially true for lower water saturations.

- Between Carlson and Killough models (due to their assumptions) predictions of Carlson is better for drainage periods. For imbibition periods, Killough model predictions are better than Carlson.

- For the mixed-wet rock, although relative permeabilities of oil/water and gas/water systems are very close to each other (for both wetting and non-wetting phases) for the 1^{st} drainage periods (1^{st} oil injection compare to 1^{st} gas injection), the difference between their behavior respect to hysteresis (alternation of

imbibition and drainage displacements) makes relative permeabilities very different for the later cycles. This means that current approach in industry to replace oil-water relative permeabilities set instead of gas-water set might be fine for the 1st drainage period, but for cases with cyclic imbibition and drainage displacements (such as WAG process) it would cause significant errors on the predicted three-phase relative permeabilities and predicted recoveries.

Chapter 6: Different Injection Scenarios

- Oil recovery by waterflood is much higher in the mixed-wet rock than in water-wet system (S_{orw} (MW) < S_{orw} (WW)). This is because of suppressed water-film flow and oil snap-off mechanisms under mixed-wet conditions. Contrarily, oil recovery by gas injection was higher for water-wet conditions compared to mixed-wet system (S_{org} (MW) > S_{org} (WW)). This is attributed to higher tendency of the oil phase to adhere to the rock surfaces (and less conductivity of oil wetting layers) in mixed-wet rocks compared with water-wet rocks (oil spreading layers).

- In mixed-wet rocks, the performance of gas injection is lower compared with waterflood (S_{orw} (MW) < S_{org} (MW)). In contrast, gas-injection performance is considerably higher than waterflood in water-wet systems (S_{orw} (WW) > S_{org} (WW)). The performance of water, gas, and WAG injection are strongly affected by the state of wettability. The new insights provided by these experiments clearly demonstrate the importance of wettability of the rock in the design of a field WAG process. It is therefore necessary to ensure a proper core-handling procedure in which the reservoir native state wettability is preserved. In cases where the wettability state of the core has changed, it is crucial to follow a suitable approach to reproduce the reservoir wettability before commencing coreflood experiments.

- For water-wet systems, alternating injection of gas and water cycles increased the oil-recovery performance of each gas injection period compared with its preceding gas injection. This means that oil recovery, based on the fraction of oil at the beginning of the gas-injection period, is highest for the third gas-injection period and lowest in the first gas-injection period. Although the same trend is

also observed for mixed-wet systems, this effect was considerably less profound in mixed-wet systems compared with water-wet systems. It should, however, be mentioned that in the mixed-wet system, most of the oil was produced in the primary stage of water flooding and hence less oil remained for recovery in subsequent stages of WAG injection.

- Comparison of the amount of oil recovered by WAG, SWAG, gas injection and waterflood reveals that, for the conditions of the performed experiments (very low gas/oil IFT), WAG has a superior performance over other injection strategies tested in mixed-wet systems. In terms of oil recovery, the order of injection strategies from highest to lowest is; WAG, water flooding, SWAG and gas injection (oil recovery in mixed-wet system: $WAG_{IDIDID} > WAG_{DIDIDIDI} >$ WF > SWAG > GF). The results also reveal that the performance of WAG injection (in mixed-wet rocks) would be adversely affected (lower oil recovery and injectivity) if WAG injection begins with a gas injection period (instead of water) (injectivity in mixed-wet system: $WAG_{IDIDID} > WAG_{DIDIDIDI}$).

- Presented results on the effects of SWAG (gas/water) ratio of 0.25 and 1.0 show that the rate of oil recovery in mixed-wet systems decreases by increasing the gas fraction (oil production rate in mixed-wet system: $SWAG_{(Qg/Qw=0.25)} > SWAG_{(Qg/Qw=1.0)}$). However, the ultimate oil recovery achieved remained almost the same for the two SWAG ratios tested (ultimate oil recovery in mixed-wet system: $SWAG_{(Qg/Qw=0.25)} \simeq SWAG_{(Qg/Qw=1.0)}$).

- In addition to the lower oil recovery obtained by SWAG injection in the mixed-wet systems, it was also noticed that SWAG injection results in considerably lower injectivity than what was observed for single-phase fluid injection (during WAG injection). Although some degree of injectivity reduction is expected when water and gas injection is combined, yet the observed reduction in injectivity for SWAG injection was disproportionate to the amount of additional oil recovery obtained from it.

Chapter 7: Hysteresis Effect on Three-Phase Relative Permeability

- The results show irreversible k_r hysteresis loops for gas under three-phase flow conditions. Gas relative permeability (k_{rg}) dropped in successive WAG cycles under both water-wet and mixed-wet conditions. k_{rg} cycle-dependent hysteresis was found to be larger in the water-wet system compared to the mixed-wet one. The results also reveal saturation history dependency for oil relative permeability (k_{ro}) curves in which k_{ro} increased in successive gas injection periods separated by water injection periods. k_{ro} improvement was larger for water-wet systems compared to mixed-wet conditions.

- In both water-wet and mixed-wet systems, for WAG_{IDIDID}, the largest k_{rw} hysteresis happens for the transition from two-phase (primary waterflooding) to three-phase system. For both WAG_{IDIDID} and $WAG_{DIDIDIDI}$ injection scenarios the hysteresis for water phase becomes minimal after the 2nd three-phase displacement (2nd water injection in IDIDID and 2nd gas injection in DIDIDIDI injection sequences).

- Conventional approaches for simulation of WAG injection are based on two-phase flow hysteresis models such as Killough and Carlson. The main assumption is that the imbibition process is reversible. In the WAG experiments reported here in which the process is started with an imbibition (water injection) period. As a result neither Killough nor Carlson model would take into account any k_{rw} hysteresis in the subsequent gas and water injection periods. This is clearly not valid since the measured data shows that k_{rw} obtained during the 1st gas injection (three-phase) is much lower than k_{rw} obtained in the 1st water injection (two-phase). For the WAG test started with primary gas injection (DIDIDIDI), Killough hysteresis model predicts that k_{rw} for the 2nd water injection should be above that of previous drainage curve and Carlson model does not consider any hysteresis all together, which is against the obtained experimental results in this study. With regards to the k_{rg} curves, these models assume that drainage relative permeability curves are always above those of the former imbibition period, which is again not supported by the results from this study.

- Contrary to the conventional approach (using two-phase hysteresis such as Carlson and Killough), Larsen and Skauge (1998) three-phase hysteresis model (WAG-hysteresis model in Eclipse) assumes that three-phase k_{rw} values for later periods of the WAG injection lies between those of primary waterflooding and 2^{nd} water injection. This assumption is not quite supported by the coreflood results in the mixed-wet core, since k_{rw} continually dropped in the later stages of $WAG_{DIDIDIDI}$ injection test.

- The results show that the importance of cyclic hysteresis of each phase depends on reservoir and operational parameters such as wettability, immobile water saturation, reservoir rock permeability and injection scenario. The presented results point out the need for development of more accurate three-phase hysteresis formulations especially for mixed-wet systems.

Chapter 8: Trapped Oil and Gas Saturations

- Both three-phase trapped gas and trapped oil saturations were larger in water-wet systems compared to what was obtained in mixed-wet systems. Measured three-phase trapped oil and gas saturations for lower permeability rock (65mD) were larger than those of the 1000 mD core sample.

- S_{orw} vs. S_{gt} curve of the water-wet system lies above that of the mixed-wet system. This means that the amount of oil that is trapped by water in the presence of gas increases as the porous medium becomes more water-wet.

- Although some previously developed empirical trap models are able to capture the trends of trapped gas and trapped oil saturations for two-phase systems (Aissaoui model for S_{gtw} and Spiteri et al. model for S_{otw}), but the observed trends in three-phase (especially for mixed-wet system) cannot be captured using available models. This further emphasises the need for developing more reliable models for fluid displacements in three-phase flow regime.

- For low IFT (near-miscible) gas/oil systems, trapped gas saturations obtained from gas/oil and gas/water systems should not be used instead of the other. The same is true for trapped saturations obtained from gas/water and oil/water systems.

- It is found that for three-phase systems under WAG injection, the S_{orw} increases linearly by decreasing the S_{gt}, and approaches to the two-phase S_{orw} (obtained after primary waterflooding) for the limit case with $S_{gt} = 0$.

- From different parameters studied here, injection scenario, permeability and oil/gas IFT had the largest effect on the slope of the S_{orw} vs. S_{gt} curve.

- Investigation of the effect of oil/gas IFT showed that for immiscible WAG injection, residual oil saturation to the waterflooding periods of the WAG injection, are minimally affected by the presence of trapped gas (although trapped gas saturations were higher than those of near-miscible WAG injection). As a result immiscible WAG injection, unlike near-miscible WAG injection, is not effective in increasing the oil recovery (reducing the residual oil saturation).

Recommendations

- In this study the effect of immobile water saturation was investigated for very-low oil/gas IFT system at water-wet condition. More study regarding the effect of immobile water saturation in two-phase and three-phase flow especially in mixed-wet condition is recommended.

- The presented investigations in this study show that the most widely used trap models are unable to predict precisely the trapped hydrocarbon saturation reached by different cycles of the WAG injection. This is especially true for Land model which is the backbone in Killough two-phase hysteresis model and also WAG three-phase hysteresis model. More extensive studies should be performed towards measurement and modelling of the trapped oil and gas saturations for both two-phase and three-phase systems in mixed-wet condition.

- In this research, systems with very-low oil/gas IFT were investigated. At the time of writing this thesis author has started working on systems with higher oil/gas IFT values (gas injection, primary waterflooding and WAG injection). Two-phase and three-phase (WAG injections) displacements under higher oil/gas IFT are recommended since they would help to better understand the recovery mechanisms and effect of oil/gas IFT on cyclic hysteresis behaviour of relative permeabilities.

- This research was focused on sandstone porous media. At the time of writing this thesis author has started working on carbonate rocks using real reservoir fluids (gas, oil and brine). Considering the large amount of the oil which exist in carbonate reservoirs and unique properties of these reservoir rocks, it is highly recommended to further investigate the effect of cyclic hysteresis and trapping in carbonate rocks with low permeability.

- In this research, the coreflood experiments were conducted in horizontal direction (whilst rotating the core along its axis to reduce the gravity segregation effects). To be able to better understand the effect of gravity forces, either horizontal displacement without rotation and/or inclined/vertical displacements are recommended.